

Enhanced Electrodeposition for the Filling of Micro-Vias

Thomas David Arthur Jones, MSc, BSc

A dissertation submitted for the qualification of Engineering
Doctorate in Photonics and Optics Technologies

Heriot-Watt University
School of Engineering and Physical Sciences

June 2017

The copyright in this thesis is owned by the author. Any quotation from the thesis or use of any of the information contained in it must acknowledge this thesis as the source of the quotation or information.

Abstract

This thesis investigated the introduction of megasound (MS) (1MHz) acoustic technology as an enhanced agitation method of an electrolyte solution for the electrochemical deposition of copper (Cu), used in electroplating processes. The thesis, carried out at Merlin Circuit Technology Ltd, studied the possibility of improving processing capabilities for use in Printed Circuit Board (PCB) industrial manufacture. Prior laboratory experiments demonstrated increased metallisation of vertical interconnect access (via) features in a Printed Circuit Board (PCB), which, if applied within manufacturing, would enable increased connectivity throughout a PCB and result in cost savings.

PCB manufacturing quality after MS-assisted Cu electroplating was assessed by measurements of the topography of the electrodeposits, using scanning electron microscopy and white-light interferometry. Cu plating rate changes were also measured on the surface of the PCB and inside the vias.

After plating Cu with MS-assistance, the macro and microscale surface composition was demonstrated to alter due to the direct influence of the acoustic waves. Systematic characteristic of the surface was conducted by varying the settings of the acoustic transducer device as well as the process parameters including electrical current distribution, bath additive chemistry and solution temperature.

MS processing was shown to produce unique Cu artefacts. Their deleterious formation was demonstrated to be influenced by acoustic standing waves and microbubble formations at the electrolyte solution/PCB interface. Causes of these artefacts, microfluidic streaming and cavitation, were also observed and controlled to reduce the creation of these artefacts.

MS plating Cu down through-hole via (THV) and blind-via (BV) interconnects was shown to produce measureable benefits. These include, for THVs, a 700 % increase of Cu plating deposit thickness within a 175 μm diameter, depth-to-width aspect ratio (ar) of 5.7:1, compared with processing under no-agitation conditions. For BVs, a 60 % average increase in Cu deposition in 150 μm and 200 μm , ar 1:1, was demonstrated against plating under standard manufacturing conditions - bubble agitation and panel movement.

Dedication

This thesis is dedicated to the British tax payer, British manufacturing and academic institutions and to the loved ones in my life.

Acknowledgements

Throughout the four and a half years spent on my engineering doctorate degree, I have had the wonderful opportunity of pursuing research for the benefit of industry in prestigious British manufacturing and academic institutions.

My work was funded by the Engineering and Physical Research Council (EPSRC) under grant number EP/G037523/1 and, so, I would first like to thank the British tax payer for enabling me to take this opportunity to perform such high-level research.

I would like to acknowledge the financial support of Merlin Circuit Technology Ltd, whose progressive, far-sighted views towards research and development in the Printed Circuit Board industry – unmatched by their UK competitors – has made this degree possible. I would like to specifically thank my industrial supervisors, Mr Dennis Price and Mr Matthew Beadel, whose calm and welcoming attitude to my extensive questions on circuit manufacture enabled successful research to be delivered on time.

I would like to thank my academic supervisors, Professor Marc Desmulliez and Dr David Flynn at Heriot-Watt University, whose essential critique of my work, on a weekly basis, helped to shape me into the professional researcher I have become.

Discussions on the fundamentals of Megasonic electroplating were conducted with Dr Nadia Strusevich and researchers at Greenwich University and Dr Suzanne Costello, at MCS Ltd., Roslin. Their assistance is greatly appreciated, as they helped to guide me to a successful design of experimentation for applying the complex Megasound technology.

Last, but definitely not least, I would like to thank the people closest to me in my life for their warm words of comfort and support throughout this time, and for their grammatical checking of my written reports which were numerous in size and volume.

ACADEMIC REGISTRY

Research Thesis Submission

Name:	Thomas David Arthur Jones		
School:	School of Engineering and Physical Sciences		
Version: <i>(i.e. First, Resubmission, Final)</i>	Final	Degree Sought:	Engineering Doctorate in Photonics & Optics Technologies

Declaration

In accordance with the appropriate regulations I hereby submit my thesis and I declare that:

- 1) the thesis embodies the results of my own work and has been composed by myself
- 2) where appropriate, I have made acknowledgement of the work of others and have made reference to work carried out in collaboration with other persons
- 3) the thesis is the correct version of the thesis for submission and is the same version as any electronic versions submitted*.
- 4) my thesis for the award referred to, deposited in the Heriot-Watt University Library, should be made available for loan or photocopying and be available via the Institutional Repository, subject to such conditions as the Librarian may require
- 5) I understand that as a student of the University I am required to abide by the Regulations of the University and to conform to its discipline.
- 6) I confirm that the thesis has been verified against plagiarism via an approved plagiarism detection application e.g. Turnitin.

* *Please note that it is the responsibility of the candidate to ensure that the correct version of the thesis is submitted.*

Signature of Candidate:		Date:	
-------------------------	--	-------	--

Submission

Submitted By <i>(name in capitals)</i> :	
Signature of Individual Submitting:	
Date Submitted:	

For Completion in the Student Service Centre (SSC)

Received in the SSC by <i>(name in capitals)</i> :			
Method of Submission <i>(Handed in to SSC; posted through internal/external mail):</i>			
E-thesis Submitted (mandatory for final theses)			
Signature:		Date:	

Table of Contents

Abstract	ii
Dedication	iii
Acknowledgements	iv
Research Thesis Submission	v
Table of Contents	vi
List of Figures	ix
List of Tables	xv
Glossary	xvi
Publications and Awards	xvii
Chapter 1 Introduction	1
1.1 Background	1
1.2 Motivation for this thesis	4
1.3 Objectives	5
1.4 Structure of thesis	6
Chapter 2 Literature Review	8
2.1 Electrochemical Processes	8
2.1.1 The Electrolysis reaction	8
2.1.2 Electrodes in Copper Plating Baths	10
2.1.3 Copper Sulphate Bath Composition	13
2.1.4 Diffusion limited transfer mechanism	15
2.1.5 Plating Current Density	16
2.1.6 Periodic Reverse-Pulse Plating	19
2.1.7 Micro-throwing power of electroplating bath	23
2.1.8 Copper electro-crystallinity	24
2.1.9 Limited current density plating	26
2.1.10 Electroless copper plating	26
2.2 Megasonic Literature	27
2.2.1 Near-field of the acoustic wave	27
2.2.2 Cu surface Crystallinity after MS plating	29
2.2.3 Megasonic-Assisted Copper Electroplating	31
2.2.4 Acoustic standing waves: Levitation and acoustic interference	32
2.2.5 Acoustic Streaming	33
2.2.6 Cavitation	37
2.2.7 Cavitation streamers: bubble cones, lens and ringlets	40
2.3 PCB composition	43
2.4 Via Interconnects	44
2.4.1 Blind via Fabrication	45
2.4.2 Through-hole Via Fabrication	47
2.4.3 Improved PCB design due to MS Plating	48
2.4.4 Alternative via filling techniques	50
2.4.5 Silicon via fill processing	51
2.5 Quality evaluations of Vias	52
2.6 General Conclusions	55
Chapter 3 Experimental Details	57
3.1 Bath Synthesis and maintenance	57

3.1.1 Cathodic efficiency for plating setup	58
3.1.2 Electroless copper plating setup and composition	59
3.2 Bath equipment Setup	59
3.2.1 Rectification and electrode connectivity	61
3.2.2 Bath dummyming	61
3.2.3 50 Hz Cathode Rail Vibration.....	62
3.2.4 PCB type used in experiments	62
3.3 Characterisation Methods	62
3.3.1 Hull Cell analysis	62
3.3.2 Microsectioning / Microscope use	63
3.3.3 White light phase shifting interferometer – measurements of roughness	64
3.3.4 Via filling quality: definition and quantification	67
3.4 Transducer setup and configuration.....	68
3.4.1 Current thieving by the transducer	75
3.4.2 Fluid circulation	76
3.4.3 Conclusions.....	79
3.5 COMSOL Simulation Setup	80
3.5.1 Evaluation of the average potential Energy Density	85
3.5.2 COMSOL scattering simulations	85
3.6 General Conclusions	85
Chapter 4 Panel Plating using Megasonic Assisted Agitation	87
4.1 Cu crystallinity variation with pressure.....	87
4.2 Transducer tangential distance variation	90
4.3 Transducer power variation	92
4.4 Current density alteration due to MS	95
4.5 Cu crystallinity variation with current density	99
4.6 Plating temperature variation.....	101
4.7 MS panel plating conclusions	103
4.7.1 Whisker growth and the impact of additional agitation alongside MS	104
4.7.2 Micro-roughening due to transducer position alteration and power change	104
4.7.3 Current density alteration due to current thieving by the transducer	105
4.7.4 Reduced plating process temperatures	106
4.7.5 Section summary	107
Chapter 5 Surface Acoustic Artefacts produced in response to Megasonic Agitation	108
5.1 Standing wave behaviour	108
5.1.1 Acoustic streaming lines.....	108
5.1.2 Ridges	110
5.1.3 Ringlets and cells	113
5.1.4 Non-regular structures and nodules.....	115
5.1.5 Conclusions.....	117
5.2 Microbubble influences	120
5.2.1 MS cavitation streamers: bubble lens, cones and bubble ringlets.....	120
5.2.2 Cavitation.....	123
5.2.3 Conclusions.....	124
5.3 General conclusions	125

Chapter 6 Plating down Through-hole Via using Megasonic Assisted Agitation	126
6.1 Introduction.....	126
6.2 MS plating down THV in the thin Cu regime	126
6.2.1 Standard bath agitation effects in comparison to MS THV plating	127
6.2.2 50 Hz vibration effects on MS THV plating.....	129
6.2.3 Conclusions.....	132
6.3 MS plating down THV in the thick Cu regime.....	133
6.3.1 Cu patterning for different THV diameters	134
6.3.2 MS Plating enhancements measured within the THV.....	139
6.3.3 Transducer angle orientation alteration	141
6.3.4 Acoustic pressure and electric current density and waveform alterations...	146
6.3.5 Conclusions.....	150
6.4 General conclusions	153
Chapter 7 Plating down Blind Via using Megasonic Assisted Agitation	154
7.1 Introduction.....	154
7.2 MS plating down BV in the Thin Copper Regime.....	154
7.2.1 Results and Analysis.....	155
7.2.2 Conclusions.....	158
7.3 MS plating down BV in the Thick Cu regime	159
7.3.1 Results and Analysis.....	159
7.3.2 Conclusions.....	162
7.4 General Conclusions	163
Chapter 8 Conclusions and Future Studies	164
8.1 Megasonic-assisted electroplating issues and enhancement	165
8.2 Further megasonic processing investigations	167
8.2.1 Megasonic plating continuation	167
8.2.2 Megasonic fundamental behaviour investigations	169
8.2.3 Further quality evaluations	171
8.3 Ending statements	172
Appendix A Statistical Analysis.....	173
Appendix B Statistical Analysis.....	176
Appendix C Megasonic Assisted Dry-film Removal	180
C.1 Introduction.....	180
C.2 Megasonic assisted dry-film developing	181
C.2.1 MS developing experimental investigation.....	182
C.2.2 MS developing results and analysis.....	184
C.2.3 Conclusions	185
C.3 Megasonic assisted dry-film stripping.....	186
C.3.1 MS stripping experimental investigation	187
C.3.2 MS stripping results and analysis	189
C.3.3 Conclusions	192
C.4 General conclusions.....	193
References	194

List of Figures

Figure 1.1 - Schematic of via interconnect PCB design.	3
Figure 1.2 - Structure of thesis	6
Figure 2.1 - Schematic of the plating cell arrangements with arrows highlighting the movements of electrons, electrical current and cupric ions. Indicated on the electrodes is the built-up Coulomb charge.....	10
Figure 2.2 - General structure for acyclic organic compound brightener additive.[30, 31]	14
Figure 2.3 - Compound structure for the leveller additive CsoHtoCUCuNn. [32]	15
Figure 2.4- A) and B) cross section schematic of the field line behaviours produced between an anode (right-hand-side) and a cathode (left-hand-side), indicated by dashed lines. C) an ideal uniform spread. [36]	18
Figure 2.5 - A plot of current density against time for a typical square, pulse current and a DC current. [40]	20
Figure 2.6 - A plot of current density against time for a typical square wave, reverse-pulse current. Indicated are the respective redox potentials, time durations of the two current orientations and their maximum magnitudes. [40]	21
Figure 2.7 - A plot of current density against time for a typical square, periodic pulse-reverse current. Indicated are the currents and time durations for the two current orientations and the intermittent time between each pulse.[45].....	22
Figure 2.8 – Cross-section schematic of plated blind via – microvia - with different Cu thicknesses highlighted on the surface of the PCB. A & B, the side wall of the via, C & D, the base of the via, E, and the region of thinnest deposit, F. [46]	24
Figure 2.9 - The variation in grain structure of electrodeposited Cu in response to variations in bath parameters. [47]	25
Figure 2.10 - Shown in A and B are SEM images of electroplated tin for 0.05 A/cm ² and 0.3 A/cm ² respectively.[48].....	26
Figure 2.11 - A diagram indicating the near-field and far-field behaviours of an acoustic wave produced from a circular transducer in the ultrasound frequency range. [53].....	28
Figure 2.12 – A simplified schematic of sound beam spread, showing change in beam spread angle, α with increasing distance given in units of near field distance, N and for a transducer of circular diameter D.[53]	29
Figure 2.13 - SEM images of 4 A/dm ² DC Cu electroplated surfaces with A) no agitation B) 2.5 W/cm ² (50%) MS and C) 5.0 W/cm ² (100%) MS. Acoustic power density evaluated at source of transducer. [11]	30
Figure 2.14 - A) the electrolyte diffusion layer schematic at a PCB surface without any forced fluid circulation. B) Modification of the diffusion layer by US agitation with US plane waves indicated by lines on the figure.....	32
Figure 2.15 - Acoustic streaming patterns tracked from 1 μ m fluorescent beads, generated in response to a driving frequency between 2.1 - 2.6 MHz for different geometrical cavities of lengths between 300 - 350 μ m. [55]	36
Figure 2.16 - A not-to-scale 2D schematic of the fluid motions within the entrance of a THV with fluid motions in the boundary layers indicated.	37
Figure 2.17 - Examples of transient cavitation. A) the steps prior to and including bubble collapse indicating the jet streaming effect. B) the implosion of an air bubble under 25kHz ultrasonic agitation, where the internal-jet stream is shown.[64, 74].....	38
Figure 2.18 - A cavitation lesion produced as a result of a high frequency pulse-burst in transparent gel. Frequency of the megasound is 3.3MHz and pulse duration is	

30 ms. Vertical upward orientation indicates direction of the acoustic pulse. Scale is 2mm.[75]	39
Figure 2.19 - SEM images showing A) & B) surface of a Cu plate after 5min and 10 min of 20 kHz ultrasound exposure, respectively. C) Surface of Ag after 10 min sonication. For both metals the transducer - sample distance 0.5 mm. Scale in images 20 μ m.[76]	40
Figure 2.20 - The conical bubble structure formed for a high intensity (> 5 W/cm ²), 20kHz transducer.[79]	41
Figure 2.21 - Schematic of short distance focusing due to the formation of a non-uniform bubble layer on the surface of the ultrasound. [79]	42
Figure 2.22 - High-resolution photograph images recording the formation of an acoustic ringlet over time.[80]	43
Figure 2.23 - A) shows a cross-section diagram of a PCB glass weave and B) a top-down image of a PCB with the Cu removed[81]. Indicated in C) is a top-down surface plot of PCB electroplated with Cu under standard DC conditions. The image was obtained from a White Light Interferometer and indicated by the colour scale is the variation in height. The length scale of the image is indicated underneath.	44
Figure 2.24 - The standard filling process for electroplated copper Blind Vias. [84]	45
Figure 2.25 - A) Two vertically stacked BV. B) Two staggered BV.	46
Figure 2.26 - D.C. plated at 1 A/dm ² with MS assistance at 1 W/cm ² showing 0.1 mm diameter BVs at ar A) 1.7:1 and B) 3:1.[15]	47
Figure 2.27 - Three-stage THV filling process from left to right showing seed layer deposition with flash plating (2 - 5 μ m Cu), X-plating (5 - 10 μ m Cu) and via filling (10 - 15 μ m Cu).[16]	48
Figure 2.28 - Microsection of 0.2 mm diameter THV, ar 8:1, after 1 A/dm ² plating formed under a laboratory setting with A) no MS agitation and B) with 250 W MS. Red arrow highlights central void. [12]	48
Figure 2.29 - 2-D build schematics for a 26 layer PCB showing copper as orange and epoxy resin/glass as green, beige and white for A) standard processing involving six bonding and ten drilling operations and B) theoretical MS processing involving four bonding and six drilling operations.	49
Figure 2.30 - Three cross-section images of Through-hole via interconnects of different size, electroplated and uniformly filled with a non-conductive polymer. ...	51
Figure 2.31 - Indicated in A) are the formations of cracks due to 100 thermal cycles in a partially filled Cu through-hole via [97]. B), C) and D) display measured data for partially filled electroplated copper through-hole vias. E) shows data for fully plated via. All are unacceptable by IPC standards IPC-A-600 [98]....	54
Figure 2.32 - An example of a TDR PCB test coupon used to measure electrical impedance from Polar Instruments Ltd.	55
Figure 3.1 - Schematic of the 500 L plating bath with components in place.....	60
Figure 3.2 - The plating setup implementing a 50 Hz mechanical vibrator.....	62
Figure 3.3 - A) top-down schematic of the plating hull cell apparatus. Units in mm. B) Plated hull cell cathodes showing top, no corrections required and bottom, 2 ml/L of Cu114.[17]	63
Figure 3.4 - An example of a microsection measurement indicating the thickness of the plated copper.	64
Figure 3.5 - A) NewView™ 8000 Series Zygo Viewmeter white light phase shifting interferometer. B) closeup of circuit under analysis head.[110]	65
Figure 3.6 - Comparison of two different surface topographies but with the same value for Ra. The top shows a 'valley structure' and the bottom a 'peak structure'.[111]	66

Figure 3.7 - Schematics of the different regions which display varying degrees of plating quality in A) THV and B) BV.....	68
Figure 3.8 - X-ray photograph of the transducer surface. Indicated in the dark regions are piezoelectric transducer crystals.[112]	69
Figure 3.9 - Setup of acoustic pressure measurement performed by HWU group prior to the thesis.[112]	69
Figure 3.10 - A) & B), profiles of the acoustic pressure distributions measured for the acoustic wave parallel to the active transducer surface, at distances 2.5 cm and 25 cm respectively. Scale on images is 3 cm. Highest pressure (0.220 MPa) indicated in red and the lowest (0.037 MPa) in blue. Transducer setting 1 MHz at 90 W. [112].....	70
Figure 3.11 - A and B show a correctly setup transducer power unit from the front and back respectively.	71
Figure 3.12 - A) & B), front and back view of transducer fixed within scaffolding.....	72
Figure 3.13 - Transducer scaffolding within plating bath.....	72
Figure 3.14 - Acoustic pulse modulator circuit.....	73
Figure 3.15 - Schematics of the plating bath with components included showing, A), a top-down view without the transducer, B), with and C) a side-on view with.....	74
Figure 3.16 - A schematic of the plating cell setup indicating tangential distance x from PCB to transducer.....	74
Figure 3.17 - A plot of the plating rate measured with transducer setup a tangential distance x to the PCB surface and outputting zero agitation.	76
Figure 3.18 - Camera rig above bath.	77
Figure 3.19 - Schematics of the plating bath setup for without the transducer A) and with B) as shown in different orientations and positions by the grey rectangles. The orientation of the emitted acoustic wave is highlighted by the arrows.	78
Figure 3.20 - Fluid motion rates evaluated with two 18" by 24" PCBs in bath for A), panel movement and the fluid pump activated and B), the transducer switched on at locations a - c.....	79
Figure 3.21 - 2D representation of the multiphysics computational configuration for acoustic scattering in COMSOL. Representation shows an acoustic wave of particular frequency interacting with an object of high acoustic impedance which is of a size similar to a half of the acoustic wavelength.	80
Figure 3.22 - A) PML setup 1 and B) a close-up of its mesh. C) PML setup 2 and D) a close-up of its mesh.	82
Figure 3.23 - Different simulation setups showing background acoustic domain positions highlighted in blue covering A) the entire fluid domain and B) a partial section modelling transducer device.	83
Figure 3.24 - Schematic of 2D simulated area for THV cavity containing A) internal PCB structure and B) a simplified approximation to PCB. C) close-up of PCB internal structure highlighting glass in white, resin in grey, Cu in orange and electrolyte in blue. D) 2D cutlines in red to map pressure within THV cavity.	84
Figure 4.1 - Top-down images of plated Cu finish on PCB after 2 A/dm ² plating for 1 hour with A) without panel movement and 225 W MS B) with and 225 W MS C) with and no MS, 0 W. Scale on the images is 3 cm.	89
Figure 4.2 - White light interferometer plots of PCB surfaces plated under 2 A/dm ² DC for 30 min showing of areas 6.1 mm ² , with cross-section profiles included underneath showing, A) a 6.1 mm ² area produced from the transducer positioned 10 cm from the PCB and outputting at 225 W, B) a 6.1 mm ² area	

	produced from the transducer positioned 1 cm and outputting at 225 W and C) a 24.4 mm ² area for no transducer.	92
Figure 4.3 -	A plot of Ra measured using a white light interferometer for areas 2.0 mm ² and 6.1 mm ² , highlighting the variation in response to transducer acoustic power output.....	94
Figure 4.4 -	Top-down images of PCB surfaces plated at 2 A/dm ² for 30 min, with the transducer setup at 1 cm showing areas 6.1 mm ² using a white light interferometry with cross section profiles included underneath. Labels A and B indicate 0 and 45 W output power, respectively.....	95
Figure 4.5 -	PCB surfaces after 1 A/dm ² plating for 30 min showing A) different plated finishes observed on a PCB surface plated with a transducer at 1 cm outputting at 225 W, B) different plated finishes observed on a PCB surface plated with a transducer at 1 cm outputting at 0 W and C) plated surface with no transducer in bath.....	97
Figure 4.6 -	Top-down images of the PCB surface after 2 A/dm ² plating for 30 min for transducer setup at 1 cm and outputting at 225 W. A), B) and C) plating for bath solution temperatures 18 °C, 25 °C and 33 °C. Scale on images 3 cm.	103
Figure 5.1 -	Acoustic streaming lines on PCB surface after MS plating at 2 A/dm ² for 30 min and the transducer setup at 1 cm and outputting at A) 225 W and B) 90 W. Scale on images 3 cm.	109
Figure 5.2 -	Cu ridges imaged using an optical camera, after plating at 2 A/dm ² for 30min with MS output at 225W and transducer setup 1 cm tangential to PCB, showing A) ridges on a PCB surface without drilled vias and B) & C) with THVs.....	110
Figure 5.3 -	Microsection cross section of ridge structures formed after 30 min plating at 2 A/dm ² with 225 W acoustic output setup at angle of 45° and a tangential distance of 31 cm, and showing A) their Cu thickness and B) distance between peaks and glass weave.	112
Figure 5.4 -	2D COMSOL scattering simulations of 1 MHz wave propagating from left to right through modelled PCB cavity, depicting high and low pressures by red and blue, accordingly. A) 3D representation of the acoustic wave. B) top-down close up of the electrolyte/PC	113
Figure 5.5 -	A) Ringlet Cu features after MS plating at 2 A/dm ² for 30 min with the transducer positioned at 1 cm and output at 450 W. B) Underlying laminate surface with Cu removed via acid etch. C) & D) Cell features observed after MS plating under same conditions for but for 150 min. Scale in images 1 mm.	114
Figure 5.6 -	MS plated ring formation of matt finish on PCB from tooling hole. Plating conditions RP plating at 1:2 A/dm ² , 10ms fw, 0.5 ms rv, for 16 hours with the transducer out putting at 450 W and setup 4.5 cm tangential to PCB. Scale 0.5 mm.	115
Figure 5.7 -	PCBs RP plated at 1:3 A/dm ² for 153 min with 450 W acoustic power and the transducer setup 4.5 cm tangential to the PCB. A) Cu nodule imaged using Koolertron Digital Microscope on the MS plated PCB surface, scale 0.5 mm. B) microsection of a nodular feature.	115
Figure 5.8 -	PCB plated at 2 A/dm ² for 30 min with MS output at 225W and transducer setup 1 cm tangential to PCB showing nodular deposits formed on the tops of acoustic-formed ridges, towards the edge of the panel.....	116
Figure 5.9-	Microscope images of irregular acoustic artefacts on surfaces MS plated for 150 min at A) 1 A/dm ² DC, with 225 W MS and B) 1:3 A/dm ² RP, with 450 W MS, with the transducer setup at 4.5 cm for both.....	117

Figure 5.10 - Bubble clustering on transducer surface highlighted by blue arrows as it outputs at 450 W. Surface imaged using optical camera through clear water solution.....	120
Figure 5.11 - Optical images of the PCB surface, right, receiving MS agitation from transducer, left, highlighted by black lines. A) & B) bubble cones extending from PCB. C) levitating bubble cluster circled in red.	122
Figure 5.12 - Optical images of ring-like bubble structures observed in bath whilst under MS agitation.	122
Figure 5.13 - Images of cavitation features after MS Cu plating obtained using A) optical microscope, scale 0.25 mm, for plating conditions 2 A/dm ² for 30 min and 450 W MS, B) Interferometer, scale 1 mm and C) SEM, scale 5 µm, for plating conditions in both 4 A/dm ² for 30 min and 225 W MS.	124
Figure 6.1 - Microsections highlighting plating performance after 45 min plating at 2A/dm ² for A) transducer setup 4.5 cm tangential to PCB and outputting at 450 W, showing a 0.36 mm diameter THV ar 4.4:1 B) Panel movement & Bubble agitation showing a 0.35 mm diameter THV, ar 4.6:1 and C) no agitation, showing a 0.40 mm diameter THV, ar 4:1.	128
Figure 6.2 - The average plating rates from four measurements, taken on samples formed after standard, MS plating at 450 W and no agitation were applied, in different regions on the THV outlined in Chapter 3, Fig 3.7.	129
Figure 6.3 - Plot of the micro-throwing power given in units of %, derived from measures of average plated thickness from the mid-point and surface of THVs of different diameter and bath agitation settings, plated under 2 A/dm ² , with the transducer at 4.5 cm and 450 W of acoustic power for 45 min.....	131
Figure 6.4 - The micro-throwing power evaluated down a 0.225 mm diameter 8:1 THV, derived from measures of plated thickness at the mid-point of the THV and the surface, plated under 1 A/dm ² for 60 min.	132
Figure 6.5 - Schematic of the acoustic transducers orientation to the PCB.....	134
Figure 6.6 - Microsections of 175 µm diameter (ar = 5.7:1), THV interconnects on a PCB electroplated at 0.5 A/dm ² , for 15.5 hours and showing A) with 450 W MS and transducer setup 4.5 cm tangential to PCB and B) plating with no bath agitation.....	136
Figure 6.7 - 2D COMSOL simulated Acoustic Pressure distributions alongside MS plating results showing, A) MS Plating with PCB flipping and B) MS Plating with no PCB flipping. Scale bar for simulation showing normalised units of acoustic pressure.....	138
Figure 6.8 - COMSOL acoustic scattering simulations of 0.15 mm diameter, ar 5.7:1 for A) little Cu and B) thick Cu. Scale bar for simulation showing normalised units of acoustic pressure.	138
Figure 6.9 - Microsections of the Cu thickness in the middle of 0.15 mm diameter, ar 5.7:1 THV, deposited at 0.5 A/dm ² for 16 hours under conditions of A) 450 W MS, B) Pulsed acoustic and C) no agitation. When used transducer setup 4.5 cm tangential to PCB.	140
Figure 6.10 - The average plating rate evaluated from ten measures of Cu thickness taken in the middle of 0.15 mm diameter, ar 5.7:1 THV, after processing under different conditions.	141
Figure 6.11 - A plot of the normalised, average potential sound energy density measured within the THV cavity in response to sonicating angle, using pressure values obtained from COMSOL simulation.	146
Figure 6.12 - Micro-throwing power evaluated within the centre of 0.325 mm diameter, ar 3.4 : 1 THVs with the transducer setup at 8 cm. THV plated for 15 hours.	148

Figure 6.13 - MS plating investigation on 0.15 mm diameter THVs changing the transducer tangential distance, electrical waveform and current density. PCB plated for 16.5 hours with 450 W MS and evaluations of micro-throwing power made from average measures of plated thickness.....	149
Figure 6.14 - A) & B) micro-sections of frosted finish at THV entrance and on PCB surface, respectively. C) image of frosted region on surface. PCB plated at 0.5 A/dm ² for 16.5 hours with the transducer setup 4.5 cm tangential to PCB and outputting at 450W.....	150
Figure 7.1 - Average plated thickness evaluated from ten measures taken from the bottom of BVs after 153 min RP plating, under different agitation conditions.....	158
Figure 7.2 – Average plated thickness evaluated from ten thickness measures taken from the bottom of BVs after 12 hours RP plating, under different agitation conditions.....	161
Figure 8.1 - MS process flow for high ar BV plating.....	168

List of Tables

Table 1.1- A brief overview of PCB manufacturing with cross-section 2-D schematics of the manufacturing process, showing PCB laminate in beige, copper in orange and yellow and photoresist in blue.	2
Table 1.2 - Outline of MS-assisted electroplating process scale-up into industry.	6
Table 3.1 - CU110 chemical composition, concentration and operating conditions.....	58
Table 3.2 – Electroless Copper solution composition as supplied by MacDermid Ltd..	59
Table 3.3 - Operational Procedure for NewView™ 8000 Series Zygo Viewmeter.....	65
Table 3.4 - Properties for the different material domains.[120-125].....	84
Table 3.5 - Simulation settings.....	85
Table 4.1 - Experimental conditions for experiment 4.1a.....	88
Table 4.2 - Experimental conditions for experiment 4.1b.	89
Table 4.3 - Macro-scale and micro-scale SEM images for surfaces plated at 4 A/dm ² for 30 min and with the transducer setup a 1 cm under varying acoustic power outputs.....	90
Table 4.4 - Experimental conditions for experiment 4.2.	91
Table 4.5 - Experimental conditions for experiment 4.3.	93
Table 4.6 – Experimental conditions for experiment 4.4.....	96
Table 4.7 - Plating behaviours observed after plating at 1 A/dm ² for 30 min across a PCB receiving 225 W MS agitation. Effects caused due to changes in electrical current distribution across PCB with estimated current density values highlighted.....	98
Table 4.8 - Experimental conditions for experiment 4.5.	100
Table 4.9 - SEM images of PCB surfaces after plating for 60 min under varying current densities and acoustic output powers, with the acoustic transducer setup at 1 cm.....	101
Table 4.10 - Experimental conditions for experiment 4.6.	102
Table 4.11 – Conclusions from Chapter 4.	107
Table 5.1- The plating conditions under which surface acoustic artefacts are produced.	117
Table 6.1 - Plating setup for Experiment 6.2.1	127
Table 6.2 - Plating setup for Experiment 6.2.2.....	130
Table 6.3 - Plating experiment setup for MS THV plating investigations 6.3.1.....	134
Table 6.4 - Plating behaviour for THVs formed under different agitation conditions and for different sized diameters. PCBs plated a 1 A/dm ² for 16.5 hour for the 0.325 mm THV and 16.2 hr for 0.475 mm THV and when used, transducer positioned tangential to PCB at 8 cm.....	135
Table 6.5 - Plating experiment setup for MS THV plating investigations 6.3.2.....	139
Table 6.6 - Plating experiment setup for MS THV plating investigation 6.3.3.	142
Table 6.7 - Plating rate measured in the middle of the THVs in response to angle orientation of the transducer with corresponding COMSOL simulated acoustic scattering distributions. Image includes of THV plated under standard agitations without MS.	144
Table 6.8 - Plating experiment setup for MS THV plating investigation 6.3.4.	147
Table 7.1 - Microsection images of 0.20 mm diameter, BVs of different ar, RP plated at 1:3 A/dm ² for 153 minutes with different agitation settings.....	156
Table 7.2 - Plating bath settings.	159
Table 7.3 - Microsection images of 0.20 mm diameter BVs of different ar, RP plated at 1:3 A/dm ² for 12 hours, with different agitation settings.	160
Table 7.4 - The average plated thickness for plating settings.	161
Table 8.1 - Investigations carried out throughout the thesis.	164

Glossary

2D	Two Dimensional
AC	Alternating Current
Ah	Amp.hours
<i>ar</i>	Aspect Ratio
BV	Blind Via
CW	Continuous Wave
Cu	Copper
DC	Direct Current
DS	Development Stage
HD	High Density
hr	Hour
HWU	Heriot-Watt University
IPC	Institute of Printed Circuits (<i>currently: Association Connecting Electronics Industries</i>)
MS	Megasonic
N	Near-field distance
PCB	Printed Circuit Board
PML	Perfectly Matched Layers
PED	Potential Energy Density
Ra	Arithmetic average height
RP	Reverse-pulse
Rq	Geometric average height
SAW	Surface Acoustic Wave
SBC	Scattering Boundary Condition
SEM	Scanning Electron Microscope
Sn	Tin
TDR	Time Domain Reflectometry
THV	Through-Hole Via
TSV	Through-Silicon Via
US	Ultrasonic
via	Vertical Interconnect Access
W	Tungsten

Publications and Awards

T.D.A. Jones, D. Flynn, M.P.Y. Desmulliez, D. Price, M. Beadel, N. Strusevich, M. Patel, C. Bailey, S. Costello. (2016) ‘Megasonic Assisted Electroplated Copper Topographies and Acoustic Artefacts’, *Circuit World*, **42**,(3) pp. 127 – 140

T.D.A. Jones, D. Flynn, M.P.Y. Desmulliez (2016). ‘Megasound Acoustic Surface Treatment Process in the Printed Circuit Board Industry’, in *Design, Test, Integration & Packaging of MEMS/MOEMS (DTIP)*, Budapest, *IEEE*, 30th May 2016, pp. 135 -138

T. Jones, M. P. Y. Desmulliez, D. Price, and A.Cobley, ‘Implementing new surface pre-treatment processes in the PCB industry through the application of acoustic agitation.’ *Journal of the Institute of Circuit Technology*, (2015). **8**(1): pp. 10-17.

N.Strusevich,M.P.Y. Desmulliez, E.Abraham, D.Flynn, T.Jones, M. Patel, C. Bailey (2013) ‘Electroplating for high aspect ratio vias in PCB manufacturing: enhancement capabilities of acoustic streaming’,*Adv.Manuf.Springer*, **1** pp. 211-217

Awarded the 2015 best young person’s article written for the Journal of the UK Institute of Circuit Technology.

Chapter 1 Introduction

1.1 Background



The Printed Circuit Board (PCB) industry is a key player in the manufacturing chain of electronic devices. PCBs sit at the heart of almost all electronic devices, and structurally support a plethora of components, including Integrated Circuits, transistors, resistors, capacitors and so on. A PCB is populated with a multitude of electro-mechanical components plus various active and passive devices such as transistors, capacitors, inductors and resistors, which enable the functionality and assembly of the PCB. Increasing the density of the components on the surface of a board enables greater functionality and use. A high density (HD) design is desirable for technology high end applications, which includes automotive, aerospace, space, defense, mobile phones, medical, networking, communications, and computer storage [1]. The current trend in PCB markets is low-technology, high-volume demand and is typically supplied by low-cost, large-scale facilities in Southeast Asia, such as China, India and Thailand. High-value, low-volume PCB markets are typically supplied by smaller sized facilities in western regions such as North America and Europe, but also economically developed eastern locations such as Japan, South Korea and Taiwan [2]. The UK PCB demand typically focuses on this latter market. Manufacturing developments bringing increased capability and cost savings to a factory in the UK would be highly desirable and enable increased market competitiveness.

The increased components densities fuelled by micro-circuit feature size reductions achieved within the silicon die components have led to more complex iterations and device designs. This, in turn, has influenced HD PCB design by accommodating increased component densities on the board, which require tracking in between components and off the board. [3, 4]

A HD PCB provides electrical connection for the transmission of data or power. The electrical connections predominantly consist of copper (Cu) features manufactured using print-and-etch processing and electrochemical deposition. Highlighted in Table 1.1 is a simplified flow chart displaying the typical manufacturing processes applied by a manufacturer, to construct a double sided or multi-layered PCB with an electrical connection running between the different copper layers in a board - referred to as an interconnect. The fabrication of an interconnect requires multiple processing stages. A key stage involves the deposition of Cu with increasing thicknesses onto a PCB substrate,

referred to as plating. The copper deposition processes are critical in defining interconnect formation quality and performance.

Table 1.1- A brief overview of PCB manufacturing with cross-section 2-D schematics of the manufacturing process, showing PCB laminate in beige, copper in orange and yellow and photoresist in blue.

<p>1. PCB laminate substrate material is chosen based on customer design. The laminate is cleaned and then depending on board size multi-bonded with other laminates, then drilled or drilled without bonding if the board has no internal layers.</p>	<div> <div>Double sided PCB</div>  <div>Drilled centre</div> </div> <div> <div>Multilayer PCB</div>  <div>Drilled centre</div> </div>
--	---

PCBs today have multiple layers of interconnections. Interconnection through a PCB is realised by a feature known as a **Vertical Interconnect Access** (via). A via either connects through the PCB as a **Through Hole Via** (THV) or as a **Blind Via** (BV), which can connect the top layer to inner layers or in between inner layers. A 2-D schematic of different via construction types, along with examples, are indicated in Figure 1.1 showing Cu in orange and PCB laminate in beige.

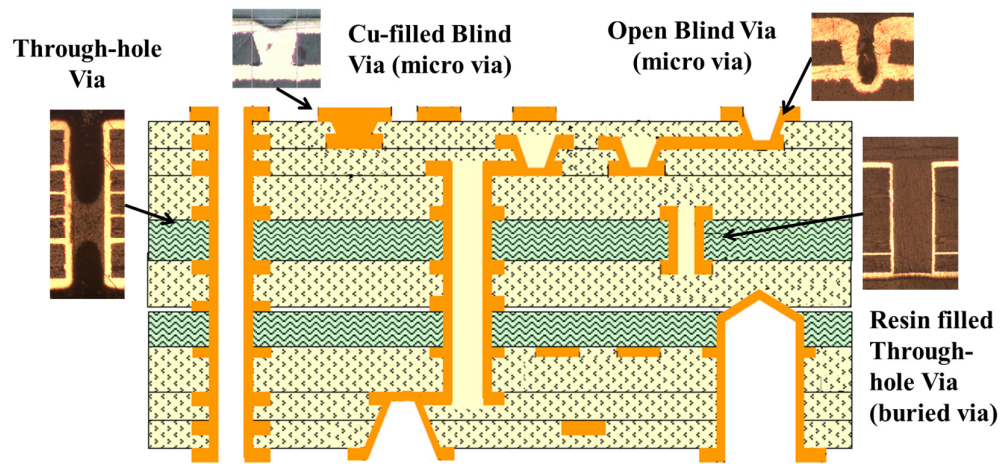


Figure 1.1 - Schematic of via interconnect PCB design.

Via interconnect manufacturing capability depends on the ability to uniformly electrodeposit a sufficient amount of Cu and to pattern surface features so that they can be fabricated to transmit signals with low bit error rates. Interconnects are metallised by electroless and electroplating processes using acidic solution chemistries. A critical process influencing interconnect quality is the electroplating of Cu, specifically the ability to circulate electrolyte solution into minuscule drilled via sizes of diameters ranging from 0.1 mm to 0.5 mm and depths from 0.4 mm to 5.0 mm.

The efficiency of an electroplating reaction depends on two factors: the concentration of Cu ions at the surface of the PCB and the electrical current available for electrodeposition.

a) Cu ion replenishment at the PCB surface influences the plating quality and deposition rate. At the solution/PCB interface a concentration gradient of Cu ions exists. Cu ions are electrodeposited from the bulk solution onto the surface - through the application of an electrical current – which reduces the Cu concentration at the surface due to the reduction of Cu ions. The most significant transport mechanism influencing the movement of Cu ions towards the surface and across the gradient is diffusion and the region from high to low concentration is referred to as the Nernst diffusion layer [2].

b) The Cu electrodeposition rate is also proportional to the electrical current, limited to a value, where additional increases to current lead to no further increases in plating rate and poor quality plating finishes.

To enable access to higher currents and thus higher plating rates with high-quality deposits, the diffusion layer thickness must be reduced by increasing the transport of Cu cations near to the PCB surface. In other words, a reduction in diffusion layer size combined with replenishment of depleted ions enables access to higher electrical currents

and quicker PCB processing time, which is desirable for PCB manufacture. This effect is possible by forcing bath convections through the use of agitation techniques of the electrolyte solution, or by altering the plating current duty cycle [5]. The first method is by enhancement of the mass transport mechanism and the second is by the introduction of a pause cycle to allow for bath convections to replenish cations. To enable the shortest processing times and the highest plating efficiencies, both techniques are typically employed [6].

1.2 Motivation for this thesis

The technological growth of high-value PCBs is currently driven by the development of boards which can propagate high frequency signals higher than 1 GHz [7] with transmission speeds over 25 Gb/s [8] and at low bit error rates (10^{-18} at 10 Gb/s [9]). Additionally, small track feature sizes are desired to allow for large board component densities. Applying these enhanced PCB properties calls for improved manufacturability capabilities of the board, specifically a) the ability to fabricate small interconnects, b) the maintenance of a low signal error and (c) high on-board device component performance, despite increasing thermal transport issues due to higher power and denser boards [10]. These issues may be addressed in PCB construction through the fabrication of THVs and BHVs of small diameters typically less than 0.2 mm and high thickness-to-width aspect ratio (ar) of the order of 8:1 for THVs and ar of 3:1 for BVs, whilst simultaneously filling the interconnect uniformly with Cu. Such interconnects would enable:

a) the increased electrical and thermal conductivity, owing to higher thermal convection through solid Cu over the standard, partially plated vias, which is extremely useful in high power applications and HD circuitry.

b) This would also permit multilayer fabrication with less thermally intensive bonding operations - due to increased BV ar beyond the current capability, 1.2:1, - increasing thereby board life time and reducing fabrication costs.

Such interconnect designs have been obtained in laboratory settings through research performed at Heriot-Watt University (HWU) [11-13]. The studies employed high frequency 1 MHz, megasound (MS) acoustic agitation to transport the electrolyte solution through via interconnects, enabling the disposition of thick deposits of copper in an electroplating process. The transport of electrolyte solution is a critical factor allowing an electrolyte solution to plate large deposits of copper down high ar interconnect features [14]. This characteristic of a electrolyte solution is referred to as its throwing power, where a high throwing power solution will produce a uniform deposition of Cu on a

surface despite a varying underlying geometry comprising of difficult-to-plate high *ar* interconnects [15].

A high micro-throwing power solution is critical in ensuring that high *ar* interconnects can be uniformly plated with 100 % Cu. The introduction of MS agitation has improved the micro-throwing power of the standard Cu electroplating solution used for PCB manufacture [16]. This was due to diffusion layer reductions and increased ion transport. This plating improvement enables interconnect formation currently not possible under existing agitation techniques or by any other process known to the author. If applied successfully within a manufacturing setting, this interconnect fabrication could bring about cost savings and technological improvements to a PCB fabricator, increasing market competitiveness within the high-value, high-technology applications and has the potential to be a disruptive technology to the industry. Fabricating a PCB with interconnects containing 100% Cu fill and high *ar* would be extremely useful and lucrative, especially in the mobile phone market which employs Cu filled THVs, of *ar* of 4:1, as these currently require high fabrication costs due to filling-chemistry and plating waveforms [17].

The technological leap realised due to MS-agitation by the Heriot-Watt team, warrants an investigation into an industry scale setup with the goal of developing a high volume manufacturing technique to fabricate PCB product with Cu filled, high *ar* via interconnects. This was carried out into a medium-size, 500 L manual plating bath at the PCB fabricators, Merlin Circuit Technology Ltd.

1.3 Objectives

The introduction of MS agitation as an electroplating technique, which is the main objective of this thesis, will be evaluated in three stages, as highlighted in Table 1.2. The sequential completion of these stages will enable the evaluation of potential to introduce the technology into manufacture. With the three stages complete, the MS technology will be gauged to see if it should be scaled up to a larger sized automated line process.

After these investigations a review will be made on the effectiveness of MS agitation applied as a PCB surface treatment.

Table 1.2 - Outline of MS-assisted electroplating process scale-up into industry.

Development stage	Purpose	Development stage outcomes
1	To become familiar with the Cu electroplating process, developing an understanding on how the introduction of MS agitation within the larger scale baths alters the electrodeposition of Cu on the surface of the PCB.	<ul style="list-style-type: none"> Determine the influence on the plating finish due to variations in plating bath parameters from standard values and settings. Define the influence on plating quality and topography due to acoustic artefacts induced by microbubble cavitation and standing wave formation.
2	Test MS plating capability down via interconnects, to evaluate the technology against existing agitation processes and determine the plating uniformity through comparisons of Cu thickness deposited inside the via and on the surface, on both THVs and BVs.	<ul style="list-style-type: none"> Resolve plating settings which provide the highest efficiency down THVs and BVs with MS agitation. Compare process plating quality to existing agitation methods.
3	Test the ability to 100% fill THVs and BVs using setting applied at Heriot-Watt University.	<ul style="list-style-type: none"> Evaluate how uniformity varies for the increase in Cu thickness deposited and compare with other available agitation process. Determine conditions leading to the largest Cu thickness plated down vias.

1.4 Structure of thesis

The thesis is organised into eight chapters displayed in Figure 1.2.

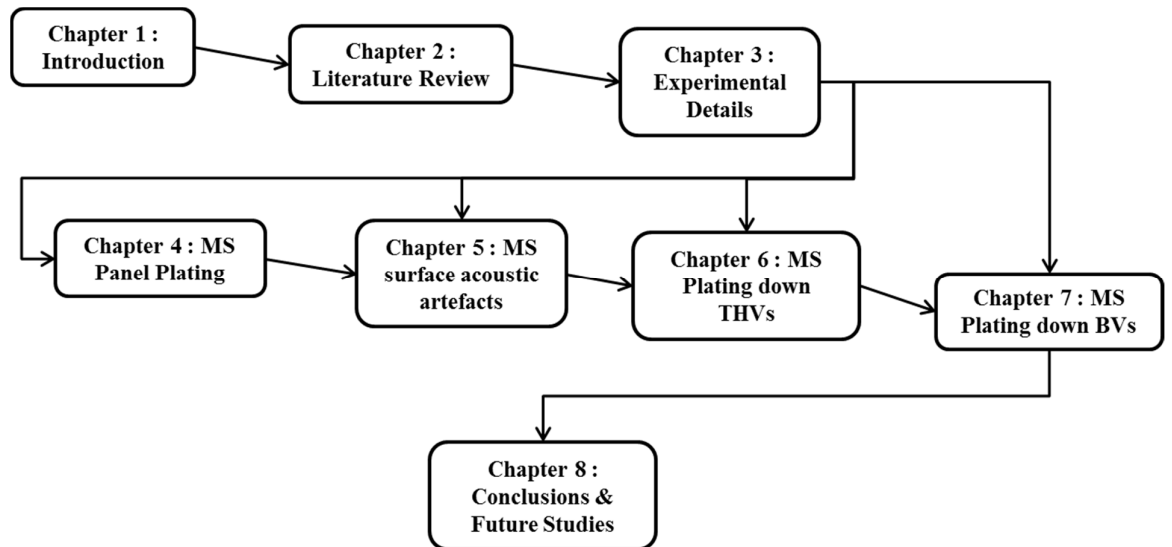


Figure 1.2 - Structure of thesis

Chapter 2 is a discussion on the background literature concerning PCB manufacturing techniques and electrochemical processes discussed within the thesis. Included is a review of the MS plating literature, highlighting the positive benefits to PCB manufacture and a discussion concerning the different effects induced due to MS agitation, observed on the macro-scale and micro-scale at the PCB surface. Finally, a

review is made of the existing THV plating techniques employed in the semiconducting industries, specifically relating to 100 % Cu fill technologies.

Chapter 3 discusses how the individual plating experiments are setup with regards to the bath chemistry and the transducer device used. It provides the experimental setup for the analytical techniques used, such as the Electron microscope. It also covers a brief investigation made into the macro-scale fluid motions observed on placement of the transducer, performed to evaluate the most efficient positioning of the device for maximum acoustic streaming coverage during plating tails.

Chapter 4 covers the first set of plating investigations looking at the MS plating influence on the surface of blank PCBs. Chapter 5 is a review of all the surface acoustic artefacts witnessed on the plated surface and a review provided into their formation. Chapter 4 and Chapter 5 address development stage 1 outlined in Table 1.1 and determine the conditions for MS plating setup to be applied for via plating.

Chapter 6 and Chapter 7 includes the sets of investigations looking into THV and BV MS plating respectively. From this development stage 2 and 3 shall be addressed as outlined in Table 1.1, resolving the conditions which enable the highest plating efficiencies using MS, for partially filled and large plated thicknesses.

Chapter 8 discusses conclusions from the experimental results and evaluates the success of the scale-up into industry and concludes with an outline on how MS-assisted processing should further continue and a description of different experiments to be performed.

Chapter 2 Literature Review

Chapter 2 is split up as follows. Section 2.1 discusses the setup of an electrochemical plating bath, outlining how composition and current density impact on Cu plating rates and crystallinity. Section 2.2 provides a review of Megasonic (MS) agitation applied within PCB manufacture, discussing its impact on the fundamental electrochemical principles behind Cu plating and the acoustic phenomena generated within electroplating baths. Section 2.3 discusses the PCB's structural composition. Section 2.4 discusses how via interconnects are manufactured and the cost savings recognised due to MS agitation. Lastly, section 2.5 discusses quality evaluation techniques applied by a PCB manufacturer.

2.1 Electrochemical Processes

Under a manufacturing setting the metallisation of Cu onto a PCB surface requires the plating operator to maintain a sophisticated control over the bath processes, so as to manipulate the electrochemical processes to behave as desired. To do this a plating line will typically be managed by a team of chemical lab technicians, who maintain chemistry levels at specification and keep the line clean of chemical waste [18]. With sufficient maintenance the plating operator is free to introduce electrical currents onto the PCB and control the Cu thickness deposited over the board and down via interconnects by $\pm 10 \mu\text{m}$. When introducing MS agitation into a plating line the same level of control is required for the electrodeposition processes.

A model does not currently exist to sufficiently describe how the ion transfer mechanisms in a Cu plating bath are manipulated by the high frequency acoustic waves and so, to describe its influence on Cu electroplating, the following section provides an outline of the electroplating mechanisms, as well as a brief description of the bath operational parameters influencing the deposition of Cu onto a PCB surface.

2.1.1 The Electrolysis reaction

Electroplating is an electrically induced chemical reaction based upon the process of electrolysis. It is comprised of electrodes submersed in an electrically conductive solution known as an electrolyte. An electrolyte consists of a chemical salt dissolved in a suitable ionising solvent to form an ion in solution. The electrolyte conductance is provided by the physical transport of charged species such, that, positively charged

species are attracted to the negatively charged cathode and negatively charged species are attracted to the positively charged anode.

Electrolysis is characterised by Faraday's laws of electrolysis, which is summarised as

$$m = \left(\frac{Q}{F}\right)\left(\frac{M}{z}\right) \quad (2.1)$$

Where m is the mass deposited; Q is the total electric charge in the electrolyte; F is the Faraday constant; M is the molar mass; and z is the valence number of the electrolyte, showing the number of electrons transferred per ion. Faradays laws of electrolysis highlight that, during the passage of current through a solution of a metal salt, the weight of the metal deposited on a cathode is proportional to both the charge passed through the solution and the equivalent weight of the metal. In other words, 1 mole of electrons will reduce 1 mole of Na^+ , $\frac{1}{2}$ mole of Ca^{2+} or $\frac{1}{3}$ mole of Al^{3+} . [19]

In electroplating, a metallic deposit is formed upon a cathode in response to an electric field applied across the salt solution. The chemical reaction for deposition occurs at the surface of the cathode, where electrons are transferred between the electrode/electrolyte. Copper sulphate is used in Cu plating and when electrolysed, metallic Cu is plated. The Cu is plated in accordance with the charge on the Cu^{2+} metal cupric ions and the direction of the electric field set up, as depicted in Figure 2.1. Displayed is the schematic for a Cu based electrolyte cell with an electric field set up between the cathode and anode, across the electrolyte solution. The direction of the current flow, I , in the solution, determines the designations of anode and cathode in the cell design, which is dependent on the bath chemistry and direction of the electric field between the electrodes.

When an electrolyte cell is formed the anode is connected to the positive pole of the electrical source, electrons are removed from the soluble anode oxidising its surface, which then dissolves into the solution as ions, in the process of electrodisolution that continuously supplies the metal ions. On the cathode the PCB is connected to the negative pole of the electrical source and electrons are added generating a negative charge. As a result the Cu^{2+} is attracted to the cathode and Cu is deposited.[20, 21]

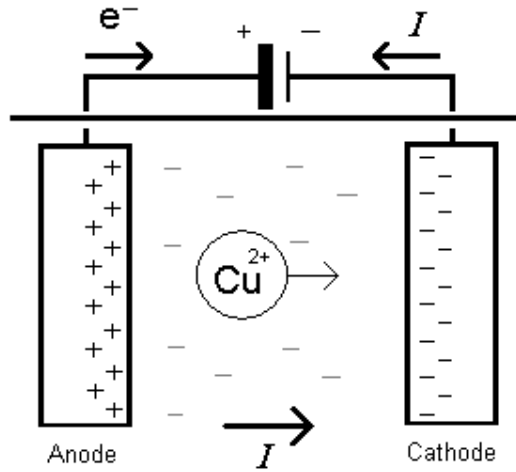


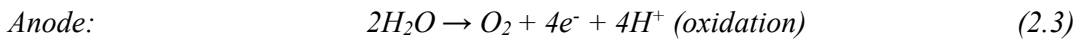
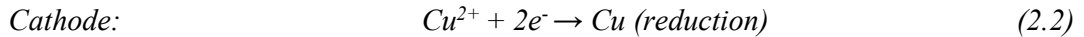
Figure 2.1 - Schematic of the plating cell arrangements with arrows highlighting the movements of electrons, electrical current and cupric ions. Indicated on the electrodes is the built-up Coulomb charge.

2.1.2 Electrodes in Copper Plating Baths

Within a Cu plating bath the deposition onto the cathode is by a reduction reaction and electrolysis is carried out using either soluble or insoluble electrodes. The two types of anode each require their own solution chemistry, maintenance procedure and bath setup to operate. The anodes are applied separately in the electroplating of via interconnects, which depends on the amount of Cu to be plated.

An insoluble anode, as the name suggests, does not dissolve into solution during electrolysis. It provides a source for electrical current but not Cu ions, which are instead supplied by additions to the bath.

The simplified reactions occurring at the electrodes using the insoluble anodes are,



On the insoluble anode the main reaction is the oxidation of water to evolve oxygen. The formation of oxygen gas contributes to the overconsumption of the organic anodes at the anode. On the cathode, cupric ions are reduced to Cu depositing onto the PCB surface [22]. Insoluble anode are used in PCB volume manufacture to 100 % fill blind vias (BV) with Cu. 100% filled BV enable connection of the surface of the PCB to the layer beneath and has a wide use in High Density circuit manufacture for smart phones [23]. In BV filling a complex interplay of bath additives are used, as explained later in

sections 2.1.3 and 2.4.1. Insoluble anodes do not change in geometry as the plating reaction occurs, unlike soluble anodes and, so, the current output is consistent across the PCB which enables improved control over the metal distribution on a batch of plated PCBs. For this reason insoluble anodes are used in BV filling [24].

The distribution of electrical current density - which controls the plating rate on a PCB surface - is influenced by the area the active anode and the cathode. The area of the anode is typically chosen to be of the same area as the cathode-PCB so as to output a more uniform current distribution. PCB size and anode size vary and so multiple anodes are applied in a plating cell to match the surface area of the PCBs. In a typical plating bath setup the number of anodes to cathode is 2:1 [25]. For the MS-plating investigations the number of anodes used in the plating cell will be chosen based around the size of the PCBs plated and the positioning of the acoustic transducer within the plating bath. The exact settings are discussed in more detail in sections 3.2.1 and 3.4 and a more in-depth discussion on the behaviour of electrical current from anodes is provided in section 2.1.5.

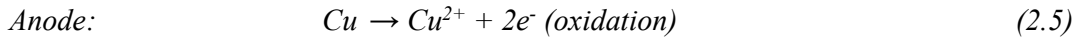
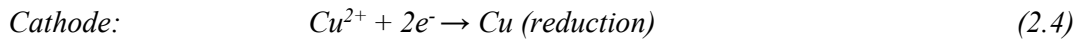
Insoluble anodes do not require the use of bath dummyming so as to build up an anodic passivation layer, see section 3.2.2. This saves time and cost of processing line start up - which can take up to six hours and use several PCB panels for dummy plating. The use of insoluble anodes also brings reduced anode maintenance as soluble anodes require regular cleaning and replenishment of the Cu in anode bags.

Insoluble anodes are typically made from expensive rare earth metals and as such their cost is higher than soluble anodes. An insoluble anode used for Cu plating comprises of a titanium base coated with 2 to 5 μm of platinum [26]. The platinum is applied so as to protect the titanium base from degradation under pulse reverse plating (RP), which occurs in the presence of chloride-containing copper sulphate electrolytes [27]. RP and chloride-containing electrolytes are used in the formation of 100 % filled BVs, see sections 2.1.6 and 2.4.1 and so the protective layer is required for insoluble anodes to be used in PCB manufacture. Another cost to insoluble anodes is the organic additive consumption is greater due to additive consumption at the anodes, where values up to eighty times greater than soluble anodes have been reported [22]. The net results is with insoluble anodes the additive maintenance is higher for a consistent output and the price of the baskets are higher.

In the MS plating investigations filling chemistry was not applied and so insoluble anodes were not used. Further experiments requiring the use of filling chemistry would have required purchasing insoluble anodes which were beyond the budget for the research. Instead soluble anodes were used.

Soluble anodes are applied in PCB volume manufacture in electroplating baths for the partial plating of Cu down THVs and BVs and on the surface of the PCB. Soluble anodes are typically made from pure copper or copper alloyed with de-oxidised phosphorous. A de-oxidised phosphorous anode is used for highly acidic baths containing organic additives. The phosphorous acts to prevent unwanted polarisation on the anode surface preventing its dissolution when not in use. Polarisation is characterised by the build-up of charge on an electrode, changing its potential. Unwanted anodic polarisation is characterised by the formation of hydrogen bubbles on an anode surface formed during electrolysis.

The simplified reaction using a soluble anode is,



On the cathode, cupric ions are reduced to Cu depositing onto the surface. The reactivity of an ion influences its ability to discharge such that, the higher the reactivity of the ion, the more likely it is to discharge. Cu^{2+} has a higher chemical reactivity than H^+ - which is also present in the plating bath - and so, the Cu^{2+} preferentially discharges rather than H^+ . On the anode the main reaction is the dissolution of Cu to Cu^{2+} . [22, 28]

The use of soluble anodes does not suffer from the high consumption of bath additives incurred by the use of insoluble anodes [22]. The copper content in baths using soluble anodes is provided by additions to the solution and by replenishment of soluble Cu balls into the anode baskets. Having Cu provided by the anodes maintains the Cu ion concentration in the bath, although dissolution of the copper into smaller balls may cause contamination within the electroplating bath, leading to unwanted particulate formation on the plated PCB surface. [29]

In the thesis soluble anodes were used with a plating chemistry formulated to partially plate via interconnects. This solution was chosen as investigations carried out previous to the thesis reported benefits to Cu plating whilst using the same solution formulations and soluble anodes [12]. Additionally, a plating line had been set up at Merlin for use with soluble anodes and, as such, to keep within project budget, investigations were performed with this.

To plate with the highest plating rate for an electrical current supplied between an anode and cathode, requires the two electrodes to display high efficiencies. The efficiency of an electroplating reaction is determined by the amount of Cu dissolved into solution from the anode and deposited onto the PCB at the cathode. The efficiency is given in

terms of a percentage of the current passing through the electrolytic cell or electrode, which accomplishes the desired chemical reaction, given as,

$$\text{Current efficiency} = 100 \times \frac{W_{Act}}{W_{Theo}} \quad (2.6)$$

where W_{Act} is the weight of the metal deposited or dissolved and W_{Theo} is the corresponding weight expected from faradays laws if there is no side reaction. The two efficiencies for the plating electrodes are referred to as the anodic and cathodic efficiency. [21]

The anodic efficiency is influenced by the passivation layer formed on the anode surface which is maintained to optimum levels by dummyming of the plating line prior to plating, as discussed in section 3.2.2 in Chapter 3. Also operation of the anode to within its specified limits outlined in section 3.2.1 in Chapter 3, prevents it from forming unwanted by product such as particulate formation within solution [6].

The cathodic efficiency is influenced by the bath agitation applied to the PCB surface, which prevents limited current plating, see section 2.1.8, and enables electrolyte replenishment, see section 2.2.2. Also maintaining the bath to within its defined chemical concentrations and bath parameters outlined in section 3.1 in Chapter 3, ensures a high cathodic plating efficiency. The cathodic efficiency for the plating setup used in the thesis was defined later on in section 3.1.1 in Chapter 3.

2.1.3 Copper Sulphate Bath Composition

Copper sulphate baths used in PCB manufacture are composed of copper sulphate solution, sulphuric acid and hydrochloric acid. Copper sulphate is the most common electrolyte, used for its ease of operation and low cost. For the MS plating investigations, plating chemistry was set up which employed the use of soluble anodes. For a soluble anode setup, the bath chemistry applied was CU110 as supplied by Schoetter Ltd. Details of this solution's makeup are discussed later in section 3.1 in Chapter 3.

Additives are used in plating baths to enable uniform plating on the board and to refine deposit characteristics. Without additives the yield for high quality deposits and plating capabilities is reduced. Additives are typically organic molecules and are available as brighteners, suppressors and levellers. The specific formulation for additives is proprietary information dependent on the chemical supplier and will vary dependent on the desired characteristics of the plating outcome [30], regardless a description of the additives typical composition will be discussed.

A brightener consists of acyclic organic compounds which is represented by the general structural formula shown in Figure 2.2. Here **R** is a lower hydrocarbon radical, which is preferably a lower aliphatic radical which may carry substituent radicals other than sulphonic groups and/or may be interrupted by heteroatoms such as sulphur, oxygen and nitrogen, **X**, **Y** and **Z** are heteroatoms such as oxygen, sulphur, and nitrogen or imino groups, at least one of them being a sulfur atom, **X'**, **Y'** and **Z'** are also heteroatoms of the type represented by **X**, **Y** and **Z** or imino groups, at least one of them being a sulfur atom, and **Q** and **Q'** are hydrogen or lower aliphatic radicals free from sulfonic groups.[31]

Brighteners contribute towards the desired plating outcome of a bright, firmly adhering, ductile metal electrodeposit from an acidic electroplating bath. The Cu solution used for deposition can vary. Dependent on the composition and conditions used in that solution different brighteners are used. The different brighteners cannot be applied universally to the different Cu solutions as each requires their own specific brightener formulation. [32]

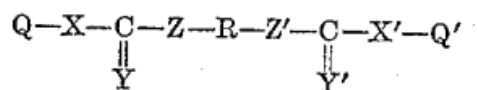


Figure 2.2 - General structure for acyclic organic compound brightener additive.[31, 32]

The suppressor also known as carriers, inhibitors or wetters, absorb at the cathode surface uniformly and suppresses the plating rate on the surface of the PCB which in turn accelerates the plating rates in recessed regions where the suppressor has failed to absorb. This is useful for ensuring a high throw power of a plating solution, as discussed in section 2.1.7 and is used in bottom-up plating of blind vias (BV), as discussed in section 2.4.1. A suppressor typically comprises of one or more high molecular weight polymers which are preferably polyether compounds. The polymers are believed to induce a catalytic effect with the specific brightener used in the Cu deposition, assisting in the formation of a bright smooth deposit formed at elevated temperatures.[33]

Levellers are preferentially heterocyclic nitrogen compounds selected from water-insoluble, metal ion-containing dyes. An example is A,B,C,D-tetrakis(pyridiniomethyl) Cu (II) phthalocyanine chloride, which is a Cu phthalocyanine, that is water-insoluble compound which after chloromethylation is manufactured into a water-soluble compound

and is reacted with pyridine. The compound has the formulation $C_{50}H_{70}CuN_4$, and has the compound structure indicated in Figure 2.3. Levellers are small molecules which preferentially attract to higher current density areas on the plated surface and selectively inhibit plating. The leveller acts in a similar fashion to the suppressor and is used in bottom-up plating of blind vias (BV) [33]

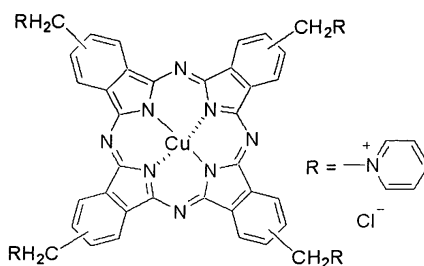


Figure 2.3 - Compound structure for the leveller additive $C_{50}H_{70}CuN_4$. [33]

In copper sulphate baths the additives are applied in varying combinations, which are influenced by whether the vias are being filled or partially plated with Cu. In the CU110 chemistry provided by Schloetter Ltd a suppressor and a brightener are used, which are the chemicals Cu 110 and Cu 114, respectively.

The suppressor aids the removal of air bubbles off the board and introduces solution on to fine features. The brightener reduces the deposit grain size and prevents ‘burning’ occurring in high current density areas, as discussed in more detail in section 2.1.8. Grain refinement is characterised by a shiny deposit and is desirable for a high quality plated finish, as it enables the successful further processing of the board in the dry-film and metal finish process lines.[34, 35]

2.1.4 Diffusion limited transfer mechanism

Different transfer mechanisms influence the deposition of ions onto the cathode. The mechanisms individually dominate and interplay over the different regions in the bath. For the copper sulphate solution the mass transfer of the Cu^{2+} ions is influenced by convective forces as well as diffusion and migration phenomena. In the plating of vias diffusion is the most dominant transfer mechanism down via interconnects and so it shall be discussed next.[36]

The ions arriving at the surface of the electrode react extremely fast relative to other processes in the bath. The flux of cations over the diffusion layer onto the cathode is described by a diffusion current density, i_c .

$$i_c = z.F.D.\frac{(c_\infty - c_c)}{\delta_N} \quad (2.7)$$

where z is the number of electrons per ion transferred; F the Faraday constant; D the diffusion constant and; c_∞ and c_c the bulk and electrode ionic concentrations, respectively. Under typical electroplating conditions c_c is less than c_∞ . When the current density is increased the cathode concentration decreases up to a point where the ion concentration at the electrode is zero. In this situation c_c is equal to zero and the current density is referred to as the diffusion-limited current density. Deposits laid down at the diffusion-limited current and beyond are powdery in nature and are of no practical use. More is discussed about the outcome of this plating condition in section 2.1.9.[36]

2.1.5 Plating Current Density

The dominant parameter defining plating rate is the magnitude of the electrical current density on the electrode. The current density for the material being plated onto the cathode is given as;

$$j = I/A \quad (2.8)$$

where I is the current intensity measured in Amps and A is the total surface area of the cathode being plated, measured in dm^2 . The area plated on the cathode is over a finite area, which is locally defined by a dry-film resist covering areas not to be plated. Electroplating the exposed area is known as pattern plating, as not all of the board surface area is plated. The exposed design will vary in size dependent on customer requirements. The current density on the surface will in turn vary dependent on the area exposed and, as such, create localised regions of high and low current density which result in non-uniform plating rates across the board.

This electrical behaviour may alternatively be described in terms of the electrical field lines. Electrical field lines are a purely geometrical construction used to visualise the electrical field at a specific location. They have the following characteristics: at a tangent to the field lines at any point gives the direction of the electric field at that point; when travelling in free space they are continuous curves which emerge from a positive charge and terminate at a negative charge; they do not intersect; and the density of the field lines represent the strength of electric field in that location and is referred to as its flux. [37]

When an electroplating reaction is induced from a rectifier electric field lines are set up between the anode-cathode. The orientation of the field lines is shown in Figure

2.4. The passage of Cu ions is indicated by the direction of the arrows from the soluble anode on the right to the cathode PCB on the left. Figure 2.4A shows an angular cathode where the current density is uniform across the cathode, apart from upon an extruding forwards-facing isolated region. This region has a small surface area and attracts a greater field line flux. As such, this region is electrically isolated and receives a greater current density and a faster copper plating rate. Figure 2.4B shows the field line behaviour for standard electroplating conditions where the anode is of a size similar to the surface area of the cathode. The current is uniform across the cathode apart from at the small-area isolated edges where the field line flux is greater and thus plating rate is greater. This setup is typical to PCB manufacture. Figure 2.4C shows the ideal field line behaviour between an anode and cathode. Here the field lines are evenly distributed across the cathode ensuring a uniform current density and a uniform plating rate. This distribution can be better approximated by introducing current thieves. A current thief is a conductive surface typically a blank PCB placed alongside a PCB circuit whilst both are electroplated. This causes field lines from electrically isolated regions to attract to the conductive ‘thief’ lowering the plating rate in that region and increasing the overall the uniformity of the Cu plating rate across the PCB circuit surface. The introduction of thieves are readily employed in standard PCB manufacture.

Current thieving and field-line behaviour are important concepts in visualising the current distribution across a PCB’s surface and the resultant plated copper thickness. In section 3.4.1 the impact on plating in response to changes to the transducer position will be considered in terms of both the electrical field lines and the resultant current density.

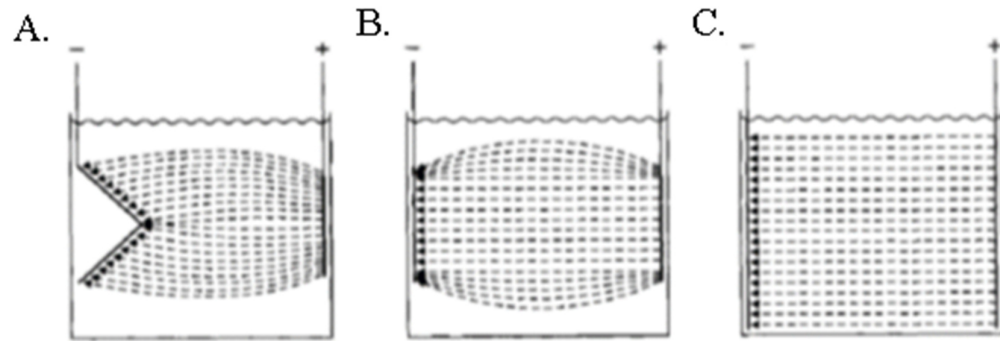


Figure 2.4– A) and B) cross section schematic of the field line behaviours produced between an anode (right-hand-side) and a cathode (left-hand-side), indicated by dashed lines. C) an ideal uniform spread. [37]

The type of plating a PCB will receive is characterised by a manufacturer in terms of the patterning of Cu on the surface of the PCB. The amount of Cu patterning on the surface of the PCB is dependent on where the PCB is in the manufacturing cycle and the customer requirements. If the PCB is to be drilled for via interconnects the board will require the holes to be made conductive. This is possible by metallising the recently drilled holes with first a conductive seed layer of electroless copper, discussed in more detail in section 2.1.10, followed by a 5 μm ‘flash’ electroplating of Cu, as outlined in Table 1.1 in Chapter 1. For flash electroplating the PCB will contain no features on the surface and will be a blank PCB. This type of board is referred to as panel plating, as the entire surface of the PCB is plated with Cu. An issue with this plating process is the amount of Cu consumed is high because of the total area required to plate, which in turn requires a large current supplied from the electrical rectifiers to output a current density to within manufacturing limits, see section 3.2.1 in Chapter 3. The other type of plating performed at PCB fabricators is pattern plating. Here the PCB is further along in the manufacturing cycle and surface of the PCB is covered by a dry-film resist in particular regions leaving areas exposed for electroplating, which include track features and via interconnects which have received flash plating. Such as setup is used to fully metallise via interconnects to a copper thickness as desired by the PCB customer. This plating configuration requires significantly less current from the rectifiers although suffers from current density control on the surface of the board due to patterning of the conductive features on the surface.[38]

When processing panels for MS plating panel plating shall be employed. This was chosen because a greater control is possible over the electrical current distribution as the

features on the surface of the board are not electrically isolated and attract overly large electrical field line flux from the anode. Dependent on the success of MS plating under this setup further investigations will be required applying MS pattern plating.

The electrical current is controlled by the plating operator altering the plating rate on the PCB of defined size. If the operator wishes to increase the plating rate then she/he will increase the current supplied by the electrical rectifier. PCB conductive areas differ dependent on the board design, where larger exposed areas receive a smaller current density, so these areas require an increased current to maintain a consistent, high plating rate.

When setting up a bath the anode size is chosen to be larger than the cathode area, to provide the most uniform electric field distribution set-up between the anode and cathode [39]. During the MS plating trials the PCB sizes will be designed taking into account changes to current density on the board and the plating current altered accordingly, to maintain consistent plating rates during the plating cycle.

2.1.6 Periodic Reverse-Pulse Plating

The ionic motion in an electrolyte is influenced by the electric field set up across it. Changing the frequency, magnitude, and directions of the electric field modulates its waveform. Changing the waveform enables unique plating results which allows for enhancement to the amount of Cu deposited down small interconnects.

The plating current discussed in section 2.1.5 was a DC waveform where the current was supplied continuously at a specific frequency. Another type of plating is pulse plating. Here electrodeposition occurs from an electrical current which has introduced periodic pauses – typically 10 ms - in its output. During a pause the electrical current drops to zero and the PCB is temporarily stopped from plating. Highlighted in Figure 2.5 pulse-current waveform where the series of pulses are of equal amplitude, periodicity and direction, and are separated by zero current. Indicated with I_A is a standard DC current. The DC ‘on’ and ‘off’ is referred to as the duty cycle and is chosen dependent on the particular plating application. A square pulse is the ideal waveform as it displays the largest duty cycle range. [40]

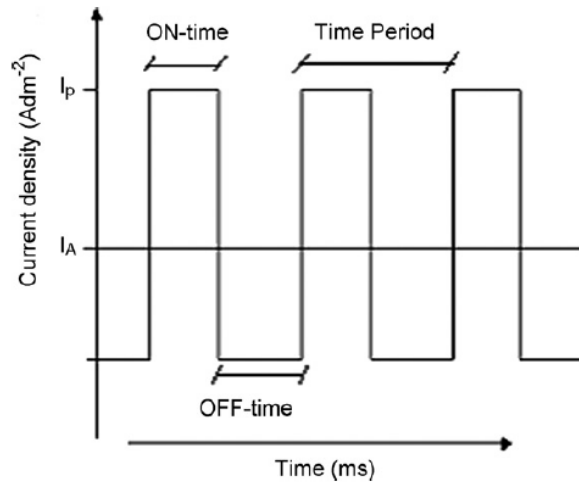


Figure 2.5 - A plot of current density against time for a typical square, pulse current and a DC current. [41]

During electrodeposition a charge layer builds up around the cathode which prevents cations from reaching the electrode surface. Regulating the pulses enables the built-up charge layer to dissipate allowing access for the cations and grain nucleation. Regions of large current density deplete ion concentrations quicker than lower current regions. During the ‘off’ cycle ions may mitigate to the depleted regions increasing the overall uniformity of the electrolyte concentration and in turn the deposition. Despite the dissipation of charge from regulation of the pulses, some charge manages to build up during the off cycle and so additives are required to ensure a uniform, high quality plating and the filling of vias [41, 42].

To improve plating further reverse-pulse (RP) plating is employed. RP introduces a change in direction between the potential maxima of the pulsed field. The brief change in current direction switches the anode and cathode around causing Cu to be stripped off the PCB. The ideal waveform is depicted in Figure 2.6 where T_c is the plating duration; T_{AA} is the stripping duration; I_c is the plating current density; and I_{AA} is the stripping current density. For this waveform the cathode plating current is also referred to as the cathodic current and the stripping current is known as the anodic current.

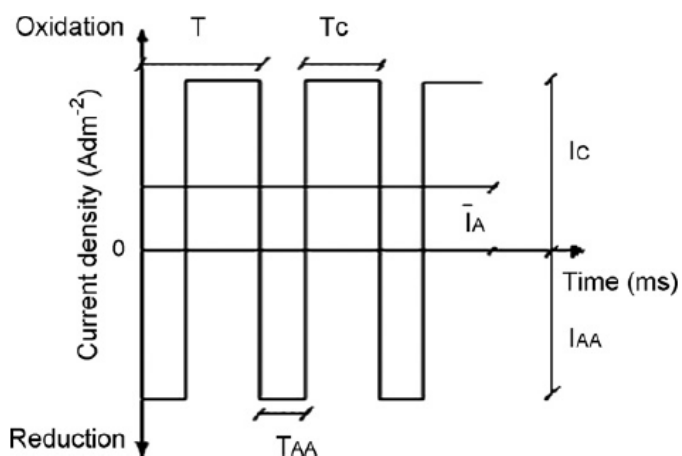


Figure 2.6 - A plot of current density against time for a typical square wave, reverse-pulse current. Indicated are the respective redox potentials, time durations of the two current orientations and their maximum magnitudes. [41]

The pinching off of via entrances and exits, and dog-bone shape plating on rectangular surfaces are unwanted common effects in electroplating [23]. With the application of RP, unwanted plating on the cathode is stripped off leading to more uniform plating during the next forward cycle. As the plating duration is longer than the stripping duration the overall net effect is plating onto the cathode. Simulations have shown that the frequency of the alternating pulse and the magnitudes of the cathodic and anodic currents influence deposition rates. For high frequency pulses (100 kHz), the plating time is enhanced and the throwing power of the two currents is increased. The throwing power is a qualitative term describing the ability to uniformly plate upon a substrate surface, regardless of the irregularity of the surface [43].

As mentioned, in pulsed plating the pause cycle between pulses enables fresh ions to diffuse into depleted regions. If the RP is short it becomes more efficient at redistributing fresh ions than the pause cycle in a pulsed current. The RP influences the soluble anode such that,

1. Copper dissolves off the cathode as described by equation 2.5 in section 2.1.2 .
2. Then the Cu crystals are transported into the bulk solution, where they may either be re-deposited in the next forwards cycle acting as a seeding layer, or dissolved into the solution [44].

RP plating enables a more uniform deposition. Under this waveform the grain structure shape can be maintained or monitored during plating [43, 45].

A final addition to improve plating is to introduce pulse plating with RP plating to form a periodic-RP current. This waveform can have its amplitude, frequency and duration modified between individual pulses. Displayed in Figure 2.7 is an ideal plating waveform where i_1 indicates the cathode plating current density; i_2 the cathode stripping, anodic current density; t_1 the plating time; t_2 the stripping time; and, t_a and t_b the pause times between pulses.

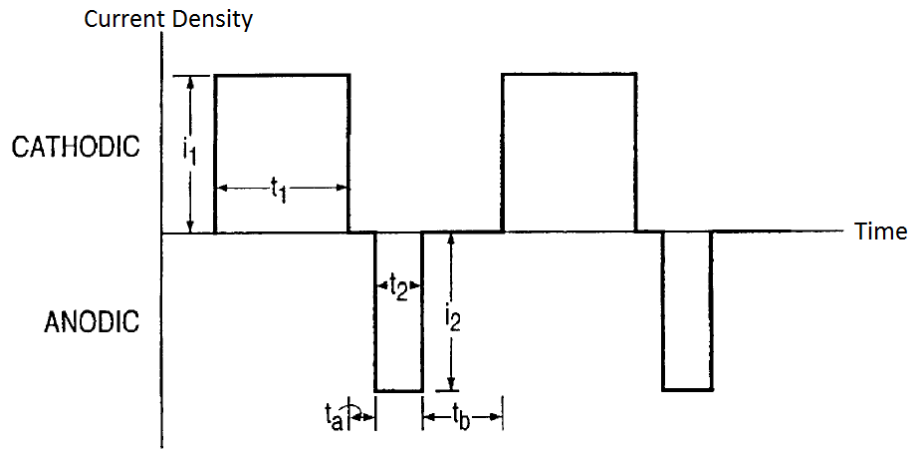


Figure 2.7 - A plot of current density against time for a typical square, periodic pulse-reverse current. Indicated are the currents and time durations for the two current orientations and the intermittent time between each pulse.[46]

To control the plating onto a cathode the parameters of pulse duration and magnitude, and the off-current durations for the cathodic and anodic pulses are manipulated. A modulated field is chosen so that the deposition is the fastest and most uniform. The ideal waveform is unique for every plating setup, as the setup is defined by via diameters, aspect ratios, plating materials, seed conductive layer and dielectric. Due to complexity of board design and volumes of batches, compromises have to be met when choosing the settings of a waveform.

The pulse in Figure 2.7 has a cathodic pulse duration longer than the anodic pulse and provides the same benefits as a RP waveform. The cathodic pulse is typically between the range of $417\mu\text{s}$ - 12.4 ms and the anodic pulse is typically less than 50 % the duration of the cathodic pulse, with best results for enhancement between 15% and 5%. As the anodic pulse duration is less than the cathodic one, the amplitude of the anodic pulse may be set to higher values to compensate for the reduced stripping time. Changing the amplitude of the pulse increases the throwing power during plating. For values too high the current density reaches a limiting value, explained in greater detail in section 2.1.9.

The frequency of the pulse train ranges from 50 Hz – 5000 Hz, preferably from 80 Hz – 1200 Hz. A pause is introduced between the pulses, which, like pulse plating, enables diffusion of ions into depleted regions on the plating surface.

With the plating rectifiers at Merlin a RP plating waveform will be used. The device can alter the current magnitude and can alter the duration of the forwards and reverse pulses, although the rectifier cannot introduce a pause between the forwards and reverse current. Larger plating lines not used in the investigation at Merlin can introduce the pause cycle and could be applied when future scaling of the technology.

2.1.7 Micro-throwing power of electroplating bath

As discussed in Section 2.1.5 the surface of a PCB will receive a variation in electrical current distribution depended on the area and geometry of Cu on the PCB surface. The ability for an electroplating solution to uniformly deposit Cu down via interconnects despite the variations in current distribution and the underlying microscale features, such as a via aspect ratio, is referred to as its micro-throwing power [15, 47]. Throwing power is influenced by a range of parameters which include metal distribution on a PCB surface; electrical conductivity; electrode polarisation; current efficiency; and geometry of via interconnect. The throwing power of a solution can be controlled through alterations to the composition of the electrolyte solution, specifically its pH, operating temperature, metal concentration and additive composition – as discussed in more detail in section 2.1.3. The micro-throwing power can be used as a quality metric to evaluate how well a plating solution can uniformly fill a via interconnect.

Highlighted in Figure 2.8 is a schematic of a plated blind via, microvia, see section 1.1 in Chapter 1, where different thicknesses are indicated. From this diagram the ratio of the average copper thickness inside the via (C, D & E) to the average surface deposit (A and B) can be evaluated as,

$$P = \frac{(C+D+E)/3}{(A+B)/2} \times 100 \quad (2.9)$$

This gives a good evaluation of the micro-throwing power and a similar equation shall be used to evaluate the MS-assisted plating quality in the thesis, see section 3.3.4 in Chapter 3.

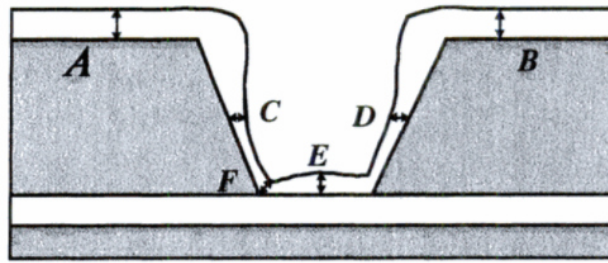


Figure 2.8 – Cross-section schematic of plated blind via – microvia - with different Cu thicknesses highlighted on the surface of the PCB. A & B, the side wall of the via, C & D, the base of the via, E, and the region of thinnest deposit, F. [15, 47]

2.1.8 Copper electro-crystallinity

The Cu electrodeposition can be regarded as a crystalline growth on a board surface. This growth may be defined by the grain size and structure of the deposit formed. The Cu deposit is initially formed at nucleation sites on a PCB surface. This mechanism is regarded as an agglomeration of adatoms. Adatoms are adsorbed atoms that lie on a crystal surface. When the crystallisation reaches a critical size, further growth occurs by additional adatoms. A more complete description of the mechanism involves discussions of the electric double layer at the board surface and on the Cu ions, which is beyond the scope of this report.

The type of electrodeposit grown can be categorised into three structural descriptions. The first is a ‘fine grain deposit’ whose properties include high density, uniformity, and random crystal orientations, which altogether highlight the correct operation of the bath parameters. The second is a ‘columnar structure’ forming deposits containing larger grains, which are of an orientation perpendicular to the PCB surface, following grain boundaries. The third is a dendritic, fibrous deposit which is described as an intermediate between the first two structures. Fine grain and columnar deposits are outlined in Figure 2.9 and show the different bath plating conditions controlling their formation.

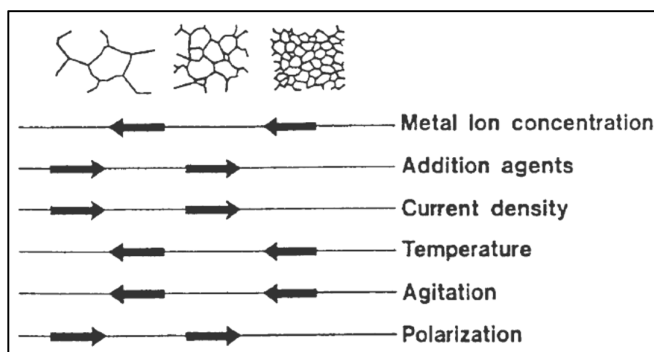


Figure 2.9 - The variation in grain structure of electrodeposited Cu in response to variations in bath parameters. [48]

Current density is an important control over the Cu plating rate, as discussed in section 2.1.5. It additionally alters the crystallinity of the deposit. Plating Cu at a current density range between 0.1 - 0.9 A/dm² will result in a slow plating rate. This current density range is below standard current densities employed in PCB manufacture. Within this range, the nucleation rate on a PCB surface is low and the growth of individual grains is favoured, leading to a columnar appearance. As a result, the large-crystal growth induces a dull Cu finish where less light is reflected off the board, because of a smaller number and size of randomly oriented crystal facets. This finish is described as a matt finish.

For current densities larger than 1 A/dm² the copper plating rate is faster. The nucleation rate is now sufficient such that crystal growth occurs more readily and smaller crystal sizes are favoured. As a result, when plating at this current density output the grain structure is described as fine-grain. Grain refinement occurs for high current densities and will form a bright, shiny deposit. The shiny finish observed is attributed to the large numbers of randomly oriented crystal facets and is typically an indicator of a hard, durable finish.

Shown in Figure 2.10 A & B, are scanning electron microscope (SEM) images of electroplated tin formed under the conditions of low and high current density, respectively. As indicated, larger crystal deposits are formed at lower current density and a fine-grain deposit formed at higher current density.[49]

In the following body of work the variation of Cu deposition in response to current density shall be discussed in Chapter 4 and its influence on deposit by MS-agitation considered.

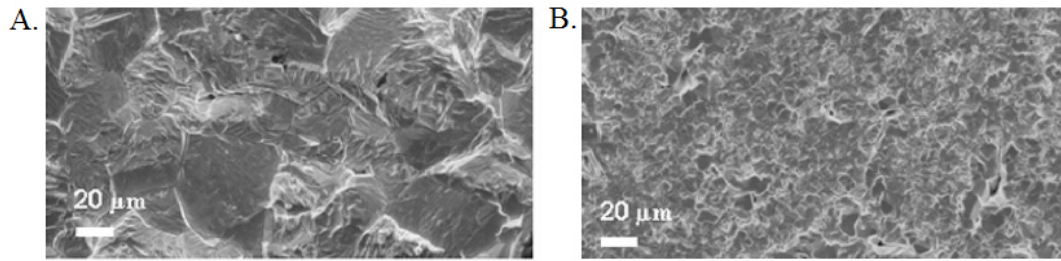


Figure 2.10 - Shown in A and B are SEM images of electroplated tin for 0.05 A/cm² and 0.3 A/cm² respectively.[49]

2.1.9 Limited current density plating

When plating at current densities at and beyond the limited current density, outlined in section 2.1.4, the copper deposit formed is loose and powdery in nature and is observed as a rough dark brown deposit. Such a deposit has been given the name of a burnt finish. It occurs on the PCB in regions of high current density which are typically at the edges of a board. It is prevented by increases to fluid convection in the regions of the high current. Increased fluid convection has been linked to a reduction in the diffusion layer at a board surface, over which Cu cations are transported across [12]. A reduction in the diffusion layer increases the limited diffusion current in that region and enables the high current regions to efficiently plate without the gross production of hydrogen bubbles.[6, 43, 50]

When applying MS agitations on the PCB surface it will be the additional role of the acoustic streaming to prevent limited current plating, by increasing the limited current on high current regions, or when plating at high current densities.

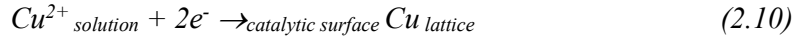
2.1.10 Electroless copper plating

Electroless plating also referred to as autocatalytic plating is a plating technique used to deposit the initial metallic coating onto a PCB surface. Its application is in the metallisation of drilled via interconnects. Electroless deposits for via fabrication are within the range of 0.5 µm to 2.0 µm dependent on the requirements of the customer. The electroless copper plating process occurs before electroplating and after the drilling of the PCB interconnects as outlined in Table 1.1 in Chapter 1. [51]

The basic formulation of proprietary electroless Cu solutions is very similar in that they are highly alkaline solutions containing: a complexing agent used to make the copper sulphate soluble at pH greater than 12; a reducing agent to enable reduction of the Cu cations to Cu metal; a caustic to maintain the pH of the bath and provide the hydroxide ions for the reducing agent oxidation; a stabiliser to ensure pH and maintain bath life time

and finally an acceleration to work in combination with the stabiliser to ensure a fast plating rate and a stable bath solution, although not all commercial formulations use this.[52]

The REDOX reactions involved in the deposition of electroless Cu are modelled by mixed-potential theory. These are the reduction reaction - the cathodic partial reaction,



And the oxidation reaction - the anodic partial reaction,



The overall reaction is a combination of the two which is,



The redox reactions both occur at the same electrode, which is the metal-solution interface.[53]

A PCB operator will vertically plate a panel within a formulated electroless Cu solution for a time outlined by the chemical suppliers, so as to form a conductive seed layer which will receive thicker deposits of copper in the follow up electroplating process. The specific conditions used in the thesis investigations are outlined in section 3.1.2 in Chapter 3.

2.2 Megasonic Literature

2.2.1 Near-field of the acoustic wave

The acoustic waves used for PCB processing operate entirely within a fluid medium. The behaviour of the acoustic wave within a bath can be subdivided into two regions, the near-field also known as the Fresnel zone and the far-field also known as the Fraunhofer zone, categorised by the distance of the propagated wave from its source as indicated in Figure 2.11. In the near-field region the amplitude of the wave undergoes a series of maxima and minima ending at a last minimum. This position reflects the natural focus of the transducer. At this point the sound wave is at maximum strength. Within the far-field the wavefront uniformity is higher than in the near-field. [54]

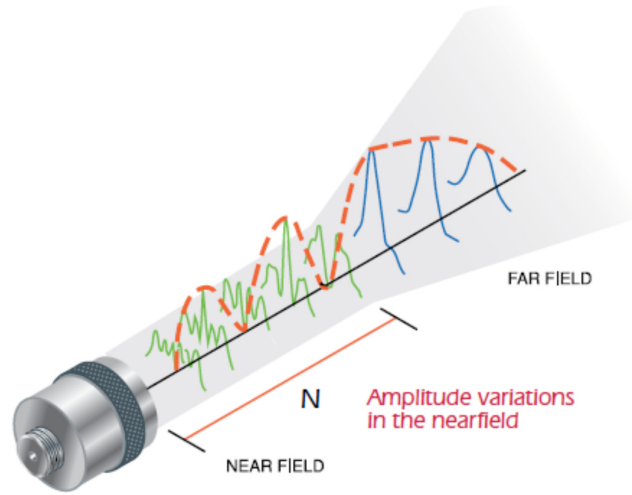


Figure 2.11 - A diagram indicating the near-field and far-field behaviours of an acoustic wave produced from a circular transducer in the ultrasound frequency range. [55]

For the 1 MHz rectangular transducer used in the investigation, the near field distance, N , for a square transducer is evaluated using the equation,

$$N = \frac{(1.35l)^2 f}{4c} \quad (2.13)$$

where l is the length of one side of the square transducer, 0.11 m; f is the frequency of the MS wave, 1×10^6 Hz; and c is the speed of sound in the electrolyte - which is approximated to water, 1480 m/s. Using these values N is evaluated as approximately 3.7 m. Beyond N the acoustic wave is within the far-field where the acoustic wave's amplitude drops to zero. In the MS investigations the distance of the transducer to the cathode will be less than 3.7 m and so will act within the near field. For this reason, any investigations involving increases to transducer distance relative to the PCB will not cause reductions of acoustic pressure to zero. [54]

The acoustic waves emitted by the transducer will undergo a beam spreading dependent on their distance from source as highlighted in Figure 2.12. Within the near field region the acoustic beam will not undergo spreading and instead focus – reduce in beam diameter - up to the near field distance N . Beyond N the beam will spread as characterised by the angle between the main lobe of the sound beam in the far field, highlighted by α in Figure 2.12.

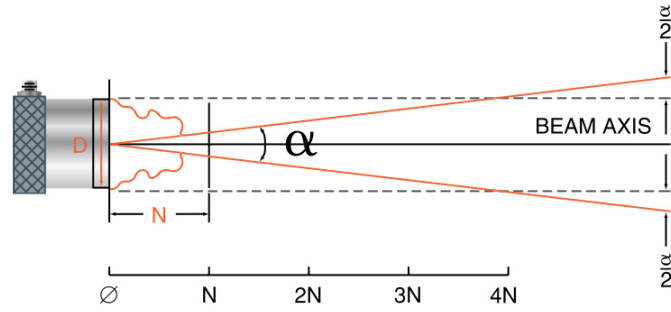


Figure 2.12 – A simplified schematic of sound beam spread, showing change in beam spread angle, α with increasing distance given in units of near field distance, N and for a transducer of circular diameter D . [55]

The beam spread angle is calculated as:

$$\alpha = 2 \sin^{-1}\left(\frac{0.44c}{fl}\right) \quad (2.14)$$

where l is the length of one side of the square transducer, 0.11 m; f is the frequency of the MS wave, 1×10^6 Hz; and c is the speed of sound in the electrolyte - which is approximated to water, 1480 m/s. Using these values the beam spread angle for the transducer used in the investigation is approximately 0.67° . [54]

For a 40 kHz US transducer of same size the beam spread will be 17° and the near field length N would be approximately 15 cm. This highlights that for lower acoustic frequencies in the US range, the acoustic beam will diverge more readily showing a poorer directionality and will reduce in intensity quicker for the same equivalent length travelled by a MS wave. MS shows a benefit to acoustic-assisted manufacture over US as a greater control is possible with the directionality of the MS waves onto a PCB surface and reductions to acoustic pressure with distance propagated will be less, enabling a greater room for placement of the transducer in the plating bath for investigations in the thesis.

2.2.2 Cu surface Crystallinity after MS plating

Prior to the current body of work, research was performed by the Heriot-Watt University (HWU) research group, highlighting the impact of MS-agitation on the morphology of electrodeposited Cu, plated under a laboratory setting at HWU [11, 56]. Surface crystallinity is an important quality metric in PCB manufacture, therefore the

impact by MS on the surface is reviewed and compared with standard processing conditions.

Figure 2.13 highlights the plating finishes obtained for without MS agitation, A; and with MS agitation, B, at 2.5 W/cm^2 ; also C, at 5.0 W/cm^2 . The acoustic power referred to the acoustic power density output by the transducer for the area of their device used [11]. The surfaces were all plated at high current density, 4 A/dm^2 . The current density defines the plating rate and is discussed in more detail in section 2.1.5. Under the current density applied a fine grain deposit is typically favoured, as discussed in section 2.1.8.

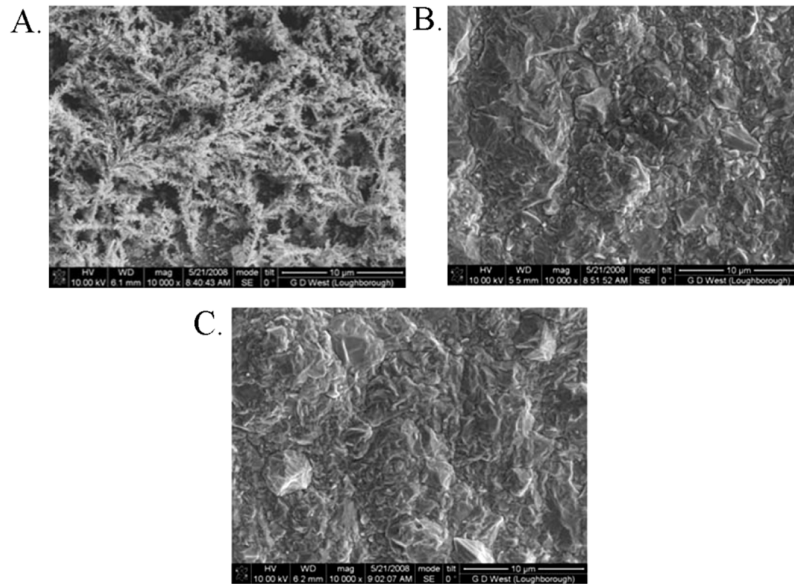


Figure 2.13 - SEM images of 4 A/dm^2 DC Cu electroplated surfaces with A) no agitation B) 2.5 W/cm^2 (50%) MS and C) 5.0 W/cm^2 (100%) MS. Acoustic power density evaluated at source of transducer. [11]

In Figure 2.13A, the Cu produced a dendritic fibre growth. A fibre growth can be deposited when the current density is high and when the bath agitation is low. Typically, at high current density Cu crystallisation on new nuclei sights is favoured rather than formation on existing grains. If bath agitation is not included - in the form of panel movement and bubble agitation - the replenishment of recently deposited Cu cations in the close vicinity of the PCB surface fails to occur. To lower the total energy of the system under this condition, Cu recrystallisation occurs favouring a dendritic growth. For this reason the result obtained in A indicates that no standard panel agitation was applied when electroplating under the experimental conditions. [48, 49]

Under MS-assistance, the two surfaces in Figure 2.13 B & C displayed similar topographies and the fibres were replaced with a polycrystalline finish comprised of large-crystal facets. The change from dendritic to polycrystalline possibly relates to increased ion replenishment near the PCB surface, caused by the forced fluid convection provided as a result of acoustic streaming. The acoustic power output was changed from 250 W to 500 W and these changes appear to have little discernible impact on the surface properties of the deposit formed.

The formation of a polycrystalline deposit indicates that, with MS, a columnar grain structure is favoured. If the bath additives operate correctly a columnar structure is unlikely at the high current densities, as discussed in more detail in section 2.1.8. However, the bath additives failing to operate could have contributed to the large grain polycrystalline deposit. The bath additives are susceptible to changes in bath operational temperature. Localised increases in temperature on the PCB surface during Cu plating are possible due to acoustic cavitation effects, which are discussed in greater detail in section 2.2.6. Increases in temperature may either speed up additive consumption in the bath [57] or denature of the additive molecule, breaking it apart under thermal stresses. With the two effects combined - ion replenishment and negative additive interference - a polycrystalline finish is favoured over a dendritic formation in their MS plating setup.

In conclusion, the results obtained previously, by the HWU research group, show that MS agitation provides replenishment of ions at the board surface, but additionally has a negative impact on the bath additive system critical for an efficient plating reaction. The additives are considered when performing surface analysis studies in the following body of work.

2.2.3 Megasonic-Assisted Copper Electroplating

Conventional techniques employed for enhancing mass transport and enabling efficient plating reactions during PCB electroplating, are achieved by applying movements to the PCB whilst agitating its surface with bubbles, or by mechanically vibrating the PCB at low frequencies (50 Hz). The increasingly small size requirement of high-value PCBs puts a strain on the ability of conventional fluid circulation techniques to enhance transport within the very small features. The introduction of high-frequency acoustic Ultrasound (US) ranging from 20 to 700 kHz, has been shown to agitate electrolyte solutions near to PCB surfaces through a variety of acousto-fluidic forces, which include acoustic streaming currents and the formation and interplay between micro-bubbles generated in solution [58]. On the introduction of 20 kHz acoustic

agitation, US forces have been shown to reduce the diffusion layer thickness over which Cu cations are transported onto the board to $0.6\ \mu\text{m}$ [59]. The low thickness values measured in the study would be difficult to obtain using convectional agitation techniques, such as the Rotating Disc Electrode, as the energies required to produce bulk flows to induce the same effect are considerably greater [60]. A schematic of the US effect is highlighted in Figure 2.14, indicating the reduced distance for Cu cations to diffuse onto the PCB from the plating solution. Reducing the diffusion layer enables the deposition of Cu at higher limiting current densities and so enabling access to higher plating currents and faster plating rates. Limited current densities are discussed in greater detail in sections 2.1.4 and 2.1.9. The introduction of 1 MHz MS agitation offers the same enhancements to plating, along with improved control over directionality of the acoustic beam on the PCB surface and a reduced loss in acoustic pressure with distance propagated, as discussed in section 2.2.1, and reduced damage to surfaces by cavitation, as the cavitation power reduces for high acoustic frequencies [61] as discussed in section 2.2.6.

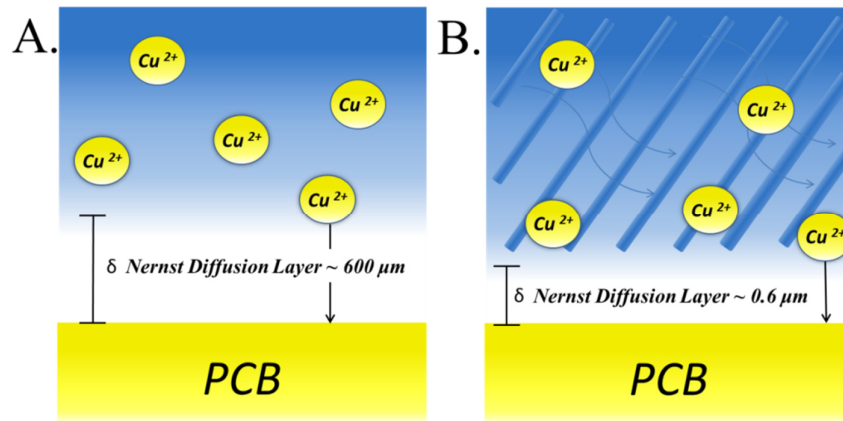


Figure 2.14 - A) the electrolyte diffusion layer schematic at a PCB surface without any forced fluid circulation. B) Modification of the diffusion layer by US agitation with US plane waves indicated by lines on the figure.

2.2.4 Acoustic standing waves: Levitation and acoustic interference

The introduction of high frequency acoustics into the PCB electroplating bath gives rise to a variety of acoustic effects. Some of the most likely effects to occur shall be discussed next.

The superposition of an oncoming travelling acoustic wave with its reflection travelling in an opposing direction, will, in the intervening fluid medium, lead to the

formation of fixed regions of high and low pressure, which correspond to pressure anti-nodes and nodes respectively. The low pressure regions - the pressure nodes – are used in manufacturing to trap and manipulate particles by the process of acoustic levitation [62]. When applying the flat MS transducer in PCB manufacture, the close proximity of the transducer device may cause standing waves to form within the intervening fluid medium.

Another standing wave effect is when an MS wave is directed onto a PCB surface, a part of the wave may be scattered and then confined to a thin layer near the board surface. The conditions for this confinement depend on the free acoustic wavelength, the acoustic impedance at the board surface and the angle scattered. The confined evanescent waves are called Rayleigh-wave Surface Acoustic Waves (SAWs), which exponentially decay perpendicularly to the board surface [63]. SAWs travel in the plane of the board and are an example of boundary layer acoustic streaming. Organic molecules attached on a rigid surface will be displaced if a SAW is generated on the surface. Organic molecular additives are attached to PCB surfaces in plating to ensure efficient deposition, as discussed in section 2.1.3. If the additives in a plating bath behave in the same manner, they may become displaced into nodal regions, which exist between the oscillating high and low pressure maximums within the SAW [64]. Additive movements may occur in a periodic fashion where regions of high and low density are formed, separated by half of the acoustic wavelength, λ . This process could interfere with the Cu electroplating on the board surface.

A SAW describes a specific acoustic condition. In the plating investigations evidence of acoustic interference effects on the PCB surface were observed, see chapters 4, 5 and 6 although their behaviours did not match the exact appearance of SAW. Further investigations beyond the scope of the thesis were required to ascertain if these acoustic effects were due to SAW formation or acoustic interference effects, and as such where the artefacts are observed in the thesis were referred to as the latter.

2.2.5 Acoustic Streaming

Acoustic streaming is the steady state flow in a fluid driven by the absorption of high amplitude acoustic oscillations. In the MS plating investigations acoustic streaming is the dominant process influencing the driving of fluid into via interconnects, enabling replenishment of electrolyte and reductions of the Nernst diffusion layer.

Acoustic streaming can be divided into subcategories, described by the individual mechanisms behind their formation, with each displaying different velocities and

magnitudes. Different streaming currents have been described in microfluidic literature and are catalogued here. This includes:

1. Eckart streaming, which is streaming within bulk solution [65],
2. inner layer boundary streaming also known as Schlichting streaming [58],
3. outerlayer boundary streaming also known as Rayleigh streaming [58],
4. streaming induced due to the flexural motions of a rigid wall by a SAW [66],
5. streaming due to the implosion of microbubbles by cavitation [67] and
6. cavitation microstreaming, which is streaming induced around microbubbles due to resonance induced motions [68].

Eckhart streaming describes the acoustic streaming occurring within the bulk solution away from the boundary layer. The Schlichting and Rayleigh streaming currents act within or near to the boundary layer. The boundary layer describes a region close to a fluid/cavity interface whereby effective viscous forces produced close to the solid alter the sound speed of the fluid and thus alter the speed and flow of any acoustic streaming currents there [69]. In large scale channels of size at least 1 mm, the two boundary layer streaming – Schlichting and Rayleigh – are significantly weaker than Eckhart streaming [70], although for microscales such as the diameter of a PCB via interconnect - 0.5 mm, boundary layer streaming is stronger than Eckhart streaming and are more significant mechanisms [65]. As such these mechanisms are more influential when describing MS plating down PCB via interconnects.

Streaming induced due to the flexural motions of a rigid surface have been attributed to increases in the Rayleigh streaming currents within a microfluidic chamber of size larger than the acoustic wavelength in solution [71]. This highlights that the acoustic streaming velocity can additionally be increased by the walls of the cavity the acoustic wave is propagating through. The size of the via interconnect in some plating configurations is larger than the length of the acoustic wavelength in solution – 1.4 mm – and so, when MS plating the walls of the via interconnects could contribute to the acoustic streaming currents formed.

Enhanced microstreaming currents occur due to the cavitation of microbubbles and microbubble resonant motions induced under acoustic fields in solution. These two effects are discussed in greater detail in sections 2.2.6 and 2.2.7, accordingly. The resonant motions of the bubbles along with the conditions for cavitation are both depended on the acoustic frequency and pressure output. Alterations to both of these can

change the streaming currents and thus influence the fluid motions within a PCB via interconnect.

It is uncertain how each of the individual streaming currents specifically influence Cu plating down via interconnects, although a brief overview of how the geometry of the acoustic streaming current is influenced will be discussed next.

When sonicating a cavity the size of a microvia, reflections of travelling acoustic waves may occur and form standing waves within [72]. These standing waves form discrete regions of high/low pressure, referred to as pressure anti-nodes and regions of zero pressure, referred to as pressure nodes. In response, the resulting fluid streaming motions are referred to as Schlichting streaming. Schlichting streaming is characterised by vorticity motions formed within the cavity, which are much smaller than the acoustic wavelength.

Highlighted in Figure 2.15 are the acoustic streaming patterns taken from [58] of fluorescent beads in solution. Vorticity is highlighted within the cavities due to fluid convection within the acoustic standing waves. The pattern of the vorticity such as their position within the cavity, pressure magnitude and fluid velocity are influenced by the acoustic properties of the resonant chamber. This includes the boundary conditions - which describe how the acoustic wave reflects or transmits at the solution/solid interface and how the acoustic pressure varies the loss mechanisms within the media and the geometry of the cavity [73]. In the top two chambers in Figure 2.15 the cavities allow flow-through and multiple streaming currents characteristic of Rayleigh streaming vortices are observed. In a cavity not enabling flow through shown on the bottom left, a single vortex of length $\lambda/2$ is seen and the final cavity in the bottom right, contains edges with sharp peaks which generates vorticity originating from the sharp peak tips. The images highlight that changes to the cavity geometry on the scale of the acoustic wavelength vastly change the microstreaming behaviour. Within via interconnects the holes drilled roughness could produce sharp peaks which could influence the vorticity within the via and the plating outcome.

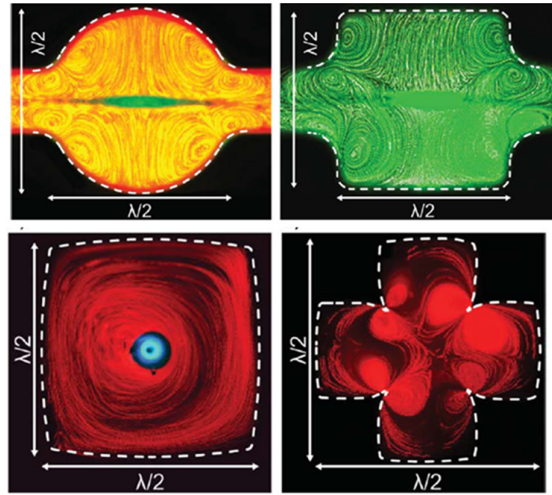


Figure 2.15 - Acoustic streaming patterns tracked from 1 μm fluorescent beads, generated in response to a driving frequency between 2.1 - 2.6 MHz for different geometrical cavities of lengths between 300 - 350 μm . [58]

The vorticity motions are altered by Eckhart streaming currents and the position of the acoustic pressure nodes [70]. Highlighted in Figure 2.16 is a not-to-scale 2D schematic, estimating the streaming behaviour inside the entrance of a Through-Hole Via (THV) cavity, in response to Eckhart streaming produced from acoustic travelling waves by a MS transducer. Different streaming currents are produced within the THV which vary due to changes in effective viscosity towards the wall of the via. These currents display different velocities and their position is defined by interactions with the acoustic pressure nodes formed within the cavity, which are separated by half of the acoustic wavelength. Such fluid behaviours are observed within microcavities and have been extensively studied for microfluidic device manufacture. [58]

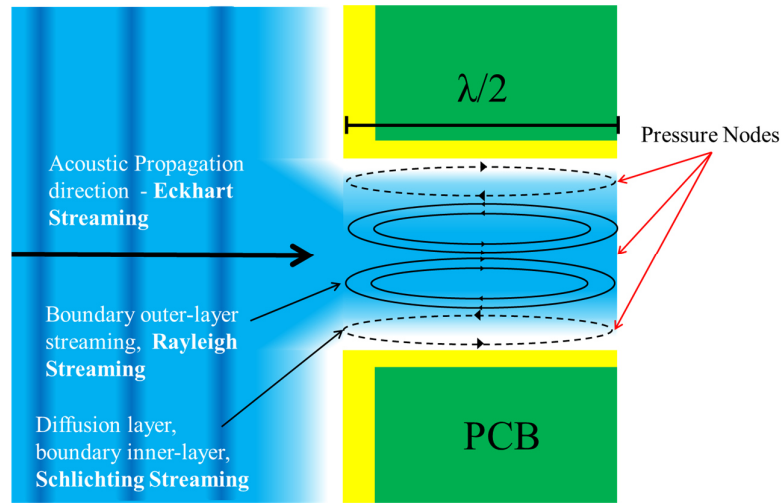


Figure 2.16 - A not-to-scale 2D schematic of the fluid motions within the entrance of a THV with fluid motions in the boundary layers indicated.

The streaming velocity is a key parameter controlling the electro-kinetics of Cu plating, which in Cu plating is increased by MS agitation. The Schlichting streaming velocity, produced towards the surface of a substrate under high frequency agitation, is proportional to the product of the square of the acoustic frequency and the transducer intensity and inversely proportional to viscosity [74]. For this reason higher frequency acoustic agitation induces faster Schlichting streaming velocities. This parameter makes MS a more desirable frequency range to plate with rather than US, as the faster velocities could enable greater electrolyte replenishment down the via interconnects. For example, the velocity was measured in [75], to increase between 100 – 500 $\mu\text{m/s}$, for increases of acoustic frequency between 1.5 and 3 MHz.

The enhancements to fluid velocity brought on by increases in acoustic frequency further warrants the use of MS over US frequencies in Cu electroplating, when plating down via interconnects.

2.2.6 Cavitation

Cavitation defines the formation of a bubble through to its collapse under high pressures. It is an effect which can be produced as a result of localised fluid medium size variations, which are brought on due to high tensile stresses occurring during the low pressure phase of an acoustic wave. Depending on the life-cycle and dynamics of the bubble, cavitation can be described as either stable or transient. Stable cavitation describes the formation of bubbles, which do not change significantly from their equilibrium positions or sizes during their lifetime cycle. Transient cavitation is regarded

as the energy release occurring from the collapse of air bubbles, when local pressures in a fluid decrease to below a minimum vapour pressure. The vapour pressure of a fluid is the absolute pressure at which the liquid vaporises or is converted to a gas at a specific temperature.[76]

Shown in Fig 2.6 is an example of transient cavitation. The transient cavitation process as a whole describes the creation of an air bubble through to its collapse. The occurrence of cavitation depends on the pressure amplitude and frequency of an acoustic wave. A pressure threshold exists below which cavitation does not occur. The value of this threshold increases with an increase in acoustic frequency. For high frequency acoustics, higher transducer powers are required to induce unstable cavitation. Unstable cavitation is unwanted in PCB manufacture due to the damage induced on its surface, as discussed below. For this reason, with MS agitation there is a lower likelihood of inducing damage than with US, making it a desirable manufacturing property.

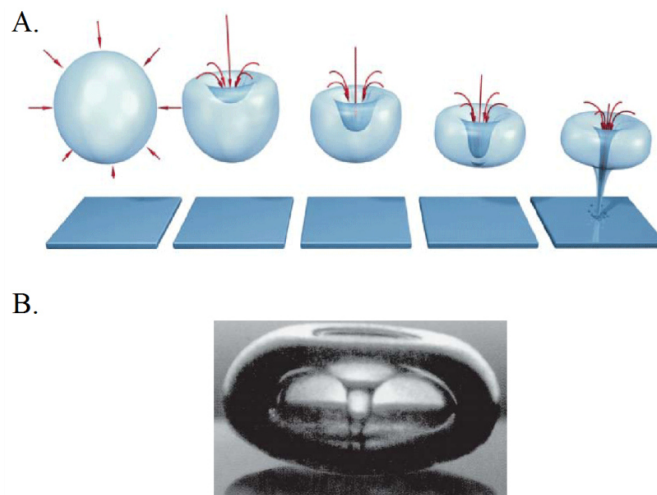


Figure 2.17 - Examples of transient cavitation. A) the steps prior to and including bubble collapse indicating the jet streaming effect. B) the implosion of an air bubble under 25kHz ultrasonic agitation, where the internal-jet stream is shown.[67, 77]

Cavitation may appear differently from the example given in Figure 2.17. Shown in Figure 2.18 is an image of cavitation produced inside a transparent gel in response to a high frequency acoustic pulse. The acoustic settings were for a frequency of 3.3 MHz and of a pulse duration of 30 ms. The pulse induced a ‘tadpole’ shaped lesion within the gel, in response to pressure variations caused by the impulse. The ‘tail’ of the lesion indicates the directional orientation of the acoustic pulse and highlights a lower pressure

region. An alternative description is that the tail region is due to the internal-jet being directed towards the low pressure region.

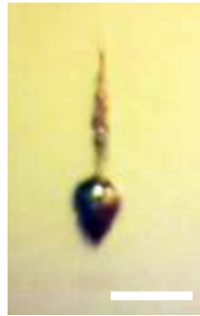


Figure 2.18 - A cavitation lesion produced as a result of a high frequency pulse-burst in transparent gel. Frequency of the megasound is 3.3MHz and pulse duration is 30 ms. Vertical upward orientation indicates direction of the acoustic pulse. Scale is 2mm.[78]

The impact of acoustic agitation upon metal surfaces has been investigated. Figure 2.19 gives examples of US-induced cavitation on metal surfaces. Shown in A and B are SEM images of copper surfaces treated under ultrasonic sonication. The surface shows increased roughness for increased processing time in the US field and the appearance of crater-like features is present. C shows the result of sonication on silver. Clearly indicated on the surface are crater-like features highlighting the appearance of cavitation. The literature results suggest that acoustic cavitation is the most significant acoustic force influencing the topography of metal surface, as indicated by the formation of craters and holes [79, 80]. Increases in roughness measured as a result of the acoustic wave are a result of cavitation intensity.

The acoustic frequency applied was in the ultrasound range and is 20 kHz. At this frequency, the energy released due to cavitation is greater than for higher frequency MS agitation operating under the same output pressures. This is because the unstable cavitation formed with US is from larger bubbles and releases a significantly greater amount of energy [61]. For this reason it is predicted that the roughness increase observed after MS sonication will not be as severe as when US processing.

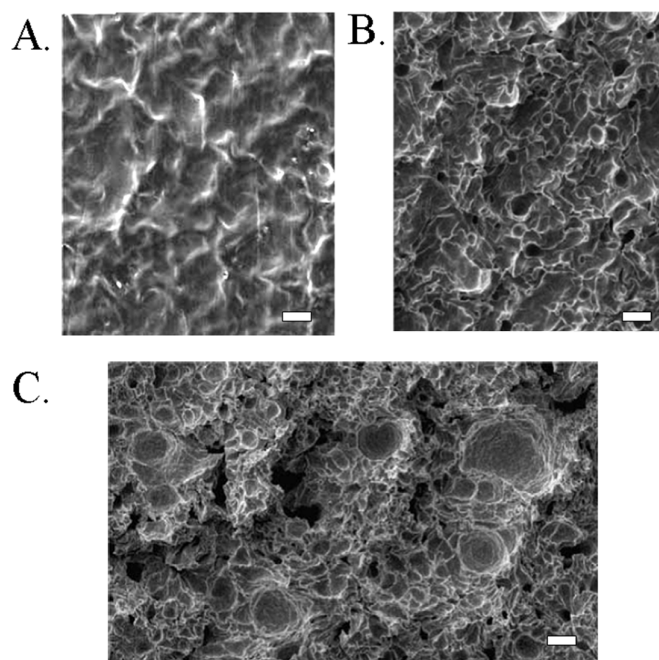


Figure 2.19 - SEM images showing A) & B) surface of a Cu plate after 5min and 10 min of 20 kHz ultrasound exposure, respectively. C) Surface of Ag after 10 min sonication. For both metals the transducer - sample distance 0.5 mm. Scale in images 20 μ m.[79]

The temperatures generated under unstable cavitation can be as high as 5000°C [67] and have been shown to generate free radicals from the thermal decomposition of molecules in high temperature zones. A free radical is an atom, molecule or ion that has unpaired valence electrons which tend to display a high chemical reactivity to other substances or themselves. Within a Cu plating bath the formation of free radicals will potentially have a negative impact on the bath concentration and the chemical additives within. Their impact on additive concentration after MS plating will be considered in the plating investigations.[76, 81]

2.2.7 Cavitation streamers: bubble cones, lens and ringlets

The pressure output of a transducer may be influenced by an interaction with bubbles generated on the surface of the device in response to acoustic resonant effects. The formation mechanisms along with their impact on pressure output will be discussed next.

Within the low pressure regions of an acoustic standing wave, particulates or gas bubbles may congregate and coalesce. In time the multi-bubble systems may lead to the formation of self-organising cavitation bubble structures, referred to as streamers.

Acoustic streamers can take many forms, which vary dependent on their generation conditions. [82]

The shape of the acoustic streamer depends on the acoustic intensity. For intensity values less than 5 W/cm^2 , observable cavitation streamers were not apparent in US investigations. For acoustic powers larger than 5 W/cm^2 a conical streamer shape has been reported as indicated in Figure 2.20. It influences the behaviour of the emitted acoustic wave and a series of unique effects are produced as a result, these are high speed fluid streaming and a focusing of the acoustic wave at distances shorter than the natural focus of the transducer. The cone is generated due to modulation of the acoustic wave by a smaller sized bubble structure formed on the surface of the transducer, which acts like an acoustic lens. [83]

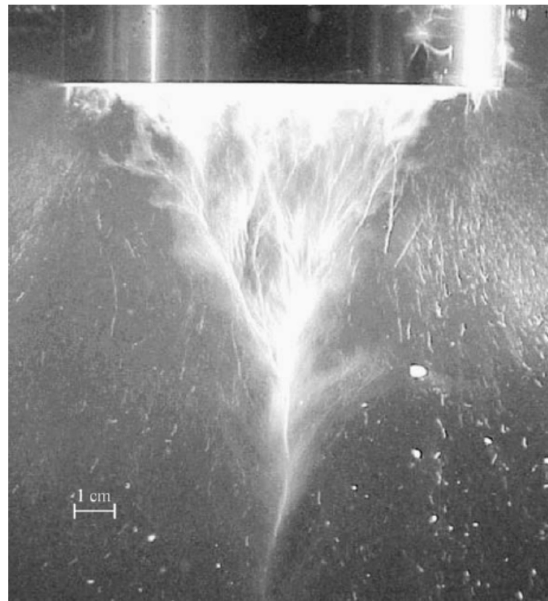


Figure 2.20 - The conical bubble structure formed for a high intensity ($> 5 \text{ W/cm}^2$), 20kHz transducer.[83]

Bubbles are attracted to the transducer surface by secondary Bjerknes forces, which are resonant attractive forces generated between individual bubbles caused by their oscillations [82]. The bubbles near to the transducer surface may then undergo further cavitation into smaller cavitation bubbles, which in turn are attracted again toward the surface. When reaching the surface the bubbles coalesce into a bubble cluster. The degree of clustering is influenced by the acoustic pressure output of the transducer. On increases to pressure, cavitation occurrence is enhanced and the bubble layer thickness grows due to the larger numbers of released bubbles. At a particular pressure the bubble layer

thickness increases until it reaches a size close to half of the wavelength of the acoustic wave. Around this size, the acoustic wave generated on the surface of the transducer is in phase with waves reflected within the bubble layer. Under this condition, a resonance phenomenon occurs whereby amplification of the pressure field happens both inside and behind the bubble layer.

If the layer continues to grow beyond the resonance thickness then resonance disappears and the acoustic pressure in the layer decreases. A reduction of pressure causes the bubble numbers to decrease and the cluster dissipates. In its entirety, the resonance layer phenomenon process tends to self-stabilise the bubble cluster thickness to a size half of the acoustic wavelength.

The bubble cluster forms into a non-uniform configuration which is thicker at the centre and is thinner, with lower bubble numbers, around the edges. The described shape is lens-like in appearance and is indicated in Figure 2.21.

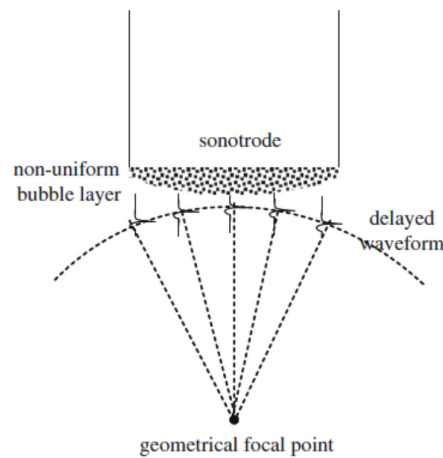


Figure 2.21 - Schematic of short distance focusing due to the formation of a non-uniform bubble layer on the surface of the ultrasound. [83]

The inhomogeneous distribution of the bubbles on the transducer surface introduces a time delay in the acoustic wave propagating outwards. As a result the resonant bubble layer acts like an acoustic lens focusing the acoustic field to shorter distances. Within the acoustic lens the microbubbles may coalesce and form larger bubbles. These bubbles grow in size until they gain enough momentum to overcome the attractive forces and break away from the surface of the transducer. The bubble is then focussed towards the focal spot generated. With multiple bubbles undergoing this process the acoustic cone is formed as indicated in Fig 2.9.

The resonant bubble structure has been shown to enhance the acoustic pressures emitted from the bubble layer, although at significantly reduced transmission distances. When processing under MS agitation, the device used operates up to 5 W/cm^2 . For this reason resonant bubble effects may influence PCB manufacturing outcome due to variations in pressure, therefore transducer distance will be considered when performing trials.

Another form of acoustic bubble streamers has been identified as ringlets. Figure 2.22 highlights the formation of bubble-rings generated from the combination of two bubble-clusters which have become detached from the transducer surface. The combination of the bubble-clusters into a bubble-ring is attributed to the focusing of the acoustic wave due to the acoustic lens effect on the transducer surface.[84]

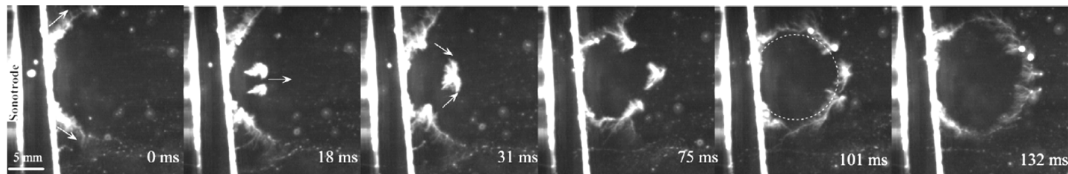


Figure 2.22 - High-resolution photograph images recording the formation of an acoustic ringlet over time.[84]

2.3 PCB composition

The structure of a PCB is comprised of a glass weave impregnated with epoxy resin. The glass weave combined with the resin provides structural and thermal stability and electrical insulation between the Cu tracks and interconnects. Each of these materials displays a different acoustic response and so will be considered when simulating the PCB setup, as discussed in Chapter 3.

The glass weave interlaces through a board as depicted in Figure 2.23 A and B. The weave impacts on the surface topography of the PCB where the knuckles of the weave can cause recesses and dimples in the electroplated Cu. The variation generated is acceptable by International Printed Circuit (IPC) standards. Highlighted in Figure 2.23C is a measure of the topography of standard electrodeposited Cu of total thickness of approximately $40 \mu\text{m}$, plated onto a PCB. The underlying glass weave has influenced the deposited Cu by inducing an approximate $5 \mu\text{m}$ variation in the surface thickness, as highlighted by the variations in colour on the plot. This indicates that the shape of the glass weave is carried forward onto the electrodeposited Cu despite the $40 \mu\text{m}$ thickness. The influence of the weave on PCB topography after MS plating will be considered in

the thesis investigations, especially when measures of surface roughness are obtained, as described in Chapter 4.

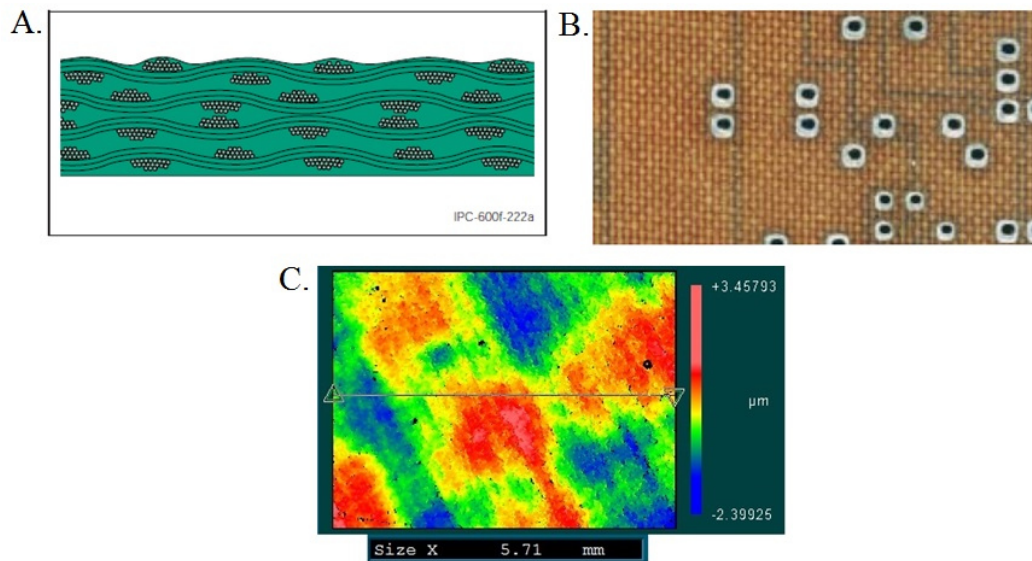


Figure 2.23 - A) shows a cross-section diagram of a PCB glass weave and B) a top-down image of a PCB with the Cu removed[85]. Indicated in C) is a top-down surface plot of PCB electroplated with Cu under standard DC conditions. The image was obtained from a White Light Interferometer and indicated by the colour scale is the variation in height. The length scale of the image is indicated underneath.

2.4 Via Interconnects

Micro-vias are currently the most common method for providing electrical interconnection between the individual layers in a circuit board. The interconnections come in three varieties, which are BV, THV and buried vias. BV currently provides interconnection between two layers in a PCB, although recent advances push the capability towards a greater number of levels. THVs connect between multiple layers in a PCB, entering through the top of the board and exiting through the back. Buried vias are a combination of both BV and THVs and are encapsulated inside the PCB in-between the layers.[86]

The chemistry required for BV filling and THV filling differs, see section 2.1.3. THV filling is influenced by convection flow, which occurs from one side of the board to the other through the THV. Electrolyte ions are refreshed as the flow directs through the via hole and this refreshment influences the deposition rate. For BVs the electrolyte flow does not pass through the BV in the same manner and the transport is instead heavily

dependent on diffusion and migration. As a result, BV deposition rates are more influenced by the bath chemistry composition than THVs.

2.4.1 Blind via Fabrication

BVs of maximum *ar* size 1.2:1 can be partially plated or filled with Cu from the bottom to the top. If choosing to fill the BV, the formation of voids or seams is an issue and so the plating rates at the base of the via, the side walls and on top are controlled [24]. The side walls and the bottom are first plated with a micro layer of Cu - by an electroless Cu deposition process - which acts as seed layer for the follow-up electrodeposition of a thicker layer of Cu. The filling of BVs is depicted in Figure 2.24 and employs a unique chemistry composition which requires its own plating bath separate from the partial plating process. The deposition rate is controlled in the tank through the use of suppressors and brighteners, where the suppressor inhibits the formation of a surface Cu layer and the brightener accelerates the trench or base features of the via. The brightener dominates the filling process. Levellers may also be added to the solution and bottom-up filling can be obtained with and without them. The leveller acts to prevent over filling of the vias resulting in a more uniform surface finish. They operate by enhancing the role of the suppressor on the surface enabling the brightener to fill the via.[87]

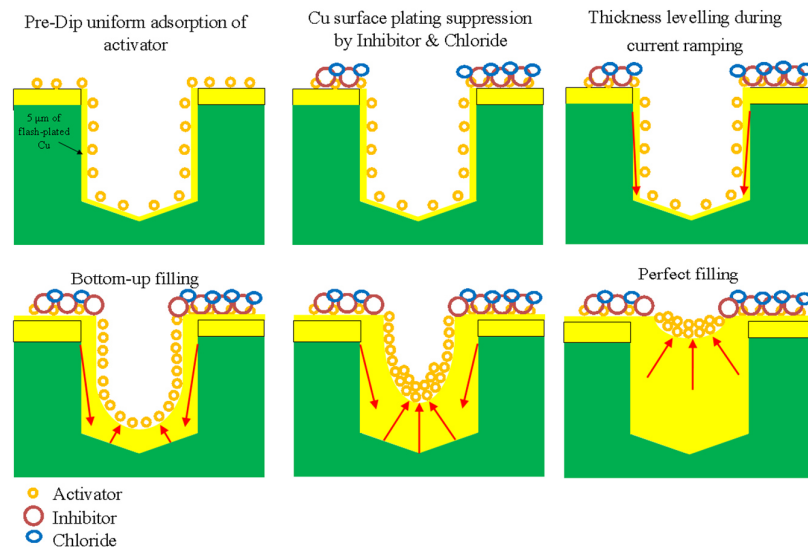


Figure 2.24 - The standard filling process for electroplated copper Blind Vias. [88]

BVs may be plated in a vertically stacked formation or singularly. Stacked vias involve multiple Blind Vias being bonded together to enable a high level of

interconnection through the board, as shown in Figure 2.25A. The negative impact of this design is multifold:

- a) the successive drilling of the vias can result in the previous via being damaged;
- b) the drill displays an alignment error of $50\mu\text{m}$ and since the diameters of the BVs can be as small as $250\mu\text{m}$, it is likely the drill will miss-align;
- c) stacked via structure is weakest at the top and at the interconnecting regions, which are prone to mechanical failures such as cracks causing electrical opens [89] and;
- d) these areas are also structurally unsound when laying down further deposits such as protective coatings and laminates [90].

For these reasons, stacked vias are difficult structures to manufacture, owing to the large amount of scrap PCBs generated to achieve the desired board yield.

An alternative, more stable design, is an off-centre or staggered stack, as indicated in Figure 2.25B. The structure is no longer mechanically unstable and does not suffer from alignment issues, or from direct process damages. Off-centre stacked vias do not, however, show the same heat dissipative capabilities as the vertically stacked vias and take up a greater amount of space on the PCB, reducing the board component density.[91]

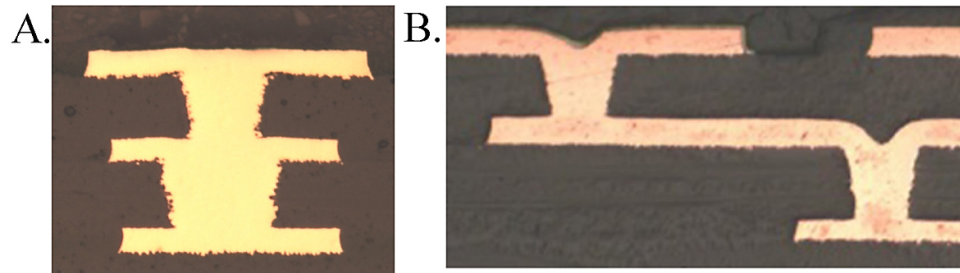


Figure 2.25 - A) Two vertically stacked BV. B) Two staggered BV.

MS-assisted electroplating studies have been performed by the research group at HWU, in non-fill chemistry plating baths, to deposit Cu down BV interconnects of different *ar*. Highlighted in Figure 2.26 are the MS plating results obtained, which show a 0.1 mm diameter BV uniformly filled with Cu at an *ar* of 3:1. This plating quality is significantly greater than obtained under standard fabrication conditions. A BV formed with a single drill operation at high *ar*, would not contain the instabilities witnessed with stacked vias and would have the positive effects of heat dissipation and a small feature size.

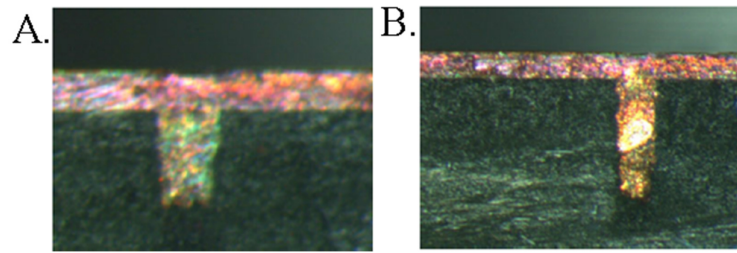


Figure 2.26 - D.C. plated at 1 A/dm^2 with MS assistance at 1 W/cm^2 showing 0.1 mm diameter BVs at ar A) 1.7:1 and B) 3:1.[16]

2.4.2 Through-hole Via Fabrication

THVs are larger than BVs. They are still considered as microvia due to their size and may be fabricated so as to pass through multiple layers in a board. A THV is typically partially filled with Cu to the customer's specification and then either left open or filled with a resin for structural stability. Under certain applications a THV may be uniformly filled with Cu, to provide high power requirements and act as a thermal heat sink. [92]

A fully filled THV is difficult to uniformly plate due to its size and voiding issues which occur. A void is an unwanted artefact occurring inside a via after fill-plating. If a board is sent on after PCB manufacture, then it will undergo soldering of packages to the board. If a soldered THV contains a void, then, under soldering, it can be exposed to temperatures as high as 260°C in a lead free soldering process [93], which causes the trapped gasses to expand and cracks to form in the via leading to electrical opens.

Void-free THV Cu filling is possible through a selective alteration of the bath chemistry and the electrical current density waveform, to enable a bottom up fill. A successful mechanism developed for manufacture by the company Atotech Ltd. is outlined in Figure 2.27 and involves a three-stage deposition process developed by the company Atotech [17]. The outcomes of the deposition are to uniformly fill THVs without voids and with a surface deposition no larger than customer specifications, which is typically within the range of $20 - 70 \mu\text{m}$. The process shown enables this, although it requires the addition of redox mediators ($\text{Fe}^{2+/3+}$), to improve conductivity of the bath, so that high plating current densities can be applied to form the complex Cu patterning down the THV. The redox mediators require additional costly machinery alongside the plating process, to maintain their performance within the bath. This process is capable of plating THV features of $100 \mu\text{m}$ diameter THV on boards $400 \mu\text{m}$ thick, with an ar of 4:1.



Figure 2.27 - Three-stage THV filling process from left to right showing seed layer deposition with flash plating (2 - 5 $\mu\text{m Cu}$), X-plating (5 - 10 $\mu\text{m Cu}$) and via filling (10 - 15 $\mu\text{m Cu}$).[17]

The studies performed by the HWU group show that with MS agitation, plating can be achieved producing a uniform filling of the THVs of diameter 0.2 mm and PCB thickness 1.6 mm, giving an ar of 8:1 [12]. The plating result is shown in Figure 2.28 and highlights that, with MS, a uniform deposit is formed down the THV with a small amount of Cu deposited on the surface. Shown in A is the plating condition without MS, highlighting the formation of a central void by the red arrow. The MS outcome shows all the key desirable attributes for THV filling and performs without additional costly chemistries or high plating currents, and with an ar greater than existing techniques. MS processing shows a greater promise than the process developed by Atotech and for that reason is chosen for study in the thesis. The benefits to plating are characterised next.

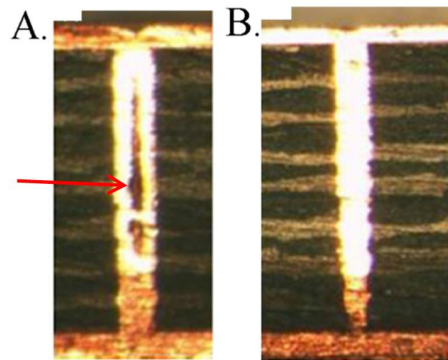


Figure 2.28 - Microsection of 0.2 mm diameter THV, ar 8:1, after 1 A/dm^2 plating formed under a laboratory setting with A) no MS agitation and B) with 250 W MS. Red arrow highlights central void. [12]

2.4.3 Improved PCB design due to MS Plating

The improvements in manufacturability brought on due to MS processing enable increased heat dissipation, increased structural stability and reduced component feature

sizes. Multilayer PCBs are fabricated by individually engineering each layer and bonding together, with potentially further drilling operations. Via fabrication capability, obtained with MS, allows for a reduced number of damaging drilling and bonding operations on high value multilayer PCBs. This enables new designs to be imagined by PCB designers.

Figure 2.29 outlines a 2-D build schematic of a 26 layer PCB as used by an engineer, where the individual layers are highlighted by showing the Cu as orange and the laminate epoxy resin/glass mixture as green, beige and white. The BVs and THVs electrically connecting the individual layers together are shown with vertical Cu lines. Highlighted in Figure 2.29A is the typical processing using standard PCB manufacturing techniques, which includes staggering the BVs as discussed in section 2.4.1. Each of the staggered BVs requires individually bonding to the PCB in a separate bonding operations before drilling and plating. Altogether, using a traditional approach the 26 Layer board is manufactured using six bonding and ten drilling operations. In Figure 2.29B the PCB is manufactured using the MS plated the high *ar* BVs outlined in Figure 2.26. Using theses the outer three layers of staggered BVs are now fabricated with a single drill operation. All together this board applied four bonding and six drilling operations and so it requires less bonding operations to construct it, increasing its lifetime and less drilling operations, reducing its manufacturing cost. These features are highly desirable for PCB manufacture and highlight a paradigm shift in processing capability, setting it apart from existing manufacturing techniques.

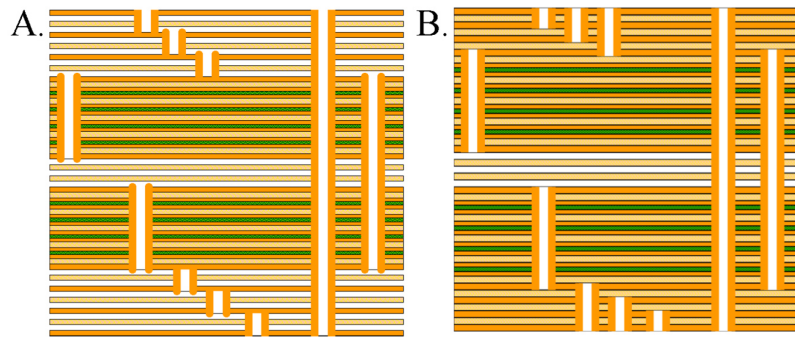


Figure 2.29 – 2-D build schematics for a 26 layer PCB showing copper as orange and epoxy resin/glass as green, beige and white for A) standard processing involving six bonding and ten drilling operations and B) theoretical MS processing involving four bonding and six drilling operations.

2.4.4 Alternative via filling techniques

A via may also be processed using a range of other techniques dependent on the PCB customer requirements. A PCB designer may want to place a via inside a board where electrical connection is provided between at least two innerlayers and is not visible from the outerlayers. This is referred to a buried via [86]. The technology enables increased functionality when board space is limited. Highlighted in Figure 2.30 are cross-section images of THV buried vias which have been partially plated with Cu to provide electrical interconnection and then filled with an epoxy based thermoset resin, using vacuum suction equipment [94].

The filling of a via with a resin instead of Cu is less desirable due to its poorer thermal transport properties, although the current manufacturing capability - defined in terms of via interconnect ar - is greater for resin filled vias than Cu filled vias, where a resin fill is typically ar 8:1 for a 0.2 mm diameter THV and ar 4:1 for a 0.2 mm diameter, respectively. Beyond these ar the filling of vias suffers from air bubble entrapment leading to voiding within the via, as discussed in section 2.4.2.

For the MS processing the ar processing capability has been shown to have been enhanced. A manufacturing combination of MS plating with resin filling of vias may yield further developments - where MS plating would be used to partially plate difficult-to-manufacture high ar interconnects and a resin filling machine used to uniformly fill the interconnect. This processing route may be useful for the customer who wishes to save on processing costs due to the reduced Cu plating time. This manufacturing process was not investigated in the thesis due to time constraints.

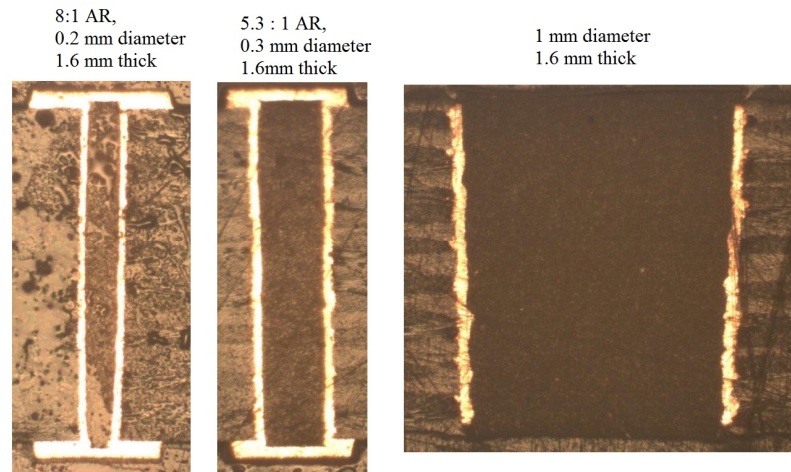


Figure 2.30 - Three cross-section images of Through-hole via interconnects of different size, electroplated and uniformly filled with a non-conductive polymer.

2.4.5 Silicon via fill processing

Via interconnects are used to connect through silicon wafers in component device manufacture and the features are referred to as Through-silicon Vias (TSV). Their construction enables high speed communication, high interconnect density and low power communication links through wafers.

The TSV is processed with a multitude of conductive materials which uniformly fill the structure. The materials used depend on the size of the TSV and its application in the wafer manufacture process. In the via-first manufacturing process TSV are made with diameters larger than 100 μm . The feature is made conductive by uniformly filling with a doped polysilicone, which is used because of thermal restrictions placed on wafer manufacturing when applying the via-first process. The via-middle process employs TSV of diameters less than 100 μm . At this size tungsten (W) is used to fill vias with *ar* larger than 10:1 and Cu is used to fill vias with *ar* less than 10:1. The two different materials are used because Cu displays increased voiding at high *ar*, whereas W improves yield due to its similar coefficient of thermal expansion with silicon, so thermal stresses can be distributed evenly between the two materials [95], although under performs structurally due to a higher intrinsic stress.[96]

When Cu filling is applied the process follows the bottom-up fill outlined in Figure 2.24 in section 2.4.1, although includes the addition of a refractory-metal barrier applied to the inner wall of the silicon via before the Cu seed. A refractory-metal is a class of metals that show a high resistance to heat and wear. The bottom-up fill suffers from

long deposition durations and so is used with a conformal plating operation to speed up overall process duration.[97]

TSV are significantly smaller than PCB vias where the smallest rigid PCB THV diameter is 150 μm . The techniques used to fill TSV suffer from voiding at larger sizes and are too slow and costly for implementation into PCB manufacture. For these reasons the TSV fill processes cannot be effectively scaled to the PCB industry. [98]

2.5 Quality evaluations of Vias

The main function of a via is to enable electrical current to pass through the PCB without electrical opens or shorts. Evaluating the quality of the fabricated via is important so as to ensure that it can pass current. A quality metric typically used by the international printed circuits (IPC) is thermal shock testing. This is applied in accordance with the quality standards IPC 6012 [99] and IPC-TM-650 2.6.8 [100]. A thermal shock test applies a high temperature to a fabricated PCB containing plated vias. The high temperatures put pressure on the PCB, causing expansion of the Cu metal. If the metal expands significantly then it can form electrical opens which prevent the flow of current and scrap the board. A thermal shock test is applied to simulate thermally intensive manufacturing operations which the board will undergo under component assembly, as discussed in section 2.4.2. The PCB is thermal shock tested to evaluate if it can survive these degrading processing conditions. The procedure is as follows:

1. A test specimen is removed from the board using a Dremel 200 Multi-tool (RS), (UK).
2. The specimen is stored in an air circulating oven at 125 ± 5 °C for one hour. It is then removed and allowed to return to a temperature of less than 30 °C.
3. The sample is covered in a solderable flux such as MEC HASL Flux W-2308 (Europe), then floated on the surface of solder for a period of three, 10 second intervals at 288 °C.
4. After the test the flux is removed prior to examination by immersing in IPA for a few seconds then blow dry with air gun.
5. The sample is then microsectioned - involving potting in a thermoset resin - and viewed under a microscope.

When viewing a THV under a microscope after thermal shock testing the most susceptible regions for failure are the barrel of the via and the corner regions. Figure 2.31 shows the results from a thermal cycle test indicating the barrel of the THV undergoing a cracking across its horizontal. The crack arises due to metal fatigue and originates at the glass substrate (FR4), on the edge of the via wall, advancing through the electrodeposited metal layer in a random fashion and typically cutting a line 20° - 50° to horizontal, also shown in Figure 2.31 B&C. Its progression through the metal corresponds to the boundaries between the plated copper crystal faces. When the crack is formed it slowly progresses out developing into a failure, which is characterised as a complete crack across the horizontal. The failure was observed after several hundred cycles of thermal testing. The likely cause of the initial crack and subsequent cracking is due to thermally driven expansion in the vertical direction of the laminate combined with compression of the barrel walls. The thermal cycling tests match observations from plating results shown in Figure 2.31 B-E. Figure 2.31D shows crack formation occurring on the corner entrance of a partially plated THV. It occurs in this region also due to expansion mismatches [101].

In the MS plating investigations thermal shock testing was not performed. Further investigations into MS processing will introduce shock testing to evaluate the quality of the MS-plated metal.

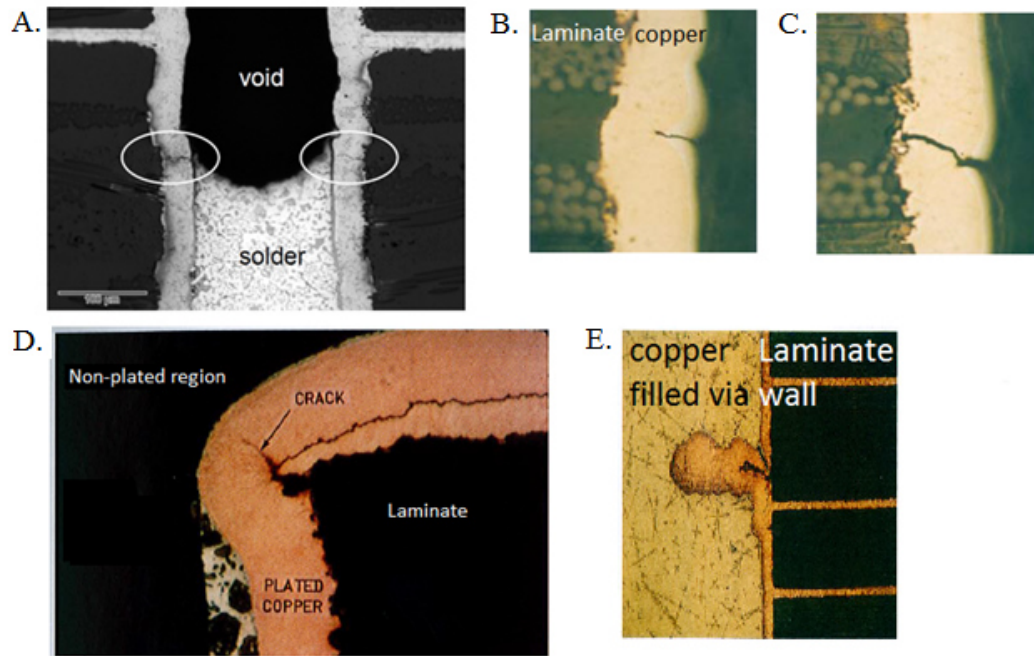


Figure 2.31 - Indicated in A) are the formations of cracks due to 100 thermal cycles in a partially filled Cu through-hole via [101]. B), C) and D) display measured data for partially filled electroplated copper through-hole vias. E) shows data for fully plated via. All are unacceptable by IPC standards IPC-A-600 [102].

An additional test of the PCB quality is to directly measure the electrical conductive properties of the PCB through impedance measurements. Impedance is a measure of the resistance to the passage of electrical current for alternating current (AC) signals [103]. Differential impedance is a test procedure evaluating the electrical resistance for high frequency signal transmission. High frequency signals are used to transmit large volumes of electrical data through a PCB [7]. If the electrical tracks are not manufactured to the customers size requirements then the electrical impedance will differ and be unable to transmit the data effectively [104].

A PCB's impedance is evaluated using the IPC-TM-650 2.5.5.7 standard [105] which employs time domain reflectometry (TDR) for measuring the characteristic impedance of a transmission line on a PCB. A transmission line is a conductor in this case a PCB, designed to conduct alternating current within the radio frequency range – higher than 30 kHz [13]. In TDR a signal is injected into a transmission line and the characteristic impedance is determined from the amplitude of the pulse reflected at the TDR/transmission line interface. The transmission line is a PCB test coupon which is fabricated within a customer's PCB panel, but is separate from their circuit design. The

coupon is designed to fit into the TDR measurement device and to accommodate high frequency signals [106]. Shown in Figure 2.32 is an example of a TDR coupon, as provided by the impedance testing equipment manufacturer Polar Instruments Ltd. If the electrical tracks inside of the test coupon are not manufactured to within coupon design requirements then it will fail to produce the required 50 Ohm impedance value. This would then indicate that the PCB panel the coupon was attached to will also be unable to perform to customer requirements, leading to scrap panels. The TDR test coupon is a quality metric on which to evaluate the quality of a fabricated PCB panel.

When MS processing PCBs, the electrical impedance properties of the MS-plated copper tracks will need to pass impedance checks, if MS processing is to have an application in high volume data transmission. TDR test coupons were not manufactured using MS plating within the thesis but are a test for future studies.



Figure 2.32 - An example of a TDR PCB test coupon used to measure electrical impedance from Polar Instruments Ltd.

2.6 General Conclusions

The electrochemical process was outlined and the individual parameters controlling the quality of a plated Cu finish were reviewed. The analysis provided a description of the conditions under which the bath operates successfully, which can be used to identify the plating conditions which have changed after MS processing.

A wide range of literature on MS has been researched which provides a background review of the fundamental principles surrounding MS-assisted Cu electroplating. A review of the acoustic wave behaviour as it propagates out from a source shows a position dependency on its pressure output, due to the natural focus of the acoustic wave. Changes to the transducer positioning shall be considered as an experimental parameter in future trials. The MS agitation shows additional improvement over US agitation due to improved directionality of the wave, which enables greater precision and control over where the acoustic energy is directed in experimentation.

Previous literature on MS-assisted electroplating was reviewed and its effect on the surface Cu deposit was evaluated. The results obtained showed a change in the Cu

surface crystallinity, due to both an increase in ion replenishment and a negative influence on the bath additives. The surface plating produced previously with MS would be an issue in PCB manufacture, as it forms a low-quality electrodeposit in terms of crystallinity. Methods to improve quality shall be investigated in the thesis by changing the acoustic power output and the plating current.

The literature describing the microscale influence on ion diffusion due to high frequency US was reviewed and enhancements were identified in the literature due to diffusion layer reduction, which lead to increased limited current densities.

A large repository of literature exists on MS agitation applied within microfluidic devices. In this work a range of acoustic artefacts were identified which play a critical role in describing the motions of microfluidic currents within micro-channels. The artefacts were influenced by microbubbles and the acoustic resonance of the chambers. These artefacts would likely be reconstructed under a MS Cu plating setting and so, to describe the results of the MS plating trials, an insight into acoustic artefacts is required to develop a description of the plating mechanism.

An analysis of a PCB internal composition was reviewed which highlighted that its construction influenced the uniformity of the surface Cu deposit. This effect was useful to consider when performing evaluations of the PCB surface after MS plating in the thesis investigations.

A description of the fabrication of via interconnects on PCBs was made and the economic benefits due to MS processing were highlighted by increases in aspect ratio size. A review was also made of wafer manufacture and the high aspect ratio TSV interconnects used in them. The size of the TSV features applied in the wafer manufacture are smaller than the features within the PCB industry and so the chemistries and Cu plating rates could not be transferred into the PCB industry to achieve the same high aspect ratios. The same plating issues were identified within wafer manufacture as in PCB manufacture and so increases to TSV plating performance may also be possible with the introduction of MS agitation, which is beyond the scope of this body of work.

A review of the different quality tests performed by a PCB manufacturer to ensure consistency in manufacture was provided. These tests were not performed in the thesis but were outlined as potential further areas to research.

Chapter 3 Experimental Details

This chapter discusses in detail the experimental setup for the different experiments performed with the Megasonic (MS) transducer. This includes section 3.1 which discusses the bath synthesis, section 3.2 for the bath setup and analysis, and section 3.3 for the characterisation methods used in the investigations. Section 3.4 evaluates the ideal transducer setup for MS plating from measures of flow rate in the bath and the impact of the transducer on plating by current thieving. The final section 3.5 discusses the experimental setup and conditions used in computation simulations of MS agitations down THV-like structures.

3.1 Bath Synthesis and maintenance

CU110 is the sulphate-based Cu plating solution used in the thesis investigations as provided by Schloetter Ltd. It is comprised of copper sulphate, which provides the cupric ions for deposition, sulphuric acid, which aids the solution conductivity in the form of sulphate ions and the chloride ions, which act as an accelerant. Hydrochloric acid (HCl) provides the chloride ions in the bath, which are essential to the correct operation of the additive system, by providing support - electrolytes to the bath, thus increasing the conductivity of the bath. With correct application the HCl and the additives enable a uniform dissolution of the anodes when plating.

The bath synthesis for CU110 chemistry is outlined in Table 3.1. When first formulating the bath, a reservoir of additive Cu111 is built up, afterwards it is maintained through addition of the Cu114 additive, which contains Cu111 within its formulation. When setting up the plating chemistry the bath composition is made up to the recommended quantities.

The sulphuric acid, copper sulphate and chloride levels are monitored through titration measures. This is performed on a monthly basis by the Company Schloetter, the suppliers to Merlin, which report back the bath levels and the substitutions required. The plating bath additives can be maintained by either the monitoring of total ampere hour (Ah) plated, or use of a Hull Cell. 'Ah' is the measure of the total electrical current supplied to a plating bath in hour units, where a current of 10 A over an hour is 10 Ah. The method of maintaining additive levels by measuring Ah is an efficient method only when a bath is continuously used, i.e. for a minimum duration of six hours a day. If a plating tank is infrequently used, the additive levels will still continue to deplete

regardless of the low load on the tank. The infrequent use of the bath in the MS plating investigations means that a hull cell is a more appropriate method of additive maintenance rather than monitoring Ah. The operation of a Hull Cell is covered in section 3.3.1.

The plating temperature of the bath should be set at 25°C, within the manufacturer's recommended range of 22°C to 35°C. Low temperatures will induce limited current plating on the PCB and increases in temperature will result in increased additive consumption [57].

Trouble shooting to find the corrective measures for problems exhibited on the PCB under standard plating can be found in the CU110 operational procedure by Schloetter. The cleanliness of the bath solution is maintained by its circulation through an external filter, which pumps at a rate of 2 - 3 bath turnovers per hour, or 970 – 1455 Litres per hour. The filter retains particles in solution of diameters 10 µm or less, removing unwanted debris fallen into the open-top baths and copper formed in solution, both of which can generate surface defects.

Table 3.1 - CU110 chemical composition, concentration and operating conditions.

Bath chemical component	Quantity	Maintenance
Sulphuric acid, H ₂ SO ₄	100 ml/L	Monitored by sending off monthly sample to Schloetter
Copper Sulphate Solution, CuSO ₄ .5H ₂ O	75 g/L	
Chloride	80 mg/L	
Starter Cu 111	7 ml/L	Monitored through hull cell analysis
Additive Cu 114	5 ml/L	
De-ionised H ₂ O	Make up to bath	Top up bath levels when dropped below ideal volume
Temperature	22 – 35 °C (25 °C ideal)	Temperature gauge within bath

3.1.1 Cathodic efficiency for plating setup

The cathodic efficiency for the plating setup used was evaluated from measures of the average plating rate on blank panels plated without the MS. The experiment was with the anode and cathode setup as outlined in Figure 3.15 in Chapter 3, although without the transducer. The bath was dummy plated before reviewing the plating efficiency, to the procedure outlined in section 3.2.2. A PCB of size 5.29 dm² was plated at 2 A/dm² for 30 min under standard agitation conditions and solution parameters.

The plating rate as recommended by the solution supplier Schloetter Ltd for 2 A/dm² output was 26.7 µm/hr [18]. The average plating rate measured across the PCB surface at five different positions was 22.0 ± 5 µm/hr which equates to a cathodic

efficiency of approximately 80 %. This low efficiency could have been due to the electrical connectivity of the rectifier to the electrodes. In the setup of an electrical rectifier the cable diameter and length are important factors influencing the power reaching the anodes. The length of cable used and their width were not evaluated before the rectifier was installed for use and were configured for a larger sizes rectifier. For this reason the resistance in the cables could have been high due to the larger current loads expected.

The low cathodic efficiency will be considered for the investigations performed in the thesis.

3.1.2 Electroless copper plating setup and composition

Prior to electroplating experiments involving via interconnects, all of the test PCBs are electroless plated with 1 μm to 2 μm of Cu. The copper is deposited down the MacDermid Ltd plating line at Merlin Circuit Technology Ltd. The chemical formulation for the electroless process along with the operational conditions are outlined in Table 3.2. The process is performed by the operators at Merlin and it is assumed for the investigation that the solution is formulated and maintained by them to the conditions outlined by Macdermid.

Table 3.2 – Electroless Copper solution composition as supplied by MacDermid Ltd.

Electroless Solution Constituent	Chemical Used	Solution Concentration (M)	Mass/Vol (g/L)	Solution/Vol (mL/L)
Copper Sulphate	Copper Sulphate	-	1.8 - 2.2	-
Caustic	NaOH	-	8.0 - 10.0	-
Chelator, Complexant	Proprietary	0.10 - 0.14	-	-
Reducing agent	Formaldehyde as HCHO 37%	-	3.5 - 4.5	5 ml/L of 37%
Stabiliser	Contained within proprietary solution	-	< 2.00	-
Accelerator	Unsure whether contained within proprietary solution	-	-	-
Temperature (°C)	40 - 46			
pH	12			

3.2 Bath equipment Setup

The plating bath used in the investigations is a 500 L tank, filled to a volume of 485 L to prevent overflow. The bath components required for correct operation includes

anode baskets, a heater and temperature gauge, inlet and outlet for the filtration convection flow, sparge pipes for bubble agitation, and a cathode rail. Highlighted in Figure 3.1 is a schematic of the plating bath with components included.

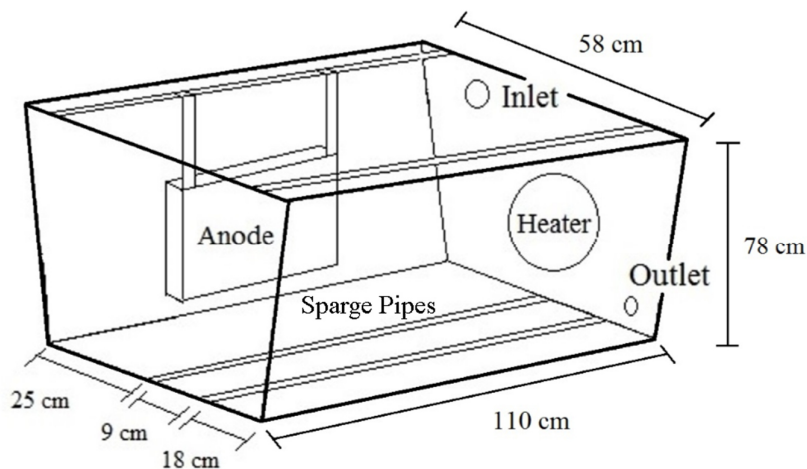


Figure 3.1 - Schematic of the 500 L plating bath with components in place.

The heating of the plating line is controlled by a temperature sensor which is submerged in the plating bath. Due to evaporation, the water level of the bath drops over time and, if it goes below the depth of the temperature sensor, the heater will switch off as a safety precaution. The heater unit, including sensor, is a Galvatek™ Fluoropolymer Immersion heater [107]. The unit is submerged within the plating line and attached to the side wall in the position indicated in Fig 3.1. When using the acoustic agitation, the heater unit shall be positioned away from the line of sight of the acoustic waves so as to negate any potential damage by cavitation.

The solution is pumped out on the wall of the bath next to the heater, where it is passed through a filtration unit housed around the back of the plating line and the filtered solution pumped back in. The pumping filtration unit includes an (AO Smith) motor. The fluid pump's internal filter requires replacing after 3 months of use and will be monitored when performing plating trials.

Sparge pipes are added at the bottom of the bath, which contain holes of increasing diameter spaced at equal intervals. These allow for an equal distribution of air pressure to escape along the pipe, ensuring that the PCB receives an equal agitation of solution, regardless of its position within the bath.

The anode is set up by hanging either a basket filled with soluble Cu balls or an insoluble titanium basket. These two setups are applied for THV plating and BV-filling plating lines, accordingly. Connectivity of the anodes shall be discussed next.

3.2.1 Rectification and electrode connectivity

To operate the plating bath efficiently, the current density drawn from the soluble anode basket and plated on the cathode surface has to be maintained within specific values. These values are the ideal operating conditions and for the anode, the Direct Current (DC) current density should be output between 0.5 A/dm^2 and 2.5 A/dm^2 and the cathode should receive between 1 A/dm^2 and 4 A/dm^2 . Electroplating outside of this scale range will encourage a non-uniform dissolution of the anode, and/or an overly large passivation layer on the anode resulting in poor current density control, leading to non-uniform, smaller than desired, plating rates. The current density on the anode and cathode is controlled by the current supplied to it. Increasing or decreasing the number of anode baskets used in PCB plating will increase or decrease the current density on the anode, respectively. In the plating trials one anode basket was used, due to the small size of the electrical rectifiers employed and the small size of the test PCBs. The tangential distance of the anode basket to the cathode PCB is 21.6 cm. This setting has been optimised for the plating bath geometry by Merlin Circuit, as it maximises the plating uniformity across the PCB [108] and was applied in PCB manufacture prior to the investigations. For this reason all the MS plating investigations shall apply this distance.

The electrical current was supplied by a Dutch Reverse Pulse Plating DRPP™ rectifier [109], which can output a DC or RP field at 1:30, forwards: reverse current, with a maximum current load of 30:90 Amps. In the investigations, plating rates on the PCB were maintained by controlling the PCB size and current output. An efficient plating reaction was ensured throughout the plating trails by accounting for the current density limits of the anode / cathode.

3.2.2 Bath dummyming

Before a bath can be efficiently operated it requires to be run for a minimum duration, to ensure that a passivation layer forms on the soluble anode so as to allow for a controllable output. If dummyming does not occur then the current density will be lower on the PCB surface than calculated using Equation 2.8 displayed in Chapter 2 in section 2.1.5. The bath is dummied for approximately 300 Ah or until it can output an approximate $10 \text{ } \mu\text{m/hr}$ plating rate on the PCB surface at 1 A/dm^2 . This plating rate is lower than the expected for the CU110 chemistry and is attributed to inefficiency in the

plating rectifier caused by a high resistance of electrical cables and not the bath chemistry, see section 3.1.1

3.2.3 50 Hz Cathode Rail Vibration

A VIBTEC™ Vibratechniques Ltd, M3/4, 4 kg, 50 Hz unit [110] was purchased and set up on the electroplating cathode rail. The unit is traditionally used to dislodge air bubbles off a PCB surface during processing. The device is set up as highlighted in Figure 3.2. It is used in THV plating trials in Chapter 6 to evaluate whether further enhancements could be made to MS agitation.

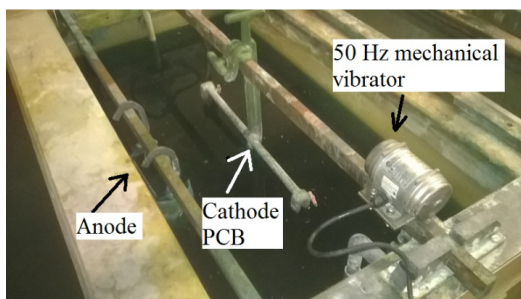


Figure 3.2 - The plating setup implementing a 50 Hz mechanical vibrator.

3.2.4 PCB type used in experiments

The PCBs used in the investigation in the thesis were Ventec Ltd, FR-481 [111] which are a standard type of FR4 material applied for general use and are not a specialist material such as PTFE or Polyimide - which is applied in high frequency signal transmission and high temperature applications [112]. The material was chosen for its relatively low cost and wide use in PCB manufacture. The standard thicknesses used with FR4 are around 1.6 mm. The material is supplied coated in a rolled Cu foil and the standard thickness typically used is 18 μm , which is also referred to in the imperial system as $\frac{1}{2}$ Oz/ft² or $\frac{1}{2}$ Oz for short. Unless otherwise stated, PCBs of this type and size shall be applied in the investigations.

3.3 Characterisation Methods

3.3.1 Hull Cell analysis

The bath additives used in the Cu plating chemistry CU110 are analysed using a Hull Cell analysis. This technique takes a sample of the plating solution, places it into the Hull Cell tank and passes a current through the solution so as to electrodeposit onto a cathode using a soluble anode. After 10 minutes of plating at 2 A/dm², the cathode is

removed from the tank and the plating finish quality is inspected, by qualitatively comparing the severity of the Cu burnt finish formed. Burning is produced in response to plating at limiting current densities and is characterised by a dark burnt / dull finish as discussed in section 2.1.9 in Chapter 2 and is easily recognised. Under an ideal additive setup no burning should be observed.

Highlighted in Figure 3.3A is the Hull Cell tank schematic, showing the cathode's angled orientation relative to the anode. At this position the electrical current distribution is uneven across the cathode and the side closest to the anode receives a higher current and a faster plating rate. The precise slope of the cathode allows the mathematical measurement of the plating rate. This configuration enables, in one plating run, to predict and measure the influence of the plating over a large range of current densities.

If the bath additives are not at the correct levels, then a burnt finish will appear spreading out from the high current region. The severity of the burnt / dull finish categorises the degree of additive replenishment required. Highlighted in Figure 3.3B is an example of two cathodes, one showing a bright finish, top, and the other showing a dull finish spreading across the board, indicated as light on the image due to contrast settings. As such, the plating solution which plated the top cathode requires no alteration and the bottom requires 2 ml/L of the Cu114 additive chemistry.

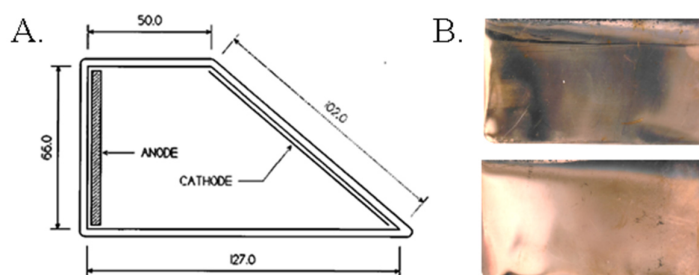


Figure 3.3 - A) top-down schematic of the plating hull cell apparatus. Units in mm. B) Plated hull cell cathodes showing top, no corrections required and bottom, 2 ml/L of Cu114.[18]

3.3.2 Microsectioning / Microscope use

The standard procedure for measuring the Cu plating on a PCB is as follows.

1. Cut out a sample (2cm by 2cm) to be sectioned using a Dremel 200 Multi-tool (RS), (UK).
2. Smooth down the side under observation with grit paper.

3. Place section into holder with smooth side facing down and place in rubber mould.
4. Create a mixture of polymer resin solution FiaFix (Struers) and pour in the required amount to fill the mould.
5. Allow to set for approximately 20 minutes until rigid.
6. Using 800 grade grit paper, grind one edge of the sample until flat and smooth.
7. Remove the 800 grade grit paper and replace with a 1200 grade grit paper. Repeat the grind, increasing the paper grit increments to provide a more uniform, smooth surface.

A Nikon Labophot™ was used and provides a resolution between $2.5\times$ and $20\times$ magnification, capable of measuring $1\text{ }\mu\text{m}$ features. An additional microscope was used to measure the surface of the PCB at a lower resolution. This was a Koolertron™ Digital Microscope. Images were obtained using both devices with accompanying computer software.

Shown in Figure 3.4 is an example of a microsection, imaged using the Labophot™, of deposited Cu. The thickness is approximated, from the copper-air side to a midpoint on the copper-FR4 side. The error associated with this measurement is $\pm 3\text{ }\mu\text{m}$ as the FR4/Cu midpoint is not certain.

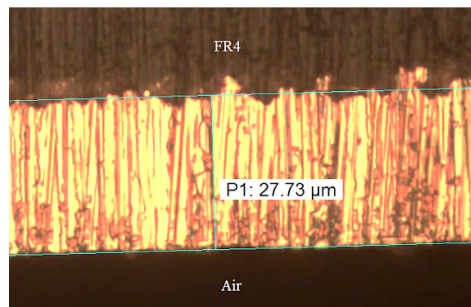


Figure 3.4 - An example of a microsection measurement indicating the thickness of the plated copper.

3.3.3 White light phase shifting interferometer – measurements of roughness

The topography of the plating results was analysed using a NewView™ 8000 Series Zygo Viewmeter white light phase shifting interferometer at HWU. The device enables a 3D topographical map of the surface to be obtained by back reflections of white light off the surface. The data output can provide 3D or 2D images of the surface and from the topographical data, the roughness can be evaluated from measures of R_a the

arithmetic mean height, Rq the geometric average height, and PV the highest to lowest distance.

The device is highlighted in Figure 3.5A and was operated by placing a flat sample under the head of the device as shown in B.

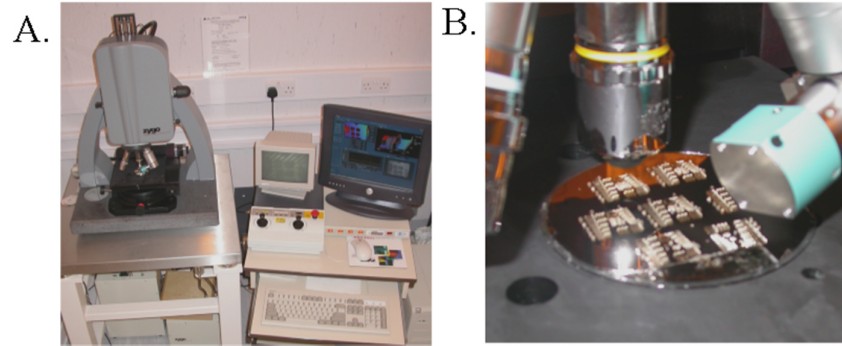


Figure 3.5 – A) NewView™ 8000 Series Zygo Viewmeter white light phase shifting interferometer. B) closeup of circuit under analysis head.[113]

The device was controlled through a computer interface using the software package MetroPro. Its operation procedure is highlighted in Table 3.3.

Table 3.3 - Operational Procedure for NewView™ 8000 Series Zygo Viewmeter.

1. Setup	Setup the motion controller and calibrate the manual stage. Set the focus of the 50X and 100X objectives.
2. Focus	Set the scan length to a length slightly greater than the peak to valley of the sample. Set the microscope starting point. Adjust the coarse focus. If no fringes, adjust stage tip/tilt. Adjust fine focus.
3. Null	Null refers to fringe minimisation. After nulling press F1 to measure.

After measuring the sample post processing was performed in MetroPro to measure the sample's surface. To quantify a surface's roughness one method is to take measurements of height from within a sampling length or area and then take an arithmetic average of peak heights and troughs from the mean height. This measurement is referred to as the Ra .

Another method is by using the root-mean-squared referred to as Rq . Rq is a description of the geometric average height of roughness-component irregularities from the mean line, measured within a sampling length or area. When compared to Ra , Rq is more sensitive to occasional variations in height over a sampling length. The main

noticeable difference between the two values is that the Rq amplifies sporadic variation in peaks or troughs whereas the Ra will average them. For this reason Ra is used in the analysis of Cu plated surfaces.

The Ra alone does not give a complete picture of a surface profile and may give a misleading interpretation. Highlighted in Figure 3.6 are two surfaces with different topographies. They each share the same Ra value, although each displays different structures indicated by a 'peak structure' or a 'valley structure'. In the plating trials it is unlikely that a valley structure would form without an external processing procedure causing a flat topography, such as by a linish. It is more likely that, after plating, a peak structure shall be formed and for this reason the Ra can be used with low risk of a misleading result.

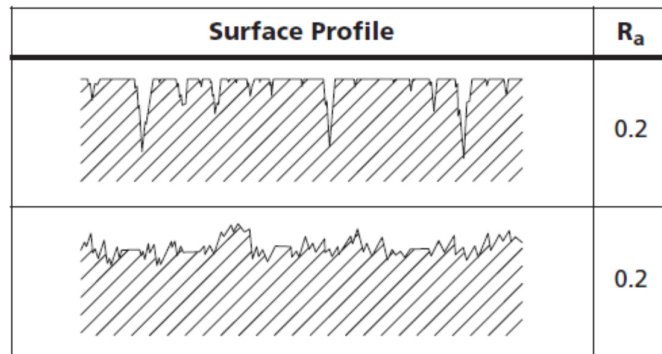


Figure 3.6 - Comparison of two different surface topographies but with the same value for Ra . The top shows a 'valley structure' and the bottom a 'peak structure'. [114]

PV provides a measure of the distance between the highest point to lowest - the peak-to-valley of an undulating feature. When used with Ra it is a useful comparison of how much the features on a surface vary in the extremes.

Ra is typically used in PCB fabrication to quantify the roughness of a surface where typically desired values are around $0.3 \mu\text{m}$ [114]. The electrical signals propagating through a PCB undergo loss due to the dielectric material, which is the PCB laminate and the conductor loss, which is the Cu tracks. The conductor loss is influenced by the scattering loss which is caused by surface roughness of the Cu and the skin effect loss. The total conductor loss increases for increases in surface roughness. The roughness of a PCB surface is also important for the successful bonding of components, as the bond strength of the Cu relies on an anchoring effect and physical and chemical adhesion.

Reducing the roughness reduces the ability to bond and so in PCB manufacture a trade-off between bond strength and signal propagation is made. [7]

In the MS plating investigations Ra was measured using the white-light interferometer and discussed in Chapter 5. These measurements assisted in evaluating the changes to the surface topography in response to MS-agitation and whether a Cu surface could be plated which would be suitable for signal transmission and bonding to.

A PCB is comprised of a glass weave encapsulated in an epoxy resin. The weave causes a natural large scale height variation, defined as waviness, of around $6\text{ }\mu\text{m}$ across the PCB surface [85]. When evaluating Ra the sample length is chosen so that the long wavelength features do not interfere with the calculation. The sampling length area chosen should be large enough to encompass the small-wavelength (roughness) features, yet small enough so that it does not include the large-wavelength (wavy) features. If the sampling length is increased to include the wavy features, then the Ra parameter will be influenced by this and increase.

When measuring the samples, area sizes 2.0 mm^2 , 6.1 mm^2 and 24.4 mm^2 were chosen so that the acoustic features plated could be measured and the large wavelength features excluded, or their effects on the measurements minimised.

3.3.4 Via filling quality: definition and quantification

The ability to deposit copper down via interconnects varies in efficiency dependent on the shape of the via feature and its size. The efficiency of Cu deposition on a PCB feature can be regarded as the amount of Cu deposited over a specific location, compared to the amount deposited in a region which is operated under the ideal electrical and chemical settings for the bath. A drop in plating rate between the two would thus highlight a drop in plating quality owing to variations in electrical or chemical performances.

During via plating the efficiency of the plating reaction was carefully maintained through the operation of the plating rectifier and the bath chemistry. When introducing MS agitation into the plating bath the chemical behaviour is effected by the forced fluid convection through the via structures. For this reason, the ability to force fluid into via features defines the plating quality. The size and shape of the via influences the ability for electrolyte chemistry to flow through the feature, as outlined in section 2.4 in Chapter 2. Highlighted in Figure 3.7A and B are cross-section schematics of THV and BV structures, respectively. Regions are highlighted which will each display different plating rates. In A, the surfaces of the THV typically receive the highest plating efficiency

and further into the via the efficiency drops. In B, a similar trend is observed, where the lowest efficiency is found at the bottom of the BV.

In the plating investigations the plating rates between the surface and inner features of the vias were measured, as these regions clearly displayed if any enhancements to the plating reaction occurred. When comparing different plating setting in the thesis the micro-throwing power will be evaluated to highlight any enhancement to plating, see section 2.1.7, in Chapter 2. This is evaluated from the average plated Cu thicknesses as,

$$\text{Micro – throwing power THV} = \frac{\text{Average thickness in middle}}{\text{Average thickness on surfaces}} \quad (3.1)$$

$$\text{Micro – throwing power BV} = \frac{\text{Average thickness at bottom}}{\text{Average thickness on surface}} \quad (3.2)$$

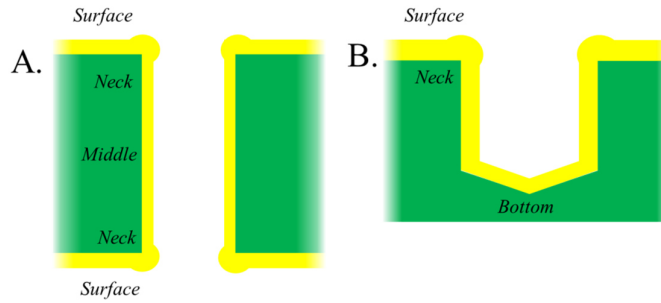


Figure 3.7 - Schematics of the different regions which display varying degrees of plating quality in A) THV and B) BV.

3.4 Transducer setup and configuration

The transducer system, manufactured by Sonosys, [67] is a square-faced submersible composed of four rectangular piezo-transducers, of size 2.5 cm by 11 cm, embedded in a steel sheet of 1.03 dm² area. The piezo-ceramic plates are highlighted internally in Figure 3.8, by an X-ray picture of the device.

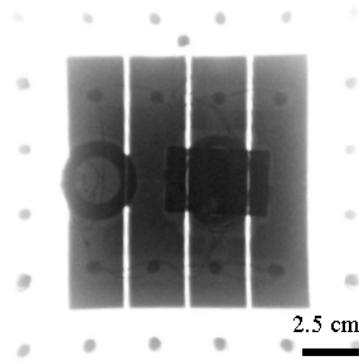


Figure 3.8 - X-ray photograph of the transducer surface. Indicated in the dark regions are piezoelectric transducer crystals.[115]

The PZT outputs a 1 ± 0.05 MHz, acoustic wave with a variable power, where, at 100 %, 500 W of electrical power is supplied to the piezoelectric emitter, which is converted to acoustic power output with a conversion efficiency of around 90 % to give 450 W of acoustic power output.

An analysis of the transducer output was made in [115], using a fibre optic hydrophone. Pressure values of the 1 MHz acoustic wave were obtained in water at set positions. The setup of the apparatus is highlighted in Figure 3.9, showing left: the 1 MHz transducer used in the thesis and right: the hydrophone device with fibre optic measuring probe tip highlighted by arrow. The entire arrangement was submerged in a de-gassed water tank. The fibre optic hydrophone probe tip was connected to a movement stage and measurements were obtained by raster scanning the probe tip over a defined area whilst the transducer was outputting.

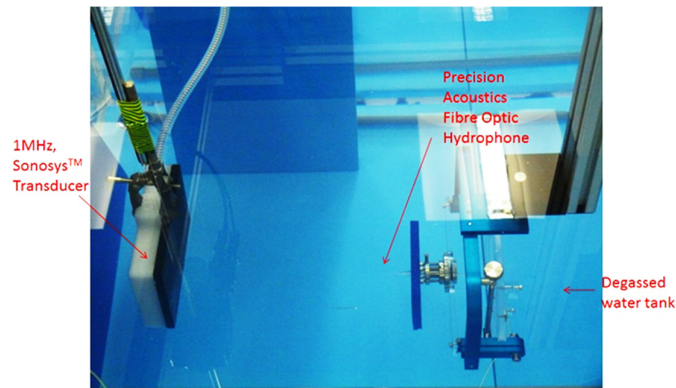


Figure 3.9 - Setup of acoustic pressure measurement performed by HWU group prior to the thesis.[115]

Pressure values were obtained from a scan of the acoustic wave profile tangential to the direction of propagation – the plane parallel to the face of the transducer – as a 1MHz wave was out put at 90 W. Two different profiles were obtained of the pressure distribution at the distances 2.5 cm and 25 cm from the surface of the transducer and were plotted in Figure 3.10A & B, respectively. They reveal that the piezo-ceramic plates influenced the distribution of the waveform, where the highest intensities were obtained from those regions. When applying the MS agitation in plating investigations the localised variations in intensity may influence the outcome. This shall be accounted for by rotating the plated surface or flipping them at set intervals during the plating cycle, to even out the influence by the MS on the overall plating.

At greater distances the acoustic pressure appears to abate, indicated by the reduction in colour intensity in Figure 3.10B. This is a surprising result as the acoustic wave was still within the near-field region at 25 cm, as the far-field was 3.7 m for the 1MHz transducer, see section 2.2.1 in Chapter 2. It is possible that the acoustic wave had not abated and was instead self-focussed as it propagated closer to the near field distance - an effect highlighted in Figure 2.12 in Chapter 2. The acoustic pressure data output in Figure 3.10 was not available for analysis in this thesis. With this data a review of the average energy density could have been applied and any pressure loss with distance could have been quantified. To quantify this another measure of the acoustic output using a hydrophone could be performed, but due to time constraints was not performed. Regardless, for the investigative experiments it was assumed that from these measures the pressured distribution would change with distance and was considered when setting up experiments.

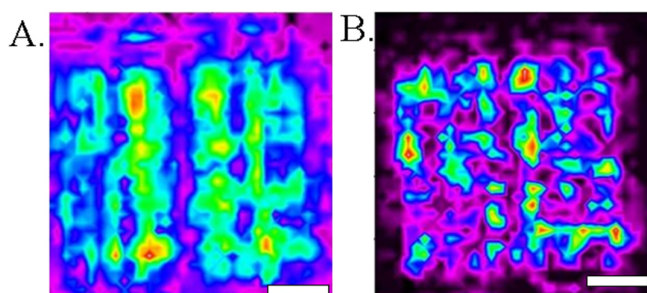


Figure 3.10 - A) & B), profiles of the acoustic pressure distributions measured for the acoustic wave parallel to the active transducer surface, at distances 2.5 cm and 25 cm respectively. Scale on images is 3 cm. Highest pressure (0.220 MPa) indicated in red and the lowest (0.037 MPa) in blue. Transducer setting 1 MHz at 90 W. [115]

The setup of the transducer for use in a plating bath shall be discussed next. Figure 3.11 shows the correct setup of the transducer power unit. Shown in A is the front, where the STANDBY and RF OK are lit up, indicating output to the transducer working correctly. Shown in B is the back of the device highlighting attached grey mains power cable, a transducer power cable and a commuter which controls the on/off output. To switch on the transducer all the components need to be in place and the commuter switched on.

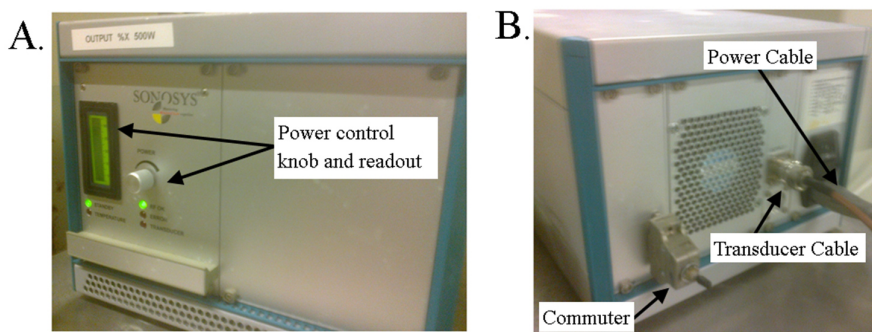


Figure 3.11 - A and B show a correctly setup transducer power unit from the front and back respectively.

The transducer device is inserted into a plating bath through the use of polypropylene scaffolding, which is resistant to the bath chemistry. The transducer face is encased within a plastic holder which allows acid proof protection of its power cable and a means to attach to scaffolding and joints so that the head may be rotated. Shown in Figure 3.12 are images of the transducer attached to the scaffolding. The unit is securely fastened in place with screws and the joints of the apparatus enable 360° motion in the *X-Y* plane and rotation / height change in the *Z*-direction. Figure 3.12A and B show front and back images of the transducer fastened.

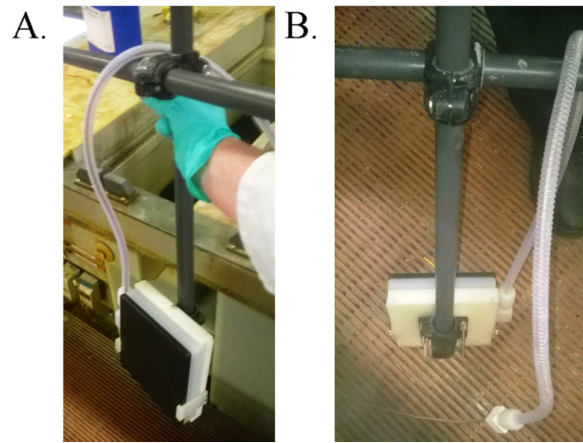


Figure 3.12 - A) & B), front and back view of transducer fixed within scaffolding.

Once the transducer is securely fastened into the scaffolding the unit may be lowered into the plating bath. Figure 3.13 shows a picture of it within the bath. It is placed on the right hand side of the cathode-PCB and opposite the anode basket, which is on the left hand side of the bath. The scaffolding is screwed into the side wall of the bath as indicated.

The transducer outputs a continuous acoustic wave (CW). The introduction of acoustic pulse operation in MS plating is investigated in Chapter 6. The pulsed output is obtained through the application of a pulse modulator to the transducer device.

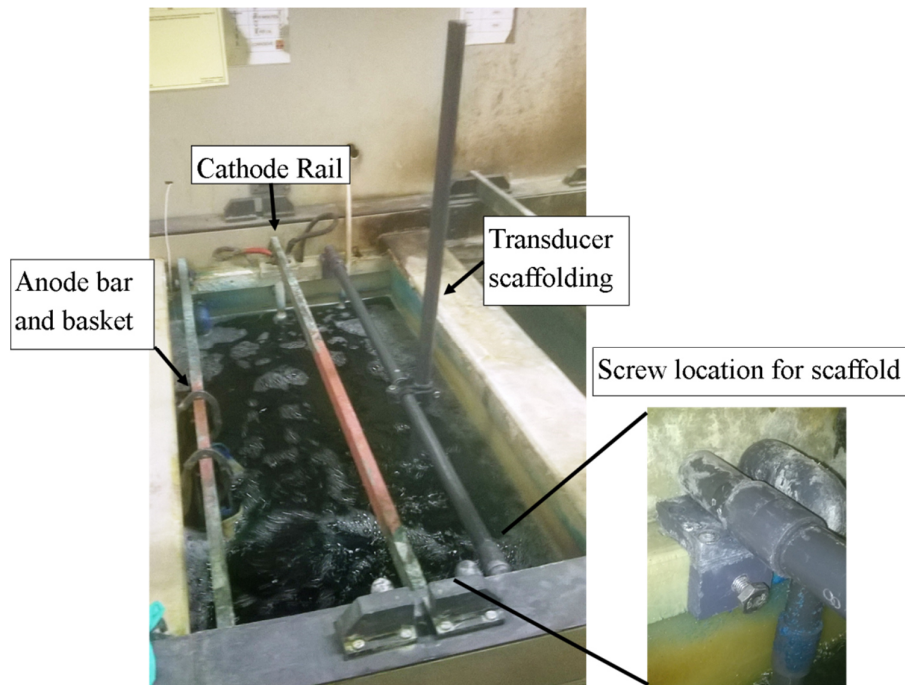


Figure 3.13 - Transducer scaffolding within plating bath.

The acoustic modulator consists of a control circuit board with an electrical connector, as shown in Figure 3.14, which is applied to the transducer unit in the place of the commuter, highlighted in Figure 3.11. Once connected to the transducer the device automatically output the acoustic wave on the setting programmed, which 7 seconds on and 17 seconds was off. This setting is controlled by ensuring that the electrical wire is attached to the port as indicated in Figure 3.14.

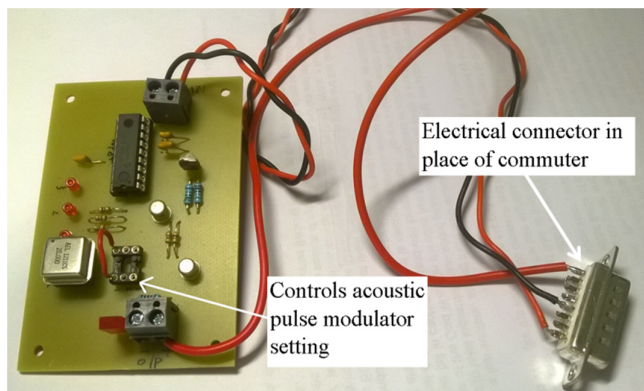


Figure 3.14 - Acoustic pulse modulator circuit.

To operate the transducer without causing damage to the device, it had to be fully submerged in solution and its surface not undergoing any physical contact with a solid surface. Figure 3.15 displays a schematic of the transducer placement within the plating bath applied during the MS plating investigations. The bath is fitted with components and is filled with solution up to 485 L. The possible movement of the transducer is indicated by the arrows. A simplified schematic of the setup of the transducer is shown in Figure 3.16 highlighting the tangential distance x from the transducer to the PCB.

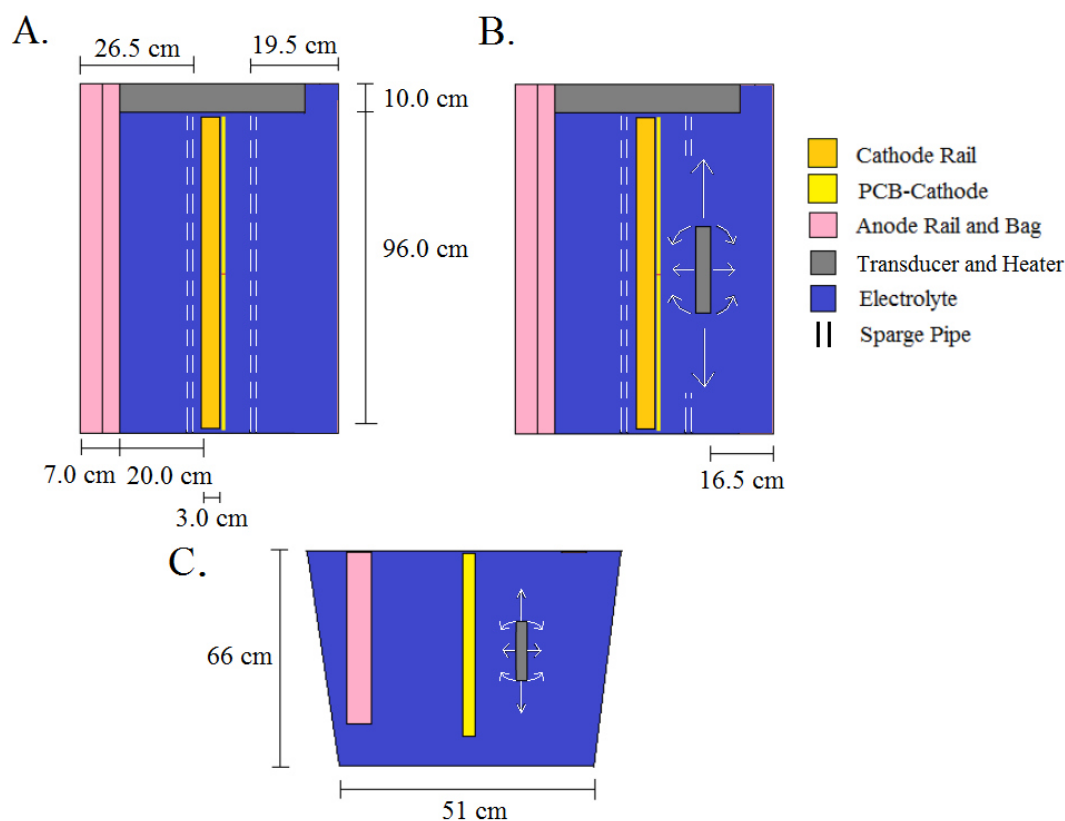


Figure 3.15 - Schematics of the plating bath with components included showing, A), a top-down view without the transducer, B), with and C) a side-on view with.

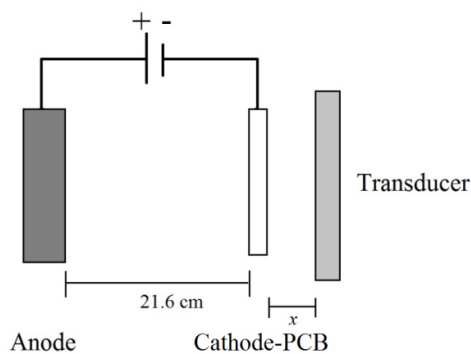


Figure 3.16 - A schematic of the plating cell setup indicating tangential distance x from PCB to transducer.

Inserting foreign objects into an electroplating bath is ill-advised due to limited space considerations. The plating bath is arranged so that sufficient fluid circulation may occur within, to maintain high plating efficiencies on the PCB surface and to allow for the electrical anodes the uniform supply of a current from the anode to the PCB cathode.

It is unknown how the transducer will influence the plating bath or how it can be set up to maximise MS effects on the PCB surface. For these reasons, it is useful before via interconnect plating trials to, *a)* evaluate how the electrical current is disrupted on the PCB surface due to potential thieving effects and, *b)* determine how the acoustic streaming behaves over the fluid medium within a 500 L plating bath. These two experiments provide an understanding of how the MS plating trials should be performed on an industrial scale, whilst maintaining the best control over the bath parameters. These are addressed next.

3.4.1 Current thieving by the transducer

If an electrically conductive surface with grounding is placed into an electroplating bath alongside a PCB, when current is applied it will be driven towards both electrical surfaces. The total current density within the bath will distribute and share with the other conductive surface, decreasing the current density on the PCB. The additional electrode is then said to act as a current thief.

With acoustic transducers setup in a plating cell, observations in [116, 117] highlight that the surface of the transducer can act as a current thief, reducing the current received at the PCB. This behaviour reduces control over the PCB current density when MS plating. The transducer acts as a current thief due to the electrical grounding. Removing the grounding is possible through the addition of a non-conductive layer upon the surface, although this interferes with the transmission properties of the device and so would have to be carefully applied in the manufacture of the transducer, so as to enable an efficient, high power output.

A series of initial MS plating trials are performed, to observe whether current thieving can be observed with the Sonosys, 1 MHz transducer. This is evaluated by looking at how plating rates on a PCB surface vary on changes to the tangential distance of the transducer from the PCB, as any Coulombic attraction by the transducer surface will decrease with distance from the source, i.e. the anode [118].

The plating bath is set up as indicated in Figure 3.15 and Figure 3.16 with the tangential distance highlighted by x and the plating performed at 1.5 A/dm² DC for 30 minutes. The transducer distances plated at are 1 cm, 4.5 cm, and 8 cm. For all trials, the acoustic power is not switched on, as the trials are only to evaluate whether or not current thieving is present with the device.

The plating performance is evaluated from the total amount of Cu plated for the plating cycle. This is determined by measuring the mass of the PCB before and after

electroplating, using a Ohaus Explorer [119] measuring balance. The difference in weight, measured as an increase, highlights the amount of Cu electroplated. From this value, the amount of Cu deposited tangential to the PCB surface is evaluated by dividing by the value for Cu density in $\text{g}/\mu\text{m}^3$, to give the volume of Cu deposited in μm^3 . This volume is then converted to μm by dividing by the total area plated and then converted to the tangential plating rate by dividing by the duration plated.

The plating trials are repeated four times and an average obtained. These values are plotted on Figure 3.17 along with their standard deviations included on the error bars. The variation is not sufficiently large as to impede analysis. Without the transducer in the bath, the plating rate is comparable to plating with the device at 4.5 cm and 8 cm away from the PCB surface. When plating with the transducer at 1 cm, the plating rate on average is 8 % less than plating without the transducer. These results show that when plating with the transducer setup at distances less than 4.5 cm from the PCB, current thieving is present, attracting electrical current away from the PCB and reducing the total amount of Cu deposited. When performing further MS plating investigations current thieving by the transducer will be considered in the setup.

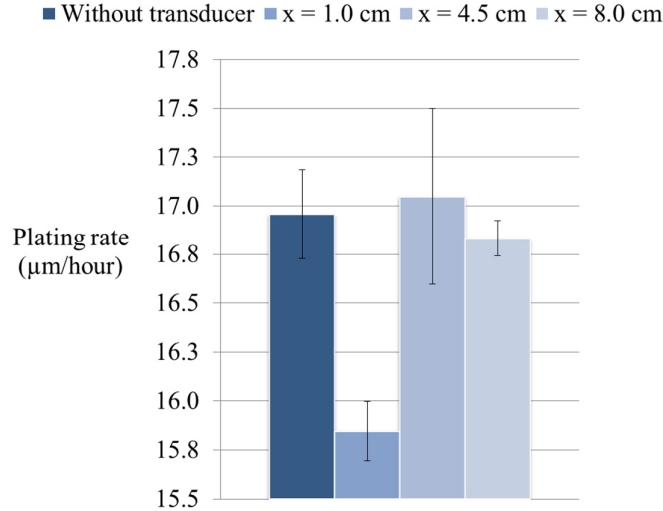


Figure 3.17 - A plot of the plating rate measured with transducer setup a tangential distance x to the PCB surface and outputting zero agitation.

3.4.2 Fluid circulation

The plating performance of Cu is heavily influenced by fluid convection within a bath, as the replenishment of Cu ions is provided from the forcing of solution around the PCB. Bath convections are influenced by the fluid pump, panel movement and sparge-

pipe bubble agitations. The introduction of MS agitation will introduce a fourth bath convection. To ensure the greatest uniformity and highest output of MS streaming onto the PCB surface, investigations are performed looking into how the transducer position alters the fluid flow rates. The solution flow is recorded from motions of food dye colourant flowing through the bath, with a Genius™ webcam installed above the plating bath, as shown in Figure 3.18.

The trials are set up by installing the transducer in positions *a* to *c*, highlighted in Figure 3.19B, where position *c* is oriented at 45° to the PCB. At each position a recording of the fluid flow is obtained, where the dye is added in front of the transducer to the positions numbered in 3.17A. MS acoustic waves are emitted from the device at 100% output corresponding to 450 W, with an orientation indicated by the arrows. From the recordings, an approximation for the fluid flow rate around the PCB is made, by measuring the distance travelled by the colourant over time. Bath agitation by bubbles is not reviewed in the trials, as it is not possible to observe the motion of the colourant within the bath when it is switched on.



Figure 3.18 - Camera rig above bath.

The trials are set up by installing the transducer in positions *a* to *c*, highlighted in Figure 3.19B by the grey rectangles, where position *c* is oriented at 45° to the PCB. At each position a recording of the fluid flow is obtained, where the dye is added in front of the transducer to the positions numbered in Figure 3.19A. MS acoustic waves are emitted from the device at 100% output corresponding to 450 W, with an orientation indicated by the arrows. From the recordings, an approximation for the fluid flow rate around the PCB is made, by measuring the distance travelled by the colourant over time. Bath agitation by bubbles is not reviewed in the trials, as it is not possible to observe the motion of the colourant within the bath when it is switched on.

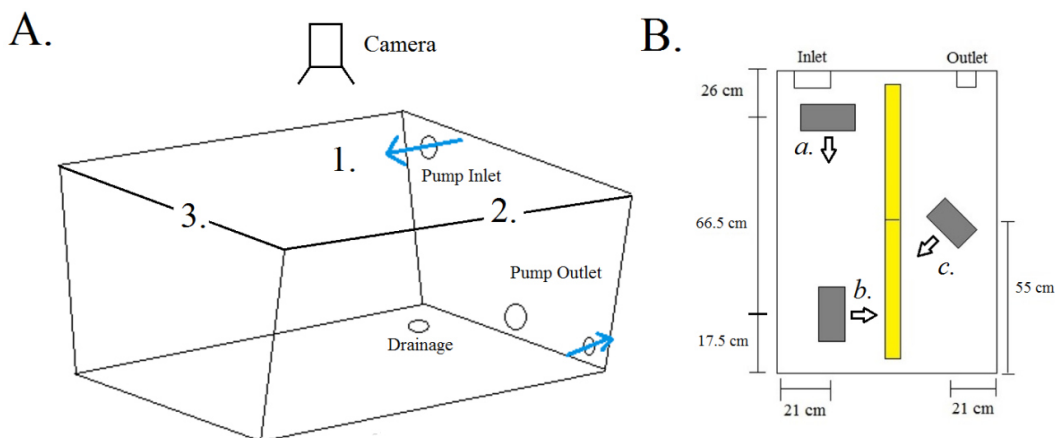


Figure 3.19 - Schematics of the plating bath setup for without the transducer A) and with B) as shown in different orientations and positions by the grey rectangles. The orientation of the emitted acoustic wave is highlighted by the arrows.

The flow rates are evaluated and displayed in Figure 3.20, showing the flow orientation and its approximate flow rate when under MS agitation. In A, the panel movement and the inlet and outlet pumps circulate solution over and around PCBs placed within the bath. The flow rates are faster around the fluid pumps due to the pumping action.

With the transducer added and switched on, as in B, the flow rates measured in response to the MS streaming are up to 150 % faster than the flow rates obtained under standard bath agitation at the same locations. The faster flow rates show that in the bulk solution, the MS acoustic streaming is considerably greater than the bath motions due to panel movement or the pump.

The transducer device is small relative to the size of a PCB and the size of the bath. The MS streaming slows by 40% as it propagates over a large distance, which is due to attenuation of the wave. To induce a larger streaming flow onto the PCB close transducer distances should be applied. When the transducer is introduced at a 45° angle to the PCB, the acoustic streaming flow spreads over the surface of the PCB as indicated by position *c* shown in Figure 3.20B. To achieve a larger coverage of the acoustic wave across the PCB an angled orientation of the transducer could be applied.

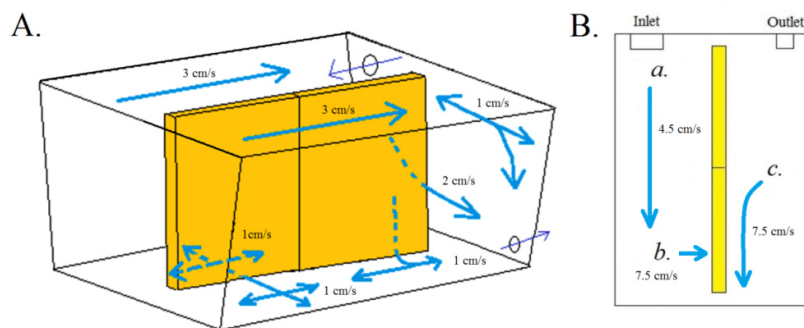


Figure 3.20 - Fluid motion rates evaluated with two 18" by 24" PCBs in bath for A), panel movement and the fluid pump activated and B), the transducer switched on at locations a - c.

3.4.3 Conclusions

The initial investigations of the transducer device setup have shown that the Sonosys 1MHz transducer acts as a current-thief and is detrimental to plating rate control within the bath. To reduce this effect, the transducer should be positioned at a tangential distance no less than 4.5 cm from the PCB. The motions of the bath fluid are analysed and reveal that a large fluid flux increase is observed due to MS streaming, although the flow rate abates with distance travelled. To maximise fluid flow rates onto the PCB, which in turn maximise the diffusion layer shrinkage, see section 2.2.3 in Chapter 2, the transducer should be placed as close as possible to the PCB surface, taking into account the current thieving effects. The area sonicated by the acoustic wave is proportional to the face of the transducer, 1.03 dm^2 , as shown in Figure 3.8, and so, to increase the coverage by the MS streaming, and thus the reduction of diffusion layer across the PCB, an angled orientation of the transducer can be applied.

When performing fluid flow experiments with the transducer damage is induced upon the polypropylene plating tank wall. The damage is indicated by a burning smell originating from the wall of the tank opposite the MS agitation and visually, by a smoky haze across the bath and the melting of the outside tank wall. These effects are present after several minutes of MS agitation at 100% output, when directed to the wall of the tank at a distance. The effect is most likely due to localised thermal increases of the portion of the wall sonicated, brought on by unstable cavitation, see section 2.2.6 in Chapter 2. The melting point of a polypropylene bath is $210 - 290 \text{ }^{\circ}\text{C}$ [120] and so the MS agitation is a considerable health risk, as is it could lead to destruction and leaking of the plating bath releasing the highly acidic chemistry. To prevent damage to the walls it is found that when the MS waves are directed towards the PCB in the middle of the bath,

they are absorbed and no damage is induced on the wall in-line with its propagation. When performing MS plating experiments for the following body of work, stray MS waves are absorbed by lining the walls of the tank with blank PCBs and by placing an anode basket in the line-of-site of the transducer behind the PCB, whether or not the anode is used for plating. It is found that applying this method results in no more occurrences of melting.

3.5 COMSOL Simulation Setup

The software package COMSOL Multiphysics is a general purpose software platform for the modelling and simulating of physics-based problems. Version 4.3b is used to model hydro-acoustic behaviour in a simulated reconstruction of the plating settings within a THV, to assist in the analysis of MS plated results. The scattering model simulation package is used as it provides a representation of travelling acoustic-wave behaviour as it scatters in response to objects within its path of propagation. The simulation operates by calculating the total acoustic field, evaluated as the sum of the background acoustic field of defined frequency and pressure, and its scatter response to objects within its path. The simulation obtained is static in that it does not propagate in time and instead provides a snap-shot of the pressure distribution at an instant. The scattering simulation operation is highlighted in Figure 3.21, which shows the total acoustic field as a superposition of the acoustic pressures, highlighting high pressure by red, low pressure by blue and no pressure with white. The figure represents an acoustic wave of particular frequency interacting with an object of high acoustic impedance of a size similar to half of the acoustic wavelength.

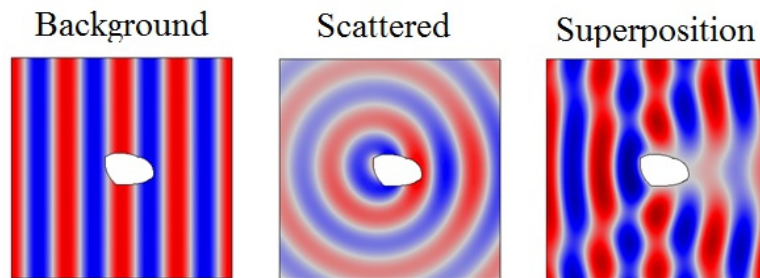


Figure 3.21 - 2D representation of the multiphysics computational configuration for acoustic scattering in COMSOL. Representation shows an acoustic wave of particular frequency interacting with an object of high acoustic impedance which is of a size similar to a half of the acoustic wavelength.

When modelling the acoustic scattering behaviour, the entire PCB cannot be reconstructed due to the large area of the plating tank relative to the small THV features on the PCB. Instead a small area is modelled in and around the THV cavity. For this reason the edges of the simulation do not represent a solid, hard boundary at which the acoustic wave is reflected, like the walls of the plating bath. Instead, the computational domain is simulated with open boundaries – that is, boundaries through which an acoustic wave will pass without any reflection. COMSOL offers several solutions for this in the form of Scattering Boundary Conditions (SBC) and Perfectly Matched Layers (PML). The PML is not a boundary condition, but rather a domain added to the exterior of the model that absorbs all outgoing waves. Although PMLs are theoretically non-reflecting, they do exhibit some reflections due to the numerical discretisation: its mesh. To minimise this reflection a mesh is applied within the PML that aligns with the anisotropy in the material. The PML will absorb propagating waves as well as evanescent waves which display superior absorption capabilities over the SBC. For this reason a PML was used instead of an SBC in the simulations.[121]

The PML domains were chosen so that they faced the oncoming travelling wave, to prevent reflection in the oncoming orientation. The PML regions were highlighted in Figure 3.22A by the blue and represent PML setup 1. This PML setup was applied under circumstances where the scattered acoustic wave did not deviate significantly from its original propagation direction. It was applied to reduce the simulation time. The simulations for which this was applied were the modelling of the acoustic wave as it propagated through the PCB board, displayed in section 5.1.2 in chapter 5.

When the acoustic wave scatters in multiple directions the entire edge of the model is allocated as a PML domain. This is highlighted in Figure 3.22C and is PML setup 2. For the simulations performed in Chapter 5 both PML setup 1 and 2 were tested and no significant changes were observed. For this reason setup 1 was performed for the remainder of the simulations in Chapter 5, which enabled a quicker simulation time. The simulation performed in Chapter 6 involved reflections in multiple directions and so setup 2 was employed to prevent reflections from the outer edge from influencing the results.

In order to dampen the outgoing acoustic waves optimally, the meshing of the PML is best performed with a quadratic mesh. For PML setup 1 & 2 this is built as highlighted in Figure 3.22B and D, respectively.

The size of the PML for all simulations was set at a third of the size of the wavelength within the solution. This specific value was taken from the COMSOL manual

on acoustic scattering, where the same setting was applied[122]. Simulations were performed (not shown) increasing the PML to a factor of two times larger than the acoustic wavelength in the solution. Regardless of the changes to PML, little variation in the scattered behaviour was qualitatively observed in the outcome, so to simplify the simulation setup, a small PML, of a third the size of the acoustic wavelength, was applied in all the simulation investigations.

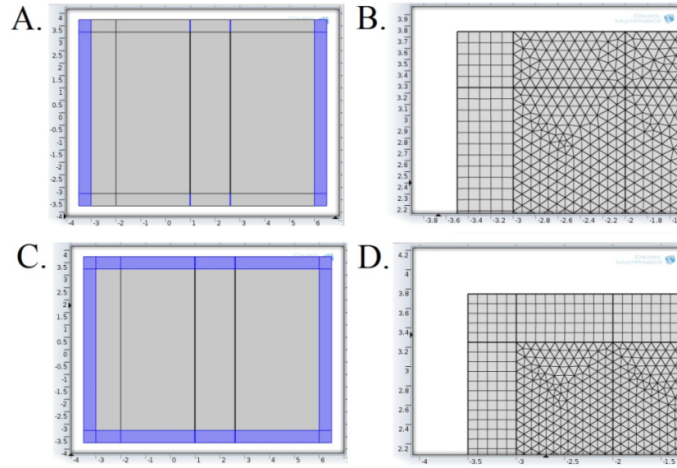


Figure 3.22 - A) PML setup 1 and B) a close-up of its mesh. C) PML setup 2 and D) a close-up of its mesh.

The scattering simulation operates by employing a background plane wave acoustic field with a chosen propagation direction. The background field is applied to the simulation by selecting a specific domain. Once an area is chosen the background field will propagate out from the area of its origin in the direction selected, reducing in intensity due to attenuation of the wave. Highlighted on Figure 3.23 is the setup of the background wave with the domain highlighted in blue. Two different setups are modelled. In A, the background field is chosen to cover over the entire electrolyte medium excluding the FR4. The purpose for this approximation is to effectively model changes in angle of propagation which will be studied later in section 6.3.3 in Chapter 6. In B, the background domain is represented by a small rectangular shape to the left of the PCB. Under this setup the transducer within the plating bath next to the PCB is more effectively modelled and is applied when simulating acoustic behaviour when the acoustic propagation remains fixed.

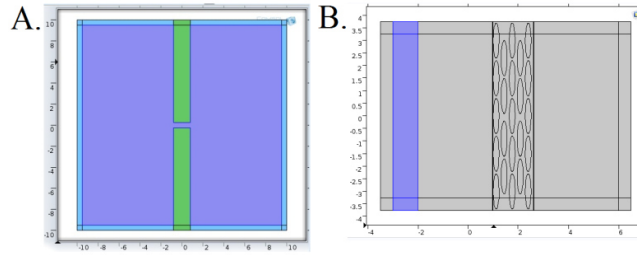


Figure 3.23 - Different simulation setups showing background acoustic domain positions highlighted in blue covering A) the entire fluid domain and B) a partial section modelling transducer device.

Cavity structures are simulated under a 2D setting to minimise simulation time and size. The THV cavity is modelled as a gap between two FR4 structures, as highlighted in Figure 3.24. COMSOL enables individual sections of a simulation to be selected where the sections are referred to as domains. Altering the acoustic properties of the domains allows an accurate model of the FR4 acoustic properties to be constructed. The simulation is set up such that the background domain is modelled in the fluid and a superposition produced by combining this field with the scatter response to the FR4.

Two models of the THV are created, one containing an approximation to the structure of the glass weave and the resin, as outlined in Figure 2.23 in Chapter 2, and the other, approximating the entire FR4 structure with one set of acoustic properties. The two models are highlighted in A, and B, accordingly. These two models are chosen as the more complex model required longer simulation duration and provides a more accurate approximation, whereas the simpler model could be performed more quickly and a wider range of parameters simulated. The individual material domains are characterised by their own sound speeds and densities, and values used are displayed in Table 3.4.

When setting up the simulation the background acoustic pressure value is input manually. Making changes to this value appears to create no noticeable variation in the pressure distribution, only the magnitude of the pressure maxima and minima. This is due to the limits of the scattering simulation as the COMSOL software makes approximations for the acoustic behaviour, only simulating linear acoustic effects rather than non-linear acoustic effects, which alter on acoustic pressure magnitude[63]. For this reason, a starter pressure of 1 Pa is chosen in all the simulations.

After the simulations investigations are performed, post processing is carried out on the simulated data. The pressure distribution within the THV cavity structure is measured on changes to transducer angle. To perform this operation multiple lines are

generated within the THV cavity using the 2D plot lines function, as indicted in Figure 3.24D. Pressure values are then obtained along these lines revealing the pressure distribution within the area plotted. Using this data, values of the acoustic potential energy density are evaluated, as will be discussed next.

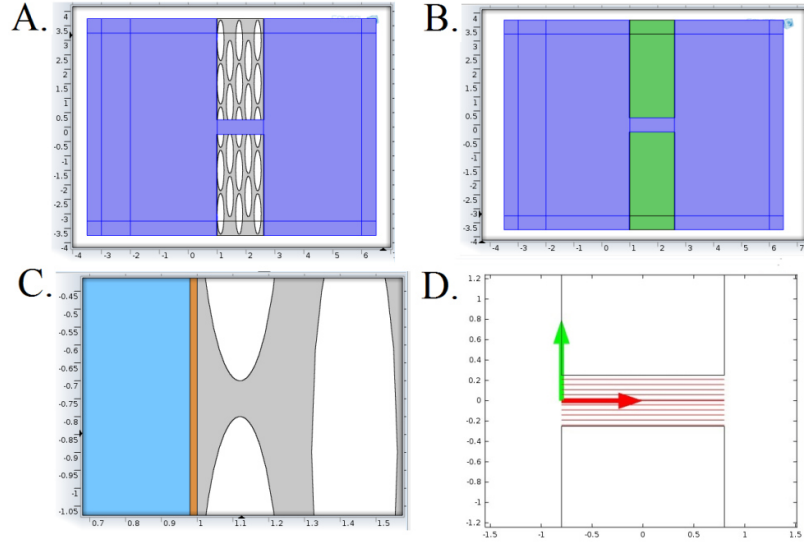


Figure 3.24 - Schematic of 2D simulated area for THV cavity containing A) internal PCB structure and B) a simplified approximation to PCB. C) close-up of PCB internal structure highlighting glass in white, resin in grey, Cu in orange and electrolyte in blue. D) 2D cutlines in red to map pressure within THV cavity.

Table 3.4 - Properties for the different material domains.[123-128]

Material Parameter	Copper	Water	Epoxy Resin	Silica Glass	FR4 Approximation
Density (kg/m^3)	8700	1000	1200	2203	1900
Sound Speed (m/s)	4600	1482	2140	5968	3602
Relative permeability (unitless)	1	-	-	1	1
Electrical Conductivity (S/m)	5.998×10^7	5.5×10^{-6}	-	1×10^{-14}	0.004
Coefficient of thermal expansion (1/K)	17×10^{-6}	-	-	0.55×10^{-6}	18×10^{-6}
Heat capacity at constant pressure ($\text{J}/[\text{kg} \cdot \text{K}]$)	385	4179	1000	703	1369
Relative permittivity	1	-	-	2.09	4.5
Thermal conductivity ($\text{W}/[\text{m} \cdot \text{K}]$)	400	0.6	0.2	1.38	0.3
Young's modulus (Pa)	110×10^9	-	-	73.1×10^9	22×10^9
Poisson's ratio (unitless)	0.35	-	-	0.17	0.28
Reference resistivity ($\Omega \cdot \text{m}$)	1.72×10^{-8}	-	-	-	-
Resistivity temperature coefficient (1/K)	0.0039	-	-	-	-
Dynamic viscosity (Pa.s)	-	1.002	0.006	-	-
Refractive Index	-	-	-	1.45	-
Ratio of specific heats (unitless)	-	1	-	-	-

3.5.1 Evaluation of the average potential Energy Density

Measures of the pressure are obtained within the THV in response to changes of the scattering behaviour. From these the average potential energy density (PED) is evaluated, which describes the displacement of an infinitesimal element from equilibrium position in response to the acoustic wave. It is given by:

$$PED = \frac{\langle p^2 \rangle}{2\rho c^2} \quad (3.3)$$

where $\langle p^2 \rangle$ is the average squared pressure over an area, ρ the density of the medium and c the speed of sound in the medium. In the simulation the PED is evaluated over a selected area using values for the sound speed and density of the medium. [73]

3.5.2 COMSOL scattering simulations

Three different simulations are performed to complement studies into MS plating behaviours on the PCB. The simulation settings are outlined in Table 3.5, along with the Chapter section they are applied in. For each simulation the PML, background domain and PCB structure are separately chosen to efficiently and effectively approximate the scattering behaviour.

Table 3.5 - Simulation settings.

Simulation Purpose	Chapter Included In	PML Setting Used	Background Domain Selection	PCB Structure	Simulation Outcome
Modelling how internal structure of the THV influenced acoustic pressure at the PCB / electrolyte interface.	CH5, Section 5.1.2	Setup 1	Small rectangle on the left hand side	Complex internal structure	Qualitative observations of the acoustic behaviour at the PCB / electrolyte interface.
Modelling the acoustic pressure distribution within THV cavities in response to changes in diameter and Cu thickness.	CH6, Section 6.3.1	Setup 2	Small rectangle on the left hand side	Simplified model	Qualitative observations of pressure distribution within THV cavity.
Modelling changes to acoustic pressure within THV in response to alteration of the background propagation orientation of the acoustic wave.	CH6, Section 6.3.3	Setup 2	Entire electrolyte domain	Simplified model	Qualitative observation of pressure distribution and quantitative measures of PED.

3.6 General Conclusions

The setup of the plating bath for experimentation was discussed, noting the individual components and their positioning within the bath. This includes the transducer device, the electrical rectifier, the anode rails and the agitation devices. The chemical

preparation of the bath was noted, mentioning the precursory dummy plating required for efficient plating.

The analytical techniques used to monitor the performance of the bath were outlined, as well as the instrumentation used to analyse the quality of the PCB after plating trials. The different definitions of a high-quality deposit were discussed, noting the regions of interest down a THV and a BV after plating.

Plating trials were performed to evaluate the effect of current thieving by the transducer on the deposition of Cu, for placements of the transducer close to the PCB. The results enabled an efficient positioning of the transducer to be evaluated, where its negative impact on plating could be minimised by placing it at a minimum distance from the PCB.

Trials were performed to evaluate the impact of the acoustic streaming force on the bulk fluid flow rates in the bath. The trials provided evidence that the acoustic waves could propagate the length of the tank under different orientations of the transducer and that its agitation increased the bulk flow rate by 150 % compared to the flow rate under panel movement agitation.

The setup for different COMSOL simulations performed and described in later chapters was outlined. Their different conditions were highlighted indicating the boundary conditions, the position of the acoustic background wave and the material properties of the simulated structures. The evaluation of the potential energy density using pressure values obtained from simulation was described and the individual simulations performed were summarised in a table.

Chapter 4 Panel Plating using Megasonic Assisted Agitation

Megasonic (MS) plating trials were performed as soon as the bath setup was prepared. The first trials investigated how the plating behaviour on the outside of the PCB was influenced by the high frequency acoustic waves. The condition of the plated Cu finish on the surface of the Printed Circuit Board (PCB) is critical to further processing and so the MS plating quality was evaluated on the surface before via plating.

A series of investigations were performed to demonstrate how the plating behaviour varied with changes to the transducer settings. These included transducer positioning and acoustic output intensity. Other parameters included bath temperature and current density. The plating was reviewed on PCBs which did not have via interconnect features or electrical tracks on their surface. When plating these boards their entire surfaces were plated with Cu which is referred to as panel plating, see section 2.1.5 in Chapter 2. It was chosen that the board would have no features to simplify the analysis of the MS-assisted Cu plated on the surfaces, as it was uncertain the exact interplay the MS plating would have with the inclusion of these features. This was addressed later in Chapters 6 and 7.

For some of the plating trials a Scanning Electron Microscope (SEM) was used at HWU to image the PCB surfaces after plating. The samples for imaging were prepared by cutting out a 1 cm² sample off the surface using a Dremel saw. The SEM device was operated and images obtained with assistance from staff at Heriot-Watt University (HWU).

4.1 Cu crystallinity variation with pressure

A PCB Cu finish provides an indicator of plating quality. For example, a ductile and uniform coverage of Cu is an example of a good plating process. If air pockets exist in a deposit then expansion of gas in the cavity may cause the board to fracture and, in the worst case scenario, result in an opening of the electrical circuit. Grain structure is influenced by all of the plating parameters, where a change made to one parameter can induce an undesired grain structure change. For this reason, the bath chemistry is carefully formulated by the chemical suppliers and maintained by the PCB fabricator, so as to ensure a high quality electrodeposit, as indicated in section 2.1.3 in Chapter 2.[129]

Plating experiment 4.1a was performed looking at how the plated finish altered with the introduction of MS and how applying additional agitation by panel movement changed the behaviour. The transducer was set up as indicated in section 3.4 in Chapter 3, under conditions outlined in Table 4.1.

Table 4.1 - Experimental conditions for experiment 4.1a.

Experiment Number	Plating Parameter Investigated	Experiment Parameters			Measurement Obtained	Purpose
4.1a	Acoustic Power	Transducer	Tangential Position to PCB X (cm)	10	Qualitative observation of Cu grain structure using an optical camera.	Reveal influence of acoustic wave on Cu surface and with the inclusion of panel movement.
			Acoustic power output (W)	0 and 225		
		Current Density (A/dm ²)	2			
		Plating Duration (min)	60			

PCBs were electroplated at 2 A/dm² separately, without panel movement and with MS agitation, with panel movement and MS and lastly with panel movement and without MS. Images of the surface finish after plating were obtained with a Samsung MultiXpress scanner and are displayed in Figure 4.1 A – C, accordingly. The pattern observed in B and C highlights areas of different Cu composition, where dark patterns relate to shinier regions. The patterns are not typically observed after plating as shown in C, highlighting that they were an effect directly produced by the acoustic wave.

The patterns produced in Figure 4.1A show a similar appearance to the acoustic wave pressure distribution output by the transducer under similar settings, as shown in Figure 3.10 in Chapter 3. The output on the PCB finish displays the pattern of the pressure wave and the individual acoustic contributions made by the four piezo-ceramic plates, which form the transducer device. The direct influence on plated finish by acoustic streaming is indicated in the dark region in the image and covers an area approximately 2.56 dm², which is of an area approximately 150 % larger than the transducer face as indicated in Chapter 3. The increase in area is due to acoustic streaming across the PCB surface.

With panel movement included, the patterns produced in Figure 4.1B show that the acoustic influence can still be witnessed, but it becomes more dispersed and uniformly distributed. The two results in A and B show that, with MS, the plated finish crystallinity displays a fine-grain, shiny deposit within the area sonicated, corresponding to the acoustic pressure distribution and that with panel movement agitation, the acoustic distribution pattern on the PCB surface becomes disturbed.

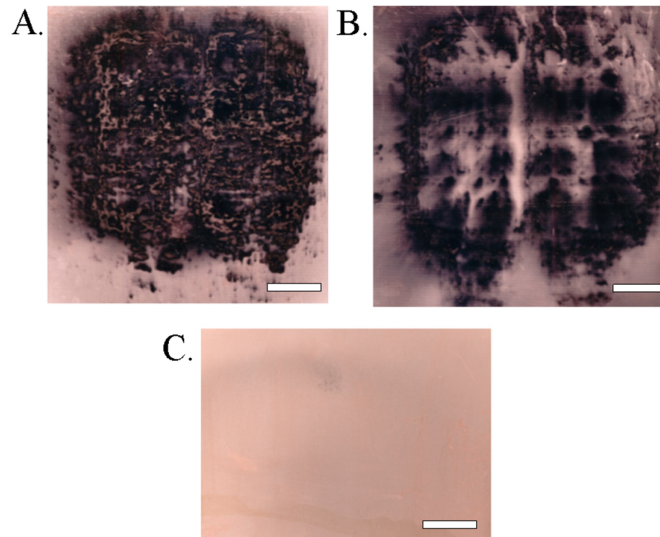


Figure 4.1 - Top-down images of plated Cu finish on PCB after 2 A/dm^2 plating for 1 hour with A) without panel movement and 225 W MS B) with and 225 W MS C) with and no MS, 0 W. Scale on the images is 3 cm.

Two further PCBs were plated in experiment 4.1b under conditions outlined in Table 4.2.

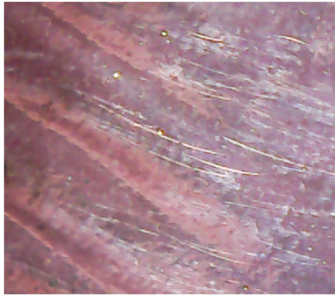

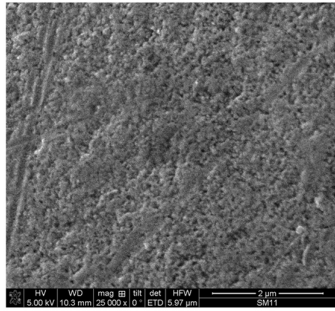
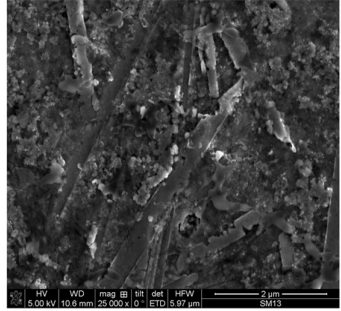
Table 4.2 - Experimental conditions for experiment 4.1b.

Experiment Number	Plating Parameters Investigated	Experiment Parameters			Measurement Obtained	Purpose
4.1b	Acoustic Power	Transducer	Tangential Position to PCB X (cm)	1	Qualitative observation of Cu grain structure using Optical Microscope and SEM.	Reveal acoustic influence on surface chemical additives.
			Acoustic power output (W)	0 and 225		
		Current Density (A/dm^2)	4			
		Plating Duration (min)	30			

PCBs were plated at 4 A/dm^2 and with the transducer set up tangentially 1 cm away from the PCB surface. Results are displayed in Table 4.3. After MS plating the finish appeared shiny in certain regions a result which is indicative of a fine grain deposit, similar to the micro-scale image of the PCB plated under silent conditions. With MS, the micro-scale SEM image revealed spiky, whisker-like, randomly oriented grains. Cu whiskers are characteristic of an electrodeposit formed by poor chemical additive performance and high current density. They are different from dendritic deposits, which have a fractal-like appearance [130]. The whiskers were layered due to diffusion-limited aggregation of the Cu. The filament/granular nature of the Cu whisker growth is due to

the uninterrupted crystal facets as they were quickly deposited on the PCB due to the high current density. The random nature of the whisker orientation is likely due to the protruding tips, which locally increase the electrical current density and enhanced their growth relative to the surrounding uniform Cu structures [131]. The spiky deposits are not prevalent over the entire surface of the PCB, enabling the appearance of a shiny deposit on the macroscale. Regardless, the spiky deposits which were present are likely to cause issues for PCB quality, particularly with reference to its structural stability, as large crystals are more susceptible to fracturing and breaking [6]. For this reason the mechanical properties of the deposit may not be sufficient to match global PCB quality standards set by the Association Connecting Electronics Industries (IPC) [132].

Table 4.3 - Macro-scale and micro-scale SEM images for surfaces plated at 4 A/dm² for 30 min and with the transducer setup a 1 cm under varying acoustic power outputs.

	4 A/dm ² , 0 W	4 A/dm ² , 225 W
Macro-scale		
Micro-scale		

4.2 Transducer tangential distance variation

The scaffolding arrangement of the transducer enables movement of the device within the plating bath. A minimum distance for the transducer has been determined in Chapter 3, to limit current-thieving effects impacting on plating rates, although little work has been performed to quantify the impact of the transducer distance on the surface finish produced. The literature suggests that reductions in distance will increase the acoustic pressure reaching the PCB due to attenuation [55]. The following investigation, 4.2, seeks to evaluate the influence on the MS plated finish produced, by changing the tangential

distance of the transducer, as the acoustic streaming force is reduced. The transducer was setup as outlined in Chapter 3 and PCBs were plated under conditions outlined in Table 4.4.

Table 4.4 - Experimental conditions for experiment 4.2.

Experiment Number	Plating Parameter Investigated	Experiment Parameters			Measurement Obtained	Purpose
4.2	Acoustic Power	Transducer	Tangential Position to PCB X (cm)	1 and 10	Quantitative measurements of Ra in response to changes to acoustic transducer tangential distance, obtained using a white light interferometer.	Notes how Ra changes with distance highlighting position-dependent influence on plated finish quality.
			Acoustic power output (W)	0 and 225		
		Current Density (A/dm ²)	2			
		Plating Duration (min)	30			

Highlighted in Figure 4.2A and B are two top-down images of the 6.1 mm² PCB surface areas processed with MS. Variations in height are indicated by changes of colour and by the cross-section profiles. The labels A and B highlight two different plated PCBs, with the transducer setup at distances of 10 cm and 1 cm, respectively, and plated under conditions outlined in Table 4.4. Dark regions in the figure can either be due to steep and vertical protrusions, depressions, or saturation of the detector due to high reflectivity of the surface. In Figure 4.2A, these dark pixels are large in size whereas in Figure 4.2B, they are more numerous but smaller. These features are observed only on PCBs which have undergone MS agitation. It is uncertain from the image if the features are peaks or depressions, although it is likely that they originate from cavitation features, as discussed in section 2.2.6 in Chapter 2. If this is the case, then the reduction of pressure of the acoustic wave due to the increase in transducer distance encourages the formation of larger cavitation features [133]. These qualitative results highlight that closer transducer distances increase the micro-roughness of the PCB surfaces, where smaller cavitation-sized features are favoured. The profile height variations in both pictures reveal similar maximum Peak-to-Valley of 2.83 μ m and 2.51 μ m, respectively.

When compared to the silent conditions highlighted in Figure 4.2C, the roughness Ra increased by 37% and 47% for the transducer, when positioned at 10 cm and 1 cm, respectively. This showed that with MS agitation the surface roughness increases significantly at large acoustic powers (225 W). As the transducer was positioned from 1 to 10 cm away from the PCB surface, measurements of Ra revealed an increase in surface roughness of 7%. This variation is relatively small and could be accounted for by random

errors in the data, brought on by the large wavy features across the PCB surface, as explained in section 3.3.3 in Chapter 3. When sampling the PCB surface, it was difficult to choose a sample area to accommodate for the waviness of the PCB, as the cavitation features varied in size. A sampling length smaller than 6.1 mm^2 would miss the features highlighted in Figure 4.2A, but not the features in Figure 4.2B [134].

Using the interferometer, measurements of Ra and Peak-to-Valley distances indicated little quantifiable variation between the two surfaces, although plots of the two surfaces displayed qualitative differences in micro-roughening. This highlights that, as the transducer-PCB distance is reduced with corresponding increase of transducer power, the larger resulting pressure increases the number of cavitation features but not their magnitude.

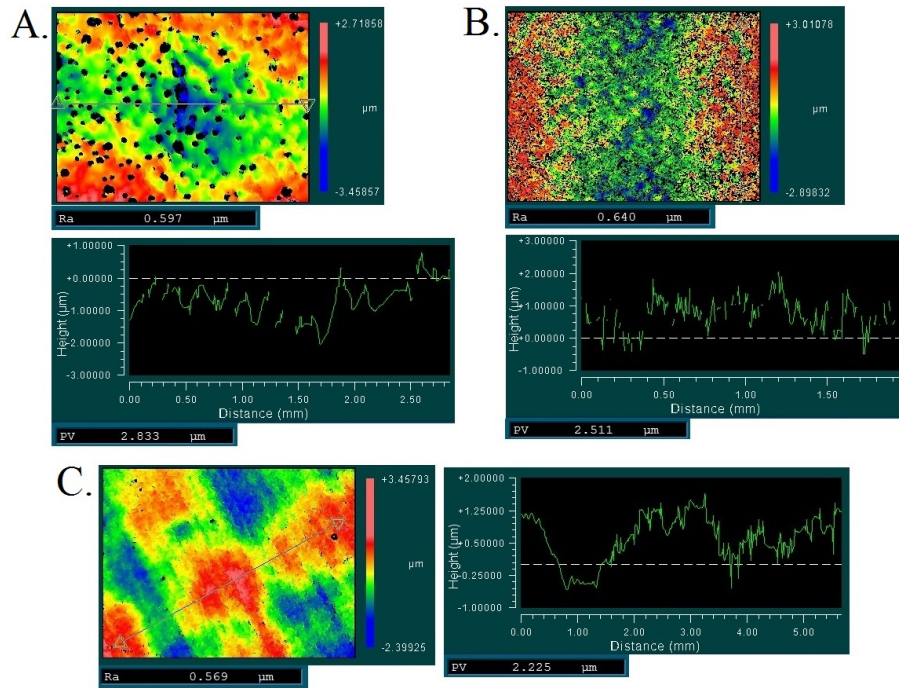


Figure 4.2 - White light interferometer plots of PCB surfaces plated under 2 A/dm^2 DC for 30 min showing of areas 6.1 mm^2 , with cross-section profiles included underneath showing, A) a 6.1 mm^2 area produced from the transducer positioned 10 cm from the PCB and outputting at 225 W, B) a 6.1 mm^2 area produced from the transducer positioned 1 cm and outputting at 225 W and C) a 24.4 mm^2 area for no transducer.

4.3 Transducer power variation

The transducer enables the output power to be controlled from 0 – 100% in increments of 5 %. It is unclear what the exact relationship is between the acoustic output

and the enhancements to plating in terms of acoustic streaming and plating rate. Characterising any variation of surface topography is vital in developing the ideal conditions for processing and so, experiment 4.3 was performed to investigate the influence of the transducer power output on the plated surface finish.

Five different PCBs were plated under increasing acoustic powers of 0 W; 45 W; 90 W; 225 W; and 450 W, under conditions outlined in Table 4.5.

Table 4.5 - Experimental conditions for experiment 4.3.

Experiment Number	Plating Parameter Investigated	Experiment Parameters			Measurement Obtained	Purpose
4.3	Acoustic Power	Transducer	Tangential Position to PCB X (cm)	1	Quantitative measurements of Ra in response to changes in acoustic transducer power output, obtained using white light interferometer.	Highlight power-dependent influence on plated finish quality.
			Acoustic power output (W)	0, 45, 90, 225 & 450		
		Current Density (A/dm ²)	2			
		Plating Duration (min)	30			

Measurements of R_a were obtained using a white light phase shifting interferometer, setup under conditions outlined in section 3.3.3 in Chapter 3. The results were plotted against power increase, as displayed in Figure 4.3. For each measurement, the transducer was set up and the same plating settings applied although changing the acoustic power per plating cycle as indicated in Table 4.5. R_a was measured over two areas, 2.0 mm^2 and 6.1 mm^2 and a single measurement was obtained for each area and for this reason an evaluation of the variation per measurement could not be made. For the small area, and for an increase of acoustic power from 45 W to 450 W, the R_a decreased by 5%. This suggests that the surface becomes smoother in response to increased acoustic agitation, which contradicts previous research into acoustic agitation effects, see previous section and section 2.2.6 in Chapter 2, which highlighted increased micro-roughening on prolonged sonication. When R_a was evaluated over a larger area, 6.1 mm^2 , it increased by 90% as the output power increased from 45 to 450 W. These results showed a different trend to those demonstrated for the smaller area. The possible reason for this switch in trend could be due to the size of the features detected. Any roughness induced due to sonication was most likely a result of cavitation. The cavitation features were typically crater-like in size. If the sample area was too small to detect the cavitation craters features, then upon increase of MS power, the increases in crater frequency or the pit depths may

not have been detected. For this reason measuring over a larger sample area appeared to detect the changes in Ra due to MS cavitation.

For the 6.1 mm² sample between 0 W and 45 W there was a 9% decrease in Ra . This was contrary to the trend observed on power increase after 90 W. It is possible that the natural variation of roughness due to the glass weave influenced this result, adding a random variation to the data. As mentioned in Chapter 3, if a sample area is large enough then it may measure long wavelength, wavy features of the underlying PCB weave. If this was the case, then Ra may randomly increase / decrease between sample measures at that scale. The low output power of the transducer may have resulted in a roughness change too small to detect over the natural variation.

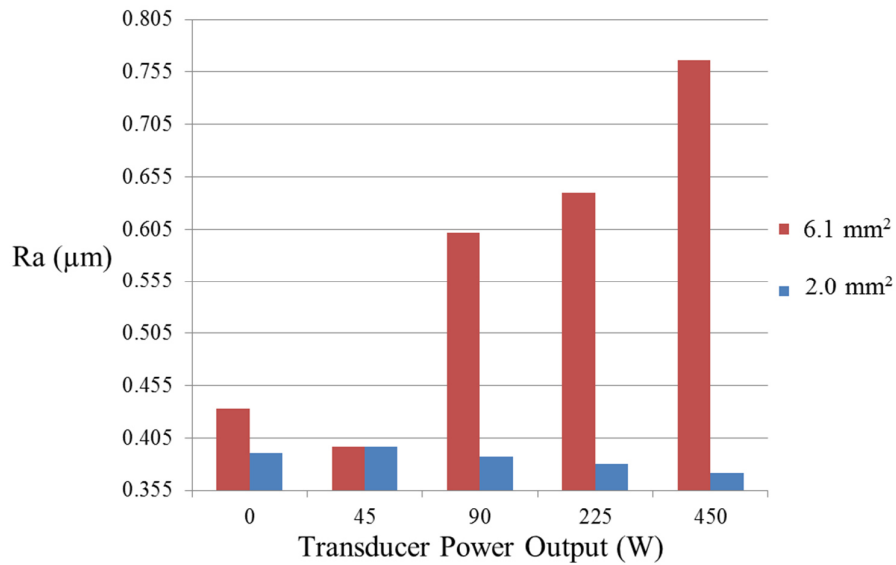


Figure 4.3 - A plot of Ra measured using a white light interferometer for areas 2.0 mm² and 6.1 mm², highlighting the variation in response to transducer acoustic power output.

To investigate this further, data from the interferometer was used to plot top-down images of the electroplated surface for 0 W and 45 W as indicated in Figure 4.4. Under silent conditions the wavy features were observed on the PCB, contributing to an approximate 2 μm Peak-to-Valley height. At 45 W, the surface displayed considerable micro-roughening, which was not detected by the interferometer in the evaluation for Ra , highlighting the limitation of the measurement device. To improve accuracy for this reading a smaller sampling area could have been used, although this would have had to be larger than 2 mm².

For transducer powers larger than 45 W the increased roughness measured was most likely due to cavitation effects, where higher acoustic pressures enhanced their frequency, as observed when the transducer was setup at smaller distance scales, as in the previous investigation in section 4.2. It is uncertain over which area-scale the impact on roughness, due to cavitation forces, was most evident, although this was observable over the 6.1 mm² scale. At this scale, the results showed that the natural undulations of the PCB laminate have an impact on the measurement for surface roughness, making it difficult to extract their influence at low power outputs.

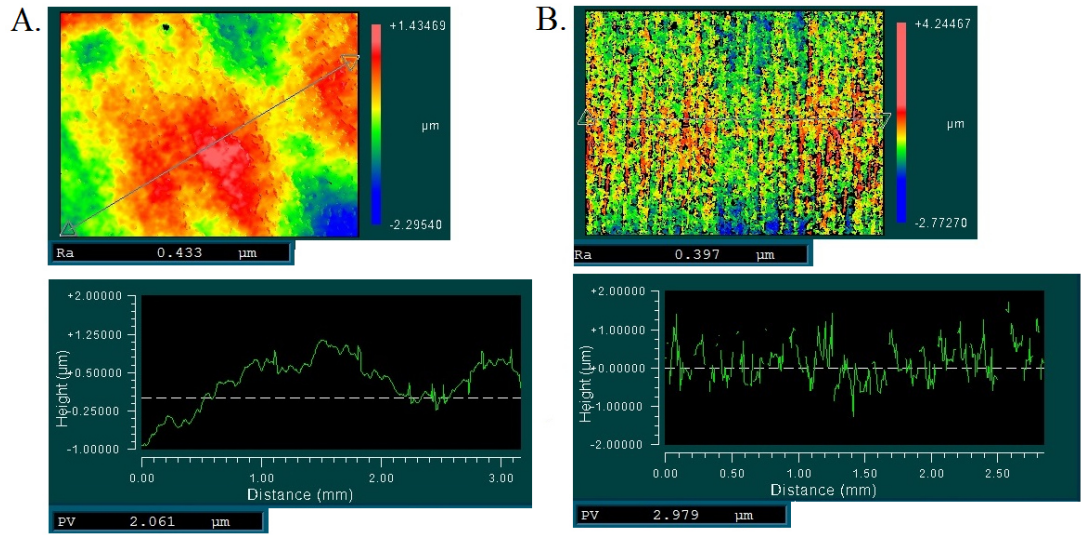


Figure 4.4 - Top-down images of PCB surfaces plated at 2 A/dm² for 30 min, with the transducer setup at 1 cm showing areas 6.1 mm² using a white light interferometry with cross section profiles included underneath. Labels A and B indicate 0 and 45 W output power, respectively.

4.4 Current density alteration due to MS

Placing the transducer at a distance close to the PCB diverted the current away from the PCB, reducing the plating rate, as outlined in Chapter 3. As such it had to be placed at a minimum tangential distance from the PCB, which would reduce the acoustic pressure reaching the surface due to attenuation. It is uncertain whether the reductions in pressure induced will reduce MS plating capability from those witnessed in previous research. For this reason an evaluation of the impact of thieving on the plated finish quality must be performed.

The following experiment, 4.4, explores how changes to transducer position altered the deposited Cu crystalline properties, through changes of the electrical current

distribution. Three PCBs were plated. One with the transducer positioned 1cm away from the PCB surface and the transducer outputting at 225 W, one with the transducer in place but no output and one without the transducer in the bath. The PCB sizes were 5.20 dm² which was larger than the 1.03 dm² area undergoing agitation. The PCBs were plated under the setting indicated in Table 4.6.

Table 4.6 – Experimental conditions for experiment 4.4.

Experiment Number	Plating Parameter Investigated	Experiment Parameters			Measurement Obtained	Purpose
4.4	Electrical Current Density	Transducer	Tangential Position to PCB X (cm)	1	Qualitative observations of Cu grain structure using SEM and optical camera in response to current density variation across PCB surface.	Highlights distance dependent current thieving effect by transducer device and characterises adverse plating produced in response.
			Acoustic power output (W)	0, 225		
		Current Density (A/dm ²)	1			
		Plating Duration (min)	30			

After the plating cycle, images were obtained of the PCB surfaces using a Samsung MultiXpress scanner. The plating results are displayed in Figure 4.5. In A, three Cu finishes were witnessed across the surface characterised by (1) a sandpaper-like texture, appearing as shiny frost-like speckles at the centre of the PCB, which typically occur at plating current densities 0.5 A/dm², (2), a smooth, bright finish surrounding the middle frosted region occurring at plating current density 1.0 A/dm² and (3), a nodular, powdery dark finish at the edge of the PCB which occurs due to limited-current plating which in this case was 2 A/dm². In B, with the transducer in place but not outputting, a similar plating effect was observed with different plating regions highlighting that the effect was not unique to when acoustic waves were present. In C, without the transducer switched on a uniform Cu deposition was obtained which was standard plating behaviour.

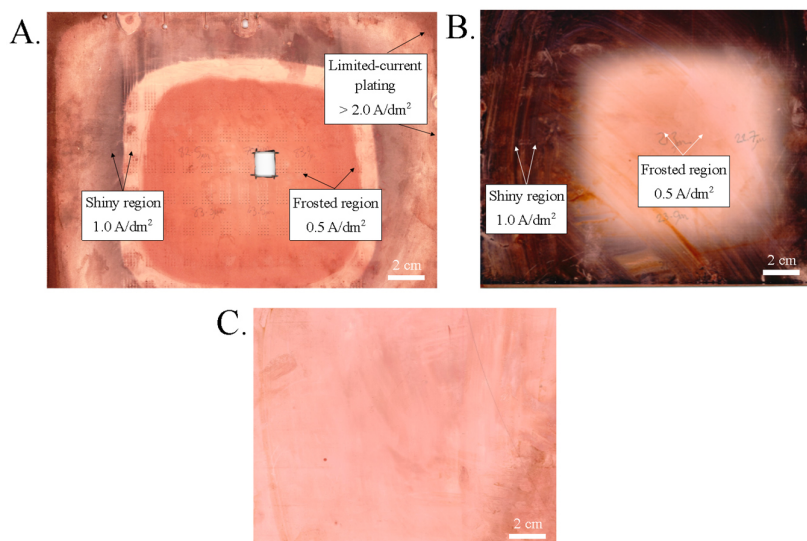
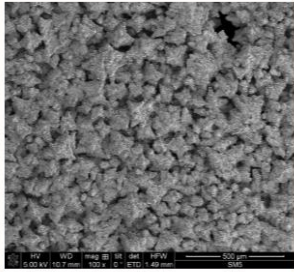
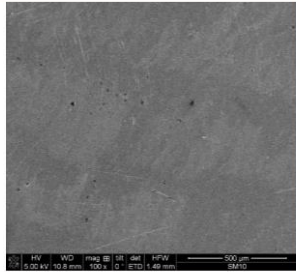
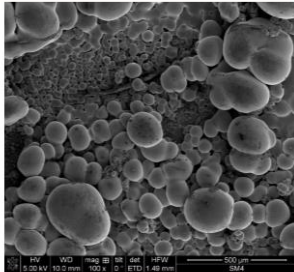
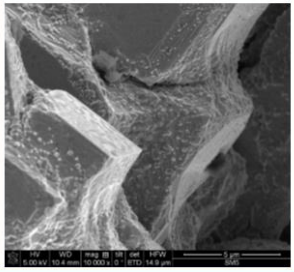
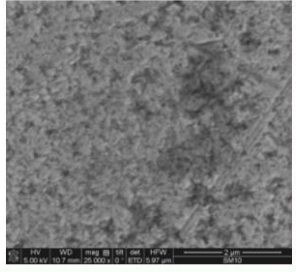
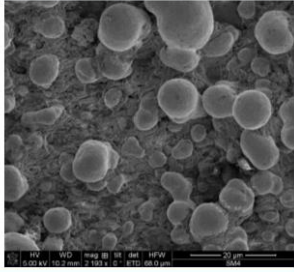


Figure 4.5 – PCB surfaces after 1 A/dm^2 plating for 30 min showing A) different plated finishes observed on a PCB surface plated with a transducer at 1 cm outputting at 225 W, B) different plated finishes observed on a PCB surface plated with a transducer at 1 cm outputting at 0 W and C) plated surface with no transducer in bath.

SEM images were obtained of the three regions indicated in Figure 4.5A and were displayed in Table 4.7 at high and low microscope resolutions. As explained in sections 2.1.5 and 2.1.3 in Chapter 2, and section 3.4.1 in Chapter 3, the three finishes are characteristic of changes brought on by variations to the electrical current distribution and the behaviour of the chemical additives across the PCB. For electroplating under current settings lower than 0.5 A/dm^2 , the SEM images show that large Cu face-centre-cubic crystals (fcc) assemble themselves in a cubic arrangement of larger crystals. The cubic arrangement could be attributed to an un-disrupted crystalline growth of the fcc structure of Cu and the deposit is columnar in nature, which suggests that the deposition occurs along individual grain boundaries [135, 136]. Evidence for individual monolayers is highlighted on the cubic structure in the high-resolution image. These layers were formed from the Cu cations being deposited from the solution onto the crystal face, indicating a step layer growth mechanism. Gaps exist between the larger crystal structures which give the deposit a highly brittle structure. During thermal cycling, the Cu metal undergoes fracturing, due to the expansion of the air pockets, resulting in the degradation of the PCB. If the electrical current levels are set up correctly and the bath chemistry is properly maintained, then a frosted finish will not be observed after plating. The appearance of the frosted finish here is due to the presence of the metallic transducer, reducing the plating

current across the PCB due to thieving. At the regions where current was stolen, the surface of the metal deposited on the PCBs shows a frosted finish indicative of plating at extremely low current densities. The frosted finish covered an area smaller than the area of the acoustic agitated area. Around the periphery of the frosting a bright and shiny Cu finish was deposited. SEM images obtained within this region, as shown in Table 4.7, highlight a compact fine grain growth of Cu, which is indicative of the standard plating behaviour expected for correct operation of the current settings and appropriate additive concentration levels. A PCB fabricated with this finish will not undergo thermal cycling issues and is desirable as a final product. To test this quality of finish the board could have undergone thermal cycling and SEM analysis performed after to highlight any fracturing of the PCB surface. Other quality metrics, not performed due to resource limitations, are discussed in section 3.3.4 in Chapter 3.

Table 4.7 - Plating behaviours observed after plating at 1 A/dm² for 30 min across a PCB receiving 225 W MS agitation. Effects caused due to changes in electrical current distribution across PCB with estimated current density values highlighted.

	Low current density Frosting ($\leq 0.5 \text{ A/dm}^2$)	Standard plating behaviour for current density (1 A/dm ²)	Limited current plating ($> 2 \text{ A/dm}^2$)
Low Magnification			
High Magnification			

At the edge of the PCB a limited current burnt finish was observed. Limited current plating is a standard plating error highlighted by a nodular, dark-brown, powdery deposit formed in regions where the current density exceeds the limited current density, which is typically at the edge of a PCB, or on isolated Cu tracks on the board surface [6]. The limited current density influences the operational limit of the current supplied to the PCB. Beyond this value the Cu cation depletion rate at the surface of the PCB is higher

than the depletion rate, as long as the fluid convection is constant. An SEM image of a limited current finish is provided in Table 4.7 at low (20 μm on scale) and high (500 μm on scale) magnifications. The finish is characterised by micro-nodules of Cu which vary in size from 5 to 250 μm in diameter. The variation in nodule size is possibly due to the fast build-up of Cu on the smaller nodules, which act as nucleation sites for the larger ones. A limited current finish is characterised by a weak deposition and is undesirable in PCB fabrication.

When plating under MS assistance in previous work, see section 4.1, there was indication that the inclusion of standard bath agitation techniques, such as panel movement and/or air bubbles, caused disruption and negated some of the benefits of acoustic wave agitation. For this reason, when plating under MS conditions, these two techniques were not included. The inclusion of panel movement and bubble agitation enables replenishment of depleted cations near the PCB surface. With the introduction of MS agitation the acoustic streaming currents produced near to the PCB surface provides the same role for ionic replenishment, enabling higher currents to be applied before limited current plating occurs, as explained in section 2.2.3 in Chapter 2. Under the plating setup, the PCB size was larger than the area agitation by the MS and so, at the edges of the PCB, the MS acoustic streaming failed to spread, reducing the streaming force and the limited current there, thus inducing limited current plating for the current supplied. The current density at the edge of the PCB was approximately 2 A/dm^2 for the 1 A/dm^2 output by the anode and thus, for this plating setup, the limited current was around 2 A/dm^2 whereas in other plating investigation, see section 4.5, the limited current density occurred at higher values.

To prevent limited current plating and frosting from entirely occurring on a board, multiple transducers could be deployed, directed at different regions on the PCB, or a transducer the size of the desired area to be plated could be implemented. Under these settings a plating finish would be obtained as highlighted in Table 4.7 under the standard plating column, where small variations in particle size and fine grain deposition are obtained.

4.5 Cu crystallinity variation with current density

A key parameter controlling the growth of Cu is the electrical current density. If the bath chemistry is maintained within a set range, then the growth of the Cu is proportional to the current density applied [19]. It is uncertain whether Cu growth is influenced by the MS agitation and whether the typical response to current density is still

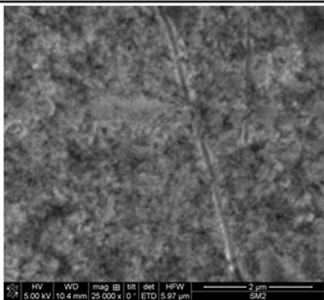
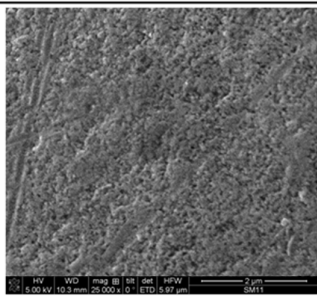
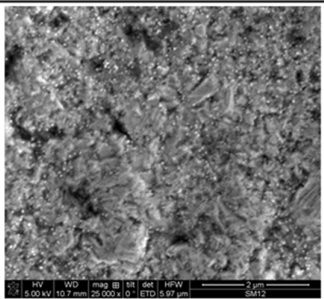
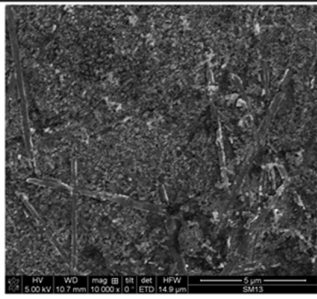
obtained. For this reason experiment 4.5 was performed plating at varying acoustic outputs and current density ranges, under settings outlined in Table 4.8.

Table 4.8 - Experimental conditions for experiment 4.5.

Experiment Number	Plating Parameter Investigated	Experiment Parameters			Measurement Obtained	Purpose
4.5	Electrical Current Density	Transducer	Tangential Position to PCB X (cm)	1	Qualitative observations of Cu grain structure using SEM in response to variation of plating current density.	Highlights changes to Cu crystallinity displaying acoustic influence on bath additives and potential performance issues.
			Acoustic power output (W)	0, 225		
		Current Density (A/dm^2)	2 & 4			
		Plating Duration (min)	60			

SEM images of the PCB surface plated under different current density regimes are provided in Table 4.9. Under silent conditions the Cu was plated at 2 A/dm^2 and 4 A/dm^2 , with standard agitation. These surfaces displayed no discernible differences and were characterised by a uniform fine grain deposition. When MS plating at 225 W and with the same current densities, the SEM images revealed different plating finishes to those produced under silent conditions. For MS plating at 2 A/dm^2 , a uniform surface deposition was observed, although a large polycrystalline deposit was also apparent. For MS plating at 4 A/dm^2 , a spiky, whisker-like growth was observed, as seen in section 4.1. The result shows that the Cu growth, under the different current density regimes, is different on the application of MS agitation due to interference with bath additives.

Table 4.9 - SEM images of PCB surfaces after plating for 60 min under varying current densities and acoustic output powers, with the acoustic transducer setup at 1 cm.

Acoustic Power	2 A/dm ²	4 A/dm ²
0 W		
225 W		

The poor performance of the bath additives can be explained by their low concentrations near the PCB surface. This could have been induced due to, a) the force of acoustic streaming waves on the PCB surface removing the additives, as displayed in [64] on organic molecules bearing a similar structure to the additives in the plating bath, b) the denaturing of the additives under large thermal increases brought on by megasound cavitation [133] and/or c) the increased depletion of additives due to temperature increases.

4.6 Plating temperature variation

The plating bath temperature is a key parameter influencing the rate of the chemical reactions within. For the correct operation of the chemical additives the plating line is maintained at 20 - 25°C depending on the chemistry used [18]. The MS agitation produces localised thermal increases due to cavitation, whose influence has been witnessed in the partial melting of the plating tank. The ability to process PCBs at reduced temperatures whilst maintaining manufacturing quality is desirable, as it would reduce overall processing costs. For this reason, MS plating performance was evaluated in experiment 4.6 for its ability to locally provide heating during PCB plating, by reducing the bath temperature controlled by its heater and observing the plated finish quality.

Three plating trials were performed under settings outlined in Table 4.1 and setup as indicated in Chapter 3.

Table 4.10 - Experimental conditions for experiment 4.6.

Experiment Number	Plating Parameter Investigated	Experiment Parameters			Measurement Obtained	Purpose
4.6	Plating Temperature	Transducer	Tangential Position to PCB X (cm)	1	Qualitative observations of the plated finish surface from images after MS plating.	Indicates temperature influence on MS plating due to interplay with bath additives.
			Acoustic power output (W)	225		
		Current Density (A/dm ²)	2			
		Plating Duration (min)	30			
		Temperature (°C)	18, 25 and 33			

Shown in Figure 4.6 are images of the MS plated surfaces produced with the temperature varied. The current distribution across the board caused a spectrum of effects the same to those reported in section 4.4, which appeared to vary in intensity on alteration of the bath temperature. The PCB shown in Figure 4.5A was plated at 18 $^{\circ}C$ and shows shiny regions in dark and matt regions in orange. A significant proportion of the board is covered by a limited current plating finish indicated by the orange-red finish. This is expected as the chemical brightener additive operates successfully at 25 $^{\circ}C$ and not below. Over the area sonicated by the transducer, a shiny plating finish is observed indicating correct additive behaviours. This is contrary to standard behaviour obtained at 18 $^{\circ}C$ and a positive result. It indicates that with MS-agitation, a lower operating temperature can be applied due to the temperature increases induced by cavitation, which maintains the correct environment for the bath additives.

Figure 4.6B and 4.6C show the plating finishes produced for bath temperatures 25 $^{\circ}C$ and 33 $^{\circ}C$, respectively. For an increase in bath temperature the limited current plating at the edge of the boards reduces, which is expected as the additives are operating under their ideal settings, although no panel movement or bubble agitation is applied and so limited current plating still occurs. Over the area sonicated a dull matt finish is produced which increases in intensity and appearance with temperature. As mentioned in section 4.5, the behaviour of the bath additives could be hindered by increases to plating temperatures, so this could be contributing to the matt finish.

The region sonicated was also characterised by vertical lines, possibly related to standing wave, acoustic interference formation on the surface and acoustic streaming,

which are discussed in greater detail in Chapter 5. As the temperature of the bath was increased, the widths of the vertical lines increase and become more readily observable. For temperatures up to 23 °C the lines were no bigger than 1 mm thick, beyond this temperature they were greater than 2 mm. If the lines are associated with acoustic interference effects, then it appears that the transport of additives and acoustic driven heat dissipation both play key roles in the observed behaviour.

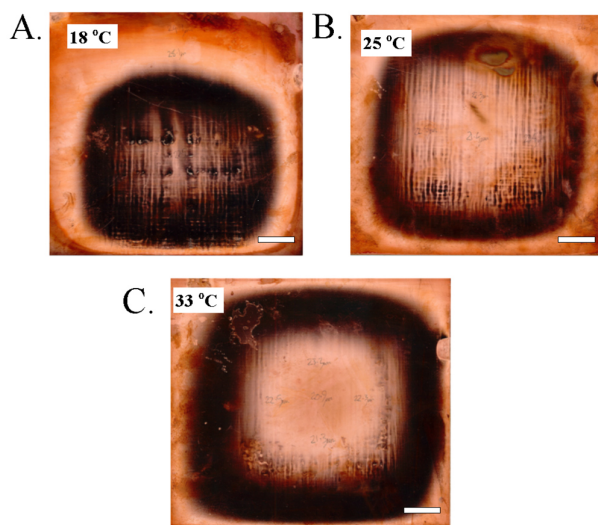


Figure 4.6 - Top-down images of the PCB surface after 2 A/dm² plating for 30 min for transducer setup at 1 cm and outputting at 225 W. A), B) and C) plating for bath solution temperatures 18 °C, 25 °C and 33 °C. Scale on images 3 cm.

4.7 MS panel plating conclusions

The influence of the MS agitation has been evaluated through changes observed in the Cu electrodeposit formed on the surface of the PCB, after applying changes to the conditions under which it is plated. This has led to the identification of unique plating properties beyond those currently reported in the MS literature. The experiments addressed development stage 1 outlined in Chapter 1, for the scale-up of the MS plating technique. The experiments also enabled a familiarisation of the MS plating behaviours through observations of the plated finish. The following topics review the outcomes of MS and how it will impact on the second integration stage, where MS is evaluated on vias.

4.7.1 Whisker growth and the impact of additional agitation alongside MS

MS plating trials investigated the influence of the acoustic power emitted by the transducer on the characteristics of the electrodeposits. On maximum acoustic output power, 450 W, observations on the macroscale revealed a shiny electrodeposit on the surface, which was expected for standard fabrication and suggested a fine-grain ductile microscale finish. On observations of its microstructure the Cu structure appeared spiky, with large whisker-like formations. Whisker growths were also observed during MS plating with high electrical currents of 4 A/dm². Whisker growth is undesirable and was the product of the high electrical currents and the large acoustic powers. The acoustic power induces an acoustic streaming force on the PCB surface as well as exothermic MS cavitation. The two effects combined could have a negative impact on the organic chemical additives on the PCB surface, which under typical plating operation, ensure grain refinement.

Thermal increases brought on by MS cavitation effects could induce denaturing of the additives and the acoustic streaming force could displace and remove the attached organic molecules. A whisker-like deposition is undesirable in PCB fabrication, due to its susceptibility to fracturing and breaking under thermal expansion, leading to reduced PCB life time and electrical shorts. To reduce the impact of this plating finish, modifications to the MS plating cycle could be implemented, such as the introduction of an off-cycle during the plating cycle, or plating at lower current densities and acoustic powers.

The additional introduction of panel movement alongside MS plating was shown to disrupt the acoustic wave, indicating that it cannot be included to enhance fluid agitation and thus plating. For this reason when MS plating via the agitation will be supplied with no additional external forces.

4.7.2 Micro-roughening due to transducer position alteration and power change

The introduction of MS agitation increased micro-roughening on the plated PCB surface. The micro-roughening appeared to increase with increases in transducer power output and on the reduction in distance of the transducer device. For smaller tangential transducer/PCB distances, attenuation of the acoustic wave was less, enabling higher acoustic powers over the PCB surface sonicated, per unit area. An increase in acoustic power is realised by increases in pressure. Increases to acoustic pressure are reported to increase the intensity of cavitation collapse [125] and, so, the micro-roughening

behaviours witnessed could be accounted for by an increase of cavitation power on transducer distance reduction and power output increase.

Controlling roughness on a plated Cu surface is important, as roughness impacts on PCB manufacture, where increases in manufacturing performance are obtained for increases to roughness up to a point, and where further increases led to electrical signal loss at high operating electrical frequency PCBs.

The current trend in PCB design is towards high interconnect density, high-frequency applications [137]. One of the goals for the introduction of MS plating is to reduce interconnect features on a PCB, reducing track pitch and providing low surface roughness of metal tracks for high frequency applications. The surface roughness values measured as a result of the MS are larger than desired for high-frequency PCB fabrication. Fabricating under these conditions is currently counter-productive for the development of future product technological trends. A reduction in roughness during MS plating could be made by making modifications to the plating cycle. Reducing the acoustic pressure output towards the end of a plating cycle would ensure that the plating finish at the end of the cycle undergoes less cavitation and a more uniform finish. Additionally, introducing an off-cycle during plating would, on average, reduce the cavitation influence. Further studies are required into the influence of more complex MS plating cycles where on/off duty cycle and acoustic pressure are altered.

During the via-plating trials the surface finish roughness produced can be overlooked in the short term, in order to investigate the Cu plating efficiency down the vias. After via plating performance is determined more complex plating cycles can be evaluated which address any unwanted roughness on the surface.

4.7.3 Current density alteration due to current thieving by the transducer

Observations were made as to how the electrical current, distributed across the PCB due to a current thieving effect, along with the acoustic streaming force reduction, influences the crystallinity of the electrodeposited metal. Prior to the investigation, it was found that increasing the transducer tangential distance reduced the current thieving effect, at around 4.5 cm from the PCB the current thieving was reduced to a negligible effect, as measured by the plating rates. In the current trials, a spectrum of finish behaviours was observed after plating which are characteristic of high and low plating currents. The behaviours were induced primarily due to thieving of electrical current away from the PCB by the presence of the transducer. The current variation induced by the close proximity of the device to the cathode surface produced the low quality plating

finish. The results show that, to form a high-quality bright plating finish when MS plating, the minimum tangential distance found previously must be applied again. This value may alter, depending on the size and shape of the transducer, as this influences the electrical field distribution in the plating bath.

Further electrochemical investigations are required to assess more thoroughly the influence of transducer surface conductivity on current thieving, as changes may be made to the transducer surface to reduce electrical conductivity, such as the deposition of a non-electrically conductive layer. However, this solution may come at the risk of reducing the acoustic power output, hampering any positive effects on plating by the MS.

When the acoustic streaming force failed to cover the entire face of the PCB, the Cu cation replenishment rate suffered in electrically isolated regions which received high field line flux, inducing unwanted limited current plating of the Cu deposit. This result shows that, for the effective fabrication of a PCB when MS plating, the acoustic agitation must cover the total plated area, especially if the panel movement and bubble agitations are switched off.

A polycrystalline finish was produced on the PCB surface with the introduction of MS at plating currents 2 A/dm^2 . This finish was also observed in research performed prior to this thesis, as indicated in Section 2.2.2 in Chapter 2, although these surfaces were MS plated at double the current density. It is possible that current thieving was present in the previous research, reducing the current plated on the surface and leading to a similar polycrystalline finish. If so, these results show that the same plating effects have been replicated between the two different plating investigations, which is a promising indicator that MS plating effects can be reproduced and are directly manipulated by the bath plating parameters.

4.7.4 Reduced plating process temperatures

The bath temperature controls the additive behaviours within the plating bath. Increases in temperature beyond the recommended can result in anode and cathode polarisation, reducing the ability to output electrical current and maintain plating rates. Reductions in bath temperatures will induce limited current plating on the PCB surface. The MS agitation induced thermal increases on the PCB surface, possibly due to cavitation effects, enabling lower than standard plating bath temperatures. This is highly beneficial in terms of energy savings and reduced process costs. For the via-plating trials the bath temperature must remain the standard, as processing at reduced temperatures reduces control over the bath chemical behaviour under MS.

Acoustic streaming lines were present on the PCB surface and were more readily observable on bath temperature increases. Their appearance was categorised by a matt finish indicative of large grain crystallinity. The lines were more apparent on temperature increases. This indicates an underlying temperature dependence on their formation. High frequency (15 - 18 kHz) acoustic streaming has been associated with increases of heat transfer coefficients between fluids and solids by up to 390 % [138]. Enhancements of this sort could be contributing to the localised movement of heat across the board, altering the bath additive behaviour under the regions sonicated. A more comparative review into the MS acoustic streaming mechanism is required to quantify the relationship between temperature and streaming line appearance.

4.7.5 Section summary

The outcomes witnessed in Chapter 4 are collated in Table 4.11.

Table 4.11 – Conclusions from Chapter 4.

Acoustic Effect	Reasoning for outcome
Formation of a whisker growth	Acoustic streaming power along with cavitation influence negatively influence bath additives hindering grain refinement.
Panel movement disrupts acoustic wave	The pattern formed on the plated CU surface altered and was dispersed when panel movement introduced, suggesting MS waves can be disturbed by medium fluid motions.
Microroughening due to transducer position and power output alteration.	The Cu microstructure was roughened on increases to acoustic pressure reaching surface.
Current thieving by transducer	Current thieving by transducer alters electrical current distribution across PCB surface changing the plating rate and encouraging unwanted deposit growths. Applying a minimum distance for transducer from PCB surface negates effect.
Reduced processing temperatures	Increases to temperature brought on by cavitation and heat transport by acoustic streaming, enabled increased performance of bath additives at lower than recommended plating temperatures.

Chapter 5 Surface Acoustic Artefacts produced in response to Megasonic Agitation

Acoustic assisted plating has been shown to strongly influence the characteristics of electrodeposited Cu. A variety of plating artefacts have been observed on the plated Printed Circuit Board (PCB) surfaces and in the bath solution near to the PCB, during and after experiments. Their formation was associated with acoustic effects produced from the Megasonic (MS) interaction with the electrodeposit, involving reflections of the acoustic wave off the PCB surface. The artefacts include periodic and aperiodic Cu features, cavitation and microbubble structuring. The artefacts were categorised under separate headings by the physical effects that influenced their formation. These were standing wave behaviours and microbubble influences. The content of Chapter 5 is split up into discussions on the individual acoustic artefacts. The behaviour of standing waves includes streaming lines, ridges, ringlets and cells, and non-regular structures and nodules. Influence of micro-bubbles includes MS cavitation streamers and cavitation. Each of these influences PCB fabrication quality and so the plating effects are discussed next along with their formation and impact.

5.1 Standing wave behaviour

The sonication of the PCB surface leads to the absorption and scattering of acoustic waves off the PCB surface. As discussed in section 2.2.4 in Chapter 2, the superposition of reflected and oncoming waves may lead to the generation of acoustic interference effects on the PCB surface. The following section discusses the different artefacts witnessed on the surface of a PCB after MS electroplating and reviews their formation and impact on PCB manufacture, offering solutions to mitigate unwanted effects.

5.1.1 Acoustic streaming lines

Highlighted in section 4.6 in Chapter 4, were images of the MS plated finish which showed the formation of lines on the surface, which took the appearance of acoustic streaming currents and showed temperature dependence. The lines were possibly formed due to the complex interplay between bath additives and forced fluid oscillations by acoustic standing waves setup at the solution / PCB interface. For this reason the lines shall be referred to as acoustic streaming lines. To further understand the relationship

between the streaming lines and acoustic output, investigation 5.1.1 was performed by altering the power output from the transducer and qualitatively observing changes in appearance.

The transducer was setup tangentially 1 cm from the PCB and was MS electroplated at 2 A/dm² for 30 min. Over the sonicated areas, images of the surface finish were obtained using the Samsung MultiXpress scanner and are highlighted in Figure 5.1. Like before, the surfaces showed parallel lines oriented vertically to the bath and were characterised by a dull matt finish appearing bright in the images. The lines were separated by approximately half of the acoustic wavelength in solution, 0.7 cm.

Between A, and B, the acoustic power was decreased. This was observed as a reduction in both intensity and occurrence of the streaming lines, over the sonicated areas. If the formation of the streaming lines is due to the movement of the bath additives on the PCB surface, then the fine-grain regions, observed as dark features in the images due to the contrast setting when obtained, are the pressure nodes of a standing wave, where the additives congregated. The large-grain matt finish regions observed as bright in the images, are the pressure maxima where the additives are displaced from. The reduction to acoustic pressure in turn reduced the displacement of the additives from their original positions. This likely led to the fainter lines and the more polished surface, as the additives were in greater concentrations on the surface at the lower acoustic intensities.

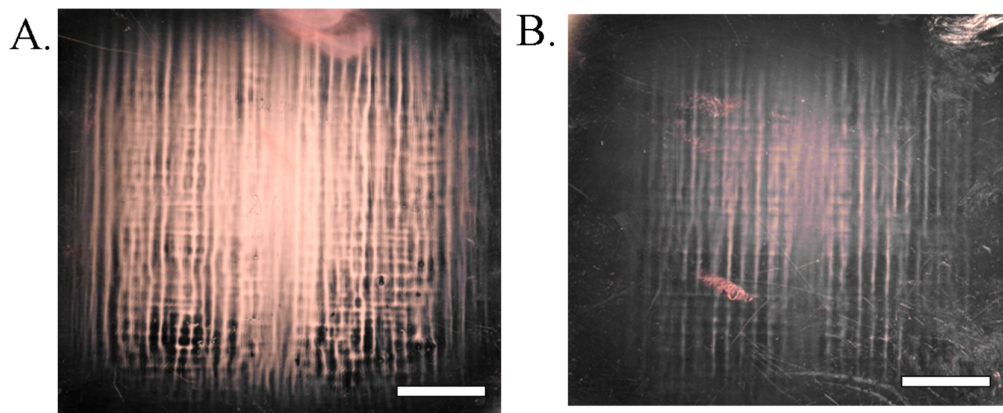


Figure 5.1 - Acoustic streaming lines on PCB surface after MS plating at 2 A/dm² for 30 min and the transducer setup at 1 cm and outputting at A) 225 W and B) 90 W. Scale on images 3 cm.

5.1.2 Ridges

After MS plating trials Cu ridge-like features were observed on the PCB surface formed after applying high plating 2 A/dm^2 or higher. Highlighted in Figure 5.2 are optical images obtained with a Koolertron™ Digital Microscope, of the PCB surfaces displaying ridges after plating at 2 A/dm^2 for 30 min, with 225 W acoustic output and the transducer placed 1 cm tangential to the PCB surface. The ridges were observed on surfaces plated without vias A) and with B) & C). They were separated by half of the acoustic wavelength, 0.7 mm, and were oriented vertically within the bath much like the streaming lines in the previous section. The ridges were formed on thicker deposits of Cu, which were produced nearer to the edge of the board where electrical isolation meant that they attracted a higher electrical field line flux and received higher plating rates, and / or towards the centre of the PCB when plating currents were applied larger than 2 A/dm^2 .

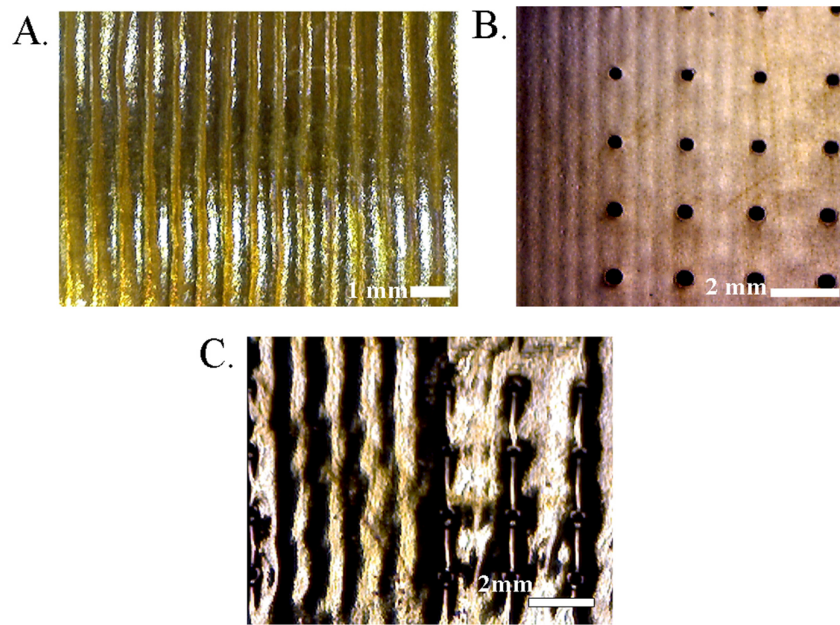


Figure 5.2 - Cu ridges imaged using an optical camera, after plating at 2 A/dm^2 for 30 min with MS output at 225 W and transducer setup 1 cm tangential to PCB, showing A) ridges on a PCB surface without drilled vias and B) & C) with THVs.

Highlighted in Figure 5.3 are microsection images of the Cu ridges deposited after 30 min of 2 A/dm^2 plating, at 225 W MS agitation. The transducer was setup as indicated in section 3.4 in Chapter 3, at an angle of 45° and a tangential distance of 31 cm.

The exact mechanism behind ridge formation was uncertain, although their appearance resembled the acoustic streaming lines. The two differed as the ridges were

more uniform in appearance, displayed a 15 μm Cu thickness variation between their peaks and troughs and were observed in locations of higher current density. In the 30 min plated at 2 A/dm^2 the copper thickness assuming a 100 % cathode efficiency, see section 2.1.2 in Chapter 2 and a correct throwing power for the solution, see section 2.1.7, should have been around 31 μm . On the peak of the ridge the thickness was 37 μm which was close to the predicted value, but at the base of the ridge the thickness was 23 μm suggesting that the plating rate had been hindered in that location. The ridges also appeared to form at large, 31 cm, and small, 1 cm, tangential distances of the transducer device setup.

The ridges occurred on both sides of the PCB, although, during some trials, they would appear greater on one side rather than the other. No noticeable trend was observed as to why this was the case. On the application of panel movement the ridges disappeared highlighting that their formation was possibly dependent on surface acoustic interference phenomena, as panel movement disrupted the resonant acoustic conditions, as shown in section 4.1 in Chapter 4. The formation of the ridges on the reverse of the board suggested that they were also influenced by the acoustic absorption properties of the PCB and possibly its internal structure. The distance between two interlacing weaves underneath the deposited copper was 775 μm which was similar to the ridge separation distance, as shown in Figure 5.3B. Additionally the weave separation was approximately half of the megasonic wavelength in solution. If an acoustic wave was absorbed by the board and transmitted through, then the glass weave may have acted like a diffraction grating [139]. This may have contributed to the scattering of the wave as it passed through, generating acoustic interference and resulting in the formation of high and low pressure variations on the side of the board opposite the transducer.

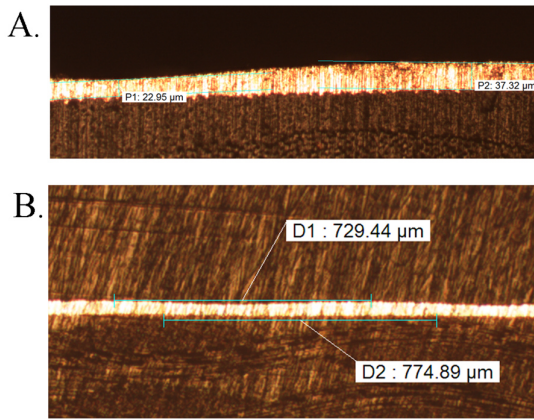


Figure 5.3 - Microsection cross section of ridge structures formed after 30 min plating at 2 A/dm² with 225 W acoustic output setup at angle of 45° and a tangential distance of 31 cm, and showing A) their Cu thickness and B) distance between peaks and glass weave.

COMSOL simulations were performed of acoustic waves scattering within a 2-D structure, modelling a detailed PCB internal structure with acoustic impedance values similar to actual. The simulation setup was discussed in section 3.5 in Chapter 3. The simulation was performed modelling a 1 MHz acoustic wave travelling from left to right through a PCB cavity structure, as indicated in Figure 5.4. The colour plots highlight the high and low pressure phases of the traveling wave as red and blue, respectively. The PCB / electrolyte interface highlighted in B, shows the pressure wave periodically varying in terms of high and low pressures in the PCB structure. This variation in pressure could have contributed to the Cu undulations observed at the PCB surface. Plating trials using PCBs of different percentage compositions of glass weave to resin could be MS plated - to highlight if board structure contributed to the appearance of Cu acoustic artefacts. These trials were beyond the scope of the Thesis.

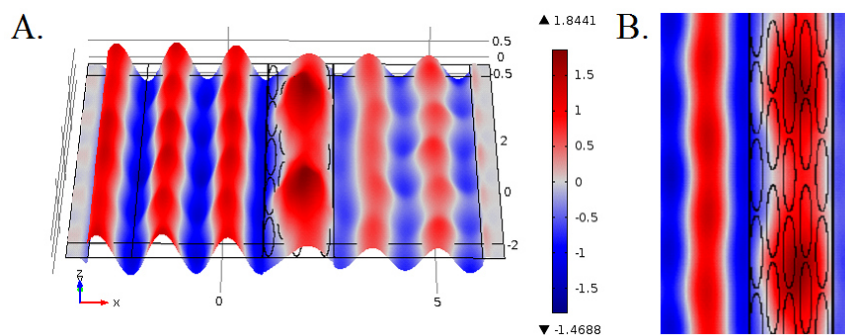


Figure 5.4 - 2D COMSOL scattering simulations of 1 MHz wave propagating from left to right through modelled PCB cavity, depicting high and low pressures by red and blue, accordingly. A) 3D representation of the acoustic wave. B) top-down close up of the electrolyte/PC

5.1.3 Ringlets and cells

After MS plating the surface of the PCB, the edge of the board would be patterned with circular features in a periodic cell-like appearance. Highlighted in Figure 5.5A is an optical image obtained using a Koolertron Digital Microscope of the PCB surface, plated at 2 A/dm^2 for 30 min, with the transducer setup tangentially 1 cm from the PCB and output at 450 W. Dark hexagonal ‘ringlets’ were formed surrounding dull circular regions where the dark regions indicated thicker plated Cu deposits. The circular features were separated by approximately 1 mm and coincided with the underlying weave structure of the PCB which was indicated in Figure 5.5B. Here the dark regions highlight the knuckles of the glass weave bundle. The similar appearance of the two surfaces suggested that after MS plating, the underlying structure was imported onto the plated finish topography.

Shown in Figure 5.5C & D is a Cu surface plated under the same conditions but for 150 min. Cell-like features were observed in regions where thicker deposits of Cu were plated on the electrically isolated features which attracted high field line flux - the edge of the board. The features varied in thickness like the Cu ridges and were formed within a similar location on the PCB. The ringlets were different from the ridges in that their separation distance was approximately 1 mm and not a half of the acoustic wavelength. A possible mechanism for their formation was that they were thicker deposits of the ringlet features mentioned in the previous paragraph, produced after longer plating cycle durations and / or higher plating current densities. The cells, as the ridges are an unwanted feature.

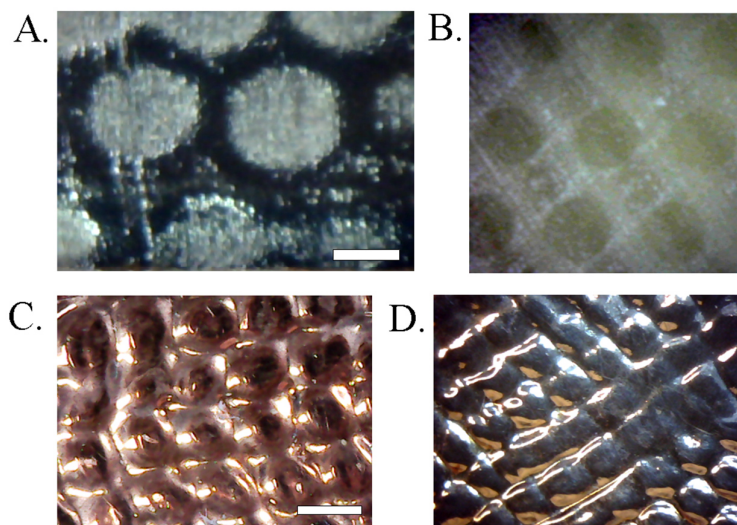


Figure 5.5 - A) Ringlet Cu features after MS plating at 2 A/dm^2 for 30 min with the transducer positioned at 1 cm and output at 450 W. B) Underlying laminate surface with Cu removed via acid etch. C) & D) Cell features observed after MS plating under same conditions for but for 150 min. Scale in images 1 mm.

The appearance of Cu ring like structures was also observed on the PCB surface, emanating from a tooling hole. Highlighted in Fig 5.6 are Cu concentric rings formed after RP plating at $1:2 \text{ A/dm}^2$ for 16 hours, under 450 W, MS agitation and with the transducer setup tangentially 4.5 cm away from the PCB. The ringlets appeared as periodic deposits of large-grain Cu growths which were observed as a dull finish on the PCB. The separation distance of the ringlets was approximately 0.7 mm or half of the acoustic wavelength. As such, their periodic appearance suggests the generation of acoustic interference effects on the PCB surface, like the streaming lines and ridges, rather than a direct imprint of the underlying weave topography. The ringlets were characterised by a deposition of large grains and a possible mechanism for their formation was that they were due to low concentrations of additives at the acoustic standing wave pressure maxima. In turn, at the pressure nodal regions, the additives would congregate, increasing in concentration and encouraging a shiny, fine grain deposit in between the matt-finish ringlets. A matt finish is unwanted in PCB fabrication as indicative of a weak and brittle structure, as shown in the image by the surface fracture in Figure 5.6.

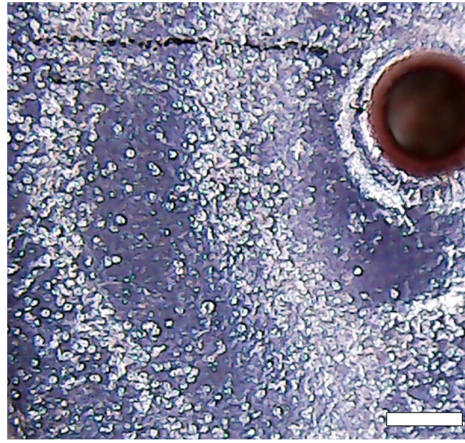


Figure 5.6 - MS plated ring formation of matt finish on PCB from tooling hole. Plating conditions RP plating at $1:2 \text{ A/dm}^2$, 10ms fw, 0.5 ms rv, for 16 hours with the transducer out putting at 450 W and setup 4.5 cm tangential to PCB. Scale 0.5 mm.

5.1.4 Non-regular structures and nodules

The last features classed under standing-wave effects are non-regular structures and nodules. Nodules are a common effect observed in standard plating due to contamination by particulates or limited current plating. Figure 5.7A highlights an isolated nodular feature observed on the PCB after RP plating at $1:3 \text{ A/dm}^2$ and with 450W MS agitation and the transducer positioned tangential at 4.5 cm. The feature and others like it were only present within the area sonicated on the PCB surface and so were most likely a direct result of MS plating. Shown in Figure 5.7B is a microsection of a nodule measuring with peak height of $4 \mu\text{m}$.

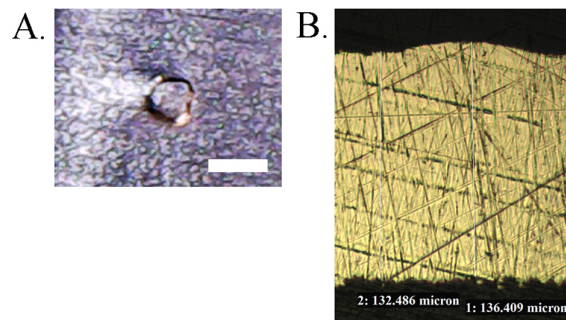


Figure 5.7 - PCBs RP plated at $1:3 \text{ A/dm}^2$ for 153 min with 450 W acoustic power and the transducer setup 4.5 cm tangential to the PCB. A) Cu nodule imaged using Koolertron Digital Microscope on the MS plated PCB surface, scale 0.5 mm. B) microsection of a nodular feature.

Nodular deposits were also observed on top of acoustic ridges as shown in Figure 5.8. The PCB was plated at 2 A/dm^2 for 30 min with MS output at 225 W and transducer setup 1 cm tangential to PCB. In this case the nodules are formed because of high plating currents towards the edge of the board and are a combination of a limited current Cu finish, see section 4.4 in Chapter 4, and acoustic interference effects. The appearance of the nodules on the ridges may not entirely be the result of the high current density. As indicated in ultrasonic research [140], micro-beads loose on a surface or in fluid medium re-arrange themselves into regions of the pressure nodes under acoustic stimulation. This self-organisation behaviour may have occurred whilst MS plating, where loose Cu particulates produced due to limited current plating and unremoved by the filter pump, were condensed together into the low pressure regions. Further investigations into particle trapping using MS would be required to indicate whether this was occurring under the plating setup.

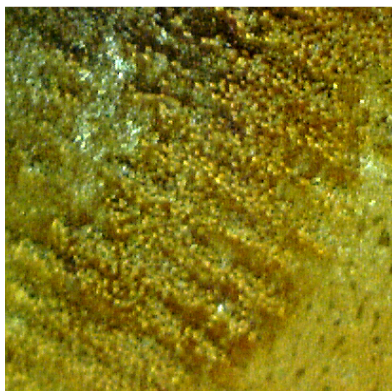


Figure 5.8 - PCB plated at 2 A/dm^2 for 30 min with MS output at 225W and transducer setup 1 cm tangential to PCB showing nodular deposits formed on the tops of acoustic-formed ridges, towards the edge of the panel.

Non-regular features were observed on the PCB surface after plating. They appeared in regions which had undergone sonication and so were attributed to MS formation. Highlighted in Figure 5.9 were plating results for surfaces formed under A, 1 A/dm^2 DC, with 225 W MS and B, 1.3 A/dm^2 RP, with 450 W MS, with the transducer setup at 4.5 cm for both. The surfaces were both plated with the transducer setup tangentially at 4.5 cm. Prior to these trials irregular features were not observed on the PCB surface when the transducer was setup tangentially. The non-regular structure formation could relate to an interplay between the electrodynamics and acoustic wave interference formation. At non-normal angles, acoustic interference formation is more

readily encouraged [141] and thus could potentially manipulate the deposition of Cu to a greater degree. When plating it is possible that shifts in the orientation of the transducer from the normal direction occur due to bath convection currents. Due to poor visibility within the bath solution, changes in position go unnoticed resulting in an angled sonication onto the PCB surface. The unwanted change in position could have aided the formation of the structures, although an exact mechanism describing their appearance is unclear.

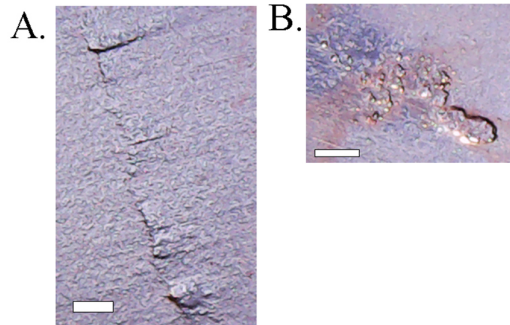


Figure 5.9- Microscope images of irregular acoustic artefacts on surfaces MS plated for 150 min at A) 1 A/dm² DC, with 225 W MS and B) 1:3 A/dm² RP, with 450 W MS, with the transducer setup at 4.5 cm for both.

5.1.5 Conclusions

For the introduction of MS-assisted plating a range of acoustic artefacts were observed on the PCB surface. Listed in Table 5.1 are the artefacts and bath parameters, which altered their appearance.

Table 5.1- The plating conditions under which surface acoustic artefacts are produced.

Observed artefact	Plating condition	Features appeared
Streaming lines / circles	Transducer position and distance	When plating at tangential distances < 10 cm.
	PCB / Transducer orientation	Streaming lines appear vertical to the orientation to the bath regardless of transducer or PCB orientation.
	Acoustic Power	Appears upon sonication of the PCB surface at 5% output (45 W) by the transducer.
	Bath Temperature	Stream line intensity shows temperature proportionality.
	PCB features	Acoustic interference Cu features appear due to interaction with surface features such as tooling holes.
Ridges	Plating currents	Occurs when current density ≥ 2 A/dm ² . Observed at edges of the PCB where electrical field line flux is high.
	Transducer position and distance	Observed when the transducer is tangential and at an angle to the PCB. Appears for transducer distances between 1 – 32 cm.
	Internal structure of PCB	Possibly influenced by position and separation of the glass weave.
Hexagonal Ringlets and Cells	Internal structure of PCB	Possibly influenced by position and separation of the glass weave.
Non-regular structures and nodules	Plating current density	Hexagonal ringlets formed at current density ~ 1 A/dm ² and cells at current density ≥ 2 A/dm ² .
	Plating currents and acoustic interference	Observed in high current regions and on the top of acoustic interference Cu ridges.
	Transducer position	Observed when the transducer face is non-normal to the PCB.

The conditions for streaming line formation were catalogued from observations obtained during all plating experiments performed in the thesis. The position of the transducer influences the appearance of the plated finish, where streaming lines were observed for tangential placements less than 10 cm. At larger distances a more randomised effect was produced as highlighted in section 4.1 in Chapter 4. This distance related dependency could have been due to the formation of an acoustic standing wave tangential to the PCB / transducer face within the fluid medium. Evidence for such effects is provided when bubble levitation occurs within the medium, which was observed and is discussed later in the Chapter in section 5.2.1. At larger distances reflections may not be able to propagate between the PCB and the transducer, negating resonant effects and the formations of the streaming lines. Due to this behaviour it was uncertain how transducer distance influenced MS via plating and so, additional investigations have been performed and are reported in Chapter 6.

The streaming lines oriented themselves vertical to the bath regardless of the position and orientation of the PCB and transducer. This highlights that the acoustic streaming mechanism was influenced by forces, which favour a vertical motion within the bath. Microbubbles are likely generated due to cavitation within the acoustic wave. If the bubbles coalesce and increase in size beyond a minimum diameter, they will be influenced by buoyancy forces [142] and so those close to the PCB surface would travel in a vertical orientation up the board. In the presence of a MS field, micro-bubble coalescence occurs [143] and acoustic streaming currents would then be influenced by the motions of these bubbles in solution [68]. If the motion of the microbubbles influences the acoustic streaming on the PCB, then this could have oriented the streaming currents into bands parallel to the motions of the bubbles. This would account for the vertical orientations observed regardless of the transducer / PCB setup.

The streaming lines appeared on the PCB regardless of the intensity of acoustic power supplied, although were reduced in appearance on power reduction. They appeared predominantly as vertical lines, although were also circular emanating from hole features. Their appearance provided the quickest indicator after electroplating that MS acoustic effects were present on the PCB. For aesthetic purposes, the removal of the streaming lines was possible by switching off the MS towards the end of the plating cycle and DC plating for the remainder of the cycle to improve finish appearance. This technique is applied in standard PCB manufacture in response to RP plating. For via plating trials in

later Chapters this technique was not applied as the surface condition was not the main objective of these investigations.

Cu ridge formation was observed and appeared to be primarily influenced by transducer position and the plating current density. Their formation was similar to the streaming lines in that the same forces appeared to influence their behaviour, although they were produced at faster plating rates. Simulations provided insights into acoustic internal reflections within the PCB, highlighting that periodic changes in pressure occurred at the solution PCB interface. These could have contributed to the standing wave behaviours observed.

The ridges were characterised by a large Cu thickness variation. The variation could have been due to the suppression of Cu deposition due to bath additive depletion, denaturing or displacement. The variation was unwanted in PCB manufacture as it was larger than the minimum acceptable by IPC specifications and so the ridges in their current form were an undesirable artefact. To prevent ridge formation the introduction of additional panel agitation strategies could be applied, disrupting the acoustic standing wave formation, although this may negate any positive MS plating effects. This was introduced in later chapters in via plating investigations.

The appearance of the ridges reduced when sonication was oriented tangential to the PCB surface, as well as when plating at lower current densities. When via plating these conditions were applied so as to minimise unwanted surface Cu variation.

Hexagonal ringlets and cell-like structures were observed on the PCB. The causes of their formation were similar to those of the Cu ridges, although they appeared to be more influenced by the underlying weave structure of the PCB rather than the acoustic wavelength properties, as measured by the separation distance between plated features. A fundamental mechanism describing their formation was uncertain, although ringlets and cells appeared to be induced by acoustic interference formation which was influenced by an interaction with the internal and external PCB features. Thickness variations were induced like Cu ridges and were an unwanted outcome for the same reasons. Their appearance was reduced by applying the same preventative conditions as for ridges.

The formation of non-regular and nodular deposits appeared on the introduction of MS plating. Their appearance did not show the underlying characteristics of the PCB internal structure or the wavelength properties of the MS agitation. A mechanism for their formation was uncertain, although like previous artefacts, appeared to be influenced by acoustic interference, internal structure of the board and transducer position. Their presence was a negative influence on surface uniformity and a method to prevent their

formation, was to improve the precision in setting up the transducer tangentially to the PCB surface.

5.2 Microbubble influences

The MS surface artefacts were not limited to standing wave behaviour and the influence of the Cu grain structure. Instead bubbles within the plating bath appear to influence the fluid dynamics near to the PCB surface and alter the topography of the Cu finish. The following section discusses the different artefacts witnessed due to microbubble behaviours within MS fields and how they impacted on PCB fabrication.

5.2.1 MS cavitation streamers: bubble lens, cones and bubble ringlets

Plating trials into dry-film removal were performed in baths filled with stripper solution, as discussed in Appendix C. This solution was transparent and enabled the transducer surface to be imaged whilst sonicating using an optical camera. Highlighted in Figure 5.10 is the transducer surface submerged within a stripper tank. Shown in light grey were microbubbles patterning the surface in positions indicated by the blue arrows. The bubbles bare a resemblance to bubble-clustering behaviours observed in US research, as discussed in section 2.2.7 in Chapter 2. If this was the same effect, then the bubbles would have interfered with the transmission properties of the transducer, inducing a focussing effect due to the bubbles acting like an acoustic lens.

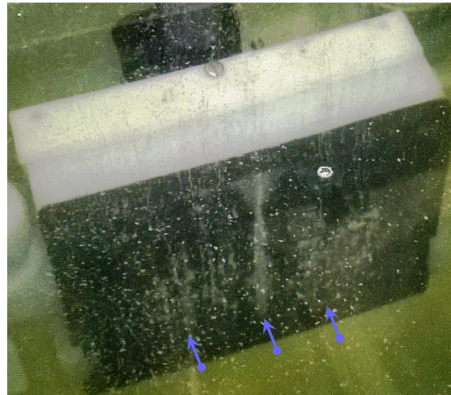


Figure 5.10 - Bubble clustering on transducer surface highlighted by blue arrows as it outputs at 450 W. Surface imaged using optical camera through clear water solution.

Photographs were taken of the transducer surface when it was set up to sonicate PCB surfaces to remove dry-film resists as discussed in greater detail Appendix C. The transducer was positioned tangentially at a distance of 1 cm and output at 450 W. Highlighted in Figure 5.11 are bubbles observed within the medium between the

transducer, outlined in black on the left of the image and the PCB - right of the image. The bubbles again showed a range of features similar in appearance to those mentioned in Ultrasonic (US) literature [62]. Shown in A & B are bubble cone structures formed between from the PCB surface and the transducer. The cones in A appeared white with their base attached to the PCB and their tips touching the transducer or protruding into the medium. The bubble cones took several seconds to form and several minutes to extend outwards from the PCB surface toward the transducer. In B the bubble cones are in the mid-process of extending outwards and so, are smaller than in A. Upon a slight mechanical tapping of the PCB the cones would dissipate and their formations start over.

The bubble cones reported previously in US literature are produced from the transducer surface. In the MS trial the bubbles were oppositely produced on the flat PCB surface parallel to the transducer. This behaviour could be explained as the acoustic waves reflecting backwards towards the transducer, treating the PCB surface as nucleation sites for cone formation. Also, a significant degree of bubbles are formed during the dry-film stripping process [144] and so could have provided a means of fuelling the growth of bubble structures from the PCB side as they were stripped off.

Bubbles were imaged in C positioned in a fixed locus in the medium. Acoustic levitation is an effect manipulated for use in manufacture[62]. Here levitation provided an indicator of the underlying physics occurring within the medium when the transducer was setup at close distances to the PCB.

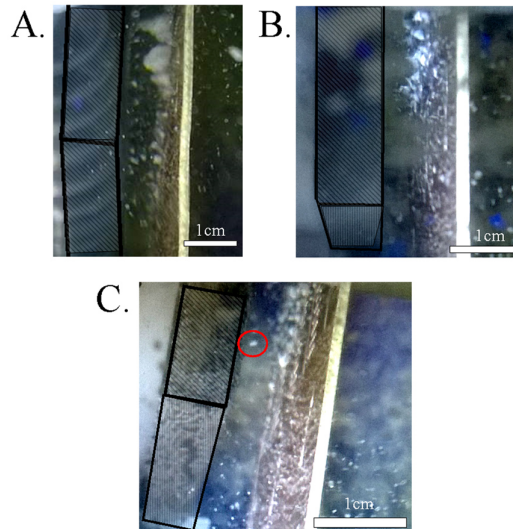


Figure 5.11 - Optical images of the PCB surface, right, receiving MS agitation from transducer, left, highlighted by black lines. A) & B) bubble cones extending from PCB. C) levitating bubble cluster circled in red.

Whilst the transducer sonicated the PCB surface in the stripping trials, bubbles were given off the transducer and the PCB surfaces. Some of the bubbles appeared as ringlets which moved under buoyancy towards the top of the bath. Photographs of the bubble-ringlets are displayed in Figure 5.12 and were only observed when MS was applied, which suggest that they are an acoustic artefact. The formations of bubble-ringlets was also reported in US investigations [84] and was attributed to acoustic bubble streamers. It is likely that the observed ringlets were due to the same effect, highlighting again the complex interplay of forces present when manufacturing under MS. The bubble-ringlets do not appear to have an adverse effect on manufacture.

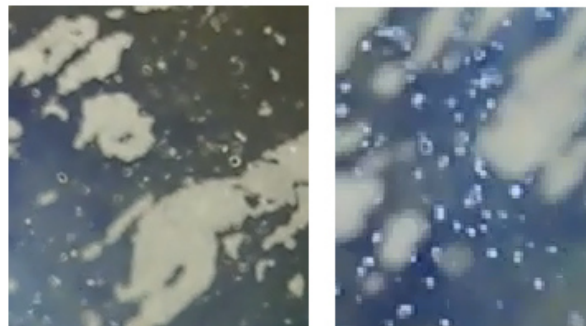


Figure 5.12 - Optical images of ring-like bubble structures observed in bath whilst under MS agitation.

5.2.2 Cavitation

Cavitation is a unique artefact observed after acoustic agitation. It varies in intensity and magnitude dependent on the acoustic pressure and frequency. Cavitation has been widely reported under US agitation [67, 78]. Cavitation can be observed on a surface because of the damage caused when highly pressurised thermal energy is released from bubble collapse. The damage is typically observed as crater-like features, although it may also be manifested as a micro-roughening of the surface. The energy released is by a jetting micro-stream. The jet stream is typically directed tangentially towards the surface the bubble is against, although it is possible for the jet stream to become directed along the surface, if the bubble undergoes influence from external, directional convection currents [78].

Figure 5.13 presents examples of cavitation recorded during the MS Cu plating investigations performed throughout the thesis. In Figure 5.13A, the Cu surface was plated at 2 A/dm² for 30 min and 450 W, MS agitation. The feature produced indicated an indentation on the deposited Cu along with a bulging feature extending upwards in the PCB's vertical orientation. The indentation was likely a crater formed from where the bubble imploded and the bulging feature possibly due to additional electrodeposition occurring on the rim of a crater feature, which due to its electrical isolation would attract electrical field lines with a greater density relative to its flat surroundings and induce higher plating currents.

Fig Figure 5.13B presents an example of cavitation observed after MS plating at 4 A/dm² for 30 min and 225 W, MS agitation. The feature was characteristic of the tadpole like appearance of cavitation[78]. The circle, of diameter of around 400 µm, was possibly a crater nucleus and the tail of length of about 2 mm the jet stream, as the bubble was directed along the surface by acoustic streaming currents. A high resolution SEM image of a MS plated PCB surface is given in Figure 5.13C. Features appear similar to the cavitation measured on the larger scale. The features, many of them occurring on the surface with the same orientation, appear to display the same nucleus and tail features, albeit at a smaller scale. Previous studies into cavitation influences have indicated that some cavitation, occurring at high frequencies (1 MHz), would be on a scale too small to be detected by standard employed techniques such as sono-luminescence [145, 146]. The cavitation features were, to the best of the author's knowledge, the first examples ever recorded for plated copper surfaces.

Circle features and pits were readily observable on the PCB's surface after MS plating. They vary in size and could be observed by eye on the macroscale and down to

the microscale. The increase of roughness mentioned in Chapter 4 could have been induced by micro-cavitation features.

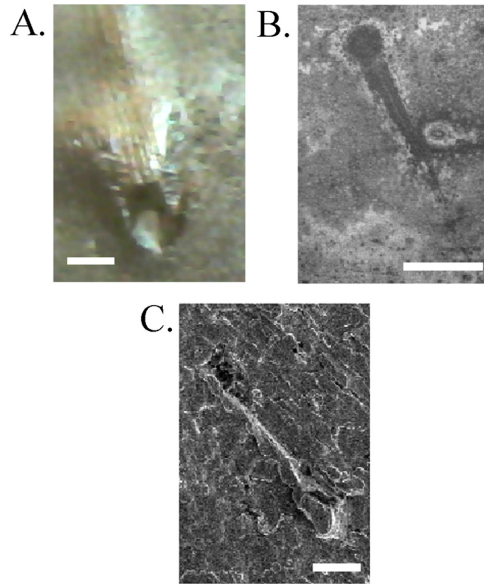


Figure 5.13 - Images of cavitation features after MS Cu plating obtained using A) optical microscope, scale 0.25 mm, for plating conditions 2 A/dm² for 30 min and 450 W MS, B) Interferometer, scale 1 mm and C) SEM, scale 5 μ m, for plating conditions in both 4 A/dm² for 30 min and 225 W MS.

5.2.3 Conclusions

The presence of bubbles during MS electroplating bath was common due to cavitation. When under MS agitation, bubbles present within the plating bath congregated into fixed positions on the PCB and transducer surfaces. Bubbles on the transducer influenced transmission properties and influenced on the PCB the acoustic streaming forces occurring there. The appearance of bubble-structuring at small transducer distance setups, highlights that nonlinear acoustic behaviours are being produced upon reduced transducer distances, where potential enhancements to streaming forces may have occurred due to the focussing of the acoustic wave [147]. This provides additional merit for later investigations, whereby small transducer tangential distance setups were applied under via plating, despite the unwanted current thieving measured previous in Chapter 3.

Damage was induced on a PCB surface due to cavitation and was reduced when increasing the frequency of the acoustic wave. In MS manufacturing damage was witnessed as changes to Cu topography, which caused an unwanted surface variation and reduced the lifetime of board.

Cavitation was the primary cause for the thermal increases observed when MS processing. Microscale localised thermal increases would have influenced the electrodynamics of the plating reactions there and potentially lead to enhanced chemical additive depletion which would have influenced deposit quality as witnessed in Chapter 4. Further investigations into thermal cavitation effects are required to sufficiently evaluate the impact of cavitation on Cu electroplating.

5.3 General conclusions

A wide range of acoustic artefacts were reported whose formation was attributed to standing wave acoustic and microbubble behaviours. The artefacts negatively influence plating as unwanted changes to surface uniformity and poor bath additive performance and as such, modifications have been suggested to counter the unwanted effects when a solution was present.

The characterisation of the different acoustic artefacts helped describe the fundamental acoustic behaviours and how they altered the bath plating parameters. The investigations combined with those from Chapter 4, provided a preliminary insight into the MS plating on the PCB surface and allowed for a range of parameters to be chosen for investigations into MS plating down via interconnects, for development stage 2 outlined in Table 1.2 in Chapter 1. With regards to the scale-up into industry progress, Development Stage 1 was completed with the end of this chapter.

Chapter 6 Plating down Through-hole Via using Megasonic Assisted Agitation

6.1 Introduction

Megasonic (MS) plating has been introduced in through-hole via (THV) plating and shown to produce significantly improved Cu plating effects over the standard agitation techniques employed, as discussed in Chapter 2 [12]. Manufacturing improvements could be obtained if settings were reproduced under manufacturing conditions, as seen by increased interconnect features through the board and improved heat dissipation. This chapter discusses investigations performed involving MS plating down THV interconnects in a 500 L plating bath. The chapter is organised into two sections. The first set of investigations addressed in section 6.2 observe plating enhancements from the deposition of Cu thicknesses around 20 μm down the THVs. This thickness is commonly applied in manufacture and requires a short plating time and therefore was a useful parameter to set, as multiple plating trials could be performed in a short time duration. Plating bath agitation was altered for these trials, to provide a standard with which to compare the MS ability to agitate the solution. These investigations addressed Development Stage 2 in Chapter 1, Table 1.2 - whereby an evaluation was made of the MS inclusion for THV plating. The second set of investigations in section 6.3 observes plating enhancements when attempting to uniformly fill the THV with Cu and to reproduce the results obtained in the previous literature. If successful, these trials would highlight the MS ability to provide vast improvements to board lifetime and thermal management. The parameters altered in this study included the THV diameter, the electric and acoustic magnitudes and waveforms, and the angle of the transducer to the Printed Circuit Board (PCB) surface. Simulations were performed alongside these investigations to provide further understanding of the acoustic behaviour within the THV.

6.2 MS plating down THV in the thin Cu regime

The performance of THV electroplating can be directly manipulated by controlling the circulation of electrolyte solution through the THV, which enables the replenishment of depleted cations in solution and reduces the Nernst diffusion layer, as discussed in Chapter 2. A range of agitation techniques are available to the PCB manufacturer as outlined in Chapter 2. Little investigation has been performed to compare the MS agitation ability with each of the standard bath agitation techniques. Quantifying

the MS ability would be extremely useful for scaling up the technology and providing a metric by which enhancement can be measured.

The following plating trials were performed depositing 20 μm of Cu down the THVs. The parameters altered were the different bath agitations.

6.2.1 Standard bath agitation effects in comparison to MS THV plating

The quality of the electrodeposit formed down the THV was categorised from the plating rates measured from three different positions, as outlined in Chapter 3. These regions were the surface, neck and middle of the THV. The thickness values were then converted into plating rate by dividing them by the total duration of time taken to plate.

Plating experiments were performed as outlined in Table 6.1.

Table 6.1 - Plating setup for Experiment 6.2.1

Experiment Number	Plating Parameter Investigated	Experiment Parameters			Measurement Obtained	Purpose
6.2.1	Bath agitations: Bubbles & Movement; MS; no agitation	Transducer	Tangential Position to PCB X (cm)	4.5	Quantitative measures of the plating rate change inside the THV in response to the bath agitations applied.	Quantifies MS ability to deposit small amounts of Cu relative to the bath agitations applied in PCB manufacture.
			Acoustic power output (W)	450		
		Current Density (A/dm ²)	DC, 2			
		Plating Duration (min)	45			
		THV diameters (mm)	0.36, 0.35 & 0.40			

Highlighted in Figure 6.1 are microsections of the plating results, where the THVs were ground down to within $\pm 25 \mu\text{m}$ of their centres. The images showed that the Cu thickness was greatest at the surface of the THV and reduced further into the via, which is typical of via plating behaviour [148]. The average plating rates were evaluated from four individual measures of thickness, at different positions within the vias and for different agitation settings and were displayed in Figure 6.2 with their standard deviations included. At the surface of the THV the plating rates did not vary considerably, although, into the THV, the behaviour changed. At the neck of the via the Cu thickness reduced compared to the surface and was greater for MS than under standard agitation.

At the middle of the THV the Cu thickness plated was, when compared to the surface, approximately 20% that of standard agitation, which was in line with expected values. With no agitation there was an approximate 50% reduction and with MS there was an approximate 80% reduction. With no agitation it was reasonable to assume that

the plating rate would be vastly reduced, but the lower value measured with MS was a surprising result, as it showed an increased hindrance to fluid circulation. This was highlighted in Figure 6.1A by the smaller deposit inside the THV for the MS setting. The variation of Cu thickness was greatest when the settings, namely ‘MS’ or ‘no agitation’, were applied. With no agitation, a large crystalline growth was favoured, see Chapter 2, this displayed poor topography uniformity and contributed to the large variation measured. When applying MS the Cu variation measured was also high, showing that uniformity did not improve with it, additionally the variation added an error to the measured thickness, making it difficult to evaluate trends.

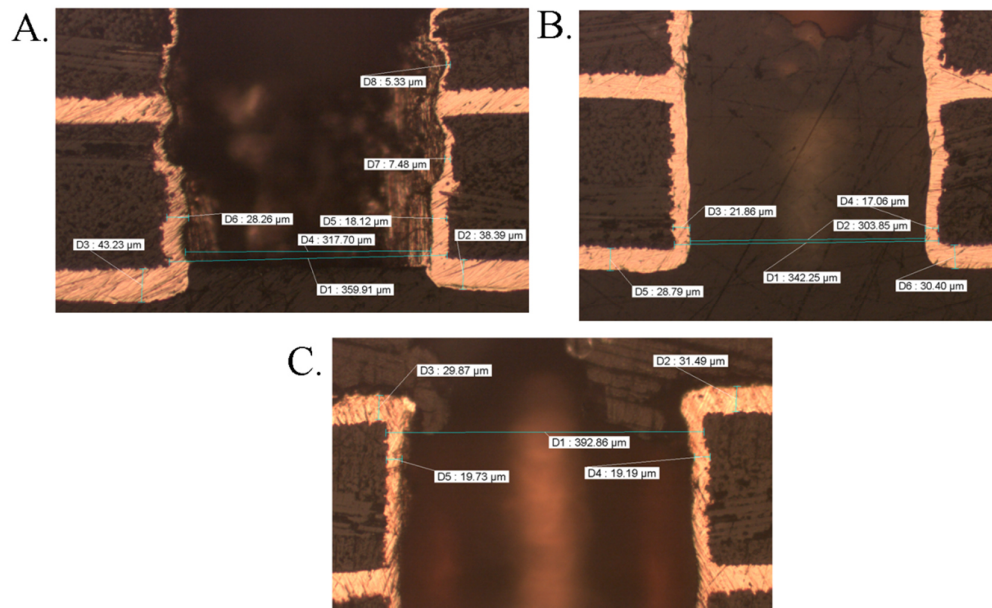


Figure 6.1 - Microsections highlighting plating performance after 45 min plating at 2A/dm² for A) transducer setup 4.5 cm tangential to PCB and outputting at 450 W, showing a 0.36 mm diameter THV at 4.4:1 B) Panel movement & Bubble agitation showing a 0.35 mm diameter THV, at 4.6:1 and C) no agitation, showing a 0.40 mm diameter THV, at 4:1.

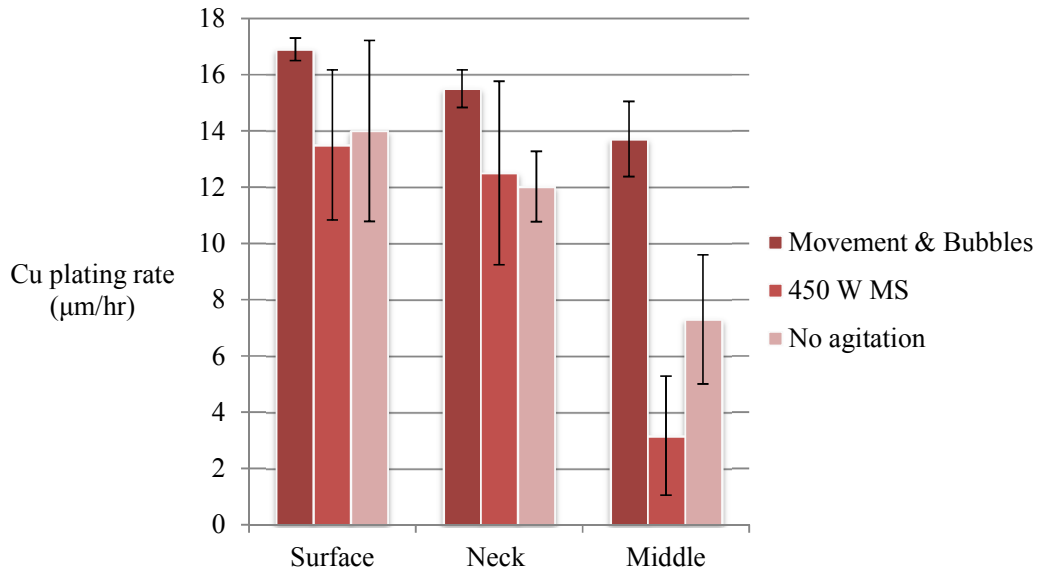


Figure 6.2 - The average plating rates from four measurements, taken on samples formed after standard, MS plating at 450 W and no agitation were applied, in different regions on the THV outlined in Chapter 3, Fig 3.7.

6.2.2 50 Hz vibration effects on MS THV plating

A drop in performance was observed in the previous section when introducing MS agitation into THV plating. The performance drop possibly related to a poor fluid circulation within the THV, where its flow was being prevented and/or a poor compatibility of the plating chemistry and the acoustic agitations. A possible related cause could be the formation of an acoustic standing wave in response to the MS within the THV. If a standing wave is set up within a cavity the overall net propagation of energy is zero, which, when translated to MS plating down a THV, means that a minimum fluid circulation into and out of the via occurs via Rayleigh streaming, as discussed in Chapter 2 [149].

A wide range of acoustic streaming mechanisms is possibly occurring within the THV. It is the goal of the plating trials to alleviate any negative acoustic effects and encourage positive effects. It is uncertain which of the microfluidic motions contribute to the plating enhancements obtained under laboratory conditions. For this reason an investigation was made to disrupt the formation of a standing wave. Disrupting the phase of a travelling acoustic wave will prevent the formation of standing waves within a cavity [150] and phase modulating transducers can be provided for this use. An alternative method of disrupting the acoustic wavefront is to induce vibrations on the THV. The transducer in use did not have phase modulation and so, to save on equipment costs, a

50Hz mechanical vibrator was purchased and setup on the cathode rail on the plating line, see Chapter 3, with the aim of disrupting the wavefront to prevent the formation of standing waves within THVs. Investigations were performed, as outlined in Table 6.2, on the impact of panel vibration on the plating thickness and the uniformity of the deposit down the THVs. The plating parameters, THV sizes and transducer position were altered to observe if these parameters had any influence on the plated thickness.

Table 6.2 - Plating setup for Experiment 6.2.2.

Experiment Number	Plating Parameter Investigated	Experiment Parameters			Measurement Obtained	Purpose
6.2.2	Bubbles & Movement; MS; no agitation; Panel vibration; THV diameter	Transducer	Tangential Position to PCB X (cm)	4.5	Quantitative measures of the plating rate change inside the THV in response to the bath agitations applied; THV diameter.	Highlights whether acoustic standing waves can be prevented with the additional introduction of 50 Hz vibration.
			Acoustic power output (W)	225 & 450		
		Current Density (A/dm ²)	1 & 2			
		Plating Duration (min)	45 & 60			
		THV diameters (mm)	0.275 and 0.475			

Highlighted in Figure 6.3 is a plot of the micro-throwing power, evaluated as the average plating thickness measured from five different THVs on same plated PCB in the middle region of the THV, divided by the average value on the surface and given as a percentage, see section 3.3.4 in Chapter 3. Included for each mean is its standard deviation. The 50 Hz vibrator was included with standard bath agitations whilst plating and the efficiencies were measured for 0.275 mm and 0.475 mm diameter THVs. For the smaller THV the micro-throw was reduced as expected due to the increased difficulty to pass solution through the smaller cross-section of the hole [151]. For the larger diameter the micro-throw was approximately 80%, as expected for the plating setting. With the introduction of MS along-side the 50 Hz vibration, there was no measurable alteration to the micro-throw, highlighting that no increased performance was obtained from a combination of the two.

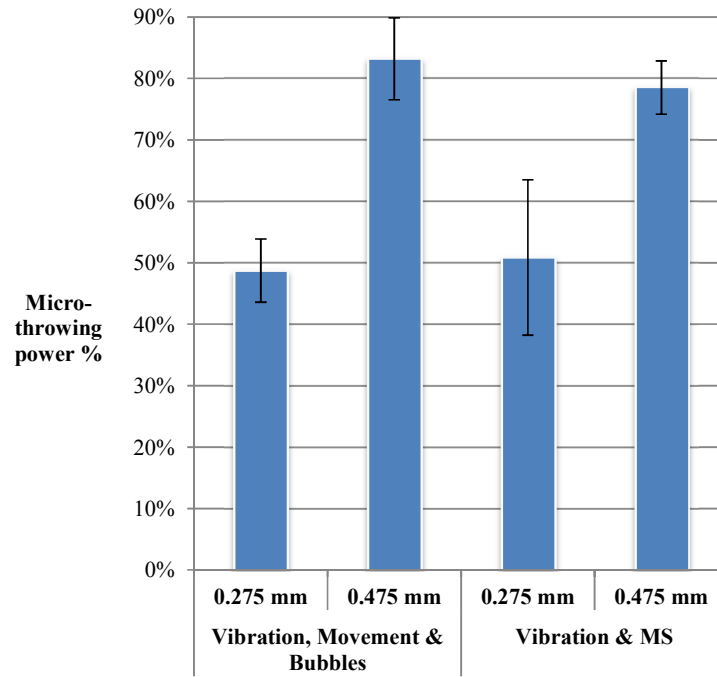


Figure 6.3 - Plot of the micro-throwing power given in units of %, derived from measures of average plated thickness from the mid-point and surface of THVs of different diameter and bath agitation settings, plated under 2 A/dm², with the transducer at 4.5 cm and 450 W of acoustic power for 45 min.

To evaluate the contribution to the plating by the combination of the 50 Hz agitation and the MS, the parameters were investigated individually on a small diameter THV at 0.225 mm and at a lower plating current density, 1 A/dm². The PCBs were plated to settings outlined in Table 6.2. Six different settings were tested and the plating micro-throwing power evaluated from average values of plating thickness obtained from five different THVs from the same PCB. The micro-throwing values are plotted on Figure 6.4 along with their standard deviations. The results highlight that, with 50 Hz agitation, the micro-throwing power is comparable to the standard agitations used in manufacture – bubble agitation and panel movement. This result is known in PCB manufacture.

The micro-throwing power was extremely small during the MS plating trials and was comparable to no agitation. The acoustic power was increased from 225 W to 450 W and a negligible increase in micro-throwing power was observed. The results highlight that the micro-throwing power obtained for the combination of vibration and MS was most likely a result of the vibration component agitating the solution through the THV and not the MS wave.

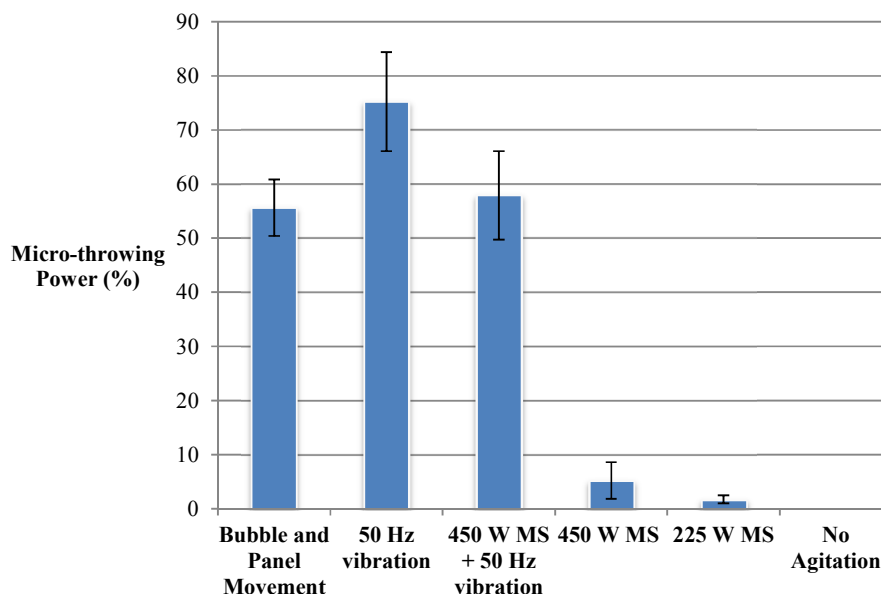


Figure 6.4 - The micro-throwing power evaluated down a 0.225 mm diameter 8:1 THV, derived from measures of plated thickness at the mid-point of the THV and the surface, plated under 1 A/dm² for 60 min.

6.2.3 Conclusions

The first investigations of the MS introduction into THV plating reveal that no enhancement of the plating occurs down the THV. This was displayed from measurements of the plated thickness, where in difficult-to-plate-regions – the centre of the THV – a minimal amount of Cu was deposited. Low thicknesses were expected in the middle of the THV, due to increased resistance to fluid motion by increased micro-fluidic effective viscous forces, although the values obtained with MS were on par with no agitation, suggesting little fluid circulation has occurred.

A possible reason for the low plating performance includes the acoustic force being too small to agitate the solution and provide the electrolyte replenishment required for efficient plating. The literature on MS agitation, highlighted in Chapter 2, has shown that the acoustic forces are sufficient to reduce the diffusion layer and replenish the electrolyte down via interconnects and so it is unlikely that it is this effect.

Another issue could be bubble entrapment within vias, as their presence prevents the deposition of Cu from solution. Agitation of the solution is required to remove bubbles and so a weak agitation of the solution will not efficiently remove these. The tear-shape of the voiding obtained when MS plating is different from the more circular appearance

of a void formed from an entrapped bubble. This suggests that bubbles have not become entrapped and that effective removal has occurred with MS.

The most likely cause for the lack of deposition was due to acoustic resonant effects, whereby net fluid motion through the THV, was hindered due to acoustic standing waves forming within [70, 152]. An investigation was made seeking to disrupt resonant acoustic modes by altering the phase of the acoustic wave at the surface of the PCB. This was attempted by the introduction of 50 Hz mechanical vibrations to the cathode PCB. The studies showed that vibration was an effective technique for circulating fluid down the THVs, producing efficiencies comparable to the standard agitation techniques. The 50 Hz vibration was effective at preventing acoustic standing wave formation indicated by an increased uniformity down the THVs, but the vibrations – such as panel movement - negated any evidence for acoustic enhanced plating and efficiencies above standard levels. For this reason the 50 Hz vibration was not used again in further investigations.

The plating trials were performed depositing small, 20 μm deposits of Cu down the THV. The previous enhancements to plating obtained by the Heriot-Watt University group were obtained when plating Cu deposits thicker than 20 μm . For this reason it is possible that a size dependency is present on the THV, where plating enhancements occur due to changes in acoustic resonant conditions for thicker deposits. When depositing between 10 μm and 20 μm of Cu onto a PCB using standard conditions, a variation of 2 - 3 μm was likely due to the distribution of electrical current across the board. This variance was carried forwards in the evaluation of the micro-throwing power, reducing the accuracy of the measurement. To reduce the error and improve evaluation of MS plating behaviours, thicker deposits of Cu down the THV were plated.

6.3 MS plating down THV in the thick Cu regime

The previous MS plating enhancements reported in literature were witnessed for depositions of Cu between 100 – 250 μm down the THVs [12]. These values were considerably thicker than those deposited in section 6.2 and were the result of higher plating current density and longer plating durations. MS plating enhancements were not witnessed down THVs when plating for short plating durations. The thick deposit plating regime was investigated, seeking to reproduce the plating enhancements witnessed in the literature, which were produced after plating durations longer than 12 hours.

Plating parameters were altered to highlight MS plating behaviour, which include the THV diameter, agitation, the acoustic and electric waveforms and the angle

positioning of the transducer. The angle of the acoustic wave's propagation relative to the PCB is defined in Figure 6.5.

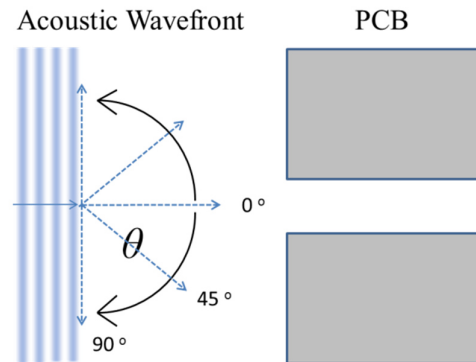


Figure 6.5 - Schematic of the acoustic transducers orientation to the PCB.

6.3.1 Cu patterning for different THV diameters

MS plating was performed on THVs of different sizes under settings outlined in Table 6.3.

Table 6.3 - Plating experiment setup for MS THV plating investigations 6.3.1.

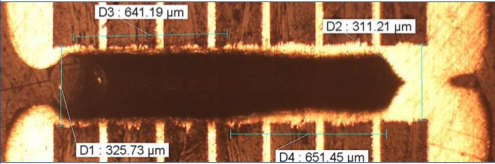
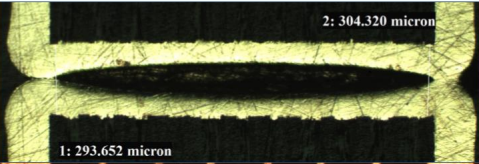
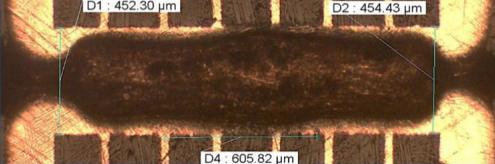
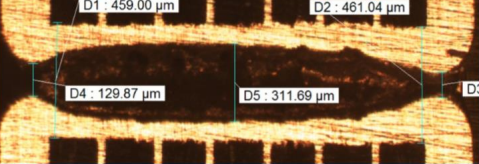
Section		Plating Parameters Altered	Experiment Parameters				Measurement Obtained	Purpose
			Transducer Settings	Current Density (A/dm ²)	THV diameter size (mm)	Plating duration (hr)		
6.3	6.3.1	THV diameter, Panel flipping	4.5 cm tangential distance, 450 W	0.5	0.175	15.50	Quantitative measures of the Cu plated thickness.	Quantified performance of MS plating deposits down THVs of different diameters in response to plating parameter changes.
			8.5 cm tangential distance, 0W & 225W	1.0	0.325	16.50		
			8.5 cm tangential distance, 0W & 225W	1.0	0.475	16.20		
			1.0 cm tangential distance, 225 W	2.0	0.525	16.75		

Typical plating behaviours show that smaller THV diameters produce a smaller deposition of Cu down the middle, as shown in Section 6.2.2. When depositing for longer plating durations the Cu behaviour displayed different characteristics than for short plating durations.

Shown in Table 6.4 are microsections of plated results, highlighting via diameters and distances between Cu plated features for 0.325 mm and 0.475 mm diameters, respectively. THV plated with 225 W MS agitation and the transducer setup 8.5 cm tangential to the PCB and with standard agitation. For THV of diameters larger than 0.30 mm the inner region contains little Cu. The Cu deposited after MS plating was characterised by variations in plated Cu thickness, where as the plating obtained with

standard agitation was characterised by a large build up at the entrance of the THV and with a smaller deposition towards the centre, characteristic of electrical field line attraction, see section 2.1.5 in Chapter 2. Periodic changes in Cu thickness after MS plating were observed on the surface of the PCB and were attributed to standing wave effects - displayed in Chapter 5. The variations here were only observed under MS plating configurations and so are again attributed to standing wave effects, like those on the surface of the PCB under MS. In section 6.2 standing wave effects were attributed to the small deposits obtained inside the THV. In Table 6.4 the plating is significantly smaller down the MS plated THVs than the standard agitation conditions – panel movement and bubbles – suggesting that standing wave formation may have influenced the outcome. The separation distance between the thick / thin Cu deposits down the MS plated THV was approximately 650 μm which is approximately half of the acoustic wavelength in solution. For this reason the deposits obtained here are also attributed with standing waves.

Table 6.4 - Plating behaviour for THVs formed under different agitation conditions and for different sized diameters. PCBs plated a 1 A/dm^2 for 16.5 hour for the 0.325 mm THV and 16.2 hr for 0.475 mm THV and when used, transducer positioned tangential to PCB at 8 cm.

	225 W MS agitation	Standard agitation
0.323 \pm 0.025 mm		
0.475 \pm 0.025 mm		

Plating trials were performed down THVs of diameter 0.175 mm with aspect ratio, ar , of 5.7:1. This diameter was chosen as it is the minimum size for THVs on a PCB at this ar and so any improvements witnessed here would reflect an increase in PCB plating capability. The PCBs were plated at 0.5 A/dm^2 , for 15.5 hours with the transducer setup 4.5 cm tangential to the PCB. These plating results were displayed in Figure 6.9 with 225W MS and without any agitation. With MS the Cu deposited down the THV vastly improved. The exact amount deposited was quantified later in section 6.3.2.

The plating outcome was significantly different from those obtained on THVs of diameters larger than 0.3 mm. Down the THV the Cu was more evenly deposited, showing pinching at the ends of the THV, which was expected under Direct Current (DC) plating conditions. The result additionally showed that MS plating enhancement was THV diameter size and board thickness dependent.

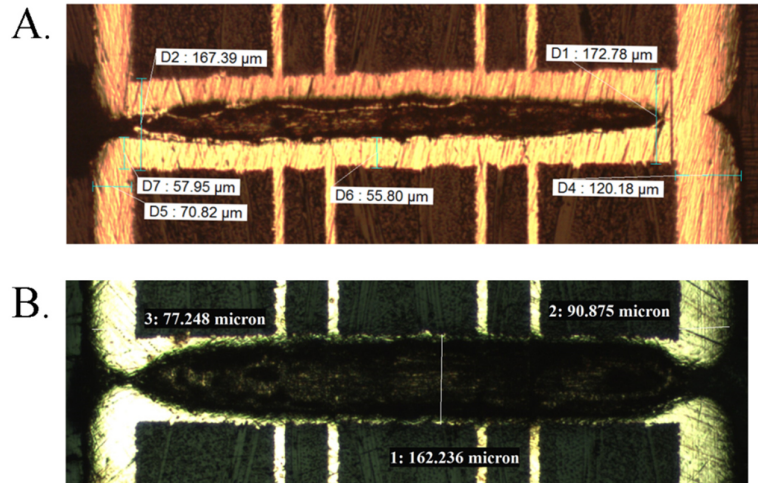


Figure 6.6 - Microsections of 175 µm diameter ($ar = 5.7:1$), THV interconnects on a PCB electroplated at 0.5 A/dm^2 , for 15.5 hours and showing A) with 450 W MS and transducer setup 4.5 cm tangential to PCB and B) plating with no bath agitation.

To provide further insight into the relationship between standing wave acoustic distribution and the Cu deposition, COMSOL acoustic scattering simulations were performed as indicated in section 3.5, Chapter 3. The simulations modelled the acoustic pressure as the acoustic wave interacted with the internal structure of the PCB, reflecting and superimposing due to the varying acoustic impedances of the individual materials. The simulation output was a pressure distribution, which was overlaid on the simulated 2D feature by a colour plot, where red represent pressure maxima, blue represent pressure minima and white represent pressure nodes – regions undergoing no pressure change.

Simulations were performed modelling 2-dimensional (2D) THV features of diameter 0.5 mm for two different acoustic plating settings. The two settings involved non-flipping and flipping the PCB at set intervals during the plating cycle. Flipping the PCB evenly distributed the Cu plating over either sides of the board and the influence by the acoustic wave. Not flipping the board led to an increased build-up of Cu on one side of the board, where the other side received a greater agitation by the MS. The plating and simulated results are shown in Figure 6.7, in A the PCB was flipped and in B it was not.

The Cu thickness on the PCB surface – shown on the left and right of the images – was of similar thickness in A and was uneven in B.

The plated result in A was a THV of diameter 0.525 mm and showed the undulating Cu pattern. Alongside was the pressure distribution plot obtained for the setup, where Cu thickness was exaggerated in the simulation at the entrance of the THV to model Cu pinching. Under this condition, three pressure nodes are observed within the THV, the first inside the THV neck, the second in the middle and the third outside the THV. The asymmetrical positioning of the node into and out of the THV on either ends, is due to the propagation direction of the acoustic wave, where, in the simulation, it is set up to travel from left to right. The extension of the pressure node outside of the cavity structure on the right is due to the end correction effect, which increases the separation distance between standing wave nodes outside of a cavity [63]. The simulated 0.5 mm diameter THV includes a pressure maximum / minimum region separated by half of the acoustic wavelength, which corresponds to a 2nd harmonic wave formed within an open-ended cylinder [153]. The undulation of the Cu in the THV appears such that the regions of minimum Cu deposition coincide with the pressure nodal regions and the thicker deposits with the pressure anti-node regions.

In B the Cu shows a thicker deposit on the anode facing side - right of the image - than the transducer facing side on the left. This is because the right receives a greater current due to its line-of-sight to the anode and the left additionally undergoes current thieving effects by the transducer. The corresponding COMSOL simulation highlighted how the acoustic pressure varied due to the asymmetric Cu deposition. It showed that the acoustic wave becomes increasingly reflected due the higher acoustic impedances of the thicker Cu - focusing the acoustic pressure wave into a pressure anti-node. The undulations observed within the THV also appear to correspond to the positioning of the pressure nodes and anti-nodes.

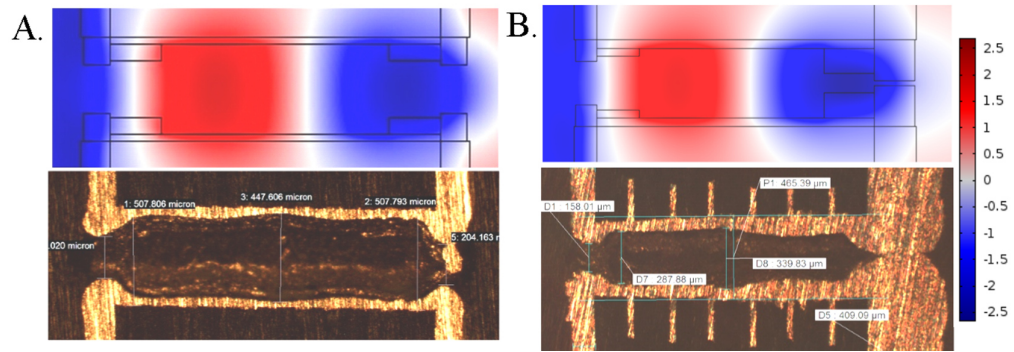


Figure 6.7 - 2D COMSOL simulated Acoustic Pressure distributions alongside MS plating results showing, A) MS Plating with PCB flipping and B) MS Plating with no PCB flipping. Scale bar for simulation showing normalised units of acoustic pressure.

Simulations were performed modelling the pressure distribution in cavities of size 0.15 mm, which were an approximation of the THV in Figure 6.8. Results were plotted for before any Cu had formed, A, and as the cavity closed up, B. The distributions are different from the pressure distributions obtained for the longer and wider cavities. Instead of a 2nd harmonic, a fundamental mode is observed, indicated by red as a single pressure anti-node formed within the cavity. In A the pressure nodes were situated outside of the THV and as the Cu thickness increased, the nodes are drawn in towards the entrances of the THV, confining the pressure anti-node.

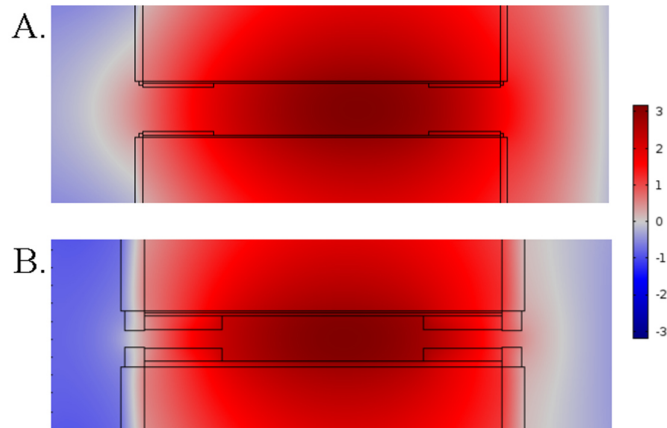


Figure 6.8 - COMSOL acoustic scattering simulations of 0.15 mm diameter, at 5.7:1 for A) little Cu and B) thick Cu. Scale bar for simulation showing normalised units of acoustic pressure.

The plating results for the different cavity diameters and lengths show that, as Cu was deposited within the THV, plating rates are influenced by the acoustic pressure distribution and the simulation results showed, conversely, that the pressure distribution changes as the Cu thickness increases over the plating lifetime.

6.3.2 MS Plating enhancements measured within the THV

The MS wave induces high energy acoustic cavitation and thermal increases on the PCB surface as explained in Chapters 5 and 4, respectively. Introducing a pause in its output reduces the MS agitation reaching the surface, but lowers the damaging thermal effects due to cavitation. The impact on plating rate due to a pulsed output is uncertain and so an investigation was performed applying an acoustic pulse modulation of 7 seconds on and 17 seconds off. The device was set up as indicated in Chapter 3.

The ability to deposit Cu with a continuous acoustic output, pulsed and no agitation, was quantified from measures of plating rates obtained in the middle of 0.15mm diameter THVs. Plating trials were performed as outlined in Table 6.5.

Table 6.5 - Plating experiment setup for MS THV plating investigations 6.3.2.

Section		Plating Parameters Altered	Experiment Parameters				Measurement Obtained	Purpose
			Transducer Settings	Current Density (A/dm ²)	THV diameter size (mm)	Plating duration (hr)		
6.3	6.3.2	Agitation settings: CW acoustic output, pulsed acoustic output & no agitation	CW acoustic output at 4.5 cm and 450 W	0.5	0.175	15.50	Quantitative measures of the Cu plated thickness.	Quantified MS plating quality obtained down THV structures in response to plating parameter changes.
			Pulse acoustic output (7 sec on and 17 sec off) at 4.5 cm and 450 W			16.00		
			Not in bath			16.00		

The plated thicknesses measured under the different settings were shown in Figure 6.9 and the evaluated average plating rates evaluated from ten measures of Cu thickness were plotted on Figure 6.10 along with their standard deviations. Results show that, under no agitation, an extremely small plating rate was obtained. This was as expected as the fluid circulation within the THV under this condition was solely due to natural fluid convections within the bath, which are slow and thus are poor at replenishing depleted Cu cations.

With MS the plating rate increased by approximately 700 % inside the THV when compared with no agitation. This was due to enhancements to acoustic streaming forces through the THV. The results obtained when applying pulsed acoustics showed a reduced plating rate compared to MS plating, although it was approximately 400 % thicker than under conditions of no agitation. This result showed that with a non-continuous supply of

acoustic agitation the solution was stirred sufficiently to produce some enhancement to plating performance, although was not as effective as continuous agitation.

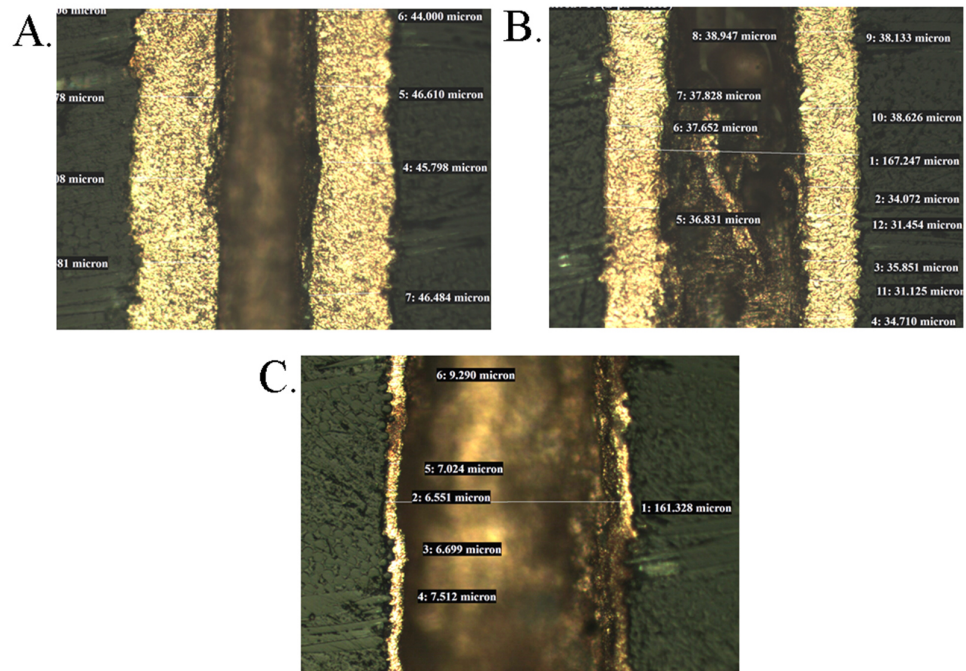


Figure 6.9 - Microsections of the Cu thickness in the middle of 0.15 mm diameter, at 5.7:1 THV, deposited at 0.5 A/dm² for 16 hours under conditions of A) 450 W MS, B) Pulsed acoustic and C) no agitation. When used transducer setup 4.5 cm tangential to PCB.

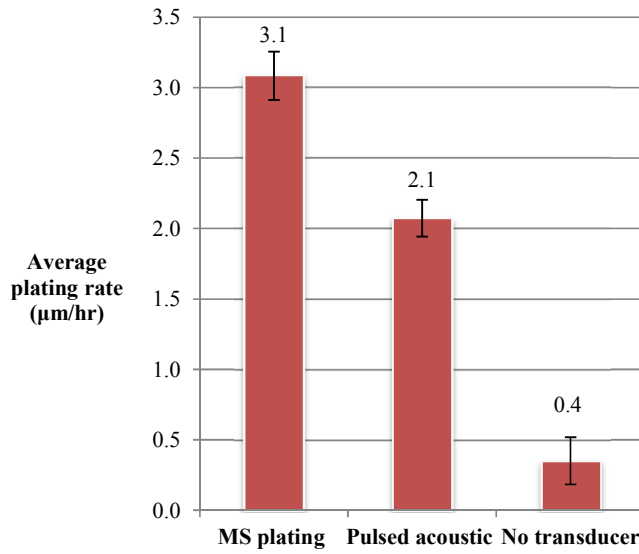


Figure 6.10 - The average plating rate evaluated from ten measures of Cu thickness taken in the middle of 0.15 mm diameter, at 5.7:1 THV, after processing under different conditions.

6.3.3 Transducer angle orientation alteration

The transducer can be placed within a wide range of orientations in the plating tank, as indicated in Chapter 3, Figure 3.15. Tangential distance of the transducer has been shown to be an important parameter influencing plating rates due to its impact on current thieving, as shown in Chapter 3, and plating uniformity, as discussed in Chapter 4. Little research has been performed attempting to quantify the change in THV plating capability in response to changes in transducer orientation to the PCB. For this reason a range of plating investigations were performed changing the angle of the transducer and distance to the PCB surface. The transducer was set up as indicated in Chapter 3 and Figure 6.5 and plated under conditions outlined in Table 6.6.

Table 6.6 - Plating experiment setup for MS THV plating investigation 6.3.3.

Section		Plating Parameters Altered	Experiment Parameters				Measurement Obtained	Purpose
			Transducer Settings	Current Density (A/dm ²)	THV diameter size (mm)	Plating duration (hr)		
6.3	6.3.3	Transducer orientation and tangential distance	1.0 cm distant, 0° orientation, 450 W	1.0	0.475	15.8	Qualitative observations of the plated behaviours response and a qualitative comparison with simulated results	Quantify MS plating behaviour on changes to transducer orientation to the PCB and THV feature sizes.
			20.4 cm distant, 25° orientation, 450 W			16.2		
			9.53 cm distant, 45° orientation, 450 W			16.0		
			14.7 cm distant, 53° orientation, 450 W			16.2		
			1.0 cm distant, 90° orientation, 450 W			16.3		
			-			16.0		

The THV diameters investigated were larger than 0.3 mm. This size was chosen as it displayed no plating enhancement with MS agitation, so changes to the agitation settings were investigated to see if an alteration could be made to improve performance.

To fit the transducer within the bath at an angled orientation, the distance from the transducer to the PCB had to be increased. This reduced the acoustic pressure reaching the PCB. Additionally, for the 0° orientation of the transducer the tangential distance was 1 cm. At this distance current thieving would have occurred, reducing the amount of Cu deposited. The two effects would have had a non-linear impact on the amount of Cu deposited, which made it difficult to provide a comparison between plating rates for the different orientations. For this reason a qualitative comparison of plating behaviours was made.

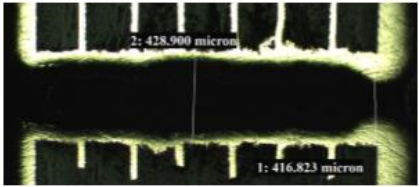
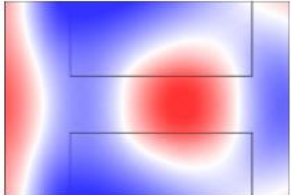
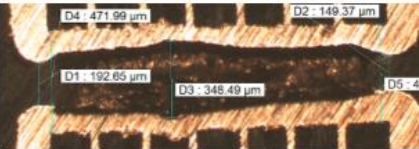
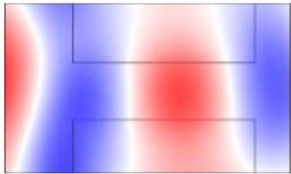
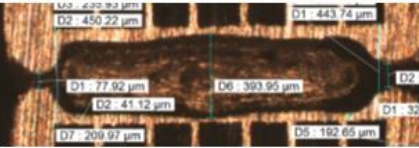
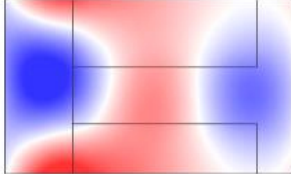
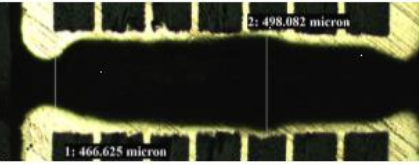
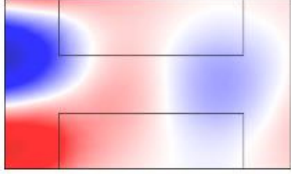
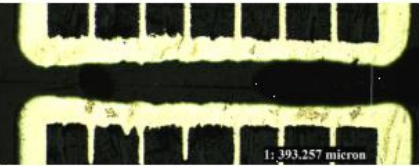

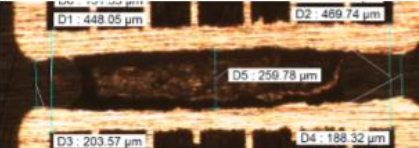

Highlighted in Figure 6.7 are micro-section images of THVs MS plated under different orientations of the Transducer. The results highlight the centre of the THV to within $\pm 50 \mu\text{m}$ of its diameter. For angles less than 90° the uniformity of the Cu deposited reduced along with its plated thickness. The plated pattern bears a resemblance to features obtained previously on THV diameters greater than 0.3 mm, see section 6.3.1, which indicates that standing wave acoustics are likely influencing the outcome. To confirm this, COMSOL simulations were performed with a setup as indicated in Chapter 3. The simulation modelled the 2D acoustic scattering distribution within a 0.5 mm diameter cavity of length 1.6 mm, for an angled orientation of the acoustic wave travelling from left to right. The simulation output is displayed in Table 6.7 alongside a corresponding micro-section image.

Qualitative observations of the simulated results show that the pressure distribution varies when the angle of the acoustic agitation is changed. The wave behaviour is influenced by the specific acoustic impedances of the FR4 structure and the

water fluid medium. The specific acoustic impedance of a medium is a measure of its opposition to acoustic flow [154]. It is given by the density of the medium multiplied by the acoustic sound speed of the structure. For the FR4 in the simulation, its value is $6.84 \times 10^6 \text{ kg.m}^{-2}.\text{s}^{-1}$, or Pa.s.m^{-1} and for the electrolyte medium, $1.48 \times 10^6 \text{ Pa.s.m}^{-1}$. As the impedance is higher in the FR4 it hinders the propagation of the wave, absorbing the acoustic energy and generating the pressure distribution within the cavity structure.

As the angle of the transducer was increased towards a 90° orientation, the acoustic pressure reduced within the cavity observed by an increase in white in the pressure plots. At a tangential orientation, the plating behaviour resembled standard processing without MS, characterised by a tear void and overplanting at the ends of the THV as shown in the image at the bottom of the table.

Table 6.7 - Plating rate measured in the middle of the THVs in response to angle orientation of the transducer with corresponding COMSOL simulated acoustic scattering distributions. Image includes of THV plated under standard agitations without MS.

Angle of Acoustic agitation ($\pm 5^\circ$)	Micro-section Image	Acoustic pressure scatter distribution
0°		
25°		
45°		
53°		
90°		
		

The acoustic energy coupled into the cavity appears to decrease for angles closer to 90°. To quantify this change the pressure values from inside the 2D THV cavity were obtained from the simulated data and the average acoustic potential energy density was evaluated in response to a change in orientation of the sonication. The energy density was

evaluated using the method outlined in Chapter 3 and values were obtained for cavities of diameters 0.5 mm, *ar* 3.2:1 and 0.2 mm, *ar* 8:1, in order to compare changes on size alterations. The results are plotted on Figure 6.11. Both sizes show that the acoustic energy is minimised when the travelling wave is tangential to the THV cavity and is at a maximum when parallel, 0°. When setting up the simulation the background acoustic pressure value was input manually. Making changes to this value appears to create no noticeable variation in the pressure distribution only the magnitude of the pressure maxima / minima. This was due to the limitations of the scattering simulation, as the COMSOL software simulates linear acoustic effects rather than non-linear acoustic effects, which alter the magnitude of the acoustic pressure [63]. For this reason the magnitude of the energy values derived from the calculation did not provide an accurate quantification of the energy within the THV. The two cavities were simulated with the same initial background pressures, so the data were normalised with respect to the largest value measured.

The smaller cavity coupled a larger potential energy density than the large-cavity. A maximum energy was coupled into the cavity at 0° which was 260 % larger in the small cavity compared to the large cavity. For both cavities the pressure coupled into the THV at this angle was significantly larger than input pressure, which indicates that the superposition of the wave within the cavities is due to constructive interference - focusing the acoustic wave. A more complete description of the behaviour requires a literature review on the topic of acoustic focusing, specifically on the behaviour at subwavelength scales.

With the data obtained of the acoustic pressure energy density. The small cavity case is more susceptible to alignment of the acoustic wave, where a change from 0° to 20° results in a 50 % drop in acoustic energy and compared to a 40 % drop for the large cavity case.

The plated results show that, at larger angles, a greater plating deposition is obtained and that Cu uniformity resembles standard processing without MS. The acoustic pressure energy density is minimised at these angles, negating acoustic effects on the plated deposit - which appear to negatively influence plating on 0.30 mm diameter THVs.

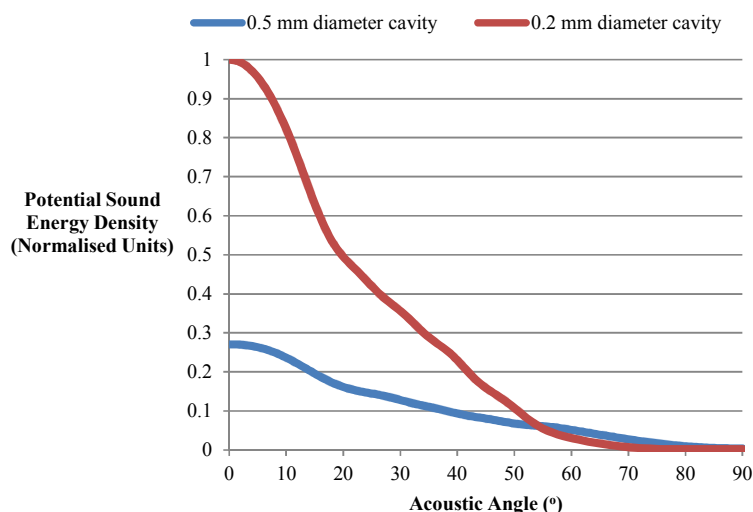


Figure 6.11 - A plot of the normalised, average potential sound energy density measured within the THV cavity in response to sonicating angle, using pressure values obtained from COMSOL simulation.

6.3.4 Acoustic pressure and electric current density and waveform alterations

The electrical current density is an important property controlling the rate at which Cu is deposited, as discussed in Chapter 2. For high current density, the plating rate is fast and the Cu deposited in the middle of the THV should be high. When using DC plating currents the opposite occurs however. The replenishment of electrolyte down the THV is controlled by the bath fluid agitation. If the replenishment rate does not increase alongside the deposition rate, then the rate of depletion overcomes repletion, reducing Cu concentration and preventing deposition. This is an unwanted result as it leads to reduced plating rates in the centre of the THV relative to the PCB surface, which is counter to the goals of depositing Cu down THVs. As such, a low current density should produce an enhanced micro-throwing power down the THV.

MS plating was performed down 0.3 mm diameter THVs, changing the electrical current density and the acoustic pressure output. The plating trials were set up under conditions outlined in Table 6.8.

Table 6.8 - Plating experiment setup for MS THV plating investigation 6.3.4.

Section		Plating Parameters Altered	Experiment Parameters				Measurement Obtained	Purpose
			Transducer Settings	Current Density (A/dm ²)	THV diameter size (mm)	Plating duration (hr)		
6.3	6.3.4	Changes to the electrical current magnitude and waveform and acoustic pressure	1.0 cm, 4.5 cm and 8.5 cm, tangential orientations, at 225W and 450 W	DC 0.5, 1.0 RP 1:2, 0.5:1	0.325, 0.175	15.0, 16.5	Quantitative measures of micro-throwing power in response to acoustic pressure, current density, electrical waveform and transducer distance variations.	Quantified enhancements due to low electrical current densities and high acoustic pressures, and an evaluation of plating waveform on MS plating performance.

Five measurements of the Cu thickness were recorded on the surface and down the middle of the PCB after 15 hours of plating and used to evaluate the average plated thickness. From this the micro-throwing power was evaluated.

Figure 6.12 shows that a lowest micro-throw is obtained for 1.0 A/dm² and 225 W acoustic output. Lowering the current density to 0.5 A/dm² reduces the plating rate on the surface and down the THV, but allows for a greater replenishment of depleted ions. As such the MS agitation was more effective and the micro-throwing power increases. An increase of acoustic output to 450 W enhances the micro-throwing power further. This is most likely due to increased replenishment of Cu cations due to the larger acoustic forces driving the solution through the THV. The results confirm that increased plating efficiencies are obtained for lower current density and that higher values may be obtained when the acoustic power is maximised. Regardless, the plating efficiencies obtained are comparable to those obtained under standard plating agitation conditions without MS, which are highlighted as 0 W at 1 A/dm² on the plot.

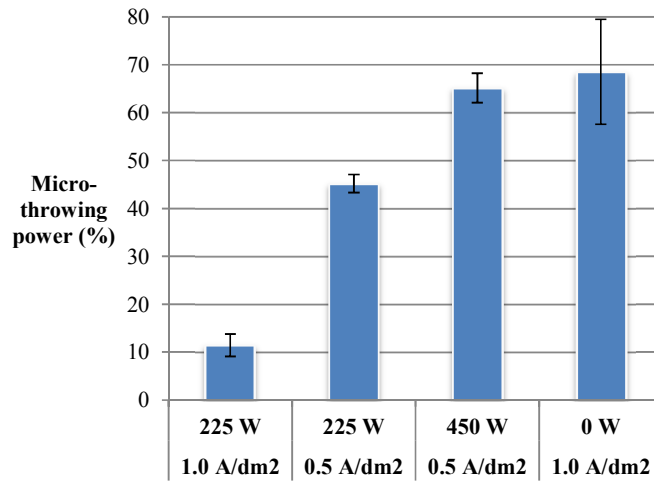


Figure 6.12 - Micro-throwing power evaluated within the centre of 0.325 mm diameter, *ar* 3.4 : 1 THVs with the transducer setup at 8 cm. THV plated for 15 hours.

Reverse pulse (RP) electroplating is the most common electrical waveform applied in PCB manufacturing, as it provides the largest deposition down via interconnects and the most uniform plating of Cu down via holes, see section 2.1.6 in Chapter 2 [155]. The largest MS plating enhancements in the current investigations are observed on 0.15 mm diameter THVs, *ar* 5.7:1 and so plating trials were performed seeking to enhance this behaviour further using RP plating.

The RP current comprises of a reverse and a forward components whose magnitude and duration are set before plating. The RP plating cycle applied under a manufacturing setting are altered depending on the desired plating outcome. To reduce the unwanted pinching effect, which occurs at the neck of vias, a large forward to reverse ratio at 1:3 is applied during the plating cycle. The negative impact of this setting is that it increases the surface roughness of the Cu deposit. [40]

An extremely low forwards current density was chosen at 0.5 A/dm². 0.5 A/dm² induced large, unwanted Cu crystalline growths, as shown in Chapter 4, and if applied with a high reverse current would amplify this growth. A compromise was made between via pinching reduction and an unwanted crystallinity by choosing the 1:2, forward:reverse, RP plating setting. The durations of the forward:reverse pulses have been chosen using recommended standard settings at 10 ms and 0.5 ms, respectively.

RP MS plating trials were performed as indicated in Table 6.8 plating for 16.5 hours, with the transducer outputting at 450 W and setup at various tangential positions. A plot of the micro-throwing power was made, indicated in Figure 6.13. At 0.5 A/dm² DC the micro-throw was around 50%. The introduction of an RP reverse current at 1:2

A/dm² reduces the micro-throw to 20%. This is likely due to the higher plating current density closing the via before electrolyte can replenish. On a reduction of the RP current density to 0.5:1 A/dm², the micro-throw increases back up to approximately 50% which is comparable to the DC setting. To increase the acoustic pressure down the THV, the tangential distance of the transducer was reduced 4.5 cm to 1 cm. At this distance current thieving occurs and reduces the plating currents in the THV but enables cation replenishment. Despite these changes the plating efficiency did not improve.

The results highlight that, introducing a reverse pulse plating cycle, did not noticeably improve the MS deposition down 0.15 mm diameter THVs.

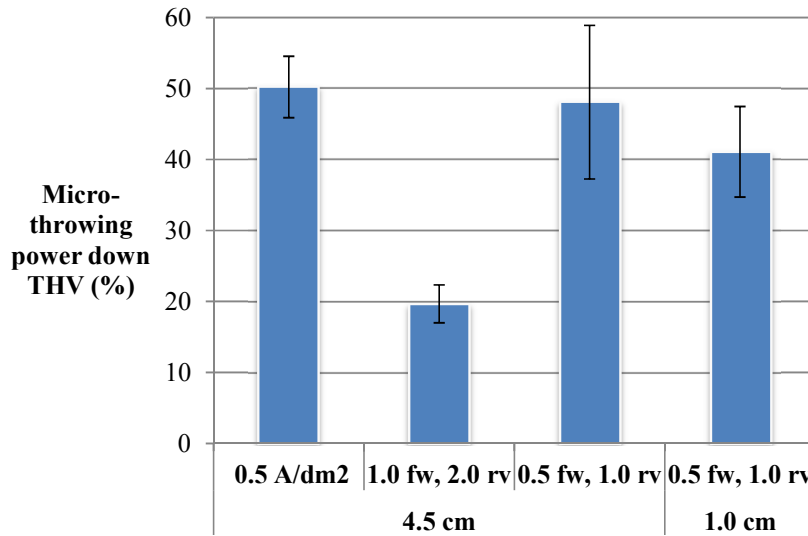


Figure 6.13 - MS plating investigation on 0.15 mm diameter THVs changing the transducer tangential distance, electrical waveform and current density. PCB plated for 16.5 hours with 450 W MS and evaluations of micro-throwing power made from average measures of plated thickness.

Plating at 0.5 A/dm² yield the highest plating efficiencies, although at this low current density a brittle and non-uniform deposition was plated. Highlighted in Figure 6.14A & B, are microsection images of the Cu deposited at the neck of a 0.15 mm diameter THV and on the surface of the board, respectively. The THV was plated for 16.5 hours and with the transducer setup at 4.5 cm and outputting at 450 W. A large Cu growth can be seen blocking the entrance of the THV and an extremely large 80 µm Cu variation was measured on the PCB surface. Blocking the entrance of the THV is not desirable as it will prevent Cu cation replenishment into the THV. Figure 6.14C shows a top-down image of the PCB surface; the frosted finish is shown in dark orange. The frosted finish

has arranged itself into patterns indicating acoustic interference pressure modes on the PCB surface - a behaviour witnessed in Chapter 5. The frosted finish produced in response to low currents is a negative effect and outweighs the positive benefits to micro-throwing power obtained within THV.

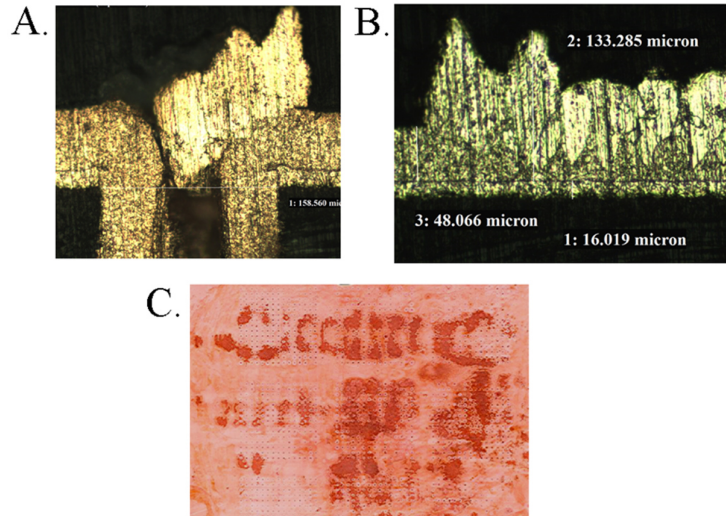


Figure 6.14 - A) & B) micro-sections of frosted finish at THV entrance and on PCB surface, respectively. C) image of frosted region on surface. PCB plated at 0.5 A/dm^2 for 16.5 hours with the transducer setup 4.5 cm tangential to PCB and outputting at 450W.

6.3.5 Conclusions

The MS plating performance was evaluated after depositing for durations longer than 15 hours down THVs of different diameters. Investigations were made to review the acoustic pressure distributions within the THV structures on changes to diameter. The results reveal a correlation between acoustic pressure distribution, cavity diameter and the amount of Cu deposited. THVs of diameters larger than 0.30 mm show no enhancement to micro-throwing power and produced plating results of a lower quality than those obtained under standard agitation conditions. Deposition did occur down those THVs and was characterised by a periodic undulating patterning which suggested influence by an acoustic standing wave. The minimum diameter a PCB THV can be fabricated with a high *ar* – larger than 1:1 - is 0.15 mm. At this size plating enhancement with the MS plating agitation was obtained which was significantly larger than plating obtained under no agitation, although it was uncertain how this enhancement compared

to the standard bath agitations as a plating result under this condition was not performed. Further studies are required including this result.

The acoustic output applied during the investigations was mostly a continuous wave but a pulsed output was additionally investigated. Introducing a pause in the acoustic output reduced the total pressure sonicating the THV, displayed by a reduced plated thickness obtained down a 0.15 mm THV when plated under that setting. Regardless, the plating obtained is greater than under no agitation plating conditions. High frequency agitations produce unwanted damage to the PCB surface, brought on due to cavitation and thermal increases as shown in Chapter 5. Reducing the acoustic agitation to a minimum whilst obtaining plating enhancement is desirable as it minimises damage to the PCB surface. Plating under pulsed conditions is a candidate method to do this.

Simulations of the acoustic pressure revealed that standing wave modes formed within the THV cavity and that they varied dependent on the diameter and size of the THV. The only increase to plating performance was obtained when the acoustic mode set up within the THV was a 1st harmonic mode. Measurements of acoustic pressure were obtained in [115] using a hydrophone inserted into a PCB-THV of diameter 0.5 mm, whilst it received 1 MHz sonication. The measurements showed that at discreet positions separated by half of the acoustic wavelength, the pressure underwent high to low variations - indicative of a standing wave. This result, along with the COMSOL simulations and the plating outcomes, provided strong evidence that the plating behaviour down THVs was influenced by the acoustic harmonic mode formed within the THV, which was influenced by the THV diameter and PCB thickness.

The COMSOL simulations allowed the acoustic pressure potential energy density to be evaluated within the THV cavity. The potential energy is one aspect of the total energy where the rest is described by the kinetic energy. The kinetic energy was not evaluated in the simulation as to do so would have required the microfluidic motions to be accurately modelled.

Evidence was shown in Chapter 2 that static acoustic waves influence microfluidic motions within a resonating cavity to form vortices. It is possible that the undulations of the Cu produced within the THVs were deposited in response to vorticity, where the electrokinetics were locally enhanced and hindered depending on the positioning of the standing acoustic wave and the induced microfluidic motions. Evidence has been given in [58, 75] that reductions in streaming currents occurs on alteration of microcavity size, when the acoustic frequency is fixed. When the THV diameter and size are altered, the resonant acoustic properties of the channel also alter, influencing microfluid motions,

which control the plating performances. To provide a more complete analysis of the MS plating behaviours, microfluid vorticity formation would need to be included into a simulation model. Such simulations have been performed and use a combination of MATLAB script and COMSOL [126].

The COMSOL scattering simulation was additionally unable to simultaneously model multiple multi-physical acoustic influences on the pressure, such as cavitation, bubble movement and acoustic streaming. All of these effects are critical factors influencing microfluidic motion under MS [156, 157] and a without a model considering each of these effects, predicting the MS plating behaviour exactly, without plating trials, was not possible.

Investigations were made altering the acoustic pressure output, the electrical current density and the electrical waveform. Increasing the acoustic pressure and reducing the electrical current density was shown to increase the amount of Cu deposited down the THV. This was possible because the two parameters enable a greater replenishment of electrolyte relative to the amount depleted within the THV. Plating at low current densities came with a caveat, in that it produced an unwanted large crystalline growth, which resulted in an unusable plated topography. 0.5 A/dm^2 is a plating current density beyond the limits of an efficient plating reaction and the improvements to plating witnessed in the investigations did not warrant its further use in manufacture.

An RP electrical plating waveform typically reduces the pinching effect which occurs at the entrances of THV, see section 2.1.6. When plating large Cu thicknesses this enables a greater amount of Cu to be deposited before the THV closes up. When applied with MS agitation, pinching was reduced, although no improvement to thickness down the THVs was obtained over DC-MS plating.

Changes to the angle of the acoustic transducer from a tangential alignment showed that the acoustic influence within the THVs reduced. The THVs plated were larger than 0.3 mm diameter and when the angle was altered from tangential, the acoustic influence reduced and the plating enhancement increased to standard values. Studies were not performed changing the acoustic angle for THV less than 0.3 mm. It was predicted that they would show the opposite - a reduction in micro-throw for changes to tangential orientation. For this reason, further investigations using MS were performed under a tangential arrangement when diameters were less than 0.3 mm.

The acoustic potential pressure energy density was evaluated within the THV cavities for different angles. The results showed that the potential acoustic energy coupled into the cavity reduced for non-tangential alignments and was reduced to a minimum for

a parallel orientation. The simulations additionally showed that smaller diameter THVs received greater acoustic pressures but were more sensitive to changes in angle change. These results highlight that alignment is an important property when setting up the transducer, where changes to orientation result in vast reductions of acoustic energy within the THV.

6.4 General conclusions

Development Stage 2 outlined in Chapter 1 sought to compare the MS-assisted agitation ability down THV interconnects to existing agitation techniques, quantified from plating experiments. The MS agitation did not show any enhancement compared to existing agitation and plating techniques. Typical bath agitations can be combined together to improve the agitation of the PCB and increase plating performance. MS agitation was susceptible to any additional fluid convection within the bath, as it disrupted the propagation of the acoustic wave. The poor performance of the MS agitation by itself and its inability to be combined with other agitations to improve its behaviour, limits its use for the electrodeposition of THVs.

Development Stage 3 outlined in Chapter 1 reviewed the ability to fill via interconnects using MS agitation. This was performed by plating PCBs beyond standard plating durations. The performance of the MS plating was influenced by the size of the THV features and the only improvement to plating performance was obtained when MS was applied on small diameter THVs, at extremely low plating current densities. The results highlighted that enhancement could be obtained, although adverse plating effects were produced in response to the low plating current densities, limiting the MS use in an industrial scale.

The plating performance obtained in laboratory settings prior to this work was not reproduced under an industrial setting. Issues with alignment of the transducer device have been reported and simulations were made which suggest that accurate alignment of the transducer with respect to the surface of the board is required to successfully couple the MS energy into the THV cavity, which possibly contributed to the plating outcomes. Due to the poor performances obtained using the 1 MHz transducer device, MS-assisted plating is not seen as a viable assist in Cu plating for the uniform filling of THV interconnects, or for use under standard plating cycles.

Chapter 7 Plating down Blind Via using Megasonic Assisted Agitation

7.1 Introduction

Megasonic (MS) plating has been introduced into Blind Via (BV) manufacture and has been shown to significantly improve the ability to deposit Cu down small diameter 0.1 mm, high *ar* 3:1, microvias [16]. The enhancements to plating by the introduction of MS agitation can lead to vast increases in Printed Circuit Board (PCB) lifetime and large improvements to technological interconnection capability, as indicated in section 2.4 in Chapter 2. For this reason a series of investigations were performed, seeking to recreate the plating behaviour witnessed within the laboratory scale investigations in [12] on a 500 L, medium scale plating bath in an industrial setting and are discussed within this chapter.

The chapter was organised into two sections. Section 7.2 looks at the plating performance for the small plating deposit regime, which represents plating thicknesses of 20 μm on the surface of the PCB. Section 7.3 addresses the thick plating deposit regime, representative of plated thicknesses larger than 70 μm on the surface of the PCB. The plating parameters and BV designs were altered to compare MS plating performance. The parameters altered include: BV diameter, *ar*, plating duration and panel modes of agitation.

7.2 MS plating down BV in the Thin Copper Regime

The PCB was drilled with BVs of different *ar*. Higher *ar* are more difficult to electroplate due to the difficulty in transporting fresh electrolyte solution through the microscale via cavities. With existing agitation techniques, BV electroplating down *ar* greater than 1.2:1 is not generally possible, for PCB manufacture with BV diameters equal to or greater than 100 μm [23].

The MS plating ability was compared with existing agitation techniques by performing plating trials on PCBs drilled with 0.15 mm and 0.20 mm diameter BVs. The different diameters were both drilled at *ar* 2:1 and 1:1. The plating performance was quantified from measures of plating rate at the bottom of the BV.

The BVs were processed by drilling the boards, followed by an electroless plating of 1 - 2 μm of Cu to form a seed layer. Unlike the other PCBs fabricated under typical BV filling as outlined in section 2.4.1 in Chapter 2, the BVs in this investigation were not

flash plated before MS plating, and were instead plated after the electroless process. This was to ensure that the Cu being plated was under MS agitation the entire electroplating of the BV.

The board plating was performed in the same plating tank and with the same chemistry as the THV plating trials in Chapter 6. For this reason the BV would not uniformly fill, as the chemistry required for this electroplating bath requires the use of insoluble anodes, which were not free for use at Merlin. Securing new ones was also costly to procure. If increases to agitation had occurred then their impact on plating rate at the bottom of the BV would have been observed, although a uniform filling was not expected.

The transducer was set up in the plating tank as indicated in Figure 3.15 in Chapter 3, with the tangential distance of the transducer to the PCB set at 4.5 cm. The PCB was set up in the bath with the BV entrance oriented towards the oncoming MS waves. This configuration allows for maximum sonication of the BV hole and was also the same as the setup applied in HWU BV trials [16].

Three different experimental settings were tested: (a) plating with no agitation, (b) plating with standard - panel movement and bubbles - and (c) plating with 450 W MS. The boards were plated under RP plating condition, 1:3 A/dm², with waveform duration, 10 ms forwards and 0.5 ms reverse. Under this setting the BV pinching would be reduced and, with 1 A/dm² in the forward plating direction, the plating rate would be slow, such that Cu could be replenished relative to the deposition without the negative impact on plating topography observed at lower currents, as displayed in Chapters 4 & 6. Under these settings the PCB was plated for 157 minutes, which was the estimated time taken to plate 20 µm of Cu on the PCB surface at the current density. The boards were rotated half way through the plating cycle to even the distribution of Cu across the board.

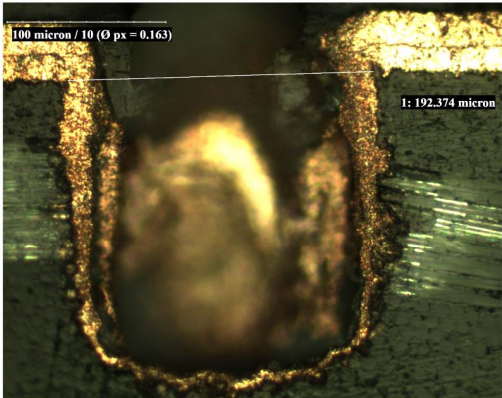
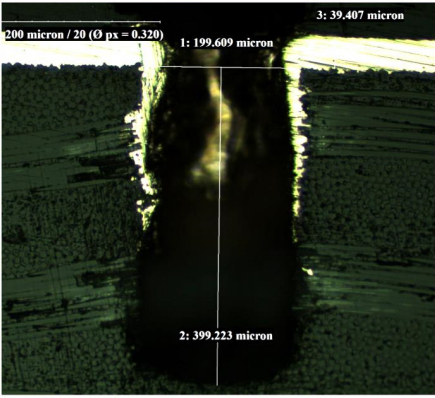
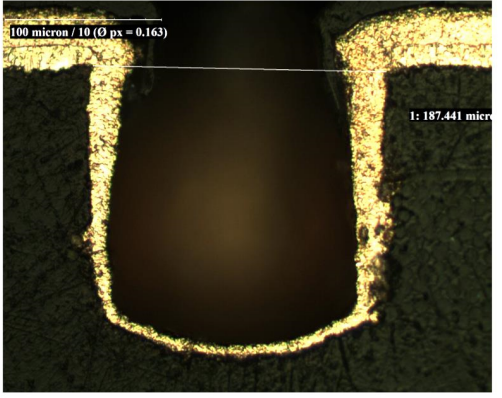
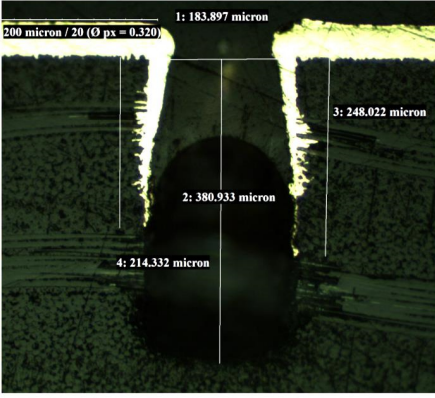
7.2.1 Results and Analysis

The plating results obtained down BVs of 0.20 mm diameter and different *ar* are indicated in Table 7.1. The plating results show that, under standard agitation and using non-filling chemistry, a small deposition of Cu occurs down the BV, characterised by a small thickness at the bottom of the via, which was expected for the plating setup.

With an increase in *ar* to 2:1, the BV showed no deposition into the via below approximately 50% of its depth. This is due to a lack of Cu seeding occurring in the electroless Cu process, because of increased microfluidic viscous forces, which prevented electrolyte circulation.

On the application of MS agitation at 450 W, at the bottom of the 1:1 BV the plated thickness appeared comparable to the standard plating. Down the 2:1 BV no deposition occurred again. The 0.15 mm BV displayed the same behaviour as the 0.20mm BV and so the plating results were not included in the table. MS plating work performed by the HWU group prior to the Thesis highlighted that 2:1 *ar* BV plating was possible with MS plating [11, 56]. They outlined that it was not certain whether the limit to the BV depth plated was due to MS electroplating or standard electroless Cu plating process performed prior to MS electroplating. The results shown here highlight that the electroless copper was the significant factor influencing the *ar* depth plated. Increases to the electroless process using MS are suggested for future research in Chapter 8.

Table 7.1 - Microsection images of 0.20 mm diameter, BVs of different ar, RP plated at 1:3 A/dm² for 153 minutes with different agitation settings.

	0.2 mm diameter 1:1 <i>ar</i>	0.2 mm diameter 2:1 <i>ar</i>
Standard agitation		
450 W MS agitation		

The plating rate was evaluated from four different thickness measurements taken at the bottom of 0.15 mm and 0.20 mm diameter BVs, plated with different agitation settings. The average thickness for each BV is plotted in Figure 7.1 along with their standard deviation included as error bars.

Statistical analysis was performed on the data as outlined in Appendix A. A Levene's test was performed to test for homogeneity of variances. Homogeneity was found and so a two-way Analysis of Variance (ANOVA) could be performed to verify statistical significance between parameters. The test was performed according to the procedures of the Statistical Analysis System [158]. The data show that, when the agitation was not considered, there was no statistical significance between the amount of Cu deposited and variation to the BV diameter, as given by $F(1,18) = 1.74$, $P = 0.203$. Statistical significance was observed between the different agitation settings as given by $F(2,18) = 65.3$, $P = 5.26 \times 10^{-9}$ indicating that changes to agitation had an effect on the amount of Cu deposited.

A plating enhancement was demonstrated compared to no agitation when applying either the standard bath agitations or MS for the two different diameters. This outcome was expected due to enhanced fluid circulation. A statistical significance was observed in the measured data between the applied bath agitation and the plated BV diameter, given by $F(2,18) = 17.4$, $P = 6.18 \times 10^{-5}$. This was observed in Figure 7.1, as the 0.15 mm diameter BV showing a greater thickness than the 0.20 mm BV. For the other agitation settings, the mean thicknesses for each BV diameter were comparable.

The measures of thickness were averaged between the two diameters for the different agitation settings. With MS agitation the average thickness between the two BV sizes was 5.8 μm , (SD = 1.3), which was approximately 4% greater than the thickness plated after standard agitation settings, 5.5 μm (SD = 1.4). The difference between the two mean thicknesses was low, although their standard deviations were high. As such, it was not possible to determine which agitation produced a more efficient plating reaction.

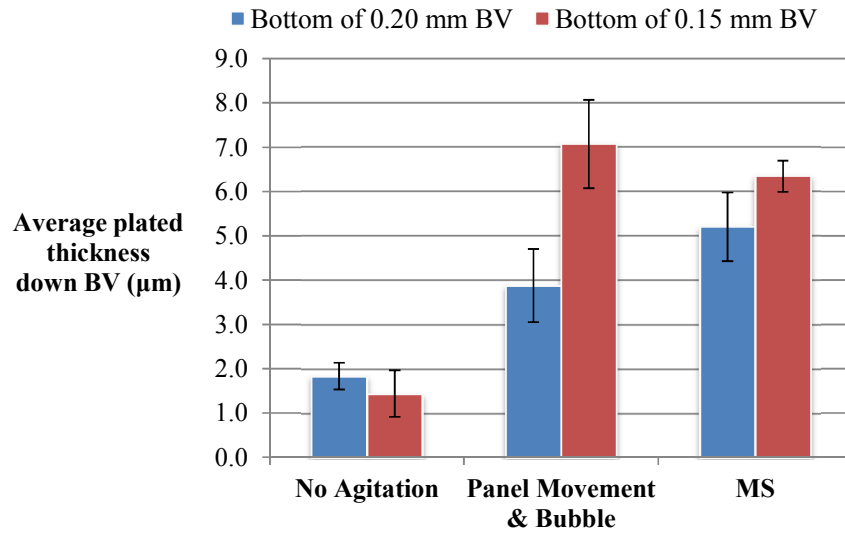


Figure 7.1 - Average plated thickness evaluated from ten measures taken from the bottom of BVs after 153 min RP plating, under different agitation conditions.

7.2.2 Conclusions

The MS plating performance was evaluated in the small thickness regime, down the smallest diameter BV sizes used in PCB design. The results were qualitatively analysed from images of the Cu deposited at the bottom of the BV. For BV with ar larger than the standard, the board failed to plate regardless of the agitation applied. This was due to the lack of Cu seeding occurring in the electroless plating process prior to Cu electroplating. The MS BV plating trials performed prior to this investigation by the HWU group, had achieved a high 3:1 ar fill, regardless of the standard electroless Cu deposition failing to deposit onto the bottom of their BVs as evidenced in [12]. The introduction of MS in the current investigation did not enhance the distance plated into the BV at high ar .

The plated thickness was quantified by changes to the plating bath agitation settings. The results highlighted, as expected, that applying agitation increased the amount of Cu deposited down the BV. The different BV diameters did not display a high, statistically significant, effect on the amount of Cu deposited and, also, it was not possible to evaluate with a high degree of accuracy whether MS agitation or the standard agitation performed the best. To provide a more comparative evaluation of the agitation performance a larger number of vias could be measured. A systematic error exists when measuring thicknesses due to the uniformity of the glass-resin PCB substrate after drilling of the BV. Laying down small deposits of Cu on top of this surface would include the poor uniformity of the substrate wall in the measurement of the Cu thickness and would

contribute to a variation within the data. Increasing the deposit thickness would reduce the impact of the underlying structure on the plated uniformity. As such, to reduce variation in the measured thickness a larger deposit can be applied.

7.3 MS plating down BV in the Thick Cu regime

The BV MS plating investigations in [16] reported a uniform filling of Cu down a 0.1 mm diameter, *ar* 3:1 BV. To achieve this, the board had to be electroplated for plating durations significantly longer than applied in Section 7.2. Plating trials performed in 7.2 revealed a similarity between the plated thicknesses obtained with standard agitation and MS and that the standard deviations were high for the methods used to achieve the plated thickness. It was not possible therefore to derive a clear indication of plating performance.

In an attempt to reproduce the previous literature findings and to reduce the variation in the measurement of the average plated thickness, MS–assistance plating trials were performed, repeating settings applied in section 7.2. The plating conditions were outlined in Table 7.2. Three different plating settings were investigated and each setup was repeated. The RP plating setting was kept the same as in section 7.2, but the duration was increased to 12 hours and the PCB was rotated every 2 hours to even the distribution of Cu across its surface.

Table 7.2 - Plating bath settings.

Plating Trial	PCB agitation	Panel Movement	Plating Duration (hours)	PCB Size (dm ²)
1	None	Panel rotation after two hours of the plating cycle	12	2.3
2				
3	Standard			
4				
5	MS			
6				

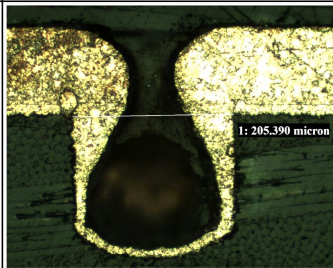
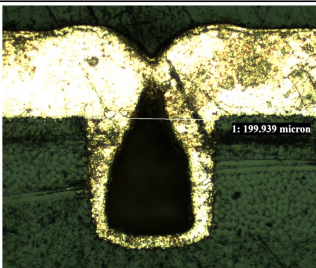
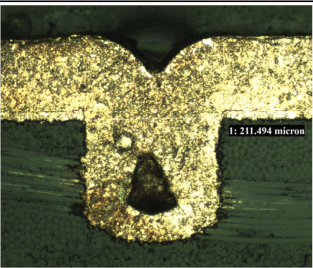
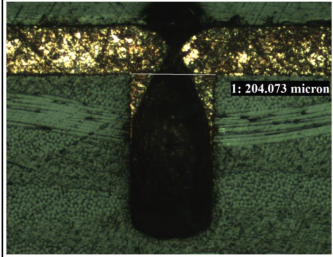
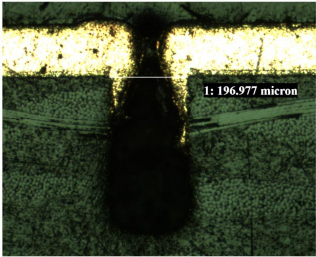
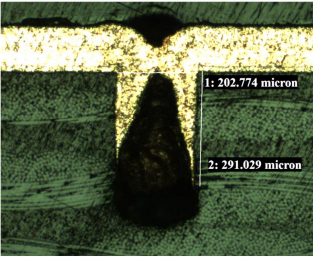
7.3.1 Results and Analysis

MS plating trials were performed with no agitation, standard and 450 W MS. Microsection images of the plating results are displayed in Table 7.3 for a 0.20 mm diameter BV with *ar* 1:1 and 2:1. With no agitation, little Cu was deposited down the BV and the neck of the BV failed to close. With standard agitation a larger thickness was deposited down the via and the entrance of the BV closed. With MS agitation a significant increase in Cu was observed within the BV, characterised by a minimum voiding in the

centre of the BV. The results clearly highlight that with MS the plating performance increases down the BV. This was likely due to increased replenishment of electrolyte down the BV because of the enhanced forcing of solution by acoustic streaming mechanisms.

The plating behaviour was analysed down 2:1 *ar* BV plated under MS agitation. With MS, the amount of Cu deposited down the 2:1 BV increased, compared to the result obtained for the no-agitation setting. The Cu electroplating stopped in the BV at the point where the Cu seed layer failed to deposit in the electroless process prior to electroplating. For this reason, despite the enhancement to electrolyte replenishment observed with MS, plating failed to occur at the bottom of high *ar* BVs as was observed in Section 7.2.

Table 7.3 - Microsection images of 0.20 mm diameter BVs of different ar, RP plated at 1:3 A/dm² for 12 hours, with different agitation settings.

	No Agitation	Standard Agitation	450 W MS Agitation
0.2 mm diameter 1:1 <i>ar</i>			
0.2 mm diameter 2:1 <i>ar</i>			

The plating thicknesses were measured in the bottom of the BV for different diameters and agitation settings and an average plating thickness was plotted on Figure 7.2 along with their standard deviations included as error bars.

Statistical analysis was performed on the data as outlined in Appendix B. A Levene's test was performed to test for homogeneity and the data was found to be nonhomogeneous despite logarithmic transformations being applied to it. As such the plated thickness was compared with the different agitations settings and BV diameters by using the two-factorial Scheirer-Ray-Hare test [159]. For this test statistical significance is found when evaluated P values are less than 0.05.

The different agitation settings produced statistically significant results given by $P = 3.9 \times 10^{-9}$, highlighting that a different plating response could be obtained when changing the agitation. There was no statistical significance between the different agitation settings and the different via diameters (plating agitation \times blind via diameter), as given by $P = 0.36$, which indicated that the via diameter had not had a significant effect on plating rate for the different agitation settings. The two BV sizes were comparatively similar, therefore the dynamics influencing deposition such as fluid circulation would not be significantly altered, contributing to the effect observed.

The data for the two diameters was averaged and the values displayed in Table 7.4 along with their standard deviation. These results show that the MS agitation increased the plating rate at the bottom of the BV by approximately 280% and 60%, compared with none and standard agitation settings, respectively.

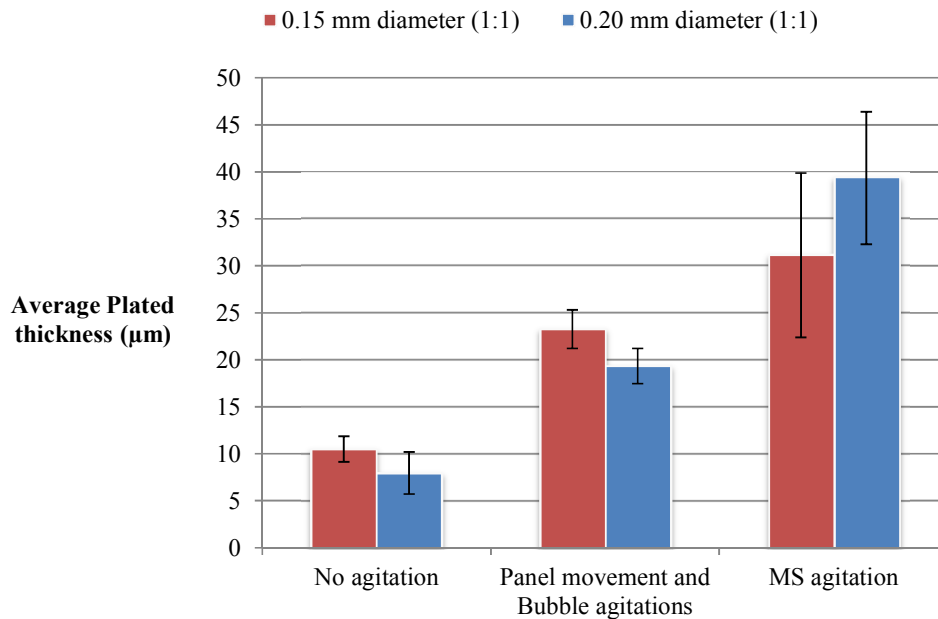


Figure 7.2 – Average plated thickness evaluated from ten thickness measures taken from the bottom of BVs after 12 hours RP plating, under different agitation conditions.

Table 7.4 - The average plated thickness for plating settings.

Plating Setting	Average Plated (µm)	Population Standard deviation (µm)
No agitation	9.2	2.3
Standard agitation	21.3	2.8
MS agitation	35.2	8.9

7.3.2 Conclusions

Plating trials were performed seeking to quantify changes to plating due to the application of MS agitation. The plating cycle was performed over a long duration so as to form a thick deposit and to reproduce plating results obtained in the literature. When evaluating the plating quality, a thicker deposit reduced the systematic error associated with the drilled hole roughness on plating thickness.

With MS agitation, a vast increase in the plating rate over standard agitation was measured within the BV. It is demonstrated that MS agitation enhances the replenishment of depleted electrolyte in the small microcavities compared to existing techniques. The replenishment is likely due to increased streaming forces. The exact mechanism behind the forcing of solution due to MS is uncertain. Evidence for standing wave patterns were not observed within the BV cavity as in the THV cavity. Additionally, changes to the cavity diameter and depth did not appear to alter the performance, although the two sizes investigated were similar and so a vast change in plating behaviour would have been unlikely. The BV diameters tested were small and the plating enhancements witnessed in THV trials occurred only on small features. For this reason, it is possible that larger diameter BVs may show some of the negative acoustic influences on plating witnessed within the THV trials. To further evaluate the MS plating performance, plating trials should be performed on larger diameter BVs.

The RP plating currents applied in the trials induced a slow plating rate. This was at the low-end of an electroplating process operation setting. Further studies are required to test the performance down faster, more process suitable, plating rates. It is expected that the plating down the BV will be reduced for these settings due to the increased depletion of electrolyte relative to the repletion rate.

Due to time constraints, in depth COMSOLTM simulations were not performed on the BVs as on the THVs. For this reason further study is required to evaluate the standing wave behaviour within BV structures, to provide a description of the MS plating mechanism for changes in BV feature size.

The BVs displayed voiding within the vias. This was expected due to the non-filling chemistries applied during the BV plating trials. Previous MS literature results had shown that a uniform filling was possible without such chemistries. These results were not reproduced.

The aspect ratio of the BV was altered and revealed that thicker deposits of Cu were obtained within the BV, although no Cu was plated over regions which had failed to Cu seed. For this reason it was not possible to electroplate Cu down BVs of high *ar* which had not received a sufficient seed. The high *ar* plating results obtained within the literature were not reproduced. To date there are no PCB solution agitation techniques which can seed Cu on high *ar* BVs [160-162].

7.4 General Conclusions

Development stage 2 outlined in Chapter 1 sought to compare the MS-assisted agitation ability down the BV interconnects to existing agitation techniques, quantified from plating experiments. A small range of BV diameters was tested, which represented high-technology configurations and the most difficult to plate via features. The MS agitation was shown to improve plating performance over the existing agitation techniques on standard aspect ratio BVs.

Development stage 3 reviewed the ability of the MS agitation to fill BV interconnects. The plating chemistry applied was not synthesised for such a setup and, as such, BV filling was not achieved. Filling chemistry employs the use of chemical additives, whose operational parameters are more susceptible to temperature changes than non-filling chemistry. The MS agitation alters the bath temperature due to cavitation and so it is likely that when applied with filling chemistry, the agitation will cause denaturing and degradation of the additives, which are essential for via filling. Regardless, these plating studies are worth investigating to further evaluate the use of MS application to BV plating. This study is discussed in more details in Chapter 9.

The plating of high *ar* features was not achieved in the MS plating studies, due to the lack of a Cu seed layer formed prior to electrodeposition in the electroless Cu plating process. It is highly desirable to plate Cu into BV of high *ar*. A possible route toward this goal is to apply MS to electroless Cu deposition, to see if a seed layer can be achieved down high *ar* BVs due to enhanced microstreaming, and then MS electroplating the seeded high *ar* features. Such a manufacturing route is possible to achieve the cost savings outlined in section 2.4.3 in Chapter 2. This experiment is outlined in greater detail in Chapter 9 along with further evaluations of BV plating trials to be performed.

Chapter 8 Conclusions and Future Studies

A list of the Megasonic (MS) plating investigations performed within this thesis is displayed in Table 0.1. Here the experiments are listed in order of appearance and a summary is provided in terms of the parameter investigated / witnessed and the experimental outcome.

Table 0.1 - Investigations carried out throughout the thesis.

Chapter / Chapter Section	Experiment Topic	Summary	
		Parameter Investigated / Witnessed	Outcome
3.4.1	Current thieving by the transducer	Current thieving produced by transducer position on PCB plating.	Tangential distance of 4.5 cm resolved as minimum distance for transducer before poor plating performance occurs.
3.4.2	Fluid circulation	Acoustic agitation impact on bulk fluid flow within the 500 L process tank.	MS induced fluid motions were found to increase up to 150% faster than the standard agitation motions.
4.	Panel plating using MS agitation	Changes to the surface Cu crystallinity on changes to MS pressure output.	MS agitation negatively interfered with organic additives attached to the PCB surface, leading to a weaker deposit.
		Influence on the surface roughness, R_a , on changes to tangential distance.	R_a increased for the inclusion of MS agitation over silent conditions. A 7% increase in surface roughness was obtained on the reduction to transducer distance.
		Transducer power variation	R_a increase was observed on the increase of acoustic power. A 10% output of MS was found to induce micro-roughening.
		Current density variation due to current thieving and MS agitation	A range of plated finishes observed with SEM images, indicating poor control of current and additives.
		Bath plating temperature variation	PCB plating capable at reduced operational temperatures due to acoustic forces. Evidence for localised variations on board surface temperature due to acoustics, which in turn increased additive consumption and reduced plating quality in high temperature regions.
5.1	Standing wave behaviour	Acoustic streaming lines	A negative influence on Cu crystallinity. Formed due to an interaction of acoustic interference, acoustic streaming currents, microbubbles and the displacement of bath additives.
		Cu ridges	Reduced the uniformity of the electrodeposit to substandard levels. Formation mechanism appeared to be influenced by internal structure of the PCB and acoustic resonance. Appearance could be prevented by reorienting the transducer and plating at low current density.
		Ringlets and cells	
5.2	Microbubble influence	MS cavitation streamers: bubble lens, cones and ringlets	Acoustic artefacts produced which influenced the sonicating pressure on the PCB surface. Effects on processing difficult to estimate without further study.
		Cavitation	Micro-scale cavitation observed on PCB providing a mechanism for increased surface roughness and temperatures.
6.2	MS plating down THV in the thin Cu regime	Bath agitation comparison when plating down THV	Substandard performance obtained when plating with MS.
		50 Hz vibrator effects on MS plating	Could not be combined with MS agitation to improve plating performance.
6.3	MS plating down THV in the thick Cu regime	Cu patterning on different THV diameters	Cu deposition down THV dependent on feature size. Standing wave effects along with Rayleigh and Schlichting streaming contributed to Cu deposition.
		MS plating enhancements within THV	Thick Cu deposits measured on THV diameter 0.15 mm showing MS streaming plating enhancement, although enhancement not compared with existing agitation techniques.

		Transducer angle orientation alteration	A reduction in MS agitation energy witness on non-normal angles to the PCB. A normal alignment found to couple largest energy into THV. Impact on plating appeared to be THV size dependent.
		Acoustic and Electric current magnitude and waveform alterations	Increasing acoustic pressure and reducing current density showed enhanced plating down THV. RP plating waveform found to produce no enhancement over DC plating.
7.2	MS plating down BV in the thin Cu regime	Plating down different BV diameters and aspect ratios	MS plating performed comparable to standard processing, although large variations were measured when evaluating the process.
7.3	MS plating down BV in the thick Cu regime	Plating down different BV diameters and aspect ratios	Errors were reduced in evaluation of plating performance, and showed that MS outperformed the standard agitation process. High aspect ratio vias did not plate.
8.2	Megasonic assisted dry-film developing	Tangential distance of transducer altered.	MS transducer performed comparably to standard agitation procedure.
8.3	Megasonic assisted dry-film stripping	MS agitation compared to existing process	MS agitation underperformed compared to standard process, likely due to operational temperature restrictions placed on bath for safe acoustic transducer operation.

The MS agitation ability to remove dry-film resists off a Printed Circuit Board (PCB) was reviewed in two processes: developing and stripping. In the developing process the MS agitation performed comparably to the standard process, quantified in terms of duration required to remove resist. When the MS was applied in stripping of the dry-film, the agitation underperformed compared to the standard process. The MS device could not operate safely within the stripping solution tank at the recommended process temperatures, therefore its poor performance could have been due to this restraint. To effectively MS process dry-film the bath would need to operate at its recommended conditions and not those applied. A transducer which indirectly provides agitations would be unaffected by high temperatures, as it is stored outside of the bath and so could be sourced for further investigations. Alternatively, a direct transducer could be sourced which can operate at higher temperatures.

MS plating experiments were performed to reproduce results obtained in the HWU labs prior to this thesis and to scale up the technology into a manufacturing environment at Merlin Circuit Technology. The plating performance could not be reproduced under the plating setup at Merlin and, because of this, the manufacturing enhancements were not realised and the process was not scaled-up for large volume manufacture. The goals set at the beginning of the thesis were obtained, as MS plating performance was evaluated in a PCB manufacturing environment and enhancements along with negative issues were witnessed. These effects are discussed next.

8.1 Megasonic-assisted electroplating issues and enhancement

A range of manufacturing issues were witnessed on application of the MS technology; these were characterised by a drop in performance of the manufactured PCB. The plating bath additive performance was negatively influenced by the MS plating

process, leading to an uncontrollable, unwanted change in the Cu crystallinity and surface roughness. The negative effects could be reduced by minimising the acoustic power, but this was counter to the goal of acoustic streaming enhancement, which was dependent on the pressure of the acoustic wave.

The acoustic wave caused resonant acoustic artefacts on the surface of the PCB, which reduced the uniformity and control of the plated deposit. The resonant effects could be prevented by using phase or frequency modulation techniques but, to apply these required a new transducer to be purchased which was costly.

Plating down the THV revealed that the plating behaviour varied, depending on the size of the feature, where no enhancement was observed on diameters equal to and larger than 0.3 mm. Manufacturing only at sizes less than 0.3 mm overlooked a wide range of THV manufacturing designs, although plating down a THV of this diameter is typically not an issue in PCB manufacture and so, was not a key area for development. Plating enhancement was measured down 0.15 mm diameter THVs which are diameters at the limit of rigid PCB THV manufacture. The enhanced processing behaviour was also attributed to resonant acoustic effects, which highlighted that the fundamental mechanism behind MS-assisted electroplating was influenced by the acoustic properties of the board and the shape of the via feature.

The MS plating showed enhancements to the plating reaction down BV compared to processing under silent conditions and the existing agitation processes. The MS plating outcome was inferior to the plating results obtained by the HWU group prior to the thesis, although it represented a vast increase over existing industry techniques. The next section discusses investigations to capitalise on this outcome and push towards a MS manufacturing technique.

The plating performance down vias was evaluated using a microsectioning procedure. This process requires the via to be sectioned at the midpoint of the via's diameter. A drilled via shows a drilling positional error of $\pm 25 \mu\text{m}$ and a size error of $\pm 25 \mu\text{m}$ and, therefore, finding the mid-point is difficult. When microsectioning, the midpoint of the via displays the smallest thickness of plated Cu and simultaneously gives the most accurate representation of the Cu thickness deposited down the via. Failing to find the mid-point will result in overlarge thickness measures and add an error to plating quality evaluation. Therefore care was taken in the plating trials to ensure that the midpoint was reached and the most accurate measure of the deposit thickness was obtained. Regardless, an improved method of evaluating the Cu deposited is by using X-ray microscopy to view inside of a via. The technique allows for a 3D view inside of the

via and is currently applied in wafer manufacture on Through-silicon Vias (TSV) [163]. The difficulty with employing X-ray microscopy is its high cost, but this procedure would help to provide insight into 3-dimensional filling behaviours and should be considered when attempting to uniformly fill a large quantity of vias with Cu, like on a ball-grid-array feature, as it could quickly evaluate if the array of vias contain any voids.

8.2 Further megasonic processing investigations

MS plating shows a plating enhancement down vias for only certain via sizes, which for THV were 0.15mm diameter and 6.7:1 aspect ratio (*ar*) and for BV 0.20mm diameter and 1:1 *ar*. At these sizes MS agitation can be used to enhance PCB manufacturing and enable an economic advantage, but before this condition can be realised in a manufacturing environment, further investigations are required. The following section is subdivided into 8.2.1, which outlines investigations looking to progress towards an MS PCB manufacturing procedure and 8.2.2, which looks to better understand fundamental MS plating behaviours and provide an improved model of the MS plating mechanism.

8.2.1 Megasonic plating continuation

Plating down BVs with *ar* greater than 1.2:1 was difficult due to effective viscous forces hindering fluid motions in small micro-cavity regions. The MS agitations were shown in the thesis investigations to induce increased electroplating in BV due to enhanced fluid replenishment. When plating down high *ar* BV the deposit failed to form, due to the electroless Cu seeding process prior to the Cu electrodeposition. During the Cu seed the bath underwent standard agitation and as such failed to deposit down *ar* larger than 1.2:1. MS could be applied within the electroless plating process, making use of its increased fluid solution movement ability to deposit 1 to 2 μm of Cu down high *ar* BVs. If MS electroless plating was successful then the BV would be MS electroplated, with the goals of depositing thicker deposits down the high *ar* features and achieving a plated high *ar* BV.

An issue with this experimental setup is that Cu electroless process operates at temperatures between 45°C and 50°C and the safe limit for operation of the transducer device is 40°C. For this reason, the plating investigation would have to operate at reduced operational temperatures, if a direct-transducer - like the one used in the thesis - was applied. Operating under this condition would have an adverse impact on the plating. MS plating could be performed at high temperatures if an indirect-transducer was used when

installed into the wall of a tank, or a direct-transducer was obtained which operates at higher temperatures.

The process steps for MS processing high *ar* BVs is outlined in Figure 0.1 and highlights that under non-filling chemistry pinching occurs at the neck of the BV. Using filling-chemistry the pinching would be reduced and the BV could be uniformly filled with Cu. MS plating with filling-chemistry is discussed next.

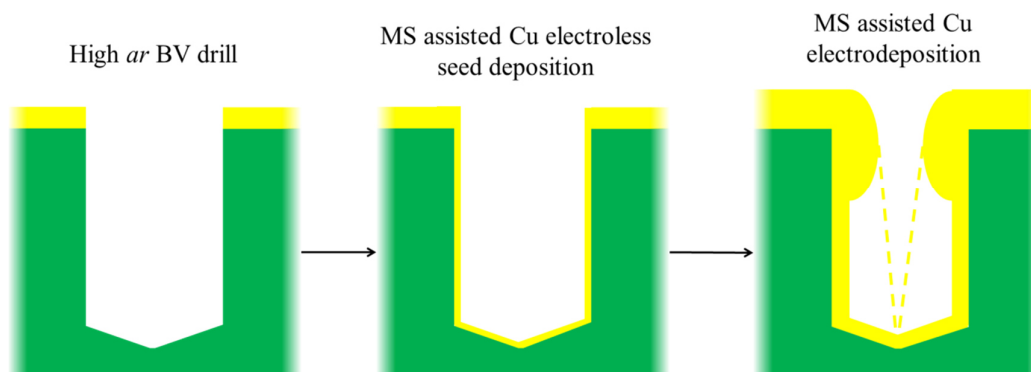


Figure 0.1 - MS process flow for high *ar* BV plating.

In Figure 0.1 the dashed line highlights the different plating behaviour obtained if bottom-up filling chemistry was to be applied, where specific bath additives enable selective Cu plating - depositing large amounts at the BV bottom and small amounts on the surface. MS plating was not performed using bottom-up filling chemistry in the thesis.

An issue with MS alongside bottom-up filling chemistry is that the bath additives are highly susceptible to increases in temperature, as their recommended operational temperature is $20 \pm 2^\circ\text{C}$. If temperatures were to increase outside of this range, the complex filling dynamics between the additives would fail to operate and the BV would not successfully bottom-up plate. MS cavitation induces high temperature changes which would likely interfere with the bath additives for via filling.

An MS plating trial using bottom-up plating chemistry was performed by the HWU group prior to the thesis, using BV110 supplied from Schloetter [12]. The trials had poor control over the bath temperature, but regardless, under this condition, plating was obtained down a 0.2 mm 1:1 *ar* BV, which had been DC plated at 2 A/dm^2 and under 250 W MS agitation for 4 hours. The micro-throwing power was evaluated by comparing the ratio of the average Cu plated on the surface / bottom of the BV and was approximately 60%. This value is high considering the poor control over temperature and the negative impact on the additives, and is a positive indicator that MS agitation had

circulated solution into the BV. For this reason MS bottom-up filling plating investigations should be performed, looking to attain 100% uniformly filled Cu deposits and should be applied in the process outlined in Figure 0.1 to uniformly fill high *ar* BVs.

8.2.2 Megasonic fundamental behaviour investigations

The transport mechanisms influencing Cu electrodeposition can be evaluated by performing voltammetry. Voltammetry is the study of current in an electrochemical cell as a function of applied electric potential. It produces plots of current I as a function of the electric potential energy E , known as a voltammogram. The shape of the plot is influenced by the rate of the electron transfer reaction, the chemical reactivity of the electroactive species and the voltage scan rate. Changing the fluid convection rate on the electrode under analysis will alter the electrical response due to diffusion layer size variation and, so, the micro-throwing power of the plating solution can be evaluated in response to agitation applied [164].

Sonovoltammetry is a type of voltammetry used to evaluate the efficiency of plating reactions, when applying high frequency acoustic waves to electrodes [59, 165]. Different configurations of the acoustic transducer may be applied, such as increased pressure and tangential distance and their impact on the Cu transport mechanisms evaluated for the plating bath chemistry used. An investigation could be made into how the electrical response changes on the cathode due to changes in position of the transducer.

US sonovoltammetry studies in [166] have shown that plating efficiency varies in different bath concentration regimes. As such it is worthwhile investigating MS sonovoltammetry and testing Cu plating under different bath concentrations, so as to perform optimisation on the plating bath chemistry.

An issue with sonovoltammetry is that the current thieving by the transducer, along with unstable cavitation, interferes with the measurement of current, adding noise [116]. The interference occurs for close positioning of the transducer to the electrode, making it difficult to extract information from a voltammogram and evaluate enhancements to mass transfer. Regardless, information can be obtained from MS sonovoltammetry studies, which would provide critical information into the MS plating behaviour within a copper sulphate solution.

The electrical impedance of the Cu plated finish influences the efficiency of the transportation of electrical signals and power across the PCB. The impedance is negatively altered on changes to the Cu grain structure, specifically when grain

boundaries exists perpendicular to the direction of signal transmission [167]. The MS studies in the thesis have highlighted that changes to Cu grain structure occur and, so, it would be useful to define how these changes influence the electrical transmission properties of the board and if changes to transducer device settings could be made to improve performance. Electrical performance can be characterised using impedance spectroscopy on PCB test samples plated after MS agitation, specifically ended impedance and differential impedance tests, which are commonly applied in PCB manufacture [168].

The surface of the Cu electrodeposit altered on the application of the MS agitation at differing powers and plating currents. High resolution Scanning Electron Microscope images were obtained of the PCB surface and from these the structural stability was analysed from a qualitative analysis of grain structure. A more quantitative analysis could be made by measuring the variation in material hardness in response to plating settings, using nano-indentation methods [169]. This would provide a more concise review of how MS influences the Cu deposit quality.

The Cu surface roughness after MS plating was measured optically using a white light phase shifting interferometer. The device suffered from saturation and failed to measure steep features. A higher resolution measure of surface roughness could be made by using an atomic force microscope and would help to reveal how the MS influences the Cu topography to a higher accuracy.

The microfluidic behaviour has been studied by the Heriot-Watt University group in [12] using a microfluidic device manufactured on Poly(methyl methacrylate) (PMMA), which revealed the characteristics of fluid circulation in via-like structures. To develop a more accurate microfluidic model to describe streaming within vias, a small 1 MHz MS transducer could be installed alongside the microfluidic channels as in [170] and acoustic agitation induced. Acoustic streaming currents would then drive the fluid motions within the channels, which could be imaged using a high speed camera by injecting into the solution fluorescent microbeads, as in [58]. This review would provide a clear insight into microfluidic behaviours occurring during MS plating, specifically measures of flow rate down high *ar* features. This investigation would be extremely useful in providing a greater understanding into the performance variations witnessed down vias of different sizes.

Simulations enable the microfluidic behaviours to be studied. In the thesis COMSOL was used to evaluate the 2D scattering of an acoustic wave in solution, in response to changes to agitation and the microcavity size. The scattering simulation did

not include a time variation and as such could not model microfluidic motions. Modelling the microfluidic motions within microcavities is important as it provides insight into the plating hydrodynamics, specifically vorticity produced in response to a driving flow, as modelled using COMSOL in [171]. To accurately model microfluidic behaviour, a value for the driving flow rate is required when setting up the simulation. This value could be obtained from measurements obtained within the MS microfluidic chamber investigation and, together, the two could provide a detailed theoretical framework into the acoustic behaviour and give a more complete description of the MS plating mechanism within vias.

Enhancements to MS THV plating were observed on small cavities, which, when simulated, produced fundamental acoustic modes within their structures. Conditions influencing mode formation are the size and specific acoustic impedance values of the microcavity. It would be worthwhile to perform a range of acoustic simulations of different PCB materials and THV sizes to consider the conditions under which the fundamental mode forms. With the conditions found, the boards could be fabricated and their MS plating performance evaluated, to see if there is a correlation between the acoustic mode and plating enhancement.

8.2.3 Further quality evaluations

The quality of the MS-plated Cu vias can be reviewed using a range of standard techniques. IPC-TM-650 2.6.8 manual [100] covers thermal shock testing which is a common test used to evaluate whether a PCB can withstand intense thermal pressures. The MS plated via interconnects had not been tested on their ability to withstand high temperatures, which is a useful standard for highlighting the quality of the metal deposit down a via.

The ability of a PCB to pass high frequency AC current for high volume signal transmission, is evaluated using the IPC-TM-650 2.5.5.7 standard [105]. This employs the use of a PCB coupon, fabricated with either external or internal Cu tracks or via interconnects, or a combination of all three, which is tested for its ability to transmit a high frequency AC electrical signal. The coupon is tested using time domain reflectometry (TDR) and the test PCB circuit referred to as a TDR coupon. A TDR coupon was not fabricated using MS plating techniques. Fabricating the coupon would provide a quick indication whether the Cu plated quality was sufficient for high frequency signal applications.

Further MS plating investigations should introduce these two PCB quality metrics to highlight the manufacturability using the acoustic technology.

8.3 Ending statements

MS introduction into Cu electroplating shows an enhancement to the electrodeposition process for certain via interconnect designs. This limits the use of the technology in application within the PCB industry. The positive impact on fabrication is challenged by adverse plating effects. Despite the initial shortcomings of the technology, remedies exist for these, although each requires a re-evaluation of the plating bath parameters. To bring about the ever-demanding increases to PCB technological development, alterations to the electrochemical setups may be required which mirror this changing landscape. Megasound technology could play a key role in this future, however further electrochemical and sonochemical investigations are needed before implementation can take place in a PCB fabrication line.

Appendix A Statistical Analysis

A Levene's test was performed on the data in Table A1 to review homogeneity. First, the data in Table A1 was subtracted the average thickness for the different parameters and the absolute was obtained and the results displayed in Table A2. Second, one-way Anova was performed on the data in Table A2 as indicated in Table A3.

Table A1- Thickness measures down BVs less the starter Cu thickness, for thin deposition plating regime.

Replicate	Cu thickness down Blind visa (μm)			
	BV diameter (mm)	No Agitation	Panel Movement & Bubbles	MS
1	0.15	2.164	7.538	5.414
2	0.15	0.792	5.862	5.032
3	0.15	1.125	8.447	6.069
4	0.15	1.673	6.432	4.305
5	0.2	1.688	5.212	6.96
6	0.2	1.938	3.074	7.821
7	0.2	2.259	3.33	5.809
8	0.2	1.444	3.889	6.083

The P value obtained was 0.27 which was greater than 0.05 and so the null hypothesis cannot be rejected and the data is homogeneous. Following this the data in Table A1 was statistically reviewed using two-way ANOVA as shown in Table A4. The results for the test are displayed in Table A5.

Table A2 - Values of average residuals from data in Table A1.

0.15mm No Agitation	0.15mm Panel Movement & Bubbles	0.15mm MS	0.2mm No Agitation	0.2mm Panel Movement & Bubbles	0.2mm MS
0.726	0.468	0.209	0.144	1.336	0.292
0.647	1.208	0.173	0.106	0.802	1.153
0.314	1.377	0.864	0.427	0.546	0.859
0.235	0.638	0.900	0.388	0.013	0.585

Table A3 - Anova: Single-Factor With Replication of data in Table A2.

SUMMARY						
<i>Groups</i>	<i>Count</i>	<i>Sum</i>	<i>Average</i>	<i>Variance</i>		
0.15 No Agitation	4	1.92	0.48	0.06		
0.15 Panel Movement & Bubbles	4	3.69	0.92	0.19		
0.15 MS	4	2.15	0.54	0.16		
0.2 No Agitation	4	1.07	0.27	0.03		
0.2 Panel Movement & Bubbles	4	2.70	0.67	0.30		
0.2 MS	4	2.89	0.72	0.14		
ANOVA						
<i>Source of Variation</i>	<i>SS</i>	<i>df</i>	<i>MS</i>	<i>F</i>	<i>P-value</i>	<i>F crit</i>
Between Groups	1.02	5	0.20	1.39	0.27	2.77
Within Groups	2.63	18	0.15			
Total	3.65	23				

Table A4 - Anova: Two-Factor With Replication of data in Table A1.

SUMMARY	No Agitation	Panel Movement & Bubbles	MS	Total
0.15				
Count	4	4	4	12
Sum	5.754	28.279	20.82	54.853
Average	1.4385	7.06975	5.205	4.571083333
Variance	0.365861667	1.327153583	0.543368667	6.594746083
0.2				
Count	4	4	4	12
Sum	7.329	15.505	26.673	49.507
Average	1.83225	3.87625	6.66825	4.125583333
Variance	0.121614917	0.908794917	0.831592917	4.793891174
Total				
Count	8	8	8	
Sum	13.083	43.784	47.493	
Average	1.635375	5.473	5.936625	
Variance	0.253215411	3.872104286	1.201012268	

Table A5 – Two-way ANOVA results for data in Table A1.

	<i>Source of Variation</i>	<i>SS</i>	<i>df</i>	<i>MS</i>	<i>F</i>	<i>P-value</i>	<i>F crit</i>	
<u>Diameter</u>	Sample	1.19	1	1.19	1.74	0.20	4.41	<i>Insignificant</i>
<u>Agitation</u>	Columns	89.18	2	44.59	65.28	5.63E-09	3.55	<i>Significant</i>
<u>Both</u>	Interaction	23.80	2	11.90	17.42	6.18E-05	3.55	<i>Significant</i>
	Within	12.30	18	0.68				
	Total	126.47	23					

Appendix B Statistical Analysis

A Levene's test was performed on the data in Table B1 to review homogeneity. First, the absolute values of the data in Table B1 less the average thickness for the parameter were obtained and the results displayed in Table B2. Second, a one-way Anova is performed on the data in Table B2 as indicated in Table B3.

Table B1 – Thickness measures down BVs less the starter Cu thickness, for thick deposition plating regime.

Replicate	BV diameter (mm)	Cu thickness down Blind vias (μm)		
		No Agitation	Panel Movement & Bubbles	MS
1	0.15	10.106	25.855	24.685
2		11.132	24.105	24.182
3		12.496	23.078	18.341
4		9.238	26.009	23.445
5		8.923	23.761	39.834
6		12.083	19.437	36.922
7		8.75	21.598	41.643
8		11.297	22.277	40.005
9	0.2	11.124	18.341	30.569
10		10.713	17.59	36.52
11		13.47	18.181	32.733
12		8.964	17.991	34.689
13		7.512	18.381	48.699
14		8.587	22.748	43.309
15		5.851	19.233	37.087
16		10.962	22.175	51.192

The P value obtained was 2.32×10^{-10} which was significantly less than 0.05 and so the null hypothesis was rejected and the data was not homogeneous. To improve homogeneity the data was transformed by applying Log10 to the data in Table B1 and performing the Levene's Test. The P value for this was 1.45×10^{-4} which was also less than 0.05. To analyse data which is not homogeneous, a Scheirer Ray Hare Test can be performed.

Table B2 - Absolute values of average residuals from data in Table B1.

0.15 mm No Agitation	0.15 mm Panel Movement & Bubbles	0.15 mm MS	0.2 mm No Agitation	0.2 mm Panel Movement & Bubbles	0.2 mm MS
0.397	2.590	6.447	1.476	0.989	9.313
0.629	0.840	6.950	1.065	1.740	3.362
1.993	0.187	12.791	3.822	1.149	7.149
1.265	2.744	7.687	0.684	1.339	5.193
1.580	0.496	8.702	2.136	0.949	8.817
1.580	3.828	5.790	1.061	3.418	3.427
1.753	1.667	10.511	3.797	0.097	1.466
0.794	0.988	8.873	1.314	2.845	11.310

Table B3 - Anova: Single-Factor with Replication of data in Table B2.

SUMMARY						
<i>Groups</i>	<i>Count</i>	<i>Sum</i>	<i>Average</i>	<i>Variance</i>		
0.15 No Agitation	8	9.99	1.25	0.33		
0.15 Panel Movement & Bubbles	8	13.34	1.67	1.63		
0.15 MS	8	67.75	8.47	5.32		
0.2 No Agitation	8	15.36	1.92	1.54		
0.2 Panel Movement & Bubbles	8	12.53	1.57	1.17		
0.2 MS	8	50.04	6.25	11.81		
ANOVA						
<i>Source of Variation</i>	<i>SS</i>	<i>df</i>	<i>MS</i>	<i>F</i>	<i>P-value</i>	<i>F crit</i>
Between Groups	375.52	5	75.10	20.67	2.32E-10	2.44
Within Groups	152.62	42	3.63			
Total	528.15	47				

The Scheirer Ray Hare test [159] was performed on the data in Table B1 using open-sourced, excel-based statistical analytical software package ‘*Real Statistics*’ obtained from <http://www.real-statistics.com/free-download/> (accessed 09/12/2016). The individual workings are highlighted in Table B4 and Table B5, and the results in Table B6.

Table B4 - Ranks evaluated for Scheirer Ray Hare test performed on data in Table B1.

BV diameter (mm)	No Agitation	Panel Movement & Bubbles	MS
0.15	8	35	34
	12	32	33
	15	29	21
	7	36	30
	5	31	43
	14	24	41
	4	25	45
	13	27	44
0.2	11	20.5	37
	9	17	40
	16	19	38
	6	18	39
	2	22	47
	3	28	46
	1	23	42
	10	26	48

Table B5 – Descriptive statistics evaluated for Scheirer Ray Hare test performed on data in Table B1.

COUNT	balanced			
	No Agitation	Panel Movement & Bubbles	MS	
0.150	8	8	8	24
0.200	8	8	8	24
	16	16	16	48
MEAN				
	No Agitation	Panel Movement & Bubbles	MS	
0.15	9.750	29.875	36.313	25.313
0.2	7.25	21.6875	42.125	23.6875
	8.500	25.781	39.219	
VARIANCE				
	No Agitation	Panel Movement & Bubbles	MS	
0.15	18.21428571	19.5535714	72.4955357	167.126359
0.2	26.78571429	14.9241071	18.6964286	231.995924
	22.66666667	33.965625	51.565625	195.989362

Table B6 – Scheirer Ray Hare Test results for data in Table B1.

	ANOVA				Alpha	0.05	
		<i>SS</i>	<i>df</i>	<i>MS</i>	<i>H</i>	<i>p-value</i>	<i>sig</i>
Diameter	Rows	31.69	1.000		0.16	0.69	no
Agitation	Columns	7588.53	2		38.72	3.91E-09	yes
Both	Inter	396.59	2		2.02	0.36	no
	Within	1194.69	42.000				
	Total	9211.50	47	195.99			

Appendix C Megasonic Assisted Dry-film Removal

C.1 Introduction

Besides the research work on electroplating vias, it was also decided to use MS agitation for the removal of particles and enhanced etching of substrates. The MS transducer device applied in electroplating studies at HWU induces acoustic pressures on the PCB surface up to 120 kPa as a result of acoustic cavitation and acoustic streaming currents [67]. These pressures are comparable to the forces induced by standard agitation techniques, although MS agitation has the unique ability to generate microstreaming currents which can remove micro-particulates from microcavity structures. Acoustic streaming currents generate a pulsating flow around micro-particulates due to vortex flow, which induce a tangential drag force lifting them off a surface [172]. This ability to agitate small microstructures has been utilised in the semiconducting industry for the last 35 years with silicon wafer cleaning [173, 174]. The increases to mass transport witnessed in MS cleaning of wafers will be utilised in this investigation for the removal of optical dry-film.

Optically activated dry-film resists are critical in PCB processing to enable electrical track definition. Dry-film is added to a PCB to protect and define the locations of the electrical features on a board. After processing, the resist has to be removed from the PCB. Removing resists can be difficult between fine-pitch electrical features of size $\leq 150 \mu\text{m}$, as it can become entrapped and lead to electrical shorts on the PCB surface. The ability to remove particulates from within small features is highly desirable, especially due to the trend in track pitch reductions. If MS agitation could assist in dry-film removal in fine pitch regions, then it would potentially improve board yields on complex designs, reducing fabrication costs, and enable enhancements in the fabrication of high-value, fine pitch boards. For this reason additional investigations will be performed into this application, looking to develop a MS-assisted dry-film removal process.

The second objective of the thesis i.e. investigations reviewing the ability to remove dry-film resists will be performed by determining, firstly, the ability to remove undeveloped dry-film resist (developing) and developed resists (stripping), from a PCB and secondly, the ability to overcome the PCB fabrication issue known as ‘mushrooming’ through the removal of dry-film.

The outcomes of these investigations will be:

- To quantify the ability of MS to remove dry-film resists.
- To evaluate the ability to overcome adverse effects on plating due to the ‘mushrooming’ effect.

A dry-film photoresist is an optically sensitive material used for the formation of a patterned coating on a Printed Circuit Board (PCB) surface. Unlike their liquid counterparts, dry films do not require the use of spinners for the deposition of the film. Films come with a certain thickness that cannot be changed. Issues with dry-film removal lead to poorly defined features and scrapped boards. To assist in the dry-film removal process, Ultrasonic (US) agitation was applied in wet chemical process tanks for wafer fabrication [175] and was shown to successfully remove the dry-film layer.

US agitation led to surface damage due to high cavitation energies. Processing at higher frequencies reduced this damage, as discussed in Chapter 2. Dry-film removal was investigated using the Megasonic (MS) transducer applied in the earlier MS plating trials. In this chapter two investigations are discussed. Section C.2 discusses the MS agitation applied for the removal of dry-film in the development stage of the process. Section C.3 examines the removal of optically active dry-film in a process referred to as stripping.

The setup of the transducer was altered in the investigations to reveal whether benefits could be obtained, in terms of technological enhancements or cost savings, for the operation of the process.

C.2 Megasonic assisted dry-film developing

MS agitation applied in the plating trials induced an aggressive force on the PCB surface due to acoustic streaming and cavitation. The transducer outputted a peak streaming force of 220 KPa, measured at a distance of 2.5 cm from the transducer surface, as indicated in Chapter 3 [115]. Sparge-pipes are used in the dry-film developing process line at Merlin to apply solution to the board surface. The forces outputted by these pipes are 120 KPa. MS processing capability was reviewed when applied to the development of the dry-film off a PCB.

Development was applied when performing the removal of either negative resists – in areas not illuminated, or positive resists – in optically activated regions. In this investigation negative resists were used. These are resists which, upon exposure to optical irradiance, increase the polymer cross linking within their molecular structure [176]. On application of developing chemistry, the areas unexposed were removed due to their weaker cohesive internal bonding. Developing away the non-activated dry-film is crucial

to the process and the duration in which to do this is referred to as the dwell time. All PCBs go through a development process and therefore any process savings achieved through dwell time reductions would be beneficial to process manufacture. Accordingly, studies were performed measuring changes to dwell time duration for the application of MS in a developer tank.

C.2.1 MS developing experimental investigation

A 225 L polypropylene process tank was purchased from Westminster Plastic for use in the dry-film developing trials. The tank was fitted with a heater, similar to the device installed in the PCB tank, as outlined in Chapter 3, to regulate the process temperature. The temperature chosen depends on the dry-film applied, which, in this case, was 29°C for the Ordyl Alpha 350 film.

The bath composition of the developer was an alkali solution, Enplate NI 418Q, provided by the suppliers Enthone. Its composition mostly consists of sodium carbonate, although, as supplied, it was modified to outperform standard solutions and to enhance ease of replenishment. It is the developer solution used at Merlin Circuit Technology. A standard bath composition comprises of 15 ml/L Enplate NI 418Q and is made-up with water to the desired mark, which, in the trials, was 185 L.

The transducer was applied in the tank as displayed in Fig C.1, highlighting a top-down schematic view of the tank showing tangential distance to the PCB, x , and the position of the heater in the top left hand corner.

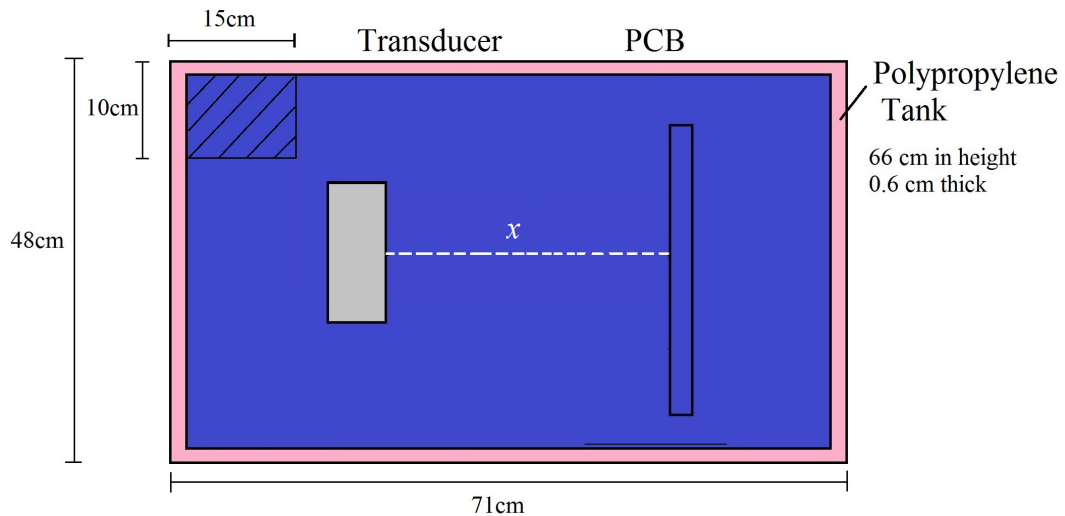


Figure C.1 - The transducer setup within the developer tank.

The dry-film used (Ordyl Alpha 350) is typically applied in outer layer manufacture. The dry-film was applied to the PCB surface using a manual lamination device, Dupont Riston LC-2400, indicated in Fig C.2. The PCBs were processed by:

1. Guillotining a panel to 6" by 6" size,
2. Cleaning the board surface using standard conveyor cleaning line, and
3. Placing into manual lamination with the aid of another operator and fed through.

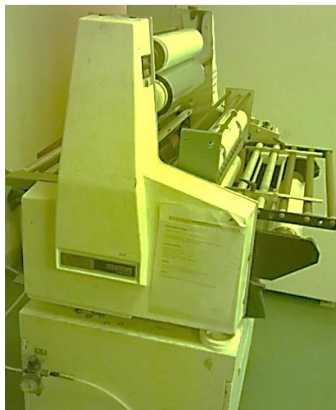


Figure C.2 - Manual dry-film lamination device.

Once the boards were successfully laminated - making sure creases had not formed on the surface - the boards were ready to be dry-film developed. At this stage the boards were optically sensitive to Ultraviolet (UV) light and so needed to be stored with no optical activation. Additionally, after lamination, the boards needed processing within six days, due to naturally induced polymerisation which increases resistance to chemical developing.

The chemical composition of the bath was analysed using a titration of the Enplate NI 418Q. The equipment and materials required were a 10 ml pipette, Phenolphthalein indicator and 0.1M Hydrochloric Acid. The procedure was as follows:

1. Pipette 10 mL of sample of the developing solution into a 250 mL beaker.
2. Add 100 mL of DI water.
3. Add 5 drops of indicator.
4. With magnetic stirrer titrate with 0.1N HCL until a colourless endpoint was reached.

With this information the concentration was calculated as: (ml of 0.1M HCL used) $\times 1.38 = \text{ml/L}$ of ENPLATE NI 418Q solution in the bath.

The developing behaviour was reviewed on the PCB by making observations as to the quality of the PCB surface after processing. Observing the dry-film removal off the board surface after developing is an acceptable method of quality review and is applied in PCB manufacture. In the developing investigations, the dwell time was evaluated by removing the PCB from the process line at specific intervals during the processing cycle and observing the quality of the changes to the dry-film removal. A single dwell time was quantified in the studies when dry-film had been entirely removed from under the area sonicated and not the entire board surface.

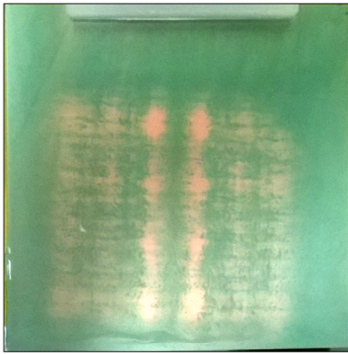

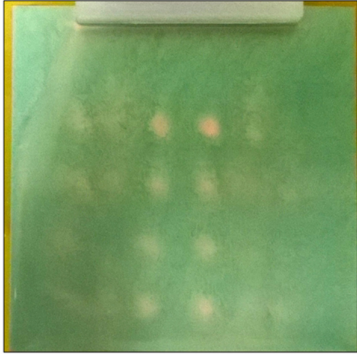

Experiments were performed evaluating the impact on dwell time as a function of the tangential distance of the transducer, as the pressure reaching the board surface depends on this value. The distances tested were 1 cm, 2 cm, 4 cm, 6 cm and 10 cm. During the investigations the transducer output was at its maximum of 450 W.

C.2.2 MS developing results and analysis

The tangential distance x was changed for different dry-film developing runs. Highlighted in Table C.1 are PCBs processed after 1 cm and 10 cm configurations. Shown in blue/green is the undeveloped dry-film on the PCB surface and the exposed Cu surface is shown in yellow. The area processed was categorised by a patterning indicative of the acoustic pressure distributions emitted by the MS transducer, as shown in Figure 3.10 in Chapter 3.

When increasing the distance of the transducer, the area processed increased, which was indicated by a larger area of dry-film removal after 75 seconds processing. The dry-film removal was poorer at larger distances, indicated by a smaller area of Cu removed after 30 seconds processing. The larger area and smaller pressures are due to attenuation of the acoustic wave, where the wave increases in area as it propagates whilst reducing in pressure.

Table C.1 - Optical images of PCB surface developed after certain process durations for MS processing at different tangential distances.

	Processing after 30 seconds	Processing after 75 seconds
MS processing at 1 cm tangential distance		
MS processing at 10 cm tangential distance		

Highlighted in Table C.2 are evaluations of the dwell time observed for different positions of x . The Dwell time was evaluated here as the time taken to remove the dryfilm under the area sonicated and not the entire surface of the board. As x increases, the dwell time increases. The standard dwell for the dry-film resist is 75 seconds. This corresponds to a maximum distance of 2 cm for the configuration of the transducer.

Table C.2 - Dwell duration recorded for different transducer positions.

Transducer Position x (± 0.5 cm)	Dwell Duration (± 15 sec)
1	75
2	75
4	82
6	82
10	90

C.2.3 Conclusions

The ability to remove dry-film was quantified by the introduction of MS agitation in the development process line. The MS agitations were shown to remove dry-film off the board successfully, at a duration comparable to standard processing time. For this

reason cost-savings were not observed on the PCB surface when processed under MS. To further evaluate potential savings, a reduction in bath concentration and operation temperature should be performed as future work, seeking to observe quality changes associated with Dwell duration.

C.3 Megasonic assisted dry-film stripping

The ‘mushroom’ plating effect is a Cu artefact occurring when a track feature over-plates and encroaches over the top of the dry-film onto the PCB surface. This effect is a negative plating feature which causes issues in the subsequent manufacturing stages.

The impact of the mushroom on follow-on processes is first encountered at the dry-film stripper line. The stripper process involves the introduction of a strong alkali solution onto the PCB surface to strip away optically activated, outer layer dry-film resists. The stripper solution traditionally causes the dry-film to swell, breaking the bonds with the base Cu and the recently plated Cu features. If a Cu feature has over-plated then the dry-film may become entrapped and fails to be effectively stripped. This results in some dry-film remaining which impacts negatively in the subsequent processes. These stages are highlighted in Fig C.3, where the swelling action of the stripper on the dry-film causes it to break away from the base Cu, where it then becomes trapped under the over-plated ‘head’.

The stripping of the dry-film is accompanied by a Cu etch process in an alkali ammoniacal etch. Under correct operation, the etchant removes the unwanted base Cu which has become recently exposed in the stripping of the dry-film, whilst leaving behind the Cu features protected by a tin (Sn) resist. This process stage enables the electrical isolation of the Cu features on the PCB design. If the dry-film becomes entrapped in between Cu tracks then it prevents the etchant from operating correctly. This is observed as a poor uniformity of the Cu tracks and a failure in etching away the unwanted base Cu, leading to short circuits. This effect is highlighted in 3 in Fig C.3.

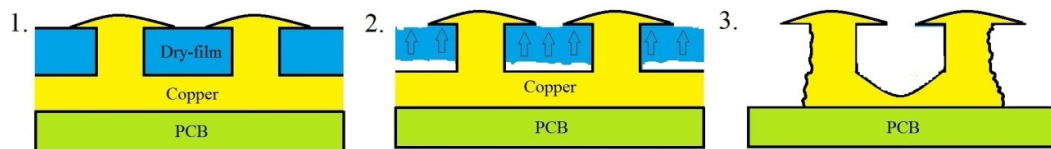


Figure C.3 - Process flow outlining mushrooming effect on dry-film removal leading to electrical short.

The mushrooming of Cu occurs when its electroplating rate is higher than desired. This increase in plating is due to an uneven distribution of the electrical current across a PCB surface, which is distributed dependent on the design of the Cu features. If a feature is electrically isolated i.e. with no surrounding Cu, then it will attract greater amounts of electrical field line flux, inducing high current and leading to unwanted plating rate increases on the feature.

Highlighted in Fig C.4A is a top view of an isolated differential pair track, where in-between the two Cu tracks unwanted Cu can be seen. Fig C.4B shows a microsection close-up of this region, where over-plating is observed by mushroom like heads. The electrical short is indicated at the base of the tracks.

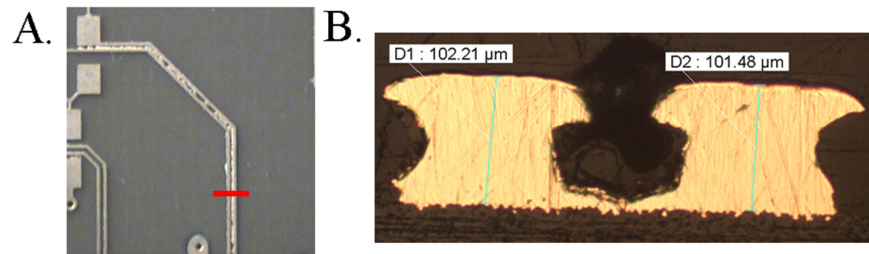


Figure C.4 - A) Top view of differential pair tracks with electrical shorts between. B) Microsection cross-section of electrical short between poorly etched tracks, from location highlighted by red in A.

MS agitation shows the ability to agitate small features due to acoustic streaming effects and thermal increases brought on by microbubble cavitation, as outlined in Chapter 2. These two acoustic effects have the potential to remove the dry-film from regions which are traditionally difficult to strip on the PCB, such as in between differential pair tracks. Removing of dry-film in microscale cavities between over-plated differential pair tracks would be highly desirable for reducing board scrap and increasing process capability. As such, investigations were performed introducing MS within a stripper solution tank to assist in dry-film stripping.

C.3.1 MS stripping experimental investigation

The MS stripping tank was set up with the equipment outlined in section C.2. The transducer was placed within the tank at a distance of 1 cm from the PCB surface, as close distances were found to produce quicker processing times, indicated in section C.2.

The stripper solution used was Ordyl Stripper 5600. The bath was made up using a 4.2% concentration with a pH of 10.5–12.5, and the remaining solution made up with

deionised water to 195 L. The recommended operational temperature of the bath is 48°C. Temperatures above 40°C cause damage to the transducer device and so the bath temperature was maintained at 33 °C which is 35% less than the recommended.

The bath composition was maintained through pH analysis. The procedure was as follows:

1. Pipette 2mL of working solution into a conical flask.
2. Add 50 mL of DI water.
3. Using a pH probe titrate to pH 4 with HCL 0.1M.

Calculation:

$$\text{ml HCL} \times 0.42 = \% \text{ Ordyl Stripper 5600 (by volume)}. \quad (7)$$

The PCB design used in the trials was made so that mushrooming would occur under standard conditions. The board design is outlined in Fig 8.5, showing the PCB surface after tin resist plating with surrounding, optically activated dry-film in dark blue. Features include differential pair tracks of width 100 µm and spacing 125 µm, which are not surrounded by Cu features and so are under electrical isolation and receive a high electrical field line flux – the conditions leading to mushrooming.

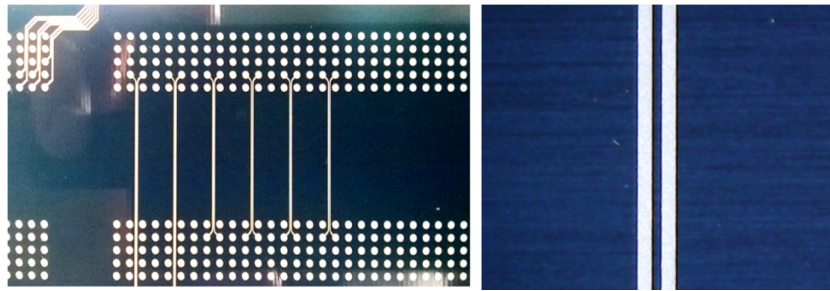


Figure C.5 - PCB design used in manufacture after tin plating, highlighting on right close-up of isolated differential pair tracks.

The manufacture of a standard outer layer PCB is indicated in Table C.3. The boards for MS processing were run through the stages 1 to 6, where at stage 5 they were added to the MS stripper tank and processed under 450 W agitation. The standard dry-film stripping is applied in a conveyor line, set at a speed of 500 mm/min. At this speed the board is under the sparge-pipe agitation of the stripper solution for 4 minutes and 19 seconds. This duration was also applied as the MS processing duration in the

investigations. After processing, the board was introduced back into the conveyor line at stage 6 and the board processed under standard settings.

Table C.3 - Manufacturing stages for outer-layer manufacture of the PCB.

Outer-layer PCB fabrication	Notes
1. Sales / Front end.	PCB was designed and put into manufacture
2. Ordyl Alpha 350 dry film added and Laser Direct Imaging exposes the features not to be removed by developer.	The dry-film is applied using the same method as in 8.2 and features are exposed so as to <u>not</u> be removed by the developer, which includes everything but the circuit design.
3. Developer	A developer removes the non-activated dry-film from the region over the electrical features, which includes the tracks, the via holes and pads.
4. Electroplating Cu and Sn resist	The circuit design features along with the via holes are plated with Cu $\sim 17\ \mu\text{m}$. Around $10\ \mu\text{m}$ Tin (Sn) is plated on top of the Cu to act as a resist, protecting the underlying Cu features in the follow up etch process.
5. Dry-film Strip	This stage involves an alkali strip of the optically activated dry-film remaining from the surface.
6. Etch-Strip	The exposed Cu is then etched using an alkali, ammoniacal etch which enables electrical isolation of the features, leaving behind the electrical tracks which were protected by the tin resist. Next, the tin resist is stripped and the PCBs features are defined on the board surface.

Once the PCBs were processed, the surface quality was imaged under a Koolertron Digital Microscope and a microsection obtained and imaged, using the process outlined in section 3.3.2 in Chapter 3. Four PCBs were processed, two with MS and two through the standard process conditions to provide a comparison.

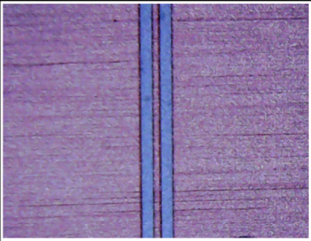
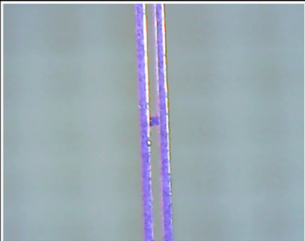
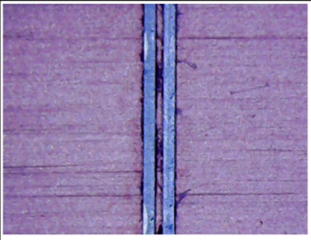
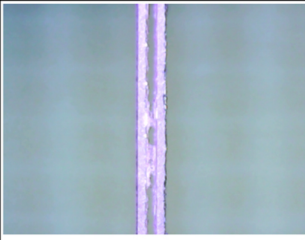
C.3.2 MS stripping results and analysis

PCBs were processed under standard conditions and MS. Top down images of the differential pair tracks on the PCB surface were shown in Table C.4 for PCBs processed with dry-film stripping and for a Cu etch and Sn resist strip. Under standard processing conditions, the dry-film was effectively stripped from the PCB revealing Cu and the Sn plated tracks. With MS agitation the dry-film was not effectively stripped around the edge of the differential pair and in-between the tracks, as shown by the dark blue filaments.

After the Cu etch and Sn strip, the differential pair displayed an electrical short between the tracks for both the standard process and the MS processed, which was due to dry-film entrapped between the two tracks preventing etching. The numbers of shorts were sparse on the standard processed board and most were correctable by running a scalpel blade in-between the tracks to sever the unwanted connection. With MS processing, electrical shorts were common on the board, as in-between the differential pair tracks a large region of un-etched Cu resided, as indicated in Table C.4.

The results highlight that the MS agitation underperformed when stripping the dry-film off the PCB, when compared to the standard operating process.

Table C.4 - Process performance comparison on over-plated differential pair tracks.

	Dry-film Stripping	Cu microetch and Sn Strip
Standard Processing		
450 W Megasonic Processing		

The MS agitation produced a non-uniform agitation of the PCB surface. This was due to the pressure distribution of the acoustic wave as it sonicated the PCB surface. Highlighted in Fig C.6 is a region of the PCB MS processed, showing Cu remaining on the surface after the Cu etch. The Cu was present where dry-film had failed to be removed by the MS. The patterning of the Cu additionally revealed the uniformity of the MS sonication, which was poor.

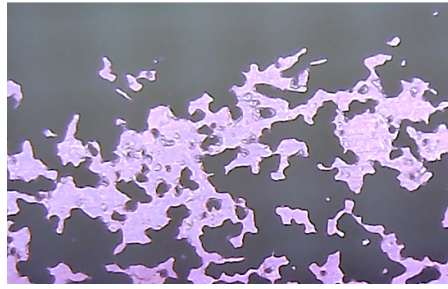


Figure C.6 - Top-down picture of PCB after MS dry-film stripping, and standard process Cu etch.

Microsections were obtained of the differential pair tracks after strip-etch-strip to reveal the uniformity of the tracks and were displayed in Fig C.7 showing, A) MS processed and B) Processed using standard procedure. The tracks were over-plated, indicated by the concave shape of the track walls. The MS processed result produced poorer track uniformity, highlighted by a greater variation in feature sizes. Compared to the standard processing conditions, the track width was approximately 20 % larger and track separation distance was approximately 40 % smaller. This outcome was an unwanted result, as the track sizes differed considerably from specification and if the board was being made for a customer it would fall outside acceptable quality requirements.

The poor uniformity obtained with MS processing was due to an impeded Cu etch, induced by dry-film remaining on the Cu features because of poor stripping. The MS device could not operate at the standard process temperature and so the temperature was lowered by 35% of the standard. Operating at the reduced temperatures could have contributed to the poor result obtained with MS agitation.

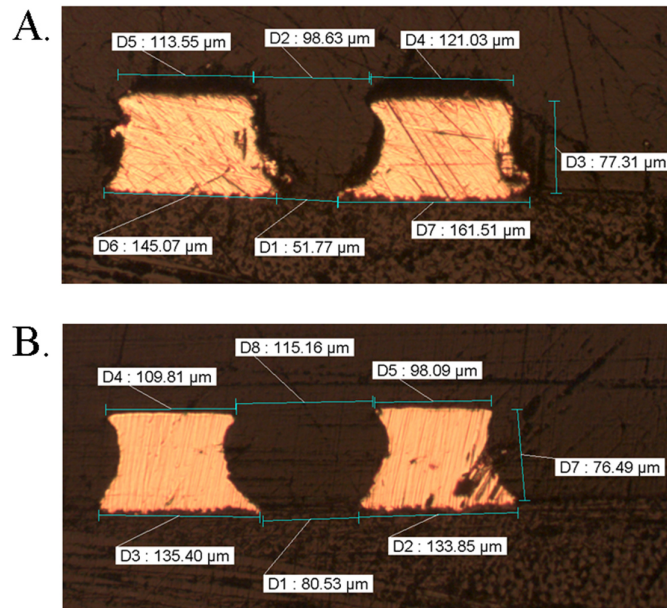


Figure C.7 - Microsection of differential pair tracks after strip-etch-strip for A) MS stripped and B) standard process.

C.3.3 Conclusions

The MS processing capability on dry-film stripping was compared with the standard processing procedure. The MS agitation was shown to aid the chemical stripping process, although failed to remove the resist in and around small features on the board. With MS processing, the bath solution had to be operated at reduced operational temperatures, due to damage induced on the acoustic transducer at the recommended setting. This condition would have negatively influenced the stripping outcome and the processing result. It is possible to induce sonication on the PCB whilst operating at standard temperatures by introducing the acoustic waves using an indirect method of agitation [177]. Indirect sonication houses the transducer unit outside the walls of the tank and excites acoustic waves through them, into the solution and onto the PCB. Using the existing transducer, such a setup would have caused large losses in the pressure output due to absorption of the acoustic waves in the tank walls and the larger propagation distances of the wave. To enable a low loss transmission, an indirect agitation transducer should be engineered by the manufacturer, where the wall of the bath is modified to enable maximum transmission. Such a device would show improved performance over the current setup and would display an increased likelihood of enabling cost savings to the stripping process, along with technological improvements.

The MS agitation displayed a poor uniformity across the PCB surface, highlighting that certain regions received dry-film sonication quicker than others. To

improve coverage of the board and uniformity, multiple transducers should be applied and / or a larger area transducer used.

C.4 General conclusions

MS agitation was shown to remove negative dry-film resists, which were non-optically and optically activated. The resists were removed in separate chemical bath processes dependent on optical activation. The optically activated dry-film failed to be removed in difficult-to-process regions and, so, quality and technological improvements were not obtained under the process settings applied. A position dependent processing capability was observed with the acoustic transducer, where ideal settings were resolved at close distances to the PCB.

The standard process line applied chemistry by multiple sparge-pipes under high pressure. The acoustic wave outputted comparable agitation pressures, although the area coverage was smaller and the uniformity was poorer. A more effective setup of the MS agitation would be to utilise it alongside sparge-pipe agitation. The transducer could then be used in manufacture when board designs were being processed containing features difficult to process under standard conditions. A conveyor process line could be used and the PCB would move to a region, receive sonication and then pass through sparge-pipe agitation to improve overall uniformity of the removal. A variety of process combinations could be applied under this configuration, each requiring its own design optimisation investigation.

The MS process quality was affected by the uniformity of the acoustic pressure distribution. The current dry-film removal process is optimised for maximum removal, but, regardless, can still underperform when processing certain board designs. The acoustic agitation has not received the same level of process optimisation and so, without such investigations, the extensive benefits to manufacture witnessed with MS wafer cleaning [178] have not yet been realised with MS dry-film removal.

References

1. Technavio 2016 'Global Printed circuit Board Market 2016 - 2017.' SKU: IRTNTR8157. Available from: <http://www.technavio.com/report/global-semiconductor-equipment-printed-circuit-board-market>. [Accessed: 3rd March 2017]
2. KPCA 'Korea PCB Industry.' Available from: <http://www.kpca.or.kr/kr/eng/Industry/industry.php>. [Accessed: 3rd March 2017]
3. B. Olney 2015 'Stackup Planning.' The PCB Design Magazine. Available from: <http://iconnect007.uberflip.com/i/525318-pcbd-june2015/21>. [Accessed: 14th May 2017]
4. M. Brizoux, A. Grivon, W.C. Maia Filho, E. Monier-Vinard, J. Stahr, and M. Morianz 2009 'Industrial PCB Development using Embedded Passive & Active Discrete Chips Focused on Process and DfR.' Available from: <http://www.ipc.org/html/review/technical-article.pdf>. [Accessed: 14th May 2017]
5. M.K. Yin,(1996) 'Duplex diffusion layer model for pulse with reverse plating ' *Elsevier, Surface & Coatings Technology*. **88**: pp. 162 - 164.
6. M.P.M. Schlesinger and M. Paunovic, 2011 *Modern Electroplating*. John Wiley & Sons.
7. T.S.S. T. Okubo, T. Hosoi, H. Tsuyoshi, F.K. Mitsui. (2013) 'Signal Transmission Loss on Printed Circuit Board in GHz Frequency Region'. in *IEEE Electrical Design of Advanced Packaging & Systems Symposium (EDAPS)*. Nara, Japan: IEEE.
8. S. Muller, T. Reuschel, R.R. Donadio, Y.H. Kwark, H.D. Bruns, and C. Schuster,(2015) 'Energy-Aware Signal Integrity Analysis for High-Speed PCB Links.' *IEEE Transactions of Electromagnetic Compatibility*. **57**(5): pp. 1226 - 1234.
9. M.V. Ierssel, T. Esmailian, A. Sheikholeslami, and P.S. Pasupathy. (2003) 'Signalling Capacity of FR4 PCB Traces for Chip-to-Chip Communications'. in *Proceedings of the 2003 International Symposium on Circuits and Systems*. IEEE.
10. S.P. Gurrum, D.R. Edwards, T. Marchand-Golder, J. Akiyama, S. Yokoya, J. Drouard, and F. Dahan. (2012) 'Generic Thermal Analysis for Phone and Tablet Systems'. in *Electronic Components and Technology Conference (ECTC), 2012 IEEE 62nd*. 2012. IEEE.
11. J.G.Kaufmann, M.P.Y.Desmulliez, Y. Tian, D. Price, M. Hughes, N. Strusevich, C. Bailey, C. Liu, and D. Hutt,(2009) 'Megasonic agitation for enhanced electrodeposition of copper.' *Microsystems and Technology*. **15**: pp. 1245-1255.
12. S. Costello, N. Strusevich, D. Flynn, R.W. Kay, M.K. Patel, C. Bailey, D. Price, M. Bennet, A.C. Jones, and M.P.Y. Desmulliez,(2013) 'Electrodeposition of copper into high aspect ratio PCB micro-via using megasonic agitation.' *Springer Verlag, Journal of Microsystems Technology*: pp. 1-8.
13. C. Nguyen, 2003 *Analysis Methods for RF, Microwave, and Millimeter-Wave Planar Transmission Line Structures*. Wiley.
14. P.C. Andricacos, E.S.D. Science, T. Division, and E.S. Meeting, 1999 *Electrochemical Processing in ULSI Fabrication and Semiconductor/metal Deposition II: Proceedings of the International Symposium*. Electrochemical Society.
15. L.J. Durney, 1984 *Graham's Electroplating Engineering Handbook*. Springer.
16. N. Strusevich, M.P.Y. Desmulliez, E. Abraham, D. Flynn, T. Jones, M. Patel, and C. Bailey,(2013) 'Electroplating for high aspect ratio vias in PCB manufacturing

- : enhancement capabilities of acoustic streaming.' *Journal of Advanced Manufacturing*, (1): pp. 211-217.
17. B. Roelfs, N. Dambrowsky, C. Erben, and S. Kenny,(2012) 'Filling through holes and blind microvias with copper using reverse pulse plating and insoluble anodes.' *Emerald Insight, Circuit World*. **38**(3): pp. 113-123.
18. Schloetter 2004 'SLOTOCOUP CU110.' Schloetter Plating Technologies. Available from: http://www.schloetter.at/fileadmin/pdf/public_eng/03/03802_E_Copper_SLOTOCOUP_CU_110.pdf. [Accessed: 14th May 2017]
19. B. Sivasankar, 2008 *Engineering Chemistry*. 1st ed., New Delhi: McGraw-Hill Education.
20. P.H. Reiger, 1994 *Electrochemistry*. 2nd ed., New York: Springer.
21. H. H. Lou and Y. Huang, 2003 *Electroplating*. Department of Chemical Engineering, Beaumont, Texas, USA: Lamar University.
22. A. J. Cobley and D.R. Gabe,(2003) 'The effect of insoluble anodes on the process control and deposit quality of acid copper electroplating baths.' *Circuit World*. **29**(4): pp. pp. 11-18.
23. H. Holden, J. Andresakis, E. Bogatin, M. Carano, K.A. Carpenter, K.H. Dietz, M. Laing, C. Vaucher, P. Viklund, and M. Wuensch, 2009 *The HDI Handbook*. 1st ed. A comprehensive high-density interconnect resource for designers, fabricators and assemblers. Po Boc 50 Seaside, OR 97138: BR Publishing, Inc.pp. 356.
24. M. Palazzola, N. Dambrowsky, and S. Kenny. (2012) 'Via Filling: Challenges for the Chemistry in the Plating Process'. in *IPC APEX EPO*. Taipei, Taiwan: IEEE.
25. A. Sato and R. Barauskas,(1995) 'Copper Plating.' *Metal Finishing*. **93**(1): pp. 223-234.
26. Schloetter. *Platinised Titanium Anodes*. Series 2017; Available from: <http://www.schloetter.co.uk/plating-equipment/platinised-titanium-anodes.htm>. [Accessed: 8th May 2017]
27. S. Menard 2006 'Insoluble Anodes For The Electroplating Industry.' PCB Fabrication. pp. 22-23. Available from: http://www.onboard-technology.com/pdf_giugno2006/060604.pdf. [Accessed: 8th May 2017]
28. G. Milazzo, 1978 *Tables of standard Electrode Potentials*. Chinchester: Wiley.
29. G.S. Mathad and V. Bakshi, 2003 *Copper Interconnects, New Contact Metallurgies/structures, and Low-k Interlevel Dielectrics II: Proceedings of the International Symposium*. Electrochemical Society.
30. M. A. Plante, S. Fairlie, B. Bailey, and I.N. Acworth 2016 'Measurement and Control of Copper Additives in Electroplating Baths by High-Performance Liquid Chromatography.' Available from: <https://tools.thermofisher.com/content/sfs/brochures/WP-71211-HPLC-Copper-Additives-Plating-Baths-WP71211-EN.pdf>. [Accessed: 5th May 2017]
31. H. Wedell and W. Strauss, 1959 *Brighteners for electroplating baths*.US 2,919,411. Germany: Dehydag gmbh. pp 1 - 3.
32. G. Bokisa, 2004 *High Speed Acid Copper Plating*.US 6,676,823 B1. USA: Taskem, Inc. pp. 1-7.
33. G. B. Larson and M. Nikolova, 2010 *Acid Copper electroplating bath composition*.EP 2195474 A2, MacDermid. 1 - 6.
34. M. Pavlov, E. Shalyt, and P. Bratin, 2012 *Chloride Analysis in Acid Copper Plating Baths*. G01N 27/26 ed.205/778.5; 205/789; 205/81. Vol. US 8,142,640 B2. United States: ECI Technology, Inc.
35. M.H. Tsai, W.J. Tsai, S.L. Shue, and C.H. Yu, 2001 *Method for Improvement of gap filling capability of electrochemical deposition of copper*. C25D 5/02 ed.205/123, US 6,224,737 B1. US. 7.

36. N. Kanani, 2006 *Electroplating: Basic Principals, Processes and Practice*, Atotech, Editor., Publisher Elsevier, Atotech: Oxford. pp. 1 - 354.
37. N.Kanani, 2006 *Electroplating Basic Principals, Processes and Practice*, ed. Atotech. Oxford: Elsevier.
38. G. Milad, 2004 *Electroplating*. McGraw-Hill Education. pp. 29.1-29.30.
39. W. Haupin,(1971) 'A scanning reference electrode for voltage contours in Aluminium smelting cells.' *Journal of metals*. **23**(10).
40. M.S. Chandrasekar and M. Pushpavanam,(2008) 'Pulse and pulse reverse plating—Conceptual, advantages and applications.' *Journal of Electrochimica Acta*. **53**(8): pp. 3313-3322.
41. M.S. Chandrasekar and M. Pushpavanam,(2008) 'Pulse and pulse reverse plating—Conceptual, advantages and applications.' *Electrochimica Acta*. **53**(8): pp. 3313-3322.
42. e.a. J.J. Kelly,(2000) 'Additive Effects during Pulsed Deposition of Cu-Co Nanostructures.' *Journal of the Electrochemical Society*. **147**(8): pp. 5.
43. S. Khorasani,(2003) 'Optimal Pulse Shapes for Periodic Reverse Electroplating.' *Iranian Journal of Science and technology*. **27**(B4): pp. 11.
44. e.a. W.Worwag. (2007) 'Copper Via Plating in Three-Dimensional Interconnects'. in *Electronic Components and Technology Conference*. 2007. Intel Corporation, Assembly Technology Development Group, 5000 W. Chandler Blvd., Chandler, AZ 85226: IEEE.
45. R. Leon, 2002 *Reverse pulse plating method* European Patent Office, EP1475463 B1.
46. E.J.Taylor, 2004 *Electrodeposition of metals in high-aspect ratio cavities using modulated reverse electric fields*. Vol. US 6,827,833 B2. United States: Faraday Technology Marketing Group. 8.
47. L.T. Romankiw and E.S.E. Division, 2000 *Electrochemical Technology Applications in Electronics: Proceedings of the Third International Symposium*. Electrochemical Society.
48. J.W. Dini, 1993 *Electrodeposition: The Materials Science of Coatings and Substrates*. Noyes Publications.
49. A. Sharma, S. Bhattacharya, S. Das, and K. Das,(2014) 'Influence of current density on surface morphology and properties of pulse plated tin films from citrate electrolyte.' *Elsevier, Journal of Applied Surface Science*. **290**: pp. 373-380.
50. M.P. M.Schlesinger, 2011 *Modern Electroplating*. John Wiley & Sons.
51. H.R. Shemilt,(1974) 'Electroless Copper Plating troubleshooting.' *Circuit World*. **1**(1): pp. pp. 7-10.
52. S. Jayalakshmi, P. Venkatesh, and P. BalaRamesh,(2016) 'RECENT ADVANCES IN ELECTROLESS COPPER DEPOSITION – A REVIEW ' *International Journal of Advanced Research in Engineering and Applied Sciences*. **5**(8): pp. pp. 1-18.
53. J.R. Henry,(2000) 'Electroless (autocatalytic) plating.' *Metal Finishing*. **98**(1): pp. 424-435.
54. J. Krautkrämer and H. Krautkrämer, 1977 *Ultrasonic testing of materials*. Springer-Verlag.
55. OlympusNDT 2006 'Ultrasonic Transducer Technical Notes.' 1-11. Available from: www.olympus-ims.com/data/File/panametrics/UT-technotes.en.pdf. [Accessed: 14th May 2017]
56. J.G. Kaufmann, M.P.Y. Desmulliez, Y. Tian, D. Price, M. Hughes, N. Strusevich, C. Bailey, C. Liu, and D. Hutt,(2009) 'Megasonic agitation for enhanced electrodeposition of copper.' *Springer, Microsystems and Technology*. **15**: pp. 1245-1255.

57. 2004 *Plating and Surface Finishing*. American Electroplaters and Surface Finishers Society.
58. M. Wiklund, R. Green, and M. Ohlin,(2012) 'Acoustofluidics 14 : Applications of acoustic streaming in microfluidic devices.' *Lab Chip*. **12**: pp. 2438 - 2451.
59. Marken. F, Akkermans. R. P, and R.G. Compton,(1996) 'Voltammetry in the presence of ultrasound: the limit of acoustic streaming induced diffusion layer thinning and the effect of solvent viscosity.' *Elsevier, Journal of Electrochemical Chemistry*. **415**: pp. 55 - 63.
60. B.G. Pollet, J.Y. Hihn, L.M. Coche, J.P. Lorimer, A. Mandroyan, and T.J. Mason,(2007) 'Transport limited current close to an ultrasonic horn: Equivalent flow velocity determination. Journal.' *Journal of the Electrochemical Society* **154**: pp. 131 - 138.
61. A. Brotchie, F. Grieser, and M. Ashokkumar,(2009) 'Effect of Power and Frequency on Bubble-Size Distributions in Acoustic Cavitation.' *Journal of Physical Review Letters*. **102**(084302): pp. 1- 4.
62. K. Feng, L. Yuanyuan, and M. Cheng,(2015) 'Numerical analysis of the transportation characteristics of a self-running sliding stage based on near-field acoustic levitation.' *Acoustical Society of America*. **136**(6): pp. 3723 - 3732.
63. S.W. Rienstra and A. Hirschberg, 2013 *IWDE 92-06: An Introduction to Acoustics*. IWDE 92-06. Eindhoven University of Technology.pp. 1-296.
64. M. Hennig, J. Neumann, A. Wixforth, J.O. Radler, and M.F. Schneider,(2009) 'Dynamic patterns in a supported lipid bilayer driven by standing surface acoustic waves.' *The Royal Society of Chemistry, Lab on a Chip*. **9**: pp. 3050-3053.
65. B. Moudjed, V. Buotton, D. Henry, H.B. Hadid, and P.J. Garandet,(2014) 'Scaling and dimensional analysis of acoustic streaming jets.'
66. L.Y. Yeo and J.R. Friend,(2014) 'Surface Acoustic Wave Microfluidics.' *Annual Review of Fluid Mechanics*. **46**(1): pp. 379-406.
67. SONOSYS 2013 'Future Technology by SONOSYS.' Efficient Megasonic Cleaning of Microstructures. Available from: <http://www.sonosys.de/en/submersible-transducer.html>. [Accessed: 15th May 2017]
68. M. Keswani, S. Raghavan, and P. Deymier,(2011) 'Study of Bubble Activity in a Megasonic Field Using an Electrochemical Technique.' *IEEE transactions on Semiconductor Manufacturing*. **24**(4): pp. 513 - 518.
69. M.N. Mikhail and M.R. El-Tantawy,(1994) 'The acoustic boundary layers: a detailed analysis.' *Journal of Computational and Applied Mathematics*. **51**: pp. 15-36.
70. W.L. Nyborg,(1957) 'Acoustic Streaming near a Boundary.' *Journal of the Acoustical Society of America*. **30**(4): pp. 329-339.
71. J. F. Spengler, W.T. Coakley, and K.T. Christensen,(2003) 'Microstreaming Effects on Particle Concentration in an Ultrasonic Standing Wave.' *American Institute of Chemical Engineers.AIChE Journal*. **49**(11): pp. pp. 2773-2782.
72. N. Strusevich, *Numerical Modelling of Electrodeposition Process for Printed Circuit Board Manufacturing*, in *School of Computing and Mathematical Sciences*. 2013, University of Greenwich: Greenwich. pp. 1-213.
73. D.H. Staelin, 2011 *Electromagnetics and Applications*. Massachusetts Institute of technology. 443.
74. M. Keswani, 2008 *Megasonic Cleaning of Wafers in Electrolyte Solutions: Possible Role of Electro-acoustic and Cavitation Effects*. University of Arizona.
75. L.A. Kuznetsova and W.T. Coakley,(2004) 'Microparticle concentration in short path length ultrasonic resonators: Roles of radiation pressure and acoustic streaming.' *Journal of the Acoustical Society of America*. **116**(4): pp. 1956 - 1966.

76. S. Martin, *Sonocrystallization of Fats*, in *Springer Briefs in Food, Health, and Nutrition*, R.W. Hartel, Editor. 2013, Springer. pp. 1-68.
77. Focus-IT. *Biological Mechanism* Series 2014; Available from: <http://eswt.net/biological-mechanism>. [Accessed: 15th May 2017]
78. Y. Zhou and X.W. Gao,(2013) 'Variations of bubble cavitation and temperature elevation during lesion formation by high-intensity focused ultrasound.' *Journal of Acoustical Society of America*. **132**(2): pp. 1683-1694.
79. S. Verdan, G. Burato, M. Comet, L. Reinert, and H. Fuzellier,(2003) 'Structural changes of metallic surface induced by ultrasound.' *Elsevier, Journal of Ultrasonics Sonochemistry*. **10**: pp. 291-295.
80. G.B. S. Verdan, M. Comet, L. Reinert, H. Fuzellier,,(2003) 'Structural changes of metallic surface induced by ultrasound.' *Elsevier, Journal of Ultrasonics Sonochemistry*. **10**: pp. 291-295.
81. P. Riesz, D. Berdahl, and C.L. Christman,(1985) 'Free Radical Generation by Ultrasound in Aqueous and Nonaqueous Solutions.' *Environ Health Perspect*. **64**: pp. 233 - 252.
82. A.A. Donnikov, 2005 *Bubble and Particle Dynamics in Acoustic Fields: Modern Trends and applications*. Bjerknes forces and translational bubble dynamics. Research signpost. 95 -143.
83. B. Dubus, C. Vanhille, C.C. Pozuelo, and C. Granger,(2010) 'On the physical origin of conical bubble structure under an ultrasonic horn.' *Journal of Ultrasonics Sonochemistry*. **17**: pp. 810-818.
84. I. Bai, J. Deng, C. Li, D. Xu, and W. Xu,(2014) 'Acoustic cavitation structures produced by artificial implants off nuclei.' *Journal of Ultrasonics Sonochemistry*. **21**: pp. 121 - 128.
85. IPC 1999 'IPC-A-600F.' Acceptability of Printed Boards IPC Association Connecting Electronics Industries Northbrook, IL 60062-6135. 2.2.1
86. X. Su, Y. Chen, W. He, S. Wang, and Z. Tao,(2013) 'Research on Manufacturing Process of Buried/Blind Via in HDI Rigid-Flex Board.' *Applied Mechanics and Materials*. **365 - 366**: pp. pp 527 - 531.
87. R. B. M. Salleh and L.C. Yung. (2015) 'Influence of acid copper plating additives on void formation during high temperature storage'. in *2015 IEEE 17th Electronics Packaging and Technology Conference (EPTC)*.
88. C. Shea and D. Ormerod. *Copper Via Fill A Solution for HDI Via-in-Pad*. Series 2007 01/10; Available from: <http://pcdandf.com/pcdesign/index.php/2007-archive-articles/2795-copper-via-fill--a-solution-for-hdi-via-in-pad>. [Accessed: 15th May 2017]
89. L.-N. Ji, Y. Gong, and Z.-G. Yang,(2010) 'Failure investigation on copper-plated blind vias in PCB.' *Microelectronics Reliability*. **50**(8): pp. 1163-1170.
90. L.-N. Ji, Z.-G. Yang, and J.-S. Liu,(2008) 'Failure Analysis on Blind Vias of PCB for Novel Mobile Phones.' *Journal of Failure Analysis and Prevention*. **8**(6): pp. 524-532.
91. P. Reid. (2012) 'Design and Construction Affects on PWB Reliability '. in *IPC APEX EXPO 2012*. Las Vegas.
92. L.B. E.Najjar, J. Nagarajan, M. Lin, M. Rzeznik, M. Lefebvre. (2012) 'Electroplating Through Hole with Different Geometry - A Novel and High Productivity Process for Through Hole Fill Plating'. in *IMPACT Conference Proceedings, IEEE*. Dow Electronic Materials.
93. Actel 2012 'Standard Reflow Profile for Standard and Lead-Free Packages.' Available from: https://www.microsemi.com/document-portal/doc_view/131105-solder-reflow-leadfree. [Accessed: 15th May 2017]

94. 'THP-100DX1 (GF) ' thermal curable gap filling dielectric. DOI: http://taiyo-america.com/docs/files/6514/6041/6525/TDS_THP-100DX1_GF_April_11_2016.pdf. [Accessed: 21st April 2017]
95. D.H. Triyoso, T.B. Dao, T. Kropewnicki, F. Martinez, R. Noble, and M. Hamilton. (2010) 'Progress and challenges of tungsten-filled through-silicon via'. in *2010 IEEE International Conference on Integrated Circuit Design and Technology*.
96. D. Diehl, H. Kitada, N. Maeda, K. Fujimoto, S. Ramaswami, K. Sirajuddin, R. Yalamanchili, B. Eaton, N. Rajagopalan, R. Ding, S. Patel, Z. Cao, M. Gage, Y. Wang, W. Tu, S.W. Kim, R. Kulzer, I. Drucker, D. Erickson, T. Ritzdorf, T. Nakamura, and T. Ohba,(2012) 'Formation of TSV for the stacking of advanced logic devices utilizing bumpless wafer-on-wafer technology.' *Microelectronic Engineering*. **92**: pp. 3-8.
97. C. Gu, H. Xu, and T. Zhang,(2009) 'Fabrication of high aspect ratio through-wafer copper interconnects by reverse pulse electroplating.' *Journal of Microelectronics and Microengineering*. **19**(6): pp. pp. 1-5.
98. J.P. Gambino, S.A. Adderly, and J.U. Knickerbocker,(2015) 'An overview of through-silicon-via technology and manufacturing challenges.' *Microelectronic Engineering*. **135**: pp. 73 - 106.
99. IPC 2014 'IPC-6012B.' Qualification and Performance Specification for Rigid Printed Boards. Available from: <http://www.ipc.org/TOC/IPC-6012B.pdf>. [Accessed: 15th May 2017]
100. IPC May 2005 'IPC-TM-650 Test Methods Manual.' 2.6.8. Available from: <https://www.ipc.org/test-methods.aspx>. [Accessed: 15th May 2017]
101. D. Susan, A. Kilgo, P. Vianco, and M. Neilsen,(2009) 'Thermal Fatigue and Failure Analysis of Cu-Plated Through Hole Solder Joints.' *Microscopy and Microanalysis*. **15**(SupplementS2): pp. 26-27.
102. 2010 'IPC-A-600, Acceptability of Printed Boards.' Association Connecting Electronics Industry, IPC 3000 Lakeside Drive, Suite 309S, Bannockburn, Illinois, 60015-1249. 99
103. L. Callegaro, 2012 *Electrical Impedance: Principles, Measurement, and Applications*. Taylor & Francis.
104. S. Y. Poh, W. C. Chew, and J.A. Kong,(1981) 'Approximate formulas for the line capacitance and characteristic impedance of microstrip line.' *IEEE transactions on microwave theory and techniques*. **MTT-29**(2): pp. 135 - 142.
105. IPC 2004 'Characteristic Impedance of lines on Printed Boards by TDR.' IPC-TM-650 2.5.5.7. 1 - 23. Available from: <https://www.ipc.org/TM/2-5-5-7a.pdf>. [Accessed: 15th May 2017]
106. J. Davis, 2006 *High-speed Digital System Design*. Morgan & Claypool Publishers.
107. Galvatek. *Flat immersion heater - Assembly type B*. Series 2016; Available from: <http://www.thermoploneurs-galvatek.com/en>. [Accessed: 15th May 2017]
108. H. Garich, L. Gebhart, E.J. Taylor, M. Inman, and H. McCrabb,(2007) 'Development and Characterization of Plating Cell Geometry for Printed Circuit Board and Packaging Applications.' *Journal of The Electrochemical Society*. **3**(16): pp. 1- 10.
109. DRPP. *Dutch Reverse Pulse Plating (DRPP)*. Series 2016; Available from: http://www.drpp.com/default.asp?id=1&id_sub=1_1&lng=e. [Accessed: 15th May 2017]
110. Vibtec. *VIBTEC Vibratetechniques LTD, Model M3*. Series 2016; Available from: www.vibtec.com/pdfs/Leaflet-18a.pdf. [Accessed: 15th May 2017]
111. Ventec 2017 'VT-481.' Laminate/Prepreg. Available from: <http://www.ventec-group.com/media/1296/vt-481.pdf>. [Accessed: 10th May 2017]

112. Ventec 2017 'Polyimide VT901.' Polyimide Laminate and Pre Preg Products. **2014**. Available from: <http://www.ventec-group.com/products/polyimide/vt-901/datasheet/>. [Accessed: 15th May 2017]
113. zygo. *NewViewTM 8000 Series*. Series 2016; Available from: <http://www.zygo.com/?/met/profilers/newview8000/>. [Accessed: 15th May 2017]
114. trelleborg 2008 'Aerospace Engineering Guide.' Trelleborg Sealing Solutions. Available from: http://www.tss.trelleborg.com/global/en/news_1/newsarchive/archive_2010/detail_pages_2010/new-aerospace-catalog.html. [Accessed: 15th May 2017]
115. S. Costello. (2011) 'Characterisation of ion transportation during electroplating of high aspect ratio microvias using megasonic agitation'. in *EMPC*. 2011. Brighton: IEEE.
116. S. Coleman and S. Roy,(2014) 'Effect of Ultrasound on mass transfer during electrodeposition for electrodes separated by a narrow gap.' *Elsevier, Journal of Chemical Engineering Science*. **11**: pp. 35-45.
117. F. Marken and R.G. Compton,(1996) 'Electrochemistry in the presence of ultrasound: the need for bipotentiostatic control in sonovoltammetric experiments.' *Elsevier, Ultrasonics Sonochemistry*. **3**: pp. S131 - s134.
118. A.V. Bakshi and U.A. Bakshi, 2009 *Electromagnetic Engineering*. Technical Publications.
119. OHAUS. *OHAUS, Explorer Analytical*. Series 2016; Available from: <http://eu-en.ohaus.com/en-eu>. [Accessed: 15th May 2017]
120. C. Hindle. *Polypropylene (PP)*. Series; Available from: <http://www.bpf.co.uk/plastipedia/polymers/PP.aspx>. [Accessed: 15th May 2017]
121. M.J.Ibrahim, *Technological Change and Economic Transformation*, in *Technological Change*, A.A.C. Teixeira, Editor. 2012, InTech.
122. COMSOL 2016 'Acoustic Scattering off an Ellipsoid.' Application ID: 12417. Available from: <https://www.comsol.com/model/acoustic-scattering-off-an-ellipsoid-12417>. [Accessed: 15th May 2017]
123. B. Verhaagen, T. Zanderink, and D.F. Rivas,(2016) 'Ultrasonic cleaning of 3D printed objects and Cleaning Challenge Devices.' *Applied Acoustics*. **103**(Part B): pp. 172-181.
124. D.C. Wood, P.J. Hazell, G.J. Appleby-Thomas, and N.R. Barnes,(2011) 'Shock behaviour of a phenolic resin.' *Journal of Materials Science*. **46**(18): pp. 5991-5999.
125. S. Ebnesajjad, 2010 *Handbook of Adhesives and Surface Preparation: Technology, Applications and Manufacturing*. Elsevier Science.
126. P. B. Muller, R. Barnkob, M. J. H. Jensen, and H. Bruus. (2012) 'COMSOL Analysis of Acoustic Streaming and Microparticle Acoustophoresis'. in *COMSOL*. Milan: COMSOL.
127. H. Überall, 1992 *Acoustic Resonance Scattering*. Gordon and Breach Science.
128. I. Fanderlik, 2013 *Silica Glass and Its Application*. Elsevier Science.
129. J.J. Yan, L.C. Chang, C.W. Lu, and W.P. Dow,(2013) 'Effects of organic acids on through-hole filling by copper electroplating.' *Electrochimica Acta*: pp. 1 - 12.
130. V. Fleury, W.A. Watters, L. Allam, and T. Devers,(2002) 'Rapid electroplating of insulators.' *Nature* **416**: pp. 716 - 722.
131. D. Minzari, F.B. Grumsen, M.S. Jellesen, P. Moller, and R. Ambat.,(2011) 'Electrochemical migration of tin in electronics and microstructure of the dendrites.' *Elsevier, Journal of Corrosion Science*. **53**: pp. 1659-1669.
132. D.M. Lee, J.T. Folkerts, F.L. Collins, A.E. Dietrich, and A. Keeney. (2010) 'Comparison of the Electrochemical and Physical Properties of Nanocrystalline

- Copper Deposition in the Fabrication of Printed Wiring Boards '. in *IPC APEX EXPO Technical Conference* Las Vegas: IPC.
133. M. Hauptmann, H. Struyf, S.D. Gendt, C. Glorieux, and S. Brems,(2013) 'Evaluation and interpretation of bubble size distributions in pulsed megasonic fields.' *Journal of Applied Physics*. **113**: pp. 1-17.
 134. ASME, 2010 *Surface Texture: Surface Roughness, Waviness and Lay*. Standards Committee B46. Designation of Surface Qualities. American Society of Mechanical Engineers.
 135. U.F. Kocks, C.N. Tomé, and H.R. Wenk, 2000 *Texture and Anisotropy: Preferred Orientations in Polycrystals and Their Effect on Materials Properties*. Cambridge University Press.
 136. J. Wang, Y. Huang, T. Yu, S. Zhu, M. Shen, W. Li, and J. Wang,(2014) 'The migration of Cu species over Cu-SAPO-34 and its effect on NH₃ oxidation at high temperature.' *Journal of the Royal Society of Chemistry, Catal. Sci. Technol.* **4**: pp. 3004-3012.
 137. J. Beers and K. Minten 2011 'PCB technology Future Trend.' IEEE 802 LAN/MAN Standards Committee. 1 - 14. Available from: http://www.ieee802.org/3/bj/public/nov11/minten_01a_1111.pdf. [Accessed: 15th May 2017]
 138. B. Tajik, A. Abbassi, M.S. Avval, A. Abdullah, and H.M. Abasi,(2013) 'Heat transfer enhancement by acoustic streaming in a closed cylindrical enclosure filled with water.' *International Journal of Heat and Mass Transfer*. **60**: pp. 230 - 235.
 139. S. C. S. Lin, B. R. Tittmann, and T. J. Huang,(2012) 'Design of acoustic beam aperture modifier using graded-index phononic crystals.' *Journal of Applied Physics*. **111**(123510): pp. 5.
 140. M.K. Tan, L.Y. Yeo, and J.R. Friend,(2009) 'Rapid fluid flow and mixing induced in microchannels using surface acoustic waves.' *Journal of Europhysics Letters* **87**: pp. 1-7.
 141. Y.H. Kim, 2010 *Sound Propagation: An Impedance Based Approach*. Wiley.
 142. G. Shi, W. Cui, M. Benchimol, Y. Liu, R.F. Mattrey, R. Mukthavaram, S. Kesari, S.C. Esener, and D. Simberg,(2013) 'Isolation of rare Tumor Cells from Blood Cells with Buoyant Immuno-Microbubbles.' *PLoS ONE*. **8**(3): pp. 1 - 9.
 143. J. Jiao, Y. He, K. Yasui, S.E. Kentish, M. Ashokkumar, R. Manasseh, and V. Lee,(2015) 'Influence of acoustic pressure and bubble sizes on the coalescence of two contacting bubbles in an acoustic field.' *Elsevier Publishers, Journal of Ultrasonics Sonochemistry*. **22**: pp. 70-77.
 144. Ordyle 2013 'ORDYLE STRIPPER 5600.' Product Data Sheet, EE.P32.GT.01-01. Available from: www.elgaeurope.it/user/download_ctg.aspx?TIPO=F...Stripper+5600.pdf. [Accessed: 15th May 2017]
 145. T. Lucke and S. Beecham,(2009) 'Cavitation, aeration and negative pressures in siphonic roof drainage systems.' *Building Serv. Eng. Res. Technol.* **30**(2): pp. 103-121.
 146. G.W. Glenn and A.A. Busnaina,(1999) 'Roles of cavitation and acoustic streaming in megasonic cleaning.' *Particulate Science and Technology: An International Journal*. **17**(3): pp. 229-238.
 147. J. Collis, R. Manasseh, P. Liovic, P. Tho, A. Ooi, and K. P. Duran,(2009) 'Cavitation microstreaming and stress fields created by microbubbles.' *Journal of Ultrasonics*. **50**: pp. 273 - 279.
 148. H. Hubner, S. R. Mertens, and D. Russ 2014 'Copper Filling of Blind Microvias and Through-Holes Using Reverse Pulse Plating.' *The PCB Magazine*. Available

from: <http://iconnect007.uberflip.com/i/306762-pcb-may2014/24>. [Accessed: 15th May 2017]

149. B.F. Hamonic, O.B. Wilson, and J.N. Decarpigny, 2012 *Power Transducers for Sonics and Ultrasonics: Proceedings of the International Workshop, Held in Toulon, France, June 12 and 13, 1990*. Springer Berlin Heidelberg.
150. S.C. Tang and G.T. Clement, (2010) 'Standing-Wave Suppression for Transcranial Ultrasound by Random Modulation.' *IEEE Transactions on Biomedical Engineering*. **57**(1): pp. 203 - 205.
151. B. Reents and S. Kenny 2002 'The influence of fluid dynamics on plating electrolyte for the successful production of blind micro-vias: Laboratory investigations leading to optimised production equipment.' Atotech Berlin, Germany.
152. J.H.M. Disselhorst and L.V. Wijngaarden, (1980) 'Flow in the exit of open pipes during acoustic resonance.' *Journal of Fluid Mechanics*. **99**(2): pp. 293-319.
153. S.N. Sen, 1990 *Acoustics, Waves and Oscillations*. Wiley.
154. P.M.C. Morse and K.U. Ingard, 1968 *Theoretical Acoustics*. Princeton University Press.
155. F.Y. Shen, W.P. Dow, A.H. Lui, J.Y. Lin, P.H. Chang, and S.M. Huang, (2013) 'Periodic Pulse Reverse Cu Plating for Through-Hole Filling.' *ECS Electrochemistry Letters*. **2**(5): pp. 3.
156. H.A. Vaidya, O. Ertunc, T. Lichtenegger, A. Delgado, and A. Skupin, (2016) 'The penetration of acoustic cavitation bubbles into micrometer-scale cavities.' *Elsevier: Ultrasonics*. **67**: pp. 190-198.
157. M.B. Dentry, L.Y. Yeo, and J.R. Friend, (2014) 'Frequency effects on the scale and behavior of acoustic streaming.' *Physical Review E*. **89**: pp. 1 - 11.
158. 2011 *SAS/STAT 9.3 User's Guide: Survey Data Analysis (Book Excerpt)*. SAS Institute.
159. J. Scheirer, W.S. Ray, and N. Hare, (1976) 'The Analysis of Ranked Data Derived from Completely Randomized Factorial Designs.' *Biometrics*. **32**(2): pp. 429 - 434.
160. W.P. Dow, Y.Y. Ming, S.Z. Liao, Y.D. Chiu, and H.C. Huang, (2008) 'Filling mechanism in microvia metallization by copper electroplating.' *Electrochimica Acta*. **53**: pp. 10.
161. W.P. Dow, M.Y. Yen, C.W. Lui, and C.C. Huang, (2008) 'Enhancement of filling performance of a copper plating formula at low chloride concentration.' *Electrochimica Acta*. **53**: pp. 3610 - 3619.
162. M.Y. Yen, M.H. Chiang, H.H. Tai, H.C. Chen, K.W. Yee, C. Li, M. Lefebvre, and M. Bayes. (2012) 'Next generation electroplating technology for high planarity, minimum surface deposition microvia filling'. in *7th International Microsystems, Packaging, Assembly and Circuits Technology Conference (IMPACT)*. Taipei: IEEE.
163. L.W. Kong, J.R. Lloyd, K.B. Yeap, E. Zschech, A. Rudack, M. Liehr, and A. Diebold, (2011) 'Applying x-ray microscopy and finite element modeling to identify the mechanism of stress-assisted void growth in through-silicon vias.' *Journal of Applied Physics*. **110**(5): pp. 53502 - 53509.
164. R.G. Compton and C.E. Banks, 2011 *Understanding Voltammetry*. Imperial College Press.
165. F. Marken, J.C. Eklund, and R.G. Compton, (1995) 'Voltammetry in the presence of ultrasound" can ultrasound modify heterogeneous electron transfer kinetics?' *Journal of Electroanalytical Chemistry*. **395**: pp. 335-339.

166. M.E. Hyde and R.G. Compton,(2002) 'How Ultrasound influences the electrodeposition of metals.' *Elsevier Publishers, Journal of Electroanalytical Chemistry*. **531**: pp. 19 - 24.
167. P.G. Huray, 2009 *The Foundations of Signal Integrity*. Wiley.
168. E. Barsoukov and J.R. Macdonald, 2005 *Impedance Spectroscopy: Theory, Experiment, and Applications*. Wiley.
169. A.C. Fischer-Cripps, 2013 *Nanoindentation*. Springer New York.
170. K. Yasuda,(2000) 'Non-destructive, non-contact handling method for biomaterials in micro-chamber by ultrasound.' *Journal of Sensors and Actuators B*. **64**: pp. 128 - 135.
171. P.B. Muller, R. Barnkob, M.J.H. Jensen, and H. Bruus. (2012) 'COMSOL Analysis of Acoustic Streaming and Microparticle Acoustophoresis'. in *COMSOL*. Milan: COMSOL.
172. P. Karimi, T. Kim, J. Aceros, J. Park, and A.A. Busnaina,(2010) 'The removal of nanoparticles from sub-micron trenches using megasonics.' *Microelectronic Engineering*. **87**: pp. 1665 - 1668.
173. N. Sinha, 2012 *Megasonic Cleaning With Controlled Boundary Layer Thickness and Associated Systems and Methods*.134/147, US 8,156,950 B2. US: Micron technology Inc. 1 - 10.
174. H. Shende, S. Singh, J. Baugh, R. Mann, U. Dietze, and P. Dress. (2011) 'MegaSonic Cleaning: Possible solutions for 22nm node and beyond'. in *Photomask Technology*. Monterey, California: SPIE
175. D. Dussault and V. Dragoi,(2012) 'Acoustic Energy : a New Tool for MEMS Manufacturing.' *Chambridge University Press: Materials Research Society Symposium Proceedings*. **1415**: pp. 1-6.
176. H.S. Nalwa, 2003 *Handbook of Photochemistry and Photobiology: Organic photochemistry*. American Scientific Publishers.
177. J. Desagher, D. Dussault, M. Beck, R. Lillard, and E. Liebscher 2016 'Direct vs. Indirect Megasonic Tank Cleaning Systems; Uniformity, Cleaning Efficiency and Cost of Ownership.' Available from: <http://www.prosysmeg.com/Papers/Direct-vs-Indirect.html>. [Accessed: 15th May 2017]
178. S. Kumari, M. Keswni, S. Singh, M. Beck, E. Leibscher, and S. Raghavan,(2012) 'Enhanced megasonic processing of wafers in MegPie using carbonated ammonium hydroxide solutions.' *Journal of Microelectronic Engineering*. **114**: pp. 148-153.